Water leaching of inorganic species from coal ash and slag generated at typical Underground Coal Gasification (UCG) temperatures

R.C Uwaoma
25452622

Dissertation submitted in partial fulfilment of the requirements for the degree *Magister Scientiae* in Chemistry at the Potchefstroom Campus of the North-West University

Supervisor: Prof CA Strydom

Co-supervisor: Prof JC van Dyk

Assistant Supervisor: Dr RH Matjie

May 2017

Declaration

I, Romanus Chinonso Uwaoma, do hereby affirm that the dissertation with the title: "**Water leaching of inorganic species from coal ash and slag generated at typical Underground Coal Gasification (UCG) temperature**", submitted in partial fulfilment of the requirement for a degree of Masters of Science (Chemistry) is my work and has not been submitted at any other university either in part or as a whole.

Signed at Potchefstroom on the **28th** day of November 2016.

……

Romanus C. Uwaoma

Acknowledgement

I express my gratitude and delightfully acknowledge the following for their contributions, assistance, help and guidance during the period if this research:

- First and foremost I would like to dedicate this work to my Heavenly Father. Through Him I received spiritual guidance, wisdom, courage and support that aided me to persevere to the end of this work.
- Prof C.A Strydom, Dr R.H Matjie and Prof J.V van Dyk, for their benevolent supervisorship, expert guidance, brilliant foresight, criticisms, invaluable suggestions and insight in the course of this investigation. I am eternally grateful to you.
- The National Research fund (NRF) and the NWU for their financial support of this investigation.
- Prof John Bunt and Prof Hein Neomagus for their assistance in terms of priceless criticisms, suggestions and guidance during the weekly meetings.
- Mr Gregory Okolo for his help with the Surface area experiments and his suggestions in making this work a success.
- Dr Louwrens Tiedt at NWU, Laboratory of Electron Microscopy, for his help with the SEM expeirments.
- Mrs Belinda Venter of the department of geology NWU for her assistance with the XRD and XRF.
- Mrs Yvonne Visagie of Eco-analytical Laboratory (centre for water science) NWU for helping with IC, ICP-OES, ICP-MS of the liquid samples.
- Prof. Cobus Kriek for helping with the leaching set up.
- My mum, dad, my Uncle Engr. Mike Uwaoma and his wife. I thank you all for all the financial support, prayers, love, patience, encouragement during the down moments, and for raising me to the person I am today. I am so grateful and amazed to have you people in my life.
- My sisters and brothers: Uncle Charles, Vincent, Marykate, Edith and Micheal, thanks guys for encouraging and cheering me up in my down moments.
- To my colleagues in the lab (Zach, Jackie, Ruthel), thank you all.
- My amiable friends, whom I hold dearly to heart: Nneka, Obinna, Charity, Boitumelo, Chris, Nnadi, David, Emeka and those back at home, thanks for supporting me through the good and the bad times.

Abstract

Underground coal gasification (UCG) is a better and more environmentally friendly way of gasifiying coal, using coal seams that are not economically viable to mine or coal seams that are deep underground. This technology has a lot of advantages in comparison with conventional or surface gasification. Recently some companies in South Africa have started to explore the practise of UCG technology for the gasification of coal. One such plant is currently being erected in the Theunissen area of the Free State Province of South Africa. With the advancement of this technology in South Africa, there is a need to study the mineralogy and water leaching of the ash and slag formed at typical temperatures of the UCG process. This study presents results obtained using a bituminous coal from the Theunissen underground coal gasification (UCG) site in the Free State Province, South Africa and results regarding the subsequent leaching from the coal and ash samples obtained after a heating process at temperatures expected during UCG.

The coal sample was blended to contain 15% of the roof and 5% of the floor samples from the Theunissen UCG site in order to mimic possible mineral compositions during a UCG process. The ash and slag samples were prepared in air at 1000, 1100, 1200 and 1300^{o}C using a furnace, and the mineralogy of the produced ash samples was characterised using various analytical methods such as XRD, XRF, FTIR, surface area (CO_2, and N_2), and SEM-EDX. Results from the XRD experiments show an increase in the crystalline phase with a decrease in the amorphous phase as the temperature of gasification increases, with mullite and quartz found to be the dominated minerals in the crystalline phase. FTIR spectroscopy results reveal the disappearance of peaks associated with certain functional groups of the carbon matrix as the temperature of gasification increases, with the appearance of peaks related to the crystalline phase of mullite. SEM results show the formation of cenospheres in the ash samples and slag as the temperature of the ashing rises. The surface area results show a reduction in surface area and porosity as the temperature of the ashing increases, with the slag at 1300^{o}C having the lowest surface area and porosity.

Leaching experiments were conducted on the coal and the ash samples (1000^{o}C, 1100^{o}C and 1300^{o}C) using two lixiviants: groundwater (GW) from the Theunissen

(UCG) site in the Free State Province, South Africa and deionised water (DW). A batch leaching method and a column leaching method was used. Some parameters were varied during the leaching tests, such as liquid to solid ratio, leaching temperature and the effect of ashing temperature on the leachability of the inorganic compounds in the ash samples. A comparison between the batch and the column leaching method indicate that more leachants were obtained using the column leaching method. The leachates obtained during the leaching study were analysed using ICP-OES, ICP-MS and IC. From the leaching results, it was found that Ca species and SO_4^{2-} ions were the most leached species and ions during the leaching tests, with a minor release of K, Mg, Al, Fe, Si, F^-, NO_2^-, NO_3^- for both leaching methods. The Cl^- and Na already in the groundwater contributed to relatively high values for these species in the leachates when the groundwater was used as lixiviant. The concentrations of the leachants increase slightly when the leaching temperature was increased from room temperature to 50°C, during the batch leaching tests. The species leached from the coal and ash samples were correlated with amounts in the original coal and ash samples. It was found that species in the leached samples were less when compared with the initial concentration of the species before leaching test. As expected fewer species leached out of the ash that was formed at 1300°C as a result of the slag being formed and the inorganic species being caught up in the melted mass.

More leachants (Ca and SO_4^{2-}) were observed using the column leaching method. The effect of ashing temperature was also investigated. It was found that the ash produced at 1300°C (fused form) produced lower concentrations of elements and ions when compared with the ash produced at 1000 and 1100°C. The amounts of the trace and heavy metals in the leachates were compared with the minimum standard requirements of the Department of Water Affairs and Forestry (DWAF) of South Africa and the Environmental Protection Agency (EPA) of USA. It was found that the concentration of the trace and heavy element were below limits as recommended by DWAF and EPA, except for Cd and Al, where slightly higher amounts were observed.

***Keywords**: Underground gasification, ash, inorganic, groundwater, mineralogy, leachate, leachants, slag*

Table of content

List of Tables

List of Figures

Abbreviations	
Abbreviation	Description
adb	Air-dried basis
d.b.	dry basis
ASTM	American Society for Testing Materials
AFT	Ash fusion temperature
BET	Brunauer-Emmett-Teller
BJH	Barrett-Joyner-Halenda
B/A	Base to acid ratio
BSE	Back scattered electrons
BTEX	Benzene, toluene, ethylbenzene and xylenes
Cdb	Carbon on a dry basis
CHNOS	Carbon, hydrogen, nitrogen, oxygen and sulfur
CTL	coal to liquid technology
dmmfb	Dry mineral matter free basis
D-R	Dubinin-Radushkevich
DTA	Differential thermal analysis
DTG	Differential thermogravimetric/thermogravimetry
DW	Deionised water
EC	Electron conductivity
ED-XRF	Energy-dispersive X-ray fluorescence
EDX	Energy dispersive X-ray spectrometer
ESKOM	South African Electricity Supply Commission
fi	Iron index
FC	Fixed carbon
FTIR	Fourier transform infrared spectroscopy
GW	Groundwater
H-K	Horvath-Kawazoe method
H/C	Hydrogen-carbon atomic ratio
IC	Ion chromatography
ICP- AES	Inductively coupled plasma atomic emission spectroscopy
ICP-OES	Inductively coupled plasma optical emission spectroscopy

Abbreviations (cont.)	
Abbreviation	Description
UICG	In-situ coal gasification (UICG)
ISO	International Organization for Standardization
LEP	Leachate extraction procedure
LOI	Loss on ignition
LTA	Low temperature ashing
m.f.b.	moisture free basis
mmb	Visible mineral matters basis
MoU	Memorandum of understanding
NWU	North-West University
O/C	Oxygen-carbon atomic ratio
PAHs	polycyclic aromatic hydrocarbon compounds (PAHs)
Ppb	Part per billion
Ppm	Part per million
PJ	petajoules
PwC	PricewaterhouseCoopers
PSD	Particle size distribution
R_s	Slagging factor
rpm	Revolution per minute
SABS	South African Bureau of Standards
SEM	Scanning electron microscopy
TA	Total alkalinity
TCLP	Toxicity characteristic leaching procedure
TDS	Total dissolved solid
TGA	Thermogravimetric analyser
Vdb	Volatile matter on a dry basis
VM	Volatile matter
vol.%	Volume percentage
wt.%	Weight percentage
XRD	X-ray diffraction
XRF	X-ray fluorescence
UCG	Underground coal gasification

Chapter 1

1.1 Introduction

This chapter introduces some background information regarding underground coal gasification (UCG) and problems encountered during the process, as well as the objectives and scope of the study. In Sections 1.2 to 1.6, the problem statement, hypotheses, research objectives and the scope of the dissertation are presented.

1.2 Problem statement

Coal offers many energy possibilities, and South Africa has some of the world's major coal deposits. Regrettably, it is not economically viable to retrieve the coal from the majority of the known reserves in South Africa (Prevost, 2003). Furthermore, the conventional methods used during surface gasification are not environmentally friendly. UCG converts organic carbon in coal to gases while still in the coal seam (in-situ). Hence, UCG promises to become a significant technique for coal utilisation, offering an alternative to the conventional coal gasification processes. The gaseous reactants during UCG are supplied by the oxidants (air or oxygen) and steam, and the coal is ignited for the underground coal combustion process (Gregg and Edgar, 1978; Walker *et al*., 2001).

UCG or in-situ coal gasification, though not a new concept, is currently attracting considerable global attention as a viable process to provide cleaner and more economical fuel from coal. This technology has the potential to exploit energy from low-grade, deep-seated, thin coal seams in a relatively economical, more environmentally friendly and more sustainable manner when compared to conventional gasification method. The UCG method can be useful to abandoned coal mines, remnants of already-exploited reserves and deposits considered uneconomical and technically difficult for existing conventional mining methods.

However, if the process is not properly managed, UCG technology has the potential to create hazardous atmospheric emissions, groundwater contamination, uncontrollable cavity growth and underground fires, mine subsidence, CO_2 pollution and human impacts such as noise, dust and increased traffic (Khadse *et al*., 2007).

During UCG, reaction products and by-products formed underground may cause unfavourable alterations in the groundwater quality. A study by Humenick *et al.* (1983) has shown that leaching from lignite ash produced at 850, 1000, and 1250°C is responsible for an array of ionic and inorganic species being released in groundwater. Due to coal pyrolysis and some of the reactions occurring during the combustion process, some toxic environmental compounds are produced which could contaminate groundwater (Liu *et al*., 2006a; Verma *et al*., 2014). Phenols, benzene, benzene derivatives (toluene, ethylbenzene and xylenes (e.g. BTEX)), and polycyclic aromatic hydrocarbon compounds (PAHs) are the most abundant organic pollutants resulting from UCG processes (Liu *et al*., 2006a; Verma *et al*., 2014). Some of the heterocyclic compounds containing nitrogen, sulfur, oxygen and heteroatom compounds may also act as groundwater contaminants (Edgar *et al*., 1981; de Graeve *et al*., 1980; Liu *et al*., 2006a, 2006b; Stanczyk *et al*., 2011; Stuermer, 1982; Verma *et al*., 2014; Yang, 2008). The inorganic species that may form during UCG include ionic compounds such as sulfates, chlorides, cyanides, and some metals and metalloid ions. These substances can migrate from the cavity and pollute underground water bodies (Edger *et al*., 1981; Liu *et al*., 2006a, 2006b; Stuermer and Yang, 2008; Stanczyk *et al*., 2011; Yang, 2009).

The ash generated during coal gasification is generally characterised in terms of the weight percentages of its constituent oxides (Fe_2O_3, Al_2O_3, MgO, MnO, V_2O_3, TiO_2, SiO_2, CaO, Na_2O, K_2O, P_2O_5, SO_3 and CrO_3) (Vassilev & Vassileva, 2005; Loubser and Verryn, 2008; Matjie, 2008). However, these constituents of ash do not represent the actual mineralogy of the ash, which consists of silicates, oxides and sulfates with small quantities of phosphates and other compounds (Vassilev & Vassileva, 2005; Vassilev & Vassileva, 2007). It is predicted that when groundwater re-enters the burning zone following a UCG process, the soluble mineral phases and non-mineral inorganics in the ash are leached out into the groundwater and carried into the surrounding formations (Bell *et al*., 2011; Burton *et al*., 2008). The gasification process during UCG is divided into various zone names: the oxidation zone, reduction zone, drying zone and pyrolysis zone. The oxidation zone is the first zone where, some coal is consumed by the exothermal reaction of reaction to give out heat (Burton *et al*., 2006). The temperature in the cavity generated from the oxidation phase can be higher than 1500 ºC (Burton *et al*., 2006).

Broadly, this study simulated groundwater leaching of inorganic species from ash formed from the coal and surrounding structures at temperatures that can be reached in a UCG plant in South Africa. The ash was prepared at typical UCG temperatures.

1.3 Hypotheses

The following hypotheses were formulated for this study:

- Knowledge of the changes in the physical, mineralogical and chemical properties of ash formed at the temperatures observed during a typical UCG process may assist in predicting the leachability of associated inorganic products in groundwater.
- The ash formed from the roof, floor of the cavity and coal seam constituents may contribute to groundwater contamination from inorganic species and unburned carbon.
- The temperature at which the UCG process occurs may influence the amounts of inorganic leachates.

1.4 Aim and Objectives

The aim of this research study is to investigate the water leaching of inorganic species from the coal ash and slag generated at typical UCG process temperatures.

Specific objectives of this study include the following:

- To investigate mineral transformation and to determine the inorganic composition of ash or slag that are formed at temperatures similar to that of a typical UCG process, using coal samples from the UCG site in Theunissen in the Free State, South Africa.
- To investigate the leaching of inorganic species from the coal and prepared ash and/or slag samples using a standard batch leaching method, and utilising water with a composition similar to that found at the Theunissen UCG site.

- To investigate leaching of inorganic species from the ash or slag formed at different relevant temperatures by using a modified column leaching method;
- To compare the standard batch and column leaching methods at room temperature.
- To compare the leaching from the coal with that from the ash and/or slag samples.
- To investigate the influence of temperature (<80°C) on leaching of inorganics species from the ash, using the batch leaching method.
- To propose the best operating temperatures for a UCG process with a view to limit leaching of inorganic compounds into the groundwater; and
- To compare the results of the trace elements obtained during the leaching process with the standard limits from the Department of Water and Forestry South Africa (DWAF) and the Environmental Protection Agency U.S (TPLC limit), in order to evaluate the environmental influence of the leached trace elements.

1.5 Outline of the study

The following will be undertaken to achieve the objectives of this study:

- The coal sample will be blended with floor and roof samples from the geological structures of the coal seam. The blended sample will be analysed for chemical, mineralogical, petrographic and physical properties prior to ashing.
- Subsequently, the blended coal sample will be ashed at the temperatures (1000 - 1300°C) typical of a UCG process, and the solid products will be characterised to understand the mineral transformation from coal to ash.
- Standard batch water leaching experiments will be conducted on the blended coal, ash and slag samples using deionised water and water obtained from the UGC site in order to compare the amounts of inorganic compounds that are leached out using these two lixiviants (groundwater and deionised water).
- All the leachates will be analysed using inductively coupled plasma optical emission spectroscopy (ICP-OES), inductively coupled plasma mass spectrometry (ICP-MS) and ion chromatography (IC) to determine the

concentrations of inorganic species and ions dissolved in water (leachates) during the leaching experiments.

- Leaching of inorganic species from the ash or slag formed at the different relevant temperatures will be studied using a modified column leaching method.
- The Influence of the leaching temperature and time during batch leaching experiments will be investigated at ambient temperature, 30°C, 40°C, and 50°C.
- XRD and XRF analyses will be performed on the blend of raw coal, roof and floor constituents, ash, and slag residues after leaching to determine the inorganic compounds remaining after the leaching process.

The outline of this study is summarised in **Figure 1.1**.

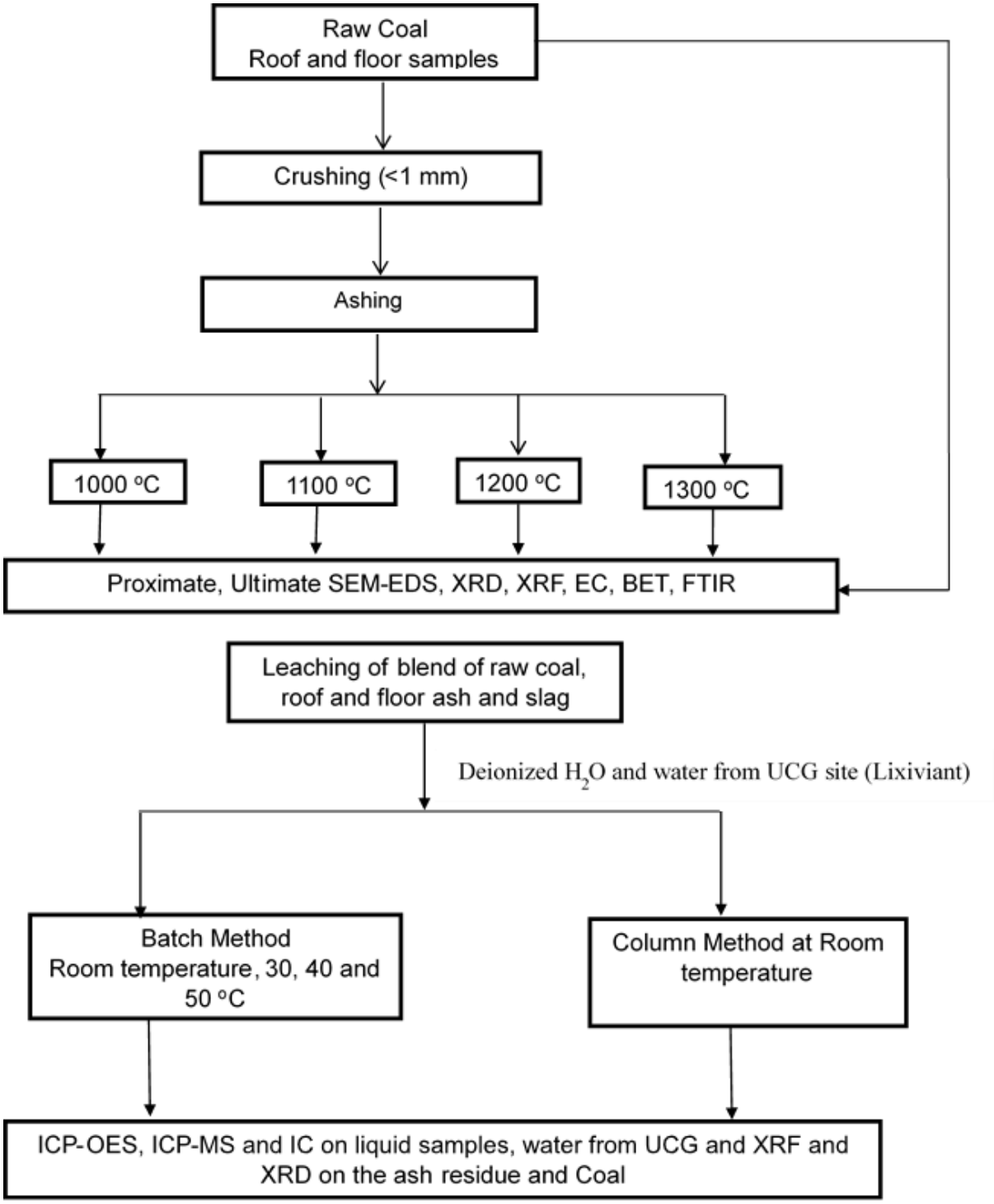

Figure 1.1: Outline of Study

1.6 Scope of the dissertation

Chapter 1: A brief introduction to the research study with some background information, motivation, hypotheses, objectives and scope of the investigation will be dealt with in this chapter**.**

Chapter 2: Background information and literature review. This chapter contains a summary of the previous studies conducted on groundwater pollution caused by ash formed at the temperatures observed during UCG.

Chapter 3: Background on experimental, analytical techniques. The focus of this chapter is on the different analytical techniques that were used to characterise the chemical, mineralogical and physical changes of the coal and ash samples. The chosen leaching methods will be discussed. The background of the analytical techniques is summarised, as well as the reasons for the selection of these techniques.

Chapter 4: Experimental procedure. This chapter contains the description of the methods of the different analytical techniques used and specifications for the instruments.

Chapter 5: Results and discussion of the changes in the chemical, mineralogical and physical properties of ash and slag formed at UCG temperatures. The results obtained from the chemical and mineralogical analyses done during the experimental part of this study are discussed in detail.

Chapter 6: Results and discussion of water leaching performed on the ash and slag. The influence of the ash and slag composition on the water leachability of the inorganic compounds is discussed. The data obtained from the various leaching methods used are compared and discussed.

Chapter 7: Conclusions and recommendations. This chapter contains a comparison and summary of the most important results, confirming or rejecting the initial hypotheses. Future research to be done is also proposed.

Chapter 2: Background and Literature review

2.1 Introduction

This chapter provides a detailed review of coal as an energy resource and its distribution in South Africa. The formation of coal, its composition (organic and inorganic) and classification will be discussed. The transformation of coal and its products, including its ashes at elevated temperatures, will be reviewed. The review will proceed by focussing on previous investigations regarding UCG in South Africa. Details of the UCG processes, the advantages and disadvantages of UCG will also be provided. Finally, the organic and inorganic contaminants formed during and after the UCG process will be reviewed.

2.2 Importance of Coal Utilisation in South Africa

The growth of any economy is dependent on the availability of energy. The three most widely globally utilised energy sources are coal, natural gas and oil (WCI, 2003). Coal has been considered as the most abundant, fastest growing and the cheapest fossil fuel in the world (Kleiner, 2008; Ye *et al*., 2013). Current estimation has shown that the consumption of coal globally accounts to about 64% when compared with 17% and 19% for natural gas and oil, respectively (OECD, 2012). Globally, coal has been one of the largest source of feedstock for power generation, production of chemicals and steel production (Buhre *et al*., 2005;; Sarwar *et al*., 2014; Ye *et al*., 2013). Presently, coal is the chief source of energy for power generation and industrial processes in South Africa and this will remain unchanged until at least 2030 (Cloke *et al*., 2003). Coal is one of the main sources of energy in developed, developing and undeveloped economies, providing 26% of global energy needs and 41% of global electricity generation (WCI, 2007). Coal has been estimated to be the second-largest source of energy production after petroleum, providing more than 27% of the energy needed, just behind the 33% contributed by petroleum with natural gas contributing 21%. As a fossil fuel, coal provides about 81% of energy demand globally with biomass providing 10%, nuclear 6%, and hydro 2% (OECD, 2012).

South Africa is the sixth-biggest coal manufacturer and the third major exporter of coal on the globe, with coal sales contributing approximately 20% of South Africa's

mineral sales (Eskom 2008; Subramoney *et al*., 2009). South Africa has an estimated recoverable coal reserve of about 53 billion tonnes (Eskom, 2008), and at the current production rate, this translates to about 200 years of coal supply. Coal production is the country's second-biggest mining sector after gold (Eskom, 2008). An average of 224 million tonnes of coal is produced yearly, 25% of which is exported, while the balance is used domestically by various coal utilisation industries (Subramoney *et al.,* 2010). Among these users are Sasol (33% for transportation fuel and petrochemical), Eskom (53% for electricity generation), metallurgical industries (12%), and household cooking and heating (2%) (Eskom, 2008; Subramoney, *et al.*, 2010).

2.3 Coal resources distribution in South Africa

Mineable and commercial coal in South Africa is extracted from different Provinces, ranging from the border with Botswana in the North-West, Limpopo, Mpumalanga and KwaZulu-Natal (Keaton Energy, 2009). These Provinces are divided into different Coalfields: the Waterberg Coalfield is located in Limpopo Province, bordering Botswana; the Highveld and Witbank coalfields are located in the Province of Mpumalanga while the Ermelo and Klip River Coalfields are in Gauteng Province (Keaton Energy, 2009). About 83% of the coal that is mined in South Africa is mined in the Highveld, Witbank, and the Klipriver Coalfields (Cairncross, 2001). A study from Cairncross (2001) estimated that the Waterberg Coalfield would be an important source of mined coal in the near future. Klipriver Coalfield is the smallest Coalfield, but it produces the country's anthracites and some of its coking coal (Cairncross, 2001; Snyman and Botha, 1993). Coal from the Free State Province is found in the Northern and Southern Free State. The coal seams found in the Free State Province are interlaminated with sandstone/mudstone and mainly composed of dull coal with high ash content. 40 - 50% of the coal resources in this Coalfield are unmineable, partly due to dolerite sills intrusions found throughout the Coalfield (Pinheiro *et al*., 1999; Snyman**,** 1998). The Coalfields in South Africa are presented in **Figure 2.1**.

Kershaw and Taylor (1995) estimated that South African coal resources consist of approximately 95% bituminous coal and 2% anthracite. Reports have shown that the majority of South African coals are mostly rich in inertinite macerals with a small

proportion of vitrinite macerals. One promising technology developed to utilise coals hitherto classified as unmineable resources and which will increase the cost effectiveness of the unmineable coals' recovery process is underground coal gasification (UCG).

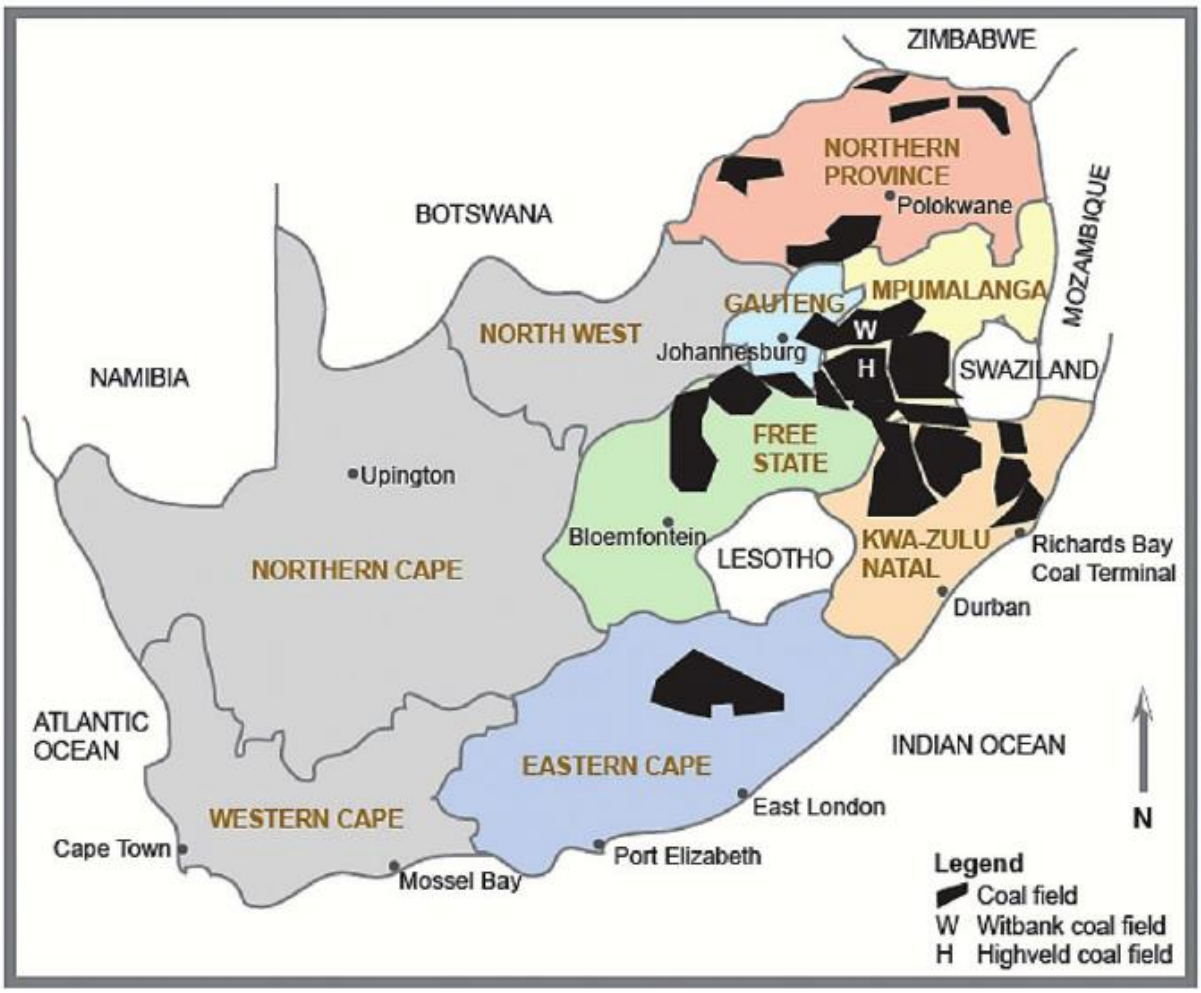

Figure 2.1: Map of South African Coalfields (Pinetown et al., 2007)

2.4 Composition of coal

Coal has its freshwater swamps and marine. High pressure and temperature assisted in trapping carbon in the peat bog that was consequently covered and buried over geological time (Meyers, 1982; Schobert, 2013; Speight, 1994). Coal contains a broad range of organic and inorganic material. Coal may be viewed as a sedimentary rock that is made up of carbonaceous organic matter (macerals) and inorganic minerals (mainly crystalline), (Harvey and Ruch, 1986; Miller, 2005). The organic components consist primarily of carbon, hydrogen, and oxygen, with smaller amounts of sulfur and nitrogen (Matjie, 2008; Ward, 2002). The inorganic

components are made up of different kinds of ash-forming compounds distributed unevenly throughout the coal (Miller, 2005).

2.4.1 Organic matter in coal (macerals)

Coal is a non-transparent heterogeneous material, made up of microscopically detectable, physically separate and chemically different organic constituents (macerals) that are mixed with small amounts of inorganic mineral matter that can be ignited to produce heat energy (Choudhury, *et al*., 2004; Osborne, 1988). The optical appearance of coal is used as a basis to describe the organic components of coal, usually referred to as macerals. Macerals have different chemical-structural properties. The macerals in coal will behave differently regarding reactivity of the coal, ash composition, amount of volatile matter released, char structure and the swelling behaviour (Benfell, 2011). The maceral composition of coal aids the prediction of the chemical, physical and optical properties of coal (Everson *et al*., 2008; Falcon and Snyman, 1986). Estimations from Schobert (2003) shows that the typical organic components of coal contain about 65-95% carbon, 2-6% hydrogen, up to 30% oxygen and a small percentage of sulfur and nitrogen for bituminous coal. The values differ for lignite and anthracite, for example.

2.4.2 Inorganic compounds in coal

The inorganic constituents in coal can occur in different forms (Benson and Holm, 1985; Benson, 1987; Ward, 1984; Ward and French, 2004), which are categorised as follows:

- Discrete crystalline or non-crystalline minerals (mineral grains);
- organically associated cations (Ca, Mg, Al, Si, Na, K, Ti and Fe); and
- salts (cations) dissolved in pore water in the coal.

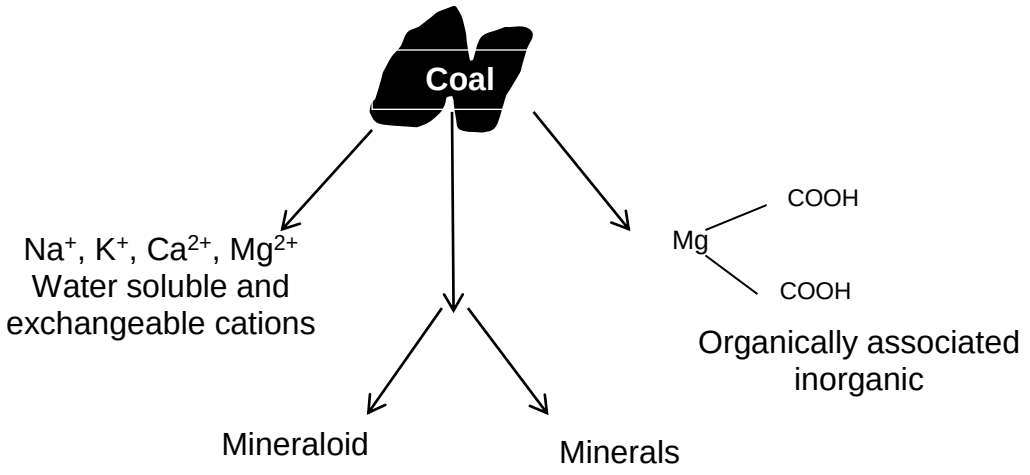

Figure 2.2: Nature of inorganic matter in coal (adapted from Ward and French, 2004)

As shown in **Figure 2.2**, the inorganic constituents of coal occur in different forms such as exchangeable ion dissolved salts, carboxylic acids or organically associated inorganics (organometallic complexes) and discrete crystalline mineral matter. This composition is primarily more significant for lower-rank coals, where organics and inorganics are related to compounds such as a carboxylate unit and organically associated inorganic elements (Schobert, 2013). Minerals in coal can originate from three main sources; namely

i plant source;

ii transportation of the minerals into the swamp and the accumulation of plants debris; and

iii percolation of water into the coal after the coal steam has been formed, which precipitates minerals into the coal.

The mineral grains make up a substantial fraction of the inorganics in coal (Benson, 1987). Bituminous and anthracite coals, which are primarily higher rank coals, contain inorganic species in the form of mineral matter, due to fewer carboxylic acid groups available in the coal structure (Schobert, 2013). Mineral matter in coal is categorized as all elements in coal excluding organic carbon (C), hydrogen (H), oxygen (O), nitrogen (N) and sulfur (S). Nevertheless, the elements such as C, H, O,

N and S may be present as an organic fusion such as H in water or water of crystallisation (hydrated) form, carbonates, sulfides, and oxides (Gluskoter, 1975). The inorganic species present with high-rank coals include silicon, aluminium and iron.

Classification of mineral matter in coal can be divided into two forms namely 'included' and 'excluded' minerals (Attalla *et al*., 2004; Matjie, 2008). 'Included' implies that the mineral is closely related to the organic matter (macerals) in the coal, while 'excluded' refers to minerals that are not held within the organic matter matrix in the coal, but are discrete grains (Attalla *et al*., 2004; Matjie, 2008; Ward and French, 2004). The amounts of organically associated (organically bound or atomically discrete) inorganic components differ inversely with coal rank. This implies that with decreasing coal rank (atomic H:C and O:C ratios increases), the portion of organically related inorganic constituents increases. The proportion of organically associated inorganic elements is much smaller than the discrete inorganic particles (extraneous minerals) in both lower-rank and higher-rank coals (Benson, 1987; Given, 1984).

The inorganic component (clays) of coal occurs mainly as minerals and trace elements. The mineral elements are made up of the following (Goblirsch *et al*., 1984; Ward and French, 2004):

i Alumino-silicates (clays) such as kaolinite, $Al_2Si_2O_5(OH)_4$ and illite, $KAl_3Si_3O_{10}(OH)_2$;

ii Oxides such as quicklime, CaO; quartz, SiO_2; hematite, Fe_2O_3; feldspars, $KAlSi_3O$, $NaAlSi_3O_8$, $CaAl_2Si_2O_8$;

iii Carbonates such as calcite, $CaCO_3$; siderite, $FeCO_3$; dolomite, $CaCO_3.MgCO_3$ and ankerite, $Ca(Fe, Mg, Mn)(CO_3)_2$; and

iv Sulfides and sulfates such as pyrite, FeS_2; marcasite, FeS_2; pyrrhotite, $Fe_{(1-x)}S$; sphalerite, ZnS; galena, PbS; stibnite, SbS; millerite, NiS and gypsum, $CaSO_4.2H_2O$.

A summary of the major minerals found in coal is presented In **Table 2.1.**

The trace elements present in coal are associated with either the mineral matter or the organic fraction. Several investigators have defined trace elements as elements that have concentrations below 1000 ppm (0.1 %) by weight in coal (Gibbs *et al*., 2004; Reed *et al*., 2001; Wang *et al*., 2007; Yiwei *et al*., 2007), while some other researchers define trace elements as having concentrations below 100 ppm (0.01 %) by weight (Bool and Helble, 1995; Xu *et al*., 2004; Yi *et al*., 2008). Most of the trace elements and radioactive elements commonly found in coal includes As, Be, Cu, Sb, B, Cd, Zn, Hg, Mn, Se, Mo, V, B, Cr, Mo, F, Sn and V. These trace elements are liberated from the carbon matrix during the coal utilisation processes. Some of the trace elements are of great concern because of their negative impact on human health and the environment. Galbreath and Zygarlicke (2004) and Swaine (2000) have identified a few of the trace elements that are harmful to humans and the environment. These trace elements include mercury, selenium, chromium, vanadium and nickel. Mercury has been associated with a neurological effect and is considered harmful to unborn kids (Zahir *et al*., 2005). Selenium has been found to be at high concentrations in some fish in Austria (Nobb *et al*., 1997). Research by Nobbs *et al*. (1997) has shown that the selenium concentration in fish from Lake Macquarie was about 12 times higher than the recommended level for human consumption. Chromium in coal can occur in two oxidation states, Cr^{3+} and Cr^{6+}. Cr^{3+} is very important for metabolic processes, but Cr^{6+} is very harmful and carcinogenic (Narukawa *et al.,* 2007). Vanadium has been claimed by researchers to be one of the major causes of cardiovascular and lung diseases, and a high concentration of nickel causes cancer to humans (Lee and Wu, 2002; Profumo *et al*., 2003). Based on the environmental effects of these trace elements, there is a need to study the leachability of these elements during and after the UCG process. Some of these trace elements such as gallium and germanium have vital commercial applications. Mineral matter and trace metals, especially calcium, potassium and iron, can have catalytic activity during the thermal processing of coals (Tomita, 2001; Lee, 2007).

Table 2.1: Principal minerals found in coal (Adapted from Ward, 2002)

	Formula	Formula	
Silicates		Carbonate	
Quartz	SiO_2	Calcite	$CaCO_3$
Chalcedony	SiO_2	Aragonite	$CaCO_3$
		Dolomite	$CaMg(CO_3)_2$
Clay minerals:		Ankerite	$(Fe,Ca,Mg)CO_3$
Kaolinite		Siderite	$FeCO_3$
Illite	$Al_2Si_2O_5\ (OH)_4$	Dawsonite	$NaAlCO_3(OH)_2$
Smectite	$K_{1.5}Al_4(Si_{6.5}Al_{1.5})O20(OH)_4$	Strontianite	$SrCO_3$
Chlorite	$Na_{0.33}(Al_{1.67}Mg_{0.33})Si_4O_{10}(OH)_2$	Witherite	$BaCO_3$
	$(MgFeAl)_6(AlSi)_4O_{10}(OH)_8$	Alstonite	$BaCa(CO_3)_2$
		Analcime	$NaAlSi_2O_6.H_2O$
Feldspar	$KAlSi_3O$	Clinoptilolite	$(NaK)_6(SiAl)_{36}O_{72}.20H_2O$
	$NaAlSi_3O_8$	Heulandite	$CaAl_2Si_7O_{18}.6H_2O$
	$CaAl_2Si_2O_8$		
		Sulfides	
Sulfates		Pyrite	FeS_2
Gypsum	$CaSO_4.2H_2O$	Marcasite	FeS_2
Bassanite	$CaSO_4.1/2H_2O$	Pyrrhotite	$Fe_{(1-x)}S$
Anhydrite	$CaSO_4$	Sphalerite	ZnS
Barite	$BaSO_4$	Galena	PbS
		Stibnite	SbS
		Others	
		Anatase	TiO_2
		Rutile	TiO_2

2.5 Coal classification

Coal is classified according to rank, which is determined by the carbon content of the coal (England *et al*., 2002). The ranks of coal consist of brown coal, lignite, sub-bituminous coal, bituminous coal and anthracite (Everson *et al*., 2008; Falcon and Snyman, 1986). Increasing mineral matter and moisture contents of coal will result in a reduction in the calorific value of the coal. This means that brown coals exhibits the lowest calorific value and anthracite possesses the highest calorific value (England *et al*., 2002). The oxygen and moisture content decrease as the rank of the coal increases. This is due to the loss of the hydroxyl, carbonyl and carboxyl groups in the coal. However, the hydrogen content remains relatively constant until the coal

reaches 89% elemental carbon content, whereafter the hydrogen content decreases with increasing coal rank (Van Krevelen, 1981). The carbon content and aromaticity thus increases with increasing coal rank, while the volatile matter content decreases. This is as a result of the loss of the aliphatic and the alicyclic groups in the coal (Borrego *et al*., 2000; Gavalas, 1982; Maroto-Valer *et al*., 1994).

2.6 Mineral matter reactions at elevated temperatures

Coal contains inorganic elements that may impact harmful behaviour during the utilisation processes that convert coal into usable products (Gupta *et al*., 1999; Huffman and Huggins, 1984). The transformation of these inorganics yields a different form of solid and volatile species. Other species formed could yield ash, fouling deposit, cause slagging, corrosion, pollution and several other problems (Gupta *et al*., 1999; Huffman and Huggins, 1984; Ward, 2002). Many reactions have been reported as being responsible for the mineral transformation in coal, ranging from oxidation, vaporisation, sulfur fixation, dehydration, reduction, solid-state interaction and recrystallisation (Gupta *et al*., 1999; Huffman and Huggins, 1984). The inorganic component of bituminous coal, which contains mineral particles such as clay minerals (kaolinite, illite), are more commonly formed, followed by quartz, bassanite and pyrite (Matjie, 2008; Van Alphen, 2005; Ward and French, 2004).

During the thermal reaction, transformation of low-rank coal under air atmosphere, the following transformations were observed between the parent coal and the ash produced, using thermo-gravimetric analysis (TGA) and differential thermal analysis (DTA): The water molecules evaporated at temperatures between 50ºC and 150ºC and gypsum ($CaSO_4.2H_2O$) dehydrated to bassanite ($CaSO_4.0.5H_2O$) and anhydrite $CaSO_4$ at 180ºC (Falcone *et al*., 1984; Falcone and Schobert, 1986). Furthermore, Falcone *et al*. (1984) and Falcone and Schobert (1986) also observed that, between 350ºC and 600ºC, there were water losses, resulting in the collapse of the clay structure with the breaking out of a cation from carboxylation, sulfate, oxides and carbonates structure. Oxidation of pyrite (FeS) to produce iron oxide occurs between 325ºC and 620ºC. At temperatures between 700ºC and 830ºC, calcite ($CaCO_3$) decomposes to calcium oxide. Quartz is stable at 1000ºC and various glassy and amorphous phases can be observed at and above 1300ºC (O'Gorman and Walter, 1973).

These mineral transformations can also be observed in studies from Grims (1962) and Bryers (1986). It was shown that, during high-temperature ashing from 400ºC to 1400ºC at intervals of 100ºC, the major minerals that were transformed were quartz, kaolinite, illite, pyrite, calcite, gypsum, dolomite and sphalerite. During this transformation, it was believed that the reaction in the minerals and the exchanges that occurred can be attributed to the mineral-mineral interactions (Matjie, 2008; Van Alphen, 2005; Ward and French, 2004). At temperatures above 600ºC, kaolinite loses its hydroxyl (OH-group) in the crystal structure to transform to alumina-silicate (meta-kaolinite) and amorphous/active quartz (Matjie, 2008; Van Alphen, 2005; Ward and French, 2004). As the temperature increases to approximately 1000ºC, the meta-kaolinite and amorphous/active quartz transformed to mullite and cristobalite, respectively (French *et al*., 2001; Matjie *et al*., 2006; Matjie, 2008; Van Dyk *et al*., 2009; Van Dyk and Waanders, 2007). Some of the amorphous quartz particles reacted at high temperatures with CaO and MgO from carbonates (dolomite and calcite) to form diopside ($CaMgSi_2O_6$) (Matjie, 2008). Some of the very reactive meta-kaolinite can react with either CaO or MgO to form a melt (Matjie *et al*., 2006). A small degree of mica, feldspar and other alumina-silicates in the coal reacted with CaO from calcite or dolomite at elevated temperatures to form anorthite ($CaAl_2Si_2O_8$) (French *et al*., 2001; Van Dyk *et al*., 2009, Van Dyk and Waanders, 2007). As the temperature decreased the anorthite crystallised from the melt. The presence of mullite, cristobalite, anorthite and diopside in the ash sample showed that there were mineral transformation and interactions at high temperature and pressure during coal gasification. The minerals mentioned below are not part of the mineral components found in coal. The summary of different mineral transformations in coal under oxidising conditions is presented in **Table 2.2.**

Table 2.2: Summary of some principal mineral transformations in coal under the oxidising conditions and the reaction temperatures (Schobert, 2013).

Temperature, ºC	Reaction or phase transformation
300	$CaSO_4.2H_2O$ (gypsum) →$CaSO_4.0.5H_2O$ (bassanite)
400	$K(Al,Mg,Fe)_2(Si,Al)_4O10(OH)_4.nH_2O$→$K(AL,Mg,Fe)_2(Si,Al)_4O_{10}(OH)_4$
	$CaSO_4.0.5H_2O$ (bassanite) → $CaSO_4$ (Anhydrite)
450	$Al_2Si_2O_5(OH)_4$ (Kaolinite) → $Al_2Si_2O_7$ (Mullite)
600	α-SiO_2 → β-SiO_2
700	$K(AL,Mg,Fe)_2(Si,Al)_4O_{10}(OH)_4$ → $K(AL,Mg,Fe)_2(Si,Al)_4O_{10}$
750	CaSO4 - NaCl eutectic melts
	Clays + $CaCO_3$ + FeS_2 → melt phase
800	$FeCO_3$ → FeO + CO_2
	$Ca(Mg,Fe)(CO_3)_2$ → CaO +MgO + CO_2 + FeO
900	K_2SO_4 - $CaSO_4$ eutectic melts
	PbS → PbO
	β- SiO_2 → Tridymite
	$CaMg(CO_3)_2$ → CaO +MgO +CO_2
	3 $CaSO_4$ + CaS → 4 CaO + 4 SO_4
950	2 $Al_2Si_2O_7$ → $Al_2O_3.3SiO_2$ + SiO_2
	FeO-FeS eutectic melts
	$CaCO_3$ → CaO (lime) + CO_2
	2 CaO + $Al_2Si_2O_7$ → $Ca_2Al_2Si_2O_7$ (anorthite) + SiO_2
	CaO + $Al_2Si_2O_7$ → $CaAL_2SiO_8$
1000	TiO_2 (anatase) → TiO_2 (rutile)
1100	$K(AL,Mg,Fe)_2(Si,Al)_4O_{10}$ forms glassy phase
1200	$Ca_2Al_2Si_2O_7$ forms glassy phase
1300	Glassy phase transforms to spinels and Si rich glass
1400	$Ca_2Al_2Si_2O_7$ and $CaAl_2SiO_8$ melts
	FeO melts
	Glassy phase → 2 $Al_2O_3.SiO_2$
1500	SiO_2 (tridymite) → SiO_2 (cristobalite)

2.7 Influence of mineral matter during coal utilisation process

Mineral matter in coal influences exploration, mining, preparation and utilisation of coal. Studies of mineral behaviour in coal which includes spreading of clay in preparation plants, development of acid(s) from pyrites and the discharge of soluble minerals have been carried out (Benson *et al*., 1987; Raask, 1985; Vorres, 1996; Gupta *et al*., 1999). Mineral-related factors involved in coal combustion, coking and gasification include catalytic activity, corrosion, fouling, slag development, erosion and the release of particulates into the atmosphere (Benson *et al*., 1987; Huffman and Huggins, 1986; Ward, 2002). The minerals can also serve as diluents (or dispersant agents) during coal conversion reactions (Matjie *et al*., 2011).

The chemical treatment of coal has been employed to decrease the mineral content of coal before utilisation. The treatment minimises the deposition of the ash during the utilisation process of coal (Vorres, 1986). Decreasing the quantities of inorganic material in coal by coal treatment increases the calorific value of the coal (Schobert et al., 2013). Alkaline and acid treatments are used to reduce alumino-silicate minerals in the coal (Vorres, 1986; Sharma and Gihar, 1988; Bolat *et al*., 1998; Okolo, 2010). The decrease of minerals in coal has been extensively studied by several investigators (Bolat *et al*., 1998;Okolo, 2010; Sharma and Gihar, 1988). However, it may not be applicable to UCG, hence an elaborate discussion of the coal treatment before usage may not necessary for the purpose of this study.

2.8 Coal Ash

Coal ash is formed during the thermal combustion and gasification processing methods used in the conversion of coal to useful products. These are combustion and gasification processes.

2.8.1 Coal ash from combustion

Coal combustion is a method where coal is burnt in a boiler for the production of electricity. The reactant gas mostly used for the combustion process is air. The air is provided to the boiler, where it reacts with the coal, liberating gases and thermal energy (Smith and Smooth, 1985; Suarrez-Ruiz and Crelling, 2008). The incombustible material that is left after the combustion process is known as ash. The

major discrepancies between combustion and gasification is the type of reactant gases used during each process.

2.8.2 Coal ash from gasification

Coal gasification is a thermo-chemical method during which the coal is transformed into synthetic gas and other products by heat and pressure. (Chen *et al*., 2009; Everson *et al*., 2008; Kühn & Plogmann, 1983; Molina & Mondragón, 1998; ; Meng *et al*., 2011; Nel, 2011; Nishiyama, 1991; Okolo, 2010; Wood *et al*., 1984). This method involves the breaking down of the coal carbon structure into its basic constituent gases namely: CO, CO_2, CH_4 and H_2. These gases that are produced can be used in the production of electricity or as a building block for industrial purposes (Chen *et al*., 2009; Okolo, 2010). Gasification reactions take place in O_2, CO_2, steam, air, or a combination of two or more of the gaseous reactants, at elevated temperatures (Okolo, 2010).

Gasification of coal happens in two phases, the first being pyrolysis, where volatile material evaporates. Pyrolysis consists of three phase: evaporation of water; devolatilisation of thermally labile volatiles; and the formation of char. The second stage is the conversion of the subsequent chars during the gasification stage under a reactive atmosphere (CO_2, O_2, air, steam, or a mixture of reactants) leading to the production of gaseous products popularly referred to as synthetic gas (syngas) and the residual non-combustible ash. The aim of this study is on underground coal gasification and thus UCG will be discussed in more detail.

2.9 Underground coal gasification (UCG)

UCG is viewed as an economically viable technique for recovering energy from coal reserves that are too deep to mine by conventional surface or strip-mining techniques (Burton *et al*., 2008; Gregg and Edgar, 1978; Kapusta and Stanczyk, 2011; Liu *et al*., 2007). Due to the shortcoming in the current coal mining technologies, 85% of the world's coal resources are classified as unmineable (Linc Energy, 2008). Estimations from Linc Energy (2008) have shown that over 5 million petajoules (PJ) of UCG syngas resources are available in the U.S.A Presently, about 1 million PJ of syngas from UCG are available in the U.S and additional 1.3 million PJ are predicted to be available in Australia. India has a projected value of 1.9

million PJ of UCG syngas available while China has over 2.2 million PJ of UCG syngas (Linc Energy, 2008). Based on the above results, it could be established that the use of UCG technology has the potential to increase the amount of useable coal resources by at least threefold.

UCG technology is, therefore, a good option in the utilisation of coal that is not economically minable (de Graeve *et al*., 1980; Edgar *et al*., 1981; Gregg and Edgar, 1978; Stanczyk *et al*., 2011; Verma *et al*., 2014; Yang, 2008). During UCG, coal is burnt underground to produce synthesis gas. The UCG technology has been available on an industrial scale and carried out in various locations across the world such as United State of America (USA), Great Britain, India, China, Australia etc (Shafirovich *et al*., 2009). The pioneering technology of UCG was developed in the 1920s and 1930s in the former Soviet Union, who was the pioneer of the technology (Gregg and Edgar, 1978). It was originally proposed by a Russian scientist, Dmitri Mendeleev, in 1888 (Gregg and Edgar, 1978). The Russian experience and success with the UCG process far surpassed those of any other country, with extensive field testing being conducted in the 1930s (Gregg and Edgar, 1978). Additional field testing of the process was done from the mid-1940s through mid-1960s by many countries, with significant testing being done by the USA and Great Britain (Gregg and Edgar, 1978). Furthermore, numerous testing processes have also been carried out in China and Europe. Results from these earlier tests suggested that the process was not efficient for energy recovery (Gregg and Edgar, 1978). However, a more recent application of the technology by Eskom in South Africa has shown that the UCG process is a promising technology on the African continent (Van der, 2008; PwC, 2008).

2.9.1 UCG in South Africa

South Africa has been using coal to liquid technology (CTL) since 1955, with all of this technology confined to surface gasification (gasification in reactors). More recently, the South African government is promoting research into the utilisation of lower grade and unmineable coals for power generation and liquid fuel production via UCG (Eskom, 2008, Van Nierop *et al.,* 2000; Van Dyk *et al.,* 2006; Van Dyk *et al.,* 2015). In 2007, the World Energy Council projected that UCG could raise the

world's usable coal reserves by as much as 70%. According to statistical estimation by Eskom, about three-quarters of the coal seams in South Africa are not mineable, and about 45 billion tonnes of this unmineable coal seams are suitable for UCG (Wild, 2014). This makes UCG an excellent alternative to the traditional gasification and combustion methods.

Eskom has developed a UCG pilot plant at Majuba Colliery, Mpumalanga, to investigate the ability to co-fire syngas with coal at Majuba power station (PwC, 2008). This site was an ideal location for a UCG pilot plant as the sub-bituminous coal found in the site cannot be mined by the traditional mining methods (PwC, 2008). On 28 October 2010, Eskom's UCG demonstration plant delivered gas to Majuba power station, and co-fired with coal to produce 3 MW of electricity (Eskom, 2010**).**

Presently African Carbon Energy (Pty) Ltd, a subsidiary of Africary, is developing a 50 MW power station which is going to use synthesis gas from the Theunissen UCG site located in the Free State Province of South Africa. According to Van Dyk *et al.,* (2015), major issues relating to the development of the project, such as environmental impact assessment, project designs, permit application, cost estimation, technology reservation and financial modelling have been finalised. Van Dyk *et al.,* (2015) also estimated that about 150 hectares of land will be used for this project and it will consume about five million tonnes of coal over the next 20 years, producing about 50 megawatts of electricity. More South African mining companies are investing in the use of UCG technology for coal gasification. A more recent one is Anglo-African Capital, who has signed a memorandum of understanding (MoU) with Gazprom, the Russian national gas company, to secure a production right for the development of UCG in South Africa. An agreement has been finalised between the two companies to partner in the use of coal located in the Springbok Flats area of Limpopo in South Africa for its UCG process. Gazprom will also partake in the pre-feasibility study of the project (http://www.miningweekly.com/anglo-africa-capital-concluded-coal-gasification-technology-deal-with-gazprom). With the advancement of this technology in South Africa, there is a need for an extensive study on the environmental impact of the UCG process in South Africa.

2.9.2 The UCG process

UCG or in-situ coal gasification (UICG), though not a new idea, is now drawing substantial global attention as a potential technique to offer a “clean” and economical fuel from coal (Khadse *et al*., 2007; Prabu and Jayanti, 2012; Yang *et al*., 2003). UCG converts coal to gas while still in the coal seam (in situ).

UCG consists of three steps: The first step is the linkage of the coal seam between injection and production wells, from the surface to the coal seam. This linkage should have a high permeability path between the injection and the production well (Britten and Thorsness, 1988; Thorsness and Rozsa, 1976). The second step involves the gasification of the coal seam through the ignition of the coal by injecting enriched air or a mixture of oxygen and steam through the injection well, which reacts chemically with the coal (Bell *et al*., 2011; Britten and Thorsness, 1988; Solcova *et al*., 2009; Thorsness and Rozsa, 1976). Finally, the third step involves the recovery of the synthesis gas (syngas) through the production well. The gas is then cleaned and utilised either as a fuel for power generation or as a chemical precursor for the production of several chemical products (e.g. hydrogen and ammonia) (Bell *et al*., 2011; Britten and Thorsness, 1988; Solcova *et al*., 2009; Thorsness and Rozsa, 1976).

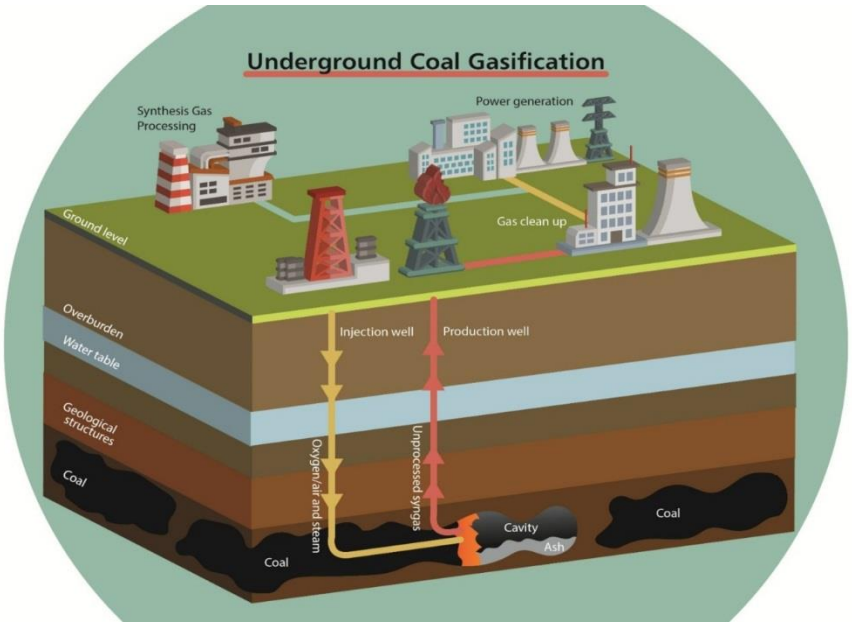

Figure 2.3: Schematic representation of the UCG process

The synthesis gases produced from a typical UCG process are composed mainly of hydrogen (H_2), carbon monoxide (CO), methane (CH_4), carbon dioxide (CO_2) and, to a lesser extent, steam (H_2O), nitrogen (N_2), and hydrogen sulfide (H_2S) (Bell *et al*., 2011; Britten and Thorsness, 1988; Solcova *et al*., 2009; Thorsness and Rozsa, 1976). A typical UCG process is illustrated in **Figure 2.3**.

2.9.3 Chemistry of UCG

The process of burning coal with air or other oxidants involves a complex series of reactions, including oxidation, partial oxidation, reduction (Boudouard reaction), hydrogenous water-gas reduction, water-gas shift conversion, methanation, hydrogenation gasification and pyrolysis reactions (Ruprecht *et al.*, 1988; Burton *et al*., 2006; Yang *et al*., 2008; Evgeny and Arivind, 2009). Some of the reactions are given below:

Oxidation reaction

$$C + O_2 \rightarrow CO_2 - 393.8 \text{ MJ/kmol} \quad (2.1)$$

Partial oxidation

$$2C + O_2 \rightarrow 2CO_2 - 231.4 \text{ MJ/kmol} \quad (2.2)$$

Oxidation

$$2\,CO + O_2 \rightarrow CO_2 - 571.2 \text{ MJ/kmol} \quad (2.3)$$

Reduction (Boudouard reaction)

$$C + CO_2 \rightarrow 2CO + 162.4 \text{ MJ/kmol} \quad (2.4)$$

Steam gasification

$$C + H_2O\,(g) \rightarrow CO + H_2 - 131.5 \text{ MJ/kmol} \quad (2.5)$$

Water-gas Shift reaction

$$CO + H_2O \rightarrow CO_2 - H_2 + 42.3 \text{ kJ/mol} \quad (2.6)$$

Methanation

$$CO + 3H_2 \rightarrow CH_4 + H_2O - 206.0 \text{ kJ/mol} \quad (2.7)$$

Hydrogenation gasification

$C + 2H_2 \rightarrow CH_4 - 87.5\ KJ/mol$ (2.8)

Pyrolysis

$Coal + Heat \rightarrow Char + Ash + HC's + CH_4 + H_2 + H_2O + CO + CO_2$ (2.9)

The UCG process may be divided into various zones: the oxidation zone, reduction zone, drying zone and pyrolysis zone. The above mentioned reactions occur in the various zones as shown in Figure 2.4.

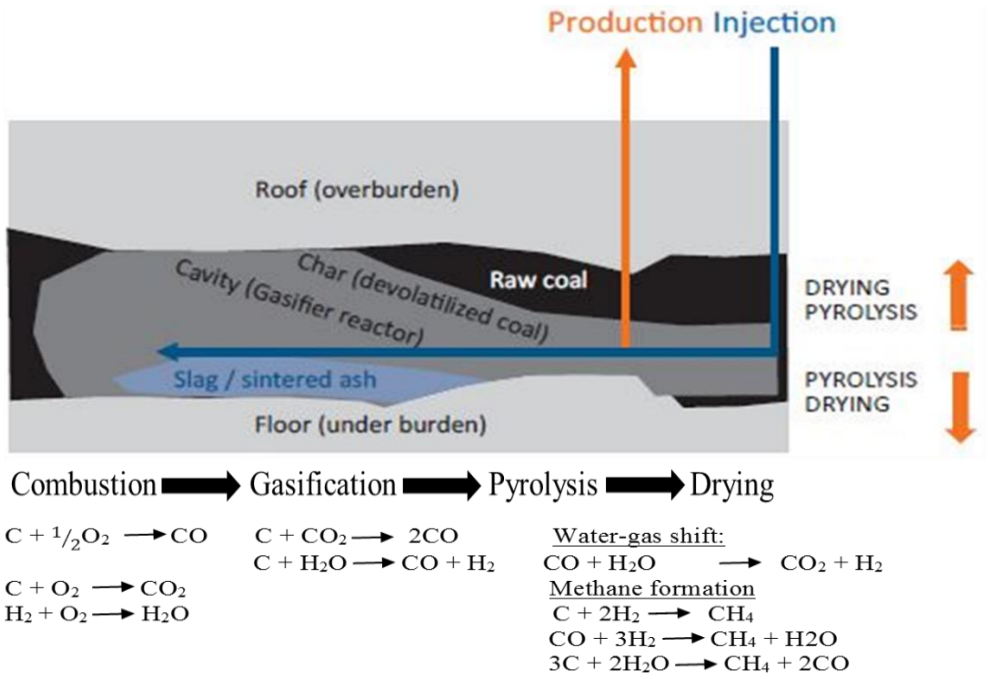

Figure 2.4: Reaction scheme of UCG (Van Dyk et al., 2015)

2.9.4 Advantages of UCG over the conventional gasification method.

A study from the Lawrence Livermore National Laboratory (California, USA) estimated that the UCG method will increase the recovery of coal in the USA by 300% (PWC, 2008; Walker, 2001). The study further claimed that the UCG method of gasification has a lower operating and capital cost when compared to the conventional or traditional method of gasification. Furthermore, the environmental and social impact of the UCG method includes the elimination of surface damages and solid waste. It also reduces SO_2 and nitrogen oxide (NO_x) emissions, particulate

matter, solid waste and surface footprints are also less when compared to the use of other gasification methods (Liu *et al.*, 2007). A Study from Meany and Maynard (2009) suggested that the use of UCG technology will reduce the accumulation of greenhouse gases in the atmosphere.

When comparing UCG and surface gasification, UCG has many other advantages over conventional gasification method. These advantages include safer working conditions, low water consumption, minimum surface disturbance, no coal transportation costs, no underground coal miners required which reduces the staff strength, when compared to surface gasification process, direct use of feedstock (coal) and water available underground, less pollution because no coal tailings are exposed to the surface and lower capital investment costs due to the absence of a manufactured gasifier (Kapusta and Stanczyk, 2011; Liu *et al*., 2007). Syngas generated from UCG typically has a relatively high content of CO and H_2 and is low in CH_4.

Burwell (1984) compared the cost of electricity generation using different technologies. This author found that the gases from UCG technology were relatively more profitable to use than the gases produced by conventional gasification methods. Massaquoi (1981) estimated that the gases produced during UCG, if used for pipeline gas, will be more cost effective than that from conventional sources, such as liquefied natural gas (LNG) and synthetic natural gas (SNG). Martelli *et al*. (2009) have shown that the use of UCG process for gasification will cut the cost of coal gasification by roughly 30 - 40 %. Blinderman and Friedman, 2006 compared the cost of electricity generated if the syngas produced from the UCG process is used for generation of electricity and the cost of electricity generated from integrated gasification combined cycle (IGCC). They found out from their study that cost of electricity generated from UCG process may be low as $24 per megawatt hour (MWh), when compared with $77 for an IGCC plant and $55 for a plant operating at with supercritical conditions (Blinderman and Friedman, 2006).

2.9.5 Disadvantages of UCG

Despite economic, environmental and technical benefits, UCG technology possibly has the following disadvantages, which include: atmospheric emissions from syngas clean-up, groundwater contamination, uncontrollable cavity growth and underground

fires. Land subsidence, which is the collapse of the cavity after the gasification process, CO_2 management and human impacts such as noise and dust are major concerns. However, land subsidence may not be a major problem, because it can be controlled by the choice of site and operational conditions (Burton et al., 2008). Therefore, groundwater contamination is the major concern during the UCG process, and the negative impact will be discussed in detail further in this section. Groundwater contamination will be divided into two parts; namely, organic and inorganic contaminations.

2.9.5.1 Contamination from organic compounds

Organic compound contaminant: It has been reported by different authors that the main compounds that contaminate groundwater during and after the underground gasification process are organic compounds (Humerick and Mattox, 1980; Kapusta and Stanczyk, 2011; Liu *et al.,* 2007). The first organic contamination was observed during the monitoring of groundwater from the gasification of lignite coal in Texas. The results obtained from the study are presented in **Table 2.3**. From the results, it was shown that different organic pollutants were observed to increase soon after the gasification period with phenols being the major contributors to the pollutant, while the minor organic contaminants were polycyclic aromatic hydrocarbons (PAHs) and heterocyclic compounds (Hummerick and Mattox, 1980; Struermer *et al*., 1982).

Table 2.3: Organic profiles of groundwater samples near Fairfield UCG site (µg/L) (Liu et al., 2007)

Component	Before gasification	Soon after gasification	One year after gasification
Total Phenols	7	10000	20
Total heterocyclic	nd	2200	nd
Two-ring PAHs	2	105	9
Three-ring PAHs	1	22	5
Four-ring PAHs	nd	7	nd
Five-ring PAHs	nd	3	nd
Total organics	10	103	34

nd- Not detected

Campbell *et al.* (1978) studied the influence of organic contaminants on the field operation of Hoe Creek UCG site in Wyoming. Their study involved the sampling of water near the burning cavity during and after the gasification process. Analyses were conducted on the water samples to determine the concentration of the following organic compounds: phenols, aromatics, carboxylic acids, aromatics, quinolones, isoquinolines and aromatics amines. Results obtained from their study showed that naphthalene, o-xylene, and z-methyl pyridine were the organic contaminants with the highest concentrations. It was also observed that Felix 1 UCG site at Hoe Creek has a high benzene concentration of about 3000 µg/L. They concluded in their study that the major organic contaminant was benzene due to the high concentration of benzene in the water. Therefore, water samples from the site should be monitored to check for the level of benzene because of its carcinogenic properties.

Kapusta and Stanczyk (2011) conducted studies on the contamination of underground water during UCG of lignite and hard coal. In their study they compared the organic and inorganic pollutants from the lignite and hard coal. Results from their study showed that the major pollutants were organic compounds such as phenols, benzene with its derivatives, polycyclic aromatics, hydrocarbons and heterocyclic with the hard coal exhibiting higher concentrations of this species when compared with the lignite coal samples. They finally concluded that the development of contaminants during UCG process is dependent on the coal rank, the elemental constituent of the coal and the temperature used during the gasification process. Since the cureent study focussed on inorganic contaminants, details of previous studies on inorganic contaminants will be discussed further below.

2.9.5.2 Contamination from Inorganic compounds

Since the present study deals with verifying the contamination of inorganic species, this review will be focussed on the previous research done on the release of inorganic species into groundwater. The section will be sub-divided into laboratory and field studies done on the release of inorganics.

The sulfur source (mainly pyrite or its polymorph marcasite, FeS_2) decomposes at elevated temperatures (800^oC) to iron oxide and SO_2. A portion of the SO_2 may be further oxidised to SO_3 and will eventually react with calcium oxide from the disintegration of calcite and dolomite to form inert $CaSO_4$ (Magee *et al*., 1973). Sulfur

compounds are considered major contaminants produced during coal thermal processing. Organically bonded sulfur existing in coal will decompose to sulfur dioxide, followed by the formation of sulfur trioxide at temperatures below 500°C in an oxidising atmosphere (Benson and Holm, 1985; Benson, 1987; Given, 1984; Reid, 1981). The alkali and alkaline earth metallic compounds in coal ash that are produced during gasification of coal may associate with sulfur oxides at high temperatures to form soluble alkali or alkaline sulfates/chlorides/carbonates such as: Na_2SO_4, K_2SO_4, NaCl, K_2CO_3, $Al_2(SO_4)_3$, $MgSO_4$ and $CaCl_2$ present in the ash samples (Reid, 1981; Benson,1987). These salts are the source of the majority of dissolved solids leached by groundwater. Inorganic elements, for example Na, Ca, Fe, K, Mg and Al, in the amorphous phase could also dissolve in water. Anhydrite ($CaSO_4$), glauberite ($Na_2Ca\ (SO_4)_2$), anorthite (Ca-feldspar and related Ca-Na aluminosilicates), quicklime (CaO), hydrated lime/portlandite ($Ca(OH)_2$) and calcite ($CaCO_3$) are insoluble in water and will report to the ash and slag materials (Bryers, 1986; Moitsheki *et al.,* 2009; Ward and French, 2004; Raask, 1985). Furthermore, lime may react with water and sulfur oxides to form portlandite ($Ca(OH)_2$) and anhydrite ($CaSO_4$) precipitates, respectively.

2.9.5.2.1 Laboratory studies

Campbell and Washington (1976) conducted laboratory-scale ash leaching experiments on coal ash samples produced at 1000°C. In their experiments, about 10 - 11 g of the ash was leached with 25 ml aliquots of deionized water. The leachate was collected and analysed for Al^{3+}, Ca^{2+} and OH^{-1} species. Results from their investigation showed that about 1.4 L of water was required to extract most of the Ca^{2+} from the ash, while about 400 mL of water was needed to leach all soluble Al^{3+}. The pH of the ash dropped from 11 to 10 after the ash was leached with 1.4 L of water. The decrease in pH observed in their study was attributed to the fact that aluminium is an amphoteric substance. A study by Campbell and Washington (1976) on preliminary laboratory and modelling investigation on the environmental influence of UCG showed that anhydrite was the only mineral that appeared to be largely unaffected by the heat treatment at temperatures below 1150ºC, showing a strong x-ray trace at all temperatures.

Humenick and Mattox (1977) studied water leaching of lignite ash samples from Texas. The char was prepared from the feed coal samples under nitrogen atmosphere at a temperature of 700°C. Also, ash was prepared from the same feed coal under air in a furnace at 1000°C. The raw lignite sample, the char and the ash produced were subjected to a batch leaching process with ground water as lixiviant for 72 hours. The leachates obtained after the leaching process were analysed for the following parameters: pH, alkalinity, SO_4^{2-}, Cl^-, Na^+, Ca^{2+}, Mg^{2+}, K^+ and NH_4^+.

From the result of the analyses, shown in **Table 2.4**, it was evident that the major ions that were leached out from the ash were Ca^{2+} and SO_4^{2-}. Also, from **Table 2.4**, the concentration of the of SO_4^{2-} increased from 1450 mg/l, 1700 mg/l and 2020 mg/l with a decrease in the lixiviant (groundwater) used during the leaching process from 192 mg/l, 94.1 mg/l and 54.4 mg/l Similar results were obtained for Ca^{2+}, having an increase in the concentration from 564 mg/l for 192 mg/l, 585 mg/l for 94.1 mg/l and 660 mg/l for 54.4 mg/l. Humenick and Mattox (1977) concluded in their study that the amount of ash sample in contact with the lixiviant decreases with equivalent rise in the concentration of the ions released, showing an inverse relationship between the ash and the groundwater used in the experiment.

Table 2.4: Leachate extraction of gasification residues (mg/l) (Humenick and Mattox, 1977)

Lixiviant (mg/l)	pH	Alkalinity	SO_4^{2-}	Cl^-	Ca^{2+}	Na^+	Mg^{2+}	K^+
			Ash					
192	10.1	144.0	1450.0	60.0	564.0	42.4	1.0	4.7
94.1	9.7	104.0	1700.0	48.0	585.0	37.0	2.4	3.8
54.7	9.1	48.0	2020.0	48.0	660.0	34.6	18.8	3.2
Blank	7.8	184.0	25.5	34.0	22.4	33.4	23.8	2.5
			Char					
9.6	31.0	50.0	184.0	20.2	25.8	3.2	-	
37.8	9.7	65.0	42.0	88.0	9.4	31.1	17.4	-
18.5	9.2	104.0	37.5	65.0	6.4	32.0	23.2	-
Blank	8.5	196.0	30.0	33.0	19	31.7	26.6	-
			Lignite					
68.1	6.5	144.0	420.0	44.0	85.0	44.4	62.0	-
35	6.8	131.0	220.0	67.0	67.5	38.4	39.0	-
17 .6	7.1	127.0	110.0	37.0	26.5	34.5	24.0	-
Blank	8.5	196.0	30.0	33.0	19.0	31.7	26.6	-

Laboratory studies have been conducted by Dalton and Campbell (1978) to measure groundwater release and transportation of pollutants predicted during UCG by high-temperature ashing of sub-bituminous coal. The following elements and ions were found in the leachate at 23°C and high pH: calcium, potassium, aluminium, barium, iron, magnesium and sulfates. Calcium ions (Ca^{2+}) and sulfate ions (SO_4^{2-}) were observed to be the major ions in the leachate. Also, high temperatures predicted lower concentrations of the elements, except for magnesium and calcium. This was attributed to high pH in the leachate, which caused a precipitation of magnesium hydroxide and calcium sulfate (Dalton and Campbell, 1978). At 25°C and low pH, Ca^{2+}, Al^{3+} and SO_4^{2-} can precipitate from the leachate in the form of ettringite, $Ca_6Al_2(SO_4)_3(OH)_{12}\cdot 26H_2O$. Dalton and Campbell (1978) conducted a leaching experiment to estimate the effect of gasifying temperature on the leaching of the

inorganic ions in ash. The lignite coal sample was heated under air in a furnace at 1000°C, 1100°C and 1200°C with a resident time (or holding time) of 4 hours. Samples were characterised using XRF and XRD. From the XRF results, it was observed that there were no major alterations in the elemental constitents of the samples as the temperature increased. However, there were significant alterations in the mineralogy of the samples. The two variations observed in the XRD result were the disappearance of Quartz (SiO_2) at 1000°C and the detection of a strong peak of calcium-aluminium silicate known as gehlenite ($Ca_2Al_2SiO_7$) at 1200°C, which was not initially detected at 1000°C. The authors suggested that the metal oxide has decomposed at a high temperature and reacted with the reactive quartz to form an insoluble silicate mineral (Dalton and Campbell, 1978). They also reported that anhydrite mineral was the only mineral that was not affected by heat during the gasification process.

Subsequently, after the ashing process, the samples were subjected to leaching experiments using natural underground water as lixiviant and a leaching temperature of 25°C. The method used for the experiment was column leaching. Leachate samples obtained after the leaching experiments were analysed for the following: pH, Ca^{2+} SO_4^{2-} $Al^{3+,}$ Mg^{2+}, Na^{+}, and K^{+}. The results of the analyses showed that the major ions that were leached were Ca^{2+} and SO_4^{2-}, with Ca^{2+} having the maximum concentration of 650 ppm for the ash produced at 1000°C, 630 ppm for the 1100°C ash, and 410 ppm for the 1200°C ash. Also, the maximum for SO_4^{2-} were 2200 ppm, 1670 ppm and 1670 ppm for the ash produced at 1000°C, 1100°C and 1200°C, respectively.

Dalton and Campbell (1978) also studied the influence of pH on the leachate and found that the pH of the leachate was 10 - 11 for the ash samples that were formed at 1000°C and 1100°C, but dropped to 7.9 for the ash sample which was produced at 1200°C. The drop in pH was attributed to the metal oxides that transformed in the ash during the high-temperature ashing and to the formation of an insoluble silicate which contains silica, which in turn reduced the hydroxide ion source in the leachate (Dalton and Campbell, 1978). Similarly, the concentration of Mg^{2+} dropped as the temperature increased. Dalton and Campbell (1978) finally concluded that the ions in the solution decrease as the temperature of the ash increases. Therefore, increasing

the peak temperature during the gasification process will lessen the concentration of ions released to groundwater.

Presented in **Table 2.5** is the comparison of laboratory and field measurements of various contaminants originating from ash. Campbell, Pellizari and Santor (1978) suggested that the comparison in **Table 2.5** will be an effective way to indicate that laboratory simulation can be used to predict the environmental effect of ions released to groundwater during and after the UCG gasification process. From their study they also found out that the major elements that were observed in the laboratory and the field study were Ca^{2+}, SO_4^{2-} and Na^{+}, with other elements found to be in lower concentrations. They also observed low concentrations of the major elements at high gasification temperatures with an increase in Mg^{2+} as the temperature of ashing increased, which was attributed to the precipitation of magnesium hydroxide at high temperatures of leaching. They concluded from their study that there was a good correllation between the elements from the laboratory and field studies.

Table 2.5: Comparison of laboratory and field measurements of numerous pollutants in the ash leachates. (Campbell, Pellizari and Santor, 1978).

Element	Field measurement sampling well in ash bed	Laboratory column leaching experiment		
		1000 °C	1100 °C	1200 °C
Ca^{2+} (ppm)	570	645	630	411
Na^{+} (ppm)	320	207	196	193
K^{+} (ppm)	57	9.7	8.9	7.7
Fe^{3+}(ppm)	0.03	<.5	-	-
Al^{3+} (ppm)	0.22	33	3.9	< .50
Mg^{2+} (ppm)	19	26	35	62
Ba^{2+} (ppm)	0	< 2.0	-	-
SO_4^{2-} (ppm)	2200	2193	2010	1667
pH (-)	10-10.5	11-1O	10.5	7.5-8.0
Conductivity (µmho/cm)	3500	3450	3100	28.5

Edgar *et al*. (1979) conducted a laboratory experiment on lignite coal samples from Texas. Ashes were prepared at 850, 1000, 1250^{o}C in a furnace under air. A batch leaching method was used during the leaching experiment and groundwater collected near Austin was used as lixiviant. The leaching temperatures used during their study were 20^{o}C for 48 hours and 80^{o}C for 72 hours . Results from their study show that calcium and sulfate were the main species in the leachate. These species were released more for ash prepared at 850^{o}C and 1000^{o}C, but were minimal for ash prepared at 1250^{o}C. Leaching temperature also played a significant role during their study with an increase in the concentration of the species from 20^{o}C to 80^{o}C leaching temperatures.

Humenick *et al*. (1983) studied water leaching of lignite coal samples from Texas. The lignite samples were ashed at 850, 1000, and 1250^{o}C in a muffle furnace under air. The samples produced from their study were characterised using XRD and the

major elements found in the ash samples generated from their study were anhydrite, quartz and mullite occurring at 1250^{o}C. Leaching was carried out using column and batch methods. Water from the underground coal site was used as lixiviant during the leaching experiment and various factors were varied during their leaching test, such as solid to liquid ratio and leaching temperatures (20 and 80^{o}C). Leachate samples were obtained after 48 hrs leaching time and the leachate was analysed for the following elements: Ca^{2+}, Mg^{2+}, Na^{+}, K^{+}, and SO_4^{2-}. Results from their experiments show that calcium and sulfate were the major ions released to the groundwater, but the concentration of these species decreased as ashing temperature increased. Also, of all the 34 trace elements tested in the leachate obtained from column method, only aluminium, arsenic, boron, phosphorous, selenium, silicon and zinc were found in th concentration of some significance.

2.9.5.2.2 Field Study

Several field test have been carried out by different authors to monitor the quality of water during and after UCG. A review of the previous tests will be dealt with in this subsection.

A field test conducted by Campbell *et al.* (1978) to monitor the quality of water near a UCG site in Hoe creek I site. In their study, samples of water were collected and the following inorganics were analysed: cyanide, boron, calcium, sulfate, ammonium, magnesium potassium, lithium, iron and bromide. The results obtained from their study show that these inorganics were observed to rise outside the burn cavity by a significant amount over the standard levels.

Mead *et al*. (1980) analysed groundwater samples from Hoe Creek III burn cavity after the UCG process. The resulting water samples were analysed for boron, fluoride, bromide, chloride, lead, lithium, sulfate, manganese, iron, calcium, lead and magnesium. Results from the analyses showed that the inorganic contamination increased after the gasification process.

A study was done by Edgar (1981) to determine the effect of *in situ* gasification of lignite coal from Texas, USA. He found that the quantity of chemical species increased during and after the UCG. The species that were observed to increase included hydrogen sulfide, methane, phenol, light hydrocarbons, oils, tars, ammonia,

carbon dioxide and polynuclear aromatic hydrocarbons. Some inorganic components also increased. These inorganics included: bicarbonate, sodium, sulfate, aluminium, arsenic, barium, boron, iron, zinc, cyanide and hydroxide (Edgar, 1981). While some of the inorganic contaminants were leached out of the burn cavity, the studies also showed that the coal seam acted as a medium for the adsorption of many of the contaminants (Gonow, 1979).

In a field study conducted by Ahern and Frazier (1980) on a UCG Tennessee colony site in Texas, water samples were collected from 3 different sites. Results from the sites showed that there is an increase in array of inorganics contaminate after the gasification process. The following soluble ash constituents were tested and found to increase, as seen in **Table 2.6**: total dissolved solid (TDS), calcium, sodium, sulfate and bicarbonates. More so, some inorganics of important concern were found to be in small amounts, which including aluminium, mercury, manganese, zinc, iron, ammonia, magnesium, selenium, hydroxides and some radioactive elements. Aherns and Frazier, (1980) concluded in their study that the difference in the site results could be attributed to coal and ash composition, natural quality of the water on the site, gasifying temperature and sampling techniques

Table 2.6: Baseline and maximum reported inorganics contaminates in 3 sites (Ahern and Frazier, 1982)

Inorganic constituents	Hoe Creek I		Hanna I		Tenn.Colony	
Cation (mg/l)	Base	Max	Base	Max	Base	Max
Ammonium	0.6	72.0	2.3	15.0	0.7	16.3
Boron	0.09	0.5	0.06	1.5	0.03	2.2
Calcium	36.0	220	15.0	32.0	8.0	94.0
Iron	0.01	37.0	0.04	8.0	0.9	92.0
lead	0.001	0.04	0.03	0.03	Nd	nd
Magnesium	10.0	60.0	9.0	15.0	2.0	22.0
Manganese	-	-	0.06	0.06	0.06	1.3
Zinc	-	-	0.2	0.2	1.8	7.0
Mercury	nd	Nd	0.001	0.001	Nd	nd
Anion (mg/l)						
Cyanide	0.01	290	-	-	nd	0.008
Sulfate	150	1230	400	1600	1	625
Thiocyanate	-	-	-	nd	Nd	0.3
TDS (mg/l)	700	3400	290	1480	290	1480
pH	7.5	6.3	8.3	5.8	8.3	5.8

nd-Not Determined

Organic and inorganic substances discussed in Sections 2.10.4.1 and 2.10.4.2, can transfer from the cavity and pollute surrounding water bodies. Liu *et al*. (2007) proposed that UCG processes introduced pollutants to the groundwater in three different ways:

- Scattering and penetrating of the pyrolysis yield of the coal seam to the surrounding rock layers;
- The discharge and scattering of pollutants with gas yield after gasification process; and
- Movement of the deposit by leaching of the ash leachants into groundwater after gasification process.

Furthermore, it has been proposed that contaminants associated with the UCG process are transported via three routes; namely mechanical dispersion, molecular diffusion and advection (heat, cold or humidity) (Burton et al., 2008; Yang *et al*., 2008; Shackhey *et al*., 2006). Pollutants from the UCG method can alter the water condition, making water sources unhealthy for human and wildlife intake (Bell *et al*., 2011).

Chapter 3: Analytical techniques

3.1 Introduction

In this chapter, the focus is on the different analytical techniques used to characterise the samples in order to determine the chemical, mineralogical and physical changes occurring during ashing. The different leaching methods to study groundwater pollution will be discussed. The experimental procedures will be discussed in Chapter 4.

The different analytical procedures used in this investigation include proximate analysis, ultimate analysis, X-ray fluorescence (XRF), X-ray diffraction (XRD), inductively coupled plasma atomic emission spectroscopy (ICP-OES), CO_2 surface area and porosity analysis, and scanning electron microscopy (SEM).

3.2 Proximate Analysis

Proximate analysis is one of the fundamental methods employed in the analysis of coal samples (Schobert *et al*., 2013; Van Alphen; 2007). Proximate analysis is employed to obtain the moisture, volatile matter, and fixed carbon contents, as well as ash yield of coal (Everson *et al.*, 2008; Everson *et al.*, 2013; Schobert *et al*., 2013). Standard analytical methods are followed during the analysis (Schobert *et al*., 2013).

Moisture content: The moisture content of coal is the water that occurs in the coal at the site, time and under the controlled condition when it is tested. Heating of coal at a temperature slightly beyond the boiling point of water (107 ± 4°C) causes a slight loss of mass from the sample, as water is evaporated from the coal sample (Schobert *et al*., 2013; Van Alphen; 2007). Moisture is an undesirable constituent of coal because it reduces the heating value (water does not burn and it uses heat energy to evaporate) and its mass increases the cost of transportation of coal. Investigators such as Illingworth (1922) and Speight (2005) have identified four different methods of measuring the moisture content in coal. These are a chemical method, an electrical method, a desiccator method and a thermal method.

Volatile matter content: The determined volatile matter percentage comprises the constituents of coal, except for moisture, which is liberated at a high temperature in the absence of oxygen (Schobert *et al*., 2013; Van Alphen; 2007). Volatile matter is

estimated by the mass percentage gaseous compounds driven off in the absence of air at approximately 950 ± 15°C for 7 minutes after a coal sample has been dried to eliminate moisture. The volatile matter gives a suggestion of the quantity of gaseous hydrocarbons that can be generated during the gasification process. Volatile matter content is a vital parameter used in the classification of coal. When reported on an ash or moisture free basis, volatile matter content varies from 2 to 50 weight percentage (wt. %) for different ranks of coal.

Fixed carbon content: The fixed carbon content of coal is the weight percentage of carbon that is left after the removal of ash yield, moisture and the volatile matter contents of the coal. It is usually obtained by difference, by subtracting the percentages of moisture, volatile matter and ash from 100% (Schobert *et al*., 2013; Van Alphen; 2007). The fixed carbon contents of coal, on moisture and ash free basis, range from 50 to about 98 wt. % (Given & Yarzab, 1978). The amount of fixed carbon in coal gives an indication of the rank of the specific coal (Speight, 2005).

Ash yield: Ash yield of coal is the non-combustible composite left after coal is heated. It denotes the bulk mineral matter after carbon, oxygen, sulfur and water (including those from clays) have been released during combustion (Given & Yarzab, 1978). Ash yield analysis is fairly straightforward, as the coal is thoroughly burnt in the air in a muffle furnace at a temperature of 725 ± 25°C and the ash yield is then expressed as a percentage of the original weight. During the process, the organic fraction of the coal is released as carbon dioxide and water vapour, whereas the mineral matter in coal transforms to form the non-combustible inorganic residue. The characteristics and quantity of ash produced are dependent on the composition and amount of the mineral matter present in the original coal (Speight, 2005). It can also give a suggestion of the value of coal. Ash yield may be evaluated on an air-dried basis and on an oven-dried basis (Given & Yarzab, 1978; Schobert *et al*., 2013; Speight, 2005; Van Alphen; 2007).

3.3 Ultimate Analysis

During ultimate analysis, which is one of the more comprehensive analyses of coal samples, various elements present in the coal sample are determined quantitatively.

The mass percentages of carbon, hydrogen, sulfur, oxygen (by difference) and nitrogen are determined by using an ultimate analyser (Schuhmann, 1952; Schobert *et al*., 2013; Van Alphen; 2007).

The amount of carbon in the mineral carbonates and the organic carbon are determined using this method of analysis. The percentage of nitrogen is presumed to be concentrated in the organic fraction. The percentage hydrogen in coal is expected to be related to the water molecules in coal in the form of water of crystallisation (hydrated) and coal structural hydrogen or organically associated hydrogen. The sulfur in coal is present in several forms such as organic sulfur, inorganic sulfides and inorganic sulfates. The inorganic sulfides and sulfates are associated with pyrites and marcasite in coal ash (Speight, 2005). The oxygen content obtained during ultimate analysis is calculated by the difference between 100% and the sum of the percentages of C, N and H (Schuhmann, 1952).

3.4 X-ray fluorescence (XRF)

An XRF spectrometer is used to determine the concentrations of elements such as the trace and major elements in coal and ash (Lu *et al*., 2001). The concentrations of the elements are measured using intensities of specific X-ray peaks. (Loubser and Verryn, 2008; Matjie, 2008). Coal ash contains elements such as Fe, Al, Mg, Mn, V, Ti, Si, Ca, Na, K, P, S, and Cr. These elements are by default reported in their elemental oxide forms; namely, Fe_2O_3, Al_2O_3, MgO, MnO, V_2O_3, TiO_2, SiO_2, CaO, Na_2O, K_2O, P_2O_5, SO_3 and CrO_3 (Loubser and Verryn, 2008; Matjie, 2008). XRF analysis is suitable for quick and precise analysis of major, minor and trace elements in coal samples. **Figure 3.1** shows a typical XRF analysis set-up for solid samples.

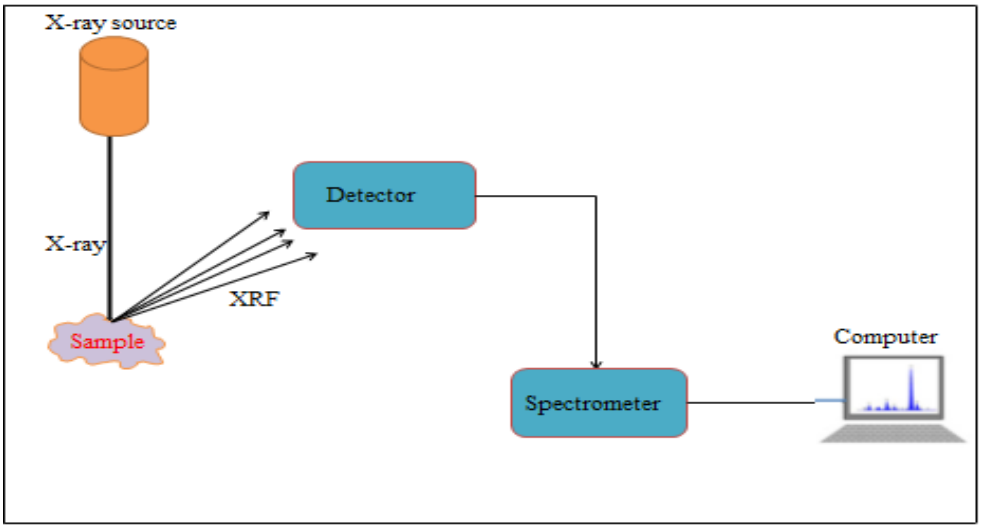

Figure 3.1: A Typical set-up for XRF analysis

X-ray tubes in the generation of secondary radiation are used during XRF analysis. Such X-ray tubes are mostly made of Chromium (Cr) or Tungsten (W) (Huggins, 2002). This method allows for the excitation of electrons produced by X-ray tube. Electrons are generated in this tube by cathodes at specific currents. This current helps in accelerating the electrons to the anode. Oxidations are avoided during this process by placing the cathode and the anode in a vacuum in order to prevent air absorption. As soon as the electrons are targeted to the anode, it generates high heat and band X-rays which are focussed onto the sample. The generated X-ray enhances the sample to radiate X-rays, which are representative of specific elements. A spectrometer is used to measure the intensities of the peaks.

There are some disadvantages to the use of XRF as a primary analytical technique for the determination of trace and minor elements in solid samples. The relative sensitivity of trace and some minor elements is low, thus the precision does not compare well to other elemental analysis methods (Huggins, 2002). Based on the low precision for the determination of trace elements with a standard XRF method, a method known as energy-dispersive XRF (ED-XRF) has been developed for the determination of trace elements. ED-XRF is conducted on coal ash that has been pelletised and bonded using $Li_2B_4O_7$. The ED-XRF analysis precision of inorganic materials relies on the surface, matrix effects, concentration, particle size and the

quality of the standard material. The precision ranges from 2 - 10% (Johnson *et al.*, 1989).

The slagging factor, R_S, the acid to base ratio, *B/A*, and the iron Index, f_i, can be calculated from the results obtained from XRF analysis (Matjie, 2008).
Slagging factor (R_S):

$$R_s = \frac{B}{A} \cdot \%TS \tag{3.1}$$

Where %TS = Percentage total sulfur.

Base/Acid Ratio:

$$\frac{B}{A} = \frac{Fe_2O_3 + Na_2O + CaO + MgO}{SiO_2 + Al_2O_3 + Ti_2} \tag{3.2}$$

Iron Index (*fi*):

$$f_i = \%Fe_2O_3 \cdot \frac{B}{A} \tag{3.3}$$

3.5 X-ray diffraction (XRD)

XRD is a method developed to qualitatively and quantitatively determine the chemical composition of crystalline and amorphous phases of powdered solid samples, including coals, chars, and ashes. This technique helps in measuring the minerals, distribution of minerals and amorphous phases in coal ash and slag (Gupta, 2007; Maity and Mukherjee, 2005; Matjie, 2008; Quanta 250 manual, 2012; Ward *et al*., 2004). The composition of coal ash is mainly made up of non-crystalline or amorphous material (aluminosilicates), crystalline material (quartz, mullite, anorthite) and small amounts of unburnt carbon, which in some cases are not visible due to the operating condition used during the heating process. With the XRD technique, different phases of minerals, based on their crystallographic properties, can be measured (Vassilev and Tascon 2003; Ward, 2002). X-ray diffraction can be used to determine the mineral component of coal and ash but does not predict the morphological features (size, association) of the minerals and particle features (Van Alphen; 2007).

Several researchers have developed different analytical methods to quantify the amounts of minerals in coal and ash samples using XRD (Rao and Gluskoter, 1973; Ward, 1977, 1978, 1989; Russell and Rimmer, 1979; Renton, 1986).

During standard XRD analysis, the sample is crushed to a fine particle size ranging from 75 – 212 µm. When the X-ray passes through the samples, the radiation from the X-ray interacts with the atoms in the samples and scatters. Constructive and destructive interferences occur when X-rays are dispersed in an orderly environment. This occurs when the proximity between the scattering points is the same order of magnitude as the frequency or wavelength of the radiation. The constructive interference is known as diffraction. The structural and composition parameters are evaluated from the intensities of the scattered X-rays as a function of the incident and scattered angles, the wavelength and polarisation.

When a beam of X-rays passes through the sample, it is reflected from all possible interplanar spacing positions to fulfil Bragg's condition for reflection. The reflected beam is identified, and a diffraction pattern is achieved. As soon as the X-ray beam strikes the sample surface at an angle, a certain portion of the beam is scattered by the atoms at the surface of the sample. The percentage of the beam that was unable to scatter enters into the next segment of the atoms where, again, some is scattered. Incident rays by atoms on the surface and also atoms deeper into the samples continue until all the rays have been scattered. The diffraction is established based on the position of the diffraction lines with respect to the diffraction angles, θ or 2θ (Skoog *et al.,* 1998). Diffraction angles are obtained by the spacing between specific numbers of planes using the empirical Bragg's equation (Equation 3.4). A schematic presentation of the XRD technique is shown in **Figure 3.2**.

$$n\lambda = 2dSin2\theta, \qquad (3.4)$$

where λ is the wavelength (*Å*) of radiation used, d is the interplanar spacing between crystallographic planes (*Å*), 2θ is the diffraction angle (rad), and constructive interference occurs when n is an integer.

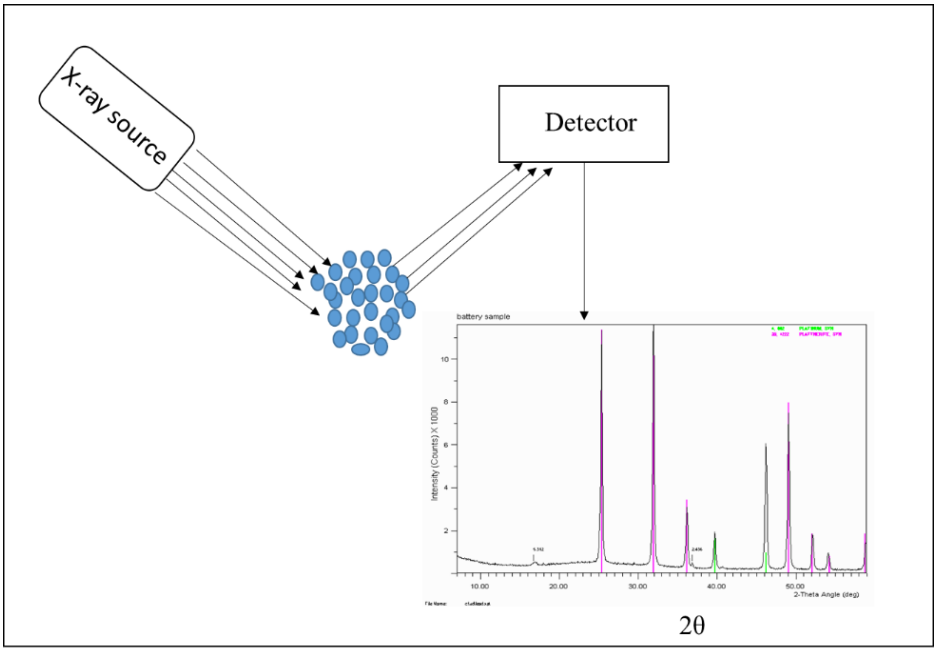

Figure 3.2: A schematic presentation of the XRD technique

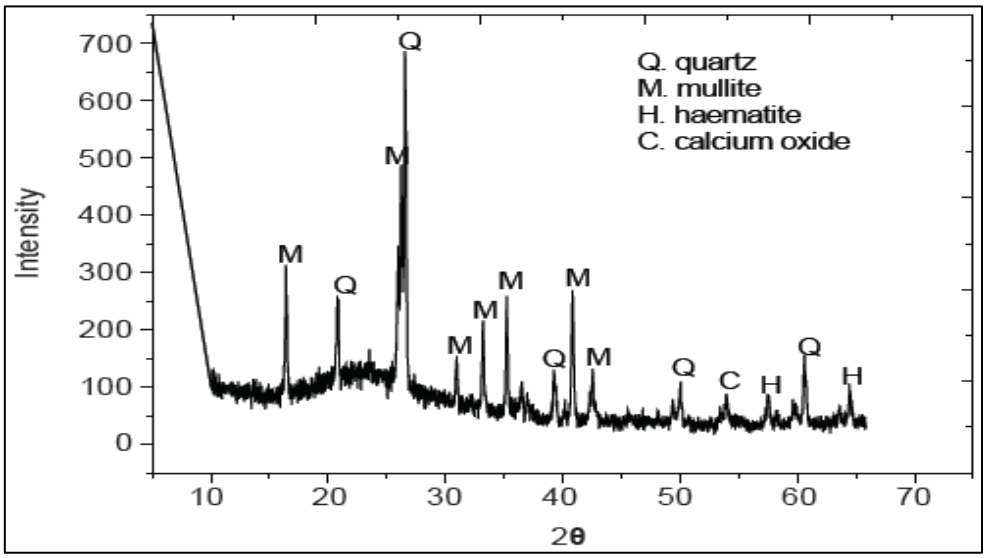

Figure 3.3: Diffraction profile (diffractogram) of coal fly ash with peaks indicating various minerals (Musapatika *et al*., 2010).

A set of peaks can be used in the identification of minerals. Peaks are assigned based on their intensities, with the crystalline mineral having the strongest peak position with the best fit. Weaker peaks confirm the presence of specific minerals. The smaller peaks are resolved simultaneously with the larger peaks and are

allocated to particular minerals (Moore and Reynolds, 1997). A typical XRD diffractogram of coal fly ash is presented in **Figure 3.3**. The Figure shows peaks for quartz (Q), mullite (M), haematite (H) and calcite (C).

Peak overlapping is one of the major problems in using quantitative XRD analysis. Such peak overlaps make it difficult for the traditional reference intensity ratio methods of quantification to be used. However, such errors can be reduced by using the Rietveld analysis method, thereby allowing for quantification of complex multi-phase systems.

3.6. Inductively coupled plasma atomic emission spectroscopy (ICP-OES)

Inductively coupled plasma optical emission spectroscopy (ICP-OES) fits into the atomic emission spectroscopy (AES) family of elemental analysis methods. ICP-OES has an advantage over atomic emission spectrometry (AES) because ICP-OES provides an improvement with regard to the quality of the ICP excitation source and many samples can be analysed at the same time, even though both of the methods use the same technique (Querol *et al*., 1996; Querol *et al*., 2001). ICP-OES may be employed to determine the concentration of over 70 elements. Since all elements are expected to release light at the same time, ICP-OES may be employed to determine the amounts of numerous elements in one step, increasing the analysis throughput (Skoog *et al*., 2007). This usefulness leads to the collective use of ICP-OES in environmental, biological, geological, and agricultural laboratories.

An ICP-OES instrument is employed to measure or quantify concentrations of elements present in leachate samples and in solids when digested with an acid. The fundamental characteristic of this process is that each element emits energy at wavelengths specific to its chemical properties. The wavelengths of the inorganic compounds that will be used for this study include: 396.1 nm (Al), 189.0 nm (As), 455.4 nm (Ba), 393.3 nm (Ca), 214.4 nm (Cd), 228.6 nm (Co), 283.5 nm (Cr), 324.7 nm (Cu), 259.9 nm (Fe), 279.5 nm (K), 769.96 nm; (Na), 589.92 nm, (Mg), 221.6 nm (Ni), 220.3 nm (Pb), and 213.8 nm (Zn) (Gomez *et al*.,2007; Huang and Schulte, 1985; Moreno *et al*., 2008).

The ICP-OES method of analysis is one of the most useful instruments as it uses a single wavelength for a particular element. The intensity of the rays generated at a

specific wavelength is related to the concentration of that element in the investigated sample. However, some parameters are needed to evaluate the concentration intensity. This can be achieved through the calibration of the sample with a known standard. (Karayigit *et al.,* 2001; Marrero *et al.,* 2007).

ICP-OES consists of an optical emission spectrometer with an atomiser that helps to scatter the solution before analysis. A plasma torch is used to excite a portion of the ions in the solution to excited electronic states. The steady energy state is achieved after the electrons in the atoms and/or ions in the excited states are relaxed to lower energy levels. Ultraviolet and visible line radiation are released, which represents the atoms and ions from which they were emitted. ICP-OES argon plasma, a hot gas with a temperature of 10 000 K, is formed in a magnetic field. The sample is usually dissolved in an organic liquid or an aqueous solution and then conveyed to the plasma by a high-velocity atomiser. The atomiser also helps in the disintegration of the liquid into smaller drops of many shapes prior to the plasma exposure. The residence time of samples in the plasma is approximately two minutes. A temperature of 5 500 K – 8 000 K is observed during this residence time. The heat generated during this period is about two to three times higher than that produced by combustion flames. As soon as the atom cools down at the observation point, radiation is emitted, which can be detected by the spectrometer. The spectrometer processes the intensities and wavelengths of radiation released by the analyte or the compound of interest. **Figure 3.4** gives a schematic representation of ICP-OES technique.

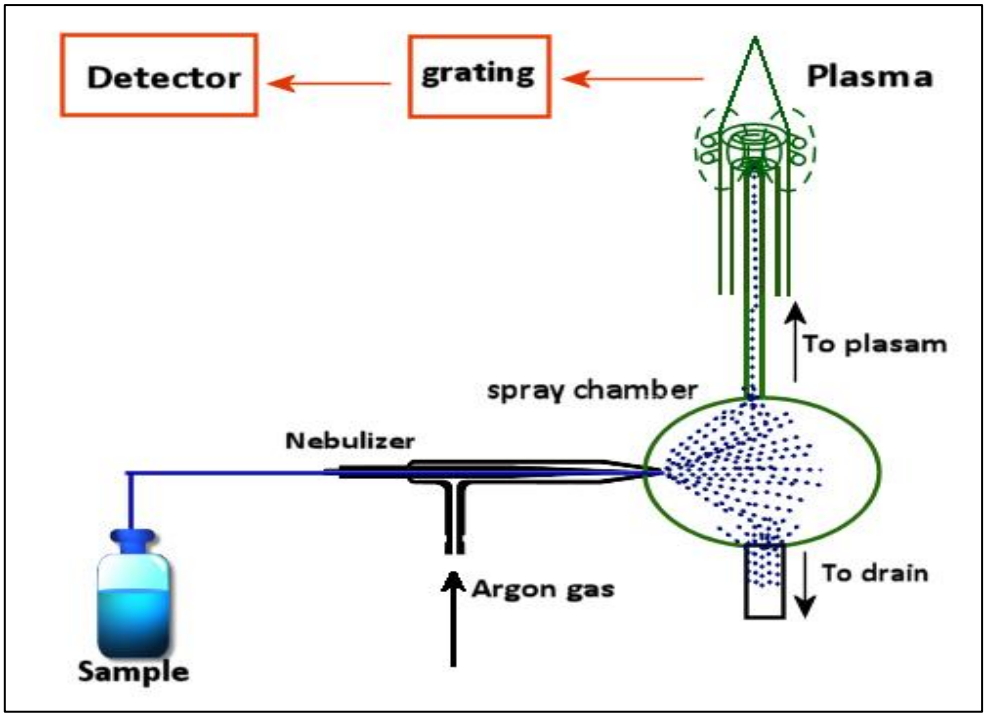

Figure 3.4: A schematic representation of ICP-OES technique

The precision of the technique is typically quoted to be ± 30% due to the interference of some elements with the detection of others (Huggins, 2002). Concentration detection as low as 1-10 parts per billion (ppb) may be identified for most elements (Skoog *et al*. 2007). Furthermore, the sensitivity of the technique is also largely dependent on the detection of the emitted radiation by the spectrophotometer. For these reasons, the technique is not appropriate for trace element identification, which is important in the characterisation of potentially hazardous leachate from coals.

3.7. Ash fusion temperature (AFT)

The standard ash fusion temperature (AFT) analysis is a test that gives an indication of the slagging and fouling characteristics of ashes. The AFT test can provide useful data that help in determining whether the specific coal is suitable for the gasification and/or combustion process, and information from AFT analysis can aid in deciding on the best gasification and combustion technique (Gupta, 2007). Ash fusion temperature of a non-mineral and mineral component of ash has an influence on the liquid formation during mineral transformation at high temperatures (Benson, 1987;

Ward, 1984). AFT has been widely acclaimed by different researchers as the most recognised method and is generally used to determine the slagging characteristics of coal.

The AFT test involves the loading of the ash or coal sample in a cone or a pyramid and placing the sample in a furnace. The sample in the furnace is heated from 1000°C to 1600°C with a heating rate of 5 -10°C /min (Wall *et al*., 1998, Wall *et al*., 1999). During the AFT test, four different temperatures are observed (Gupta *et al*, 1998; Seggiapi, 1999; Van Dyk *et al*, 2005; Wall *et al*., 1998, 1999). The initial or deformation temperature (IDT) is the stage at which the ash starts to soften and get sticky at the tip of the cone or pyramid. The softening temperature (ST) is the temperature at which the height and the width of the pyramid and the cone are equal. The hemispherical temperature is the temperature where the height of the cone is equal to half of the cone width. The fluid or flow temperature is the temperature at which the ash flows freely. The height of the cone is 1.5 mm. Characteristic shapes of the solid material during ash fusion tests are shown in **Figure 3.5**.

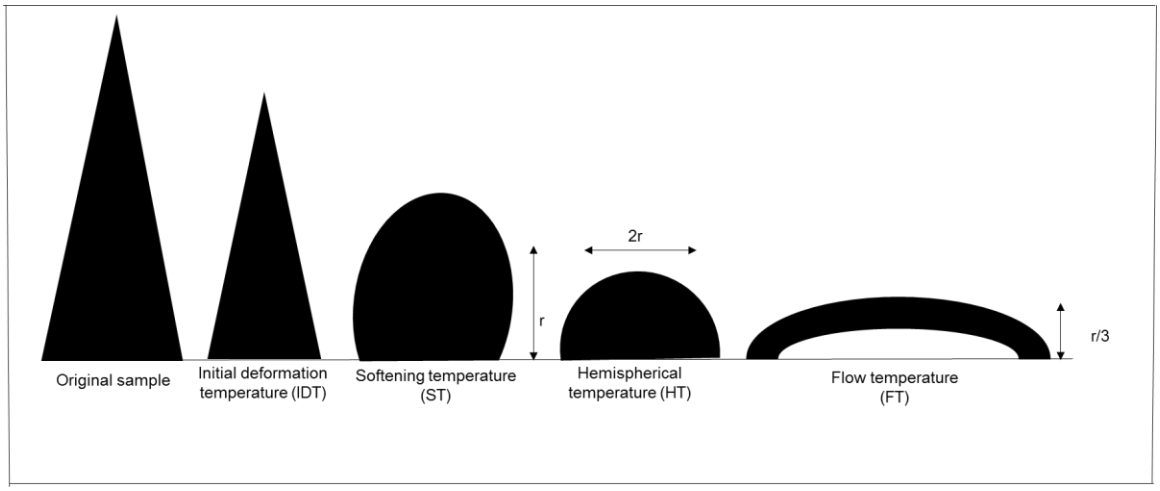

Figure 3.5: Characteristic shapes of the solid material during an ash fusion test

However, the method has its setbacks as it is a very subjective experimental procedure depending on the analyst's observations (Gupta, 2007; Van Dyk and Waanders, 2007; Van Dyk *et al.,* 2009; Wall *et al*., 1999). One of the disadvantages is that this subjective method is not as reproducible as some other methods. Kahraman *et al.* (1998) analysed samples of ceramic tiles and managed a repeatability of ± 10°C. They found that the difference in AFT are between 30°C and 50°C when the same instrument and operators were used, and between 80°C and 150°C when different operators and different instruments were used. Other investigators have reported a variation in the reproducibility of ATF data from 20°C to 100°C (Özbayoğlu & Özbayoğlu, 2006). Gupta (2007) attempted to address the major causes of variation in the reproducibility of results from AFT and attributed this also to the low heating rate used for the analysis, which impacts on the ash composition.

3.8 Scanning electron microscopy (SEM)

The scanning electron microscope (SEM-EDS) is an instrument that can be used on smooth or fragmented coal and ash surfaces to measure the mineral composition of the coal and ash (Creelman and Ward, 1996; Ward and French, 2004). It is a physical characterisation method used to study the morphology of a solid substance. SEM uses a focussed beam of high-energy electrons to generate a variety of signals at the surface of the sample. The signals resulting from the electron sample interface give information on the sample properties, including external morphology (texture), chemical constituents, crystalline arrangement and positioning of materials that make up the coal and ash sample (FEI, 2012).

SEM-EDS analysis can be performed on a Quanta 250 field emission gun (FEG) scanning electron microscope with environmental scanning electron microscope (ESEM) capabilities. This analytical tool can characterise conductive and non-conductive samples with an optional beam deceleration mode. The Quanta series can produce a fast and accurate analysis due to stable high beam currents (up to 2 µA). The SEM is coupled with an energy dispersive X-ray spectrometer (EDS), diffracted back-scattered electron-, and backscattered electron (BSE) accessories.

The SEM method of analysis firstly involves the preparation of the carbon coating of samples and subsquent placeing of the samples in a vacuum inside a chamber. Since the SEM equipment operates with electrons, solid samples are coated with carbon to allow conduction of electricity. After the coating of the samples, they are placed in a vacuum chamber for 30 min or more. As soon as air is pumped out of the column, an electron gun emits electrons of high energy. The beams emitted by the electron gun move down through magnetic lenses that are set up to focus on the sample. The scanning coil located at the bottom of the column helps in moving the focussed beam to the specimen. Once the focussed beam reaches the sample, secondary electrons are produced from the surface of the sample. The secondary detector counts the number of electrons and transfers the signals to the amplifiers. The screen displays images formed from the secondary electrons released from the sample. The schematic description of the SEM method of analysis is shown in **Figure 3.6**

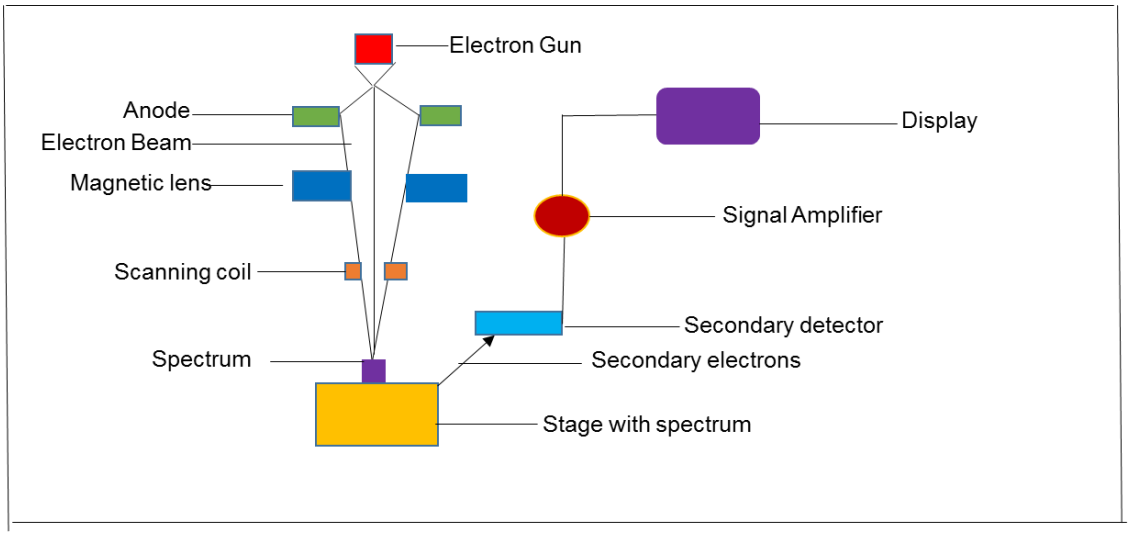

Figure 3.6: Schematic diagram of a typical SEM

3.9 CO_2 surface area (BET)

The surface area of ash and coal are evaluated from the physical adsorption data of an adsorbate gas (CO_2 or N_2) on the surface of the solid adsorbent (coal or ash). Adsorption of gas molecules occurs onto the solid's surfaces, which include the pore networks. (Gregg and Sing, 1967). Physical properties such as porosity and surface area of the sample are helpful parameters to be measured, as they are useful in

determining the performance and behaviour of solid materials (Gregg and Sing, 1982).

The adsorbent gas normally used to measure the coal or ash surface area is CO_2, due to the small molecular weight of the gas and its high average kinetic energy (Walker *et al*., 1988). Van Niekerk *et al*. (2008) compared the adsorption and desorption of CO_2 and N_2 on bituminous coals. They found that adsorption and desorption of CO_2 have a greater activation energy of adsorption in comparison to N_2, which could be attributed to the fact that CO_2 diffuses faster through the coal pore network at a lower temperature (Van Niekerk *et al*., 2008). CO_2 adsorption usually gives larger surface areas than nitrogen adsorption (Walker *et al*., 1988; Larsen *et al*., 1995). The surface area of samples is more commonly determined using the Dubinin-Radushkevich (D-R) and Brunauer-Emmet-Teller (BET) methods at a relative pressure range of 0.02 to 0.30 (Nandi and Walker, 1964; Hurt *et al*., 1991; Malumbazo, 2011).

3.10 ATR-FTIR Analysis

FTIR has been used by various authors to qualitatively identify the organic and inorganic functional groups in coal and ash materials (Criado *et al*., 2005; Fernandez-Jimenez and Palomo, 2005; Lee and Van Deventer, 2002a,b; Lucia *et al*., 2014; Swanepoel and Strydom, 2002; Sembiring *et al*., 2014). FTIR is a qualitative method of analysing spectra and assigning peaks obtained from coal and ash samples, based on methods described by previous investigators (Alessio *et al*., 2000; Beran *et al*., 2001; Criado *et al*., 2005; Fernandez-Jimenez and Palomo, 2005a; Lee and van Deventer, 2002a, b; Mukherjie and Srivastava, 2006; Sembiring *et al*., 2014; Swanepoel and Strydom, 2002; Suraj *et al*., 2007)

3.11 IC Method

Ion chromatography (otherwise known as ion exchange chromatography) is an analytical technique which helps in the separation of ions and polar molecules based on their affinity to the ion exchanger. Ion-exchange chromatography retains analyte molecules on the column based on ionic interactions. The surface of the stationary phase displays ionic functional groups (R-X) that interact with analyte ions of opposite charge. This type of chromatographic method is further subdivided into

cation exchange chromatography and anion-exchange chromatography. The ionic compound consisting of the cationic species M+ and the anionic species B- can be retained by the stationary phase.

Cation exchange chromatography retains positively charged cations because the stationary phase displays a negatively charged functional group:

$$R{-}X{-}C{+} + M{+}B{-} \leftrightarrow R{-}X{-}M{+} + C{+} + B{-} \quad (3.1)$$

Anion exchange chromatography retains anions using positively charged functional group:

$$R{-}X{+}A{-} + M{+}B{-} \leftrightarrow R{-}X{+}B{-} + M{+} + A{-} \quad (3.2)$$

The ion strength of either C+ or A- in the mobile phase can be adjusted to shift the equilibrium position, thus retention time (Haddad and Jackson, 1990).

3.12 ICP-MS Method

An Inductively coupled plasma mass spectrometry (ICP-MS) system comprises four main parts, namely; the sample introduction system, plasma region, interface and mass spectrometer region (see **Figure 3.7**).

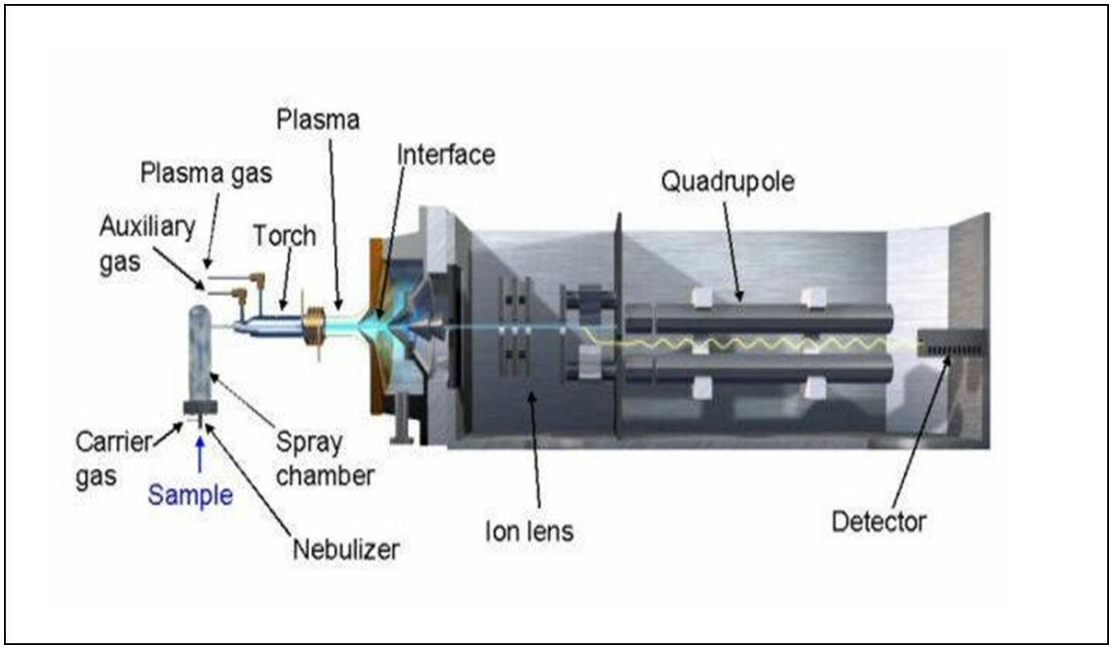

Figure 3.7: Schematic representation of a quadrupole ICP – MS set up (Source: Wolf, 2005)

The high temperature ICP aids for the alteration of the atoms of the elements in the sample to ions (Wolf, 2005). These ions are then transmitted to the mass spectrometer via the interface cones. At the interface region, the ions, travelling in the presence of argon sample stream at atmospheric pressure (1 – 2 torr), gets transferred to the mass spectrometer which is maintained at low pressure (10-5 torr). This is achieved through the combination of the sampler and skimmer cones which creates an intermediate vacuum region. The main purpose of the cones is to sample the centre portion of the ion beam coming from the ICP torch. Also, due to the small diameters of the orifices in the sampler and skimmer cones, ICP-MS has some restrictions as to the amount of total dissolved solids in the samples (ideally less than 0.2 % total dissolved solids is recommended). A shadow stop blocks the photons coming from the ICP torch so as to prevent the intense light from reaching the mass spectrometer. The ions from the ICP source are then focused by the electrostatic lenses in the system. Once the ions enter the mass spectrometer, they are separated by their mass-to-charge ratio (Wolf, 2005). In this work, a quadrupole mass spectrometer instrument was used because they are reasonably priced and also provide good resolution (up to 1 atomic mass unit). Other types of mass spectrometer that could be interfaced to the ICP include the magnetic double sector, time of flight, ion cyclotron resonance analyzers, these are however expensive and mostly used for specialized applications such as isotope analysis which were not required in this work. Once the ions have been separated by their mass-to-charge ratio, they must then be detected or counted by a suitable detector such as a discrete dynode detector which operates either in a pulse – counting or analog mode (Wolf, 2005).

Internal standards are widely used in ICP-MS analyses to correct for variations in the instrument response as the analysis proceeds (drift) and to calculate the analyte concentrations of the samples. Accurate correction for non-spectral interferences is also possible using an internal standard with mass number close to that of the analyte element(s). The use of an internal standard with mass number close to that of the analyte improves the precision of data obtained from ICP-MS. When a number of elements over a considerable mass range are to be determined, several internal standards have to be used.

ICP-MS can be used to measure most of the elements in the periodic table and to determine the concentration up to part per billion down to part per trillion. ICP-MS method of analysis has advantage when compared to other elemental analysis method such as graphite furnace atomic absorption spectroscopy (GFAAS). This advantages include its superior detection capability, higher sample throughput, and the ability to carry out isotopic analysis (Wolf, 2005).

3.13 Methods to investigate water-leaching of coal

Leaching is a process used to remove soluble species from a solid. The method of leaching can vary with the following factors: the mass and particle size of the sample, the volume of the leachate (lixiviant) solution, time, delivery method and temperature (Van der Sloot *et al*., 1997). Most leaching processes are conducted at ambient temperature, but consdiering the nature of the coal seam and cavity during UCG process this current study consider leaching at a slightly higher leaching temperature (50^{o}C).

Various properties of ash (physical and chemical) influence leaching behaviours. The physical properties include particle size, shape, surface area exposed to leaching, the porosity of the medium, flow rate of the leaching lixiviant, temperature during leaching, physical properties of the leaching lixiviant, and the heterogeneity of the ash material (Van der Sloot *et al*., 1997). The chemical properties of ash that influence the leaching performance include: the pH of the ash, the pH of the lixiviant used in complexation with inorganic species, equilibrium-based reactions (relatively quick chemical dissolution reactions), kinetic-based reactions (relatively slow desorption reactions), and solubility/desorption characteristics of constituents (Van der Sloot *et al*., 1997). The internal pore structure, the ratio of the particle area to the occupied volume by the particles and the size of the particle in the ash all regulate the surface at which the dissolution from solid to liquid can occur during the leaching process, as a function of the surface exposed to the leaching lixiviant (Van der Sloot *et al*., 1997).

3.13.1 Batch leaching procedure

The batch leaching procedure is a technique in which a sample is positioned in a precise volume of the leachate (lixiviant) solution for a given period (Pendowski, 2003). In most cases, the method involves agitation or stirring to ensure that the sample and the solution are in equilibrium or homogeneous. After the leaching is completed, the leachate is filtered and prepared for analysis. The batch leaching process is schematically described in **Figure 3.8**.

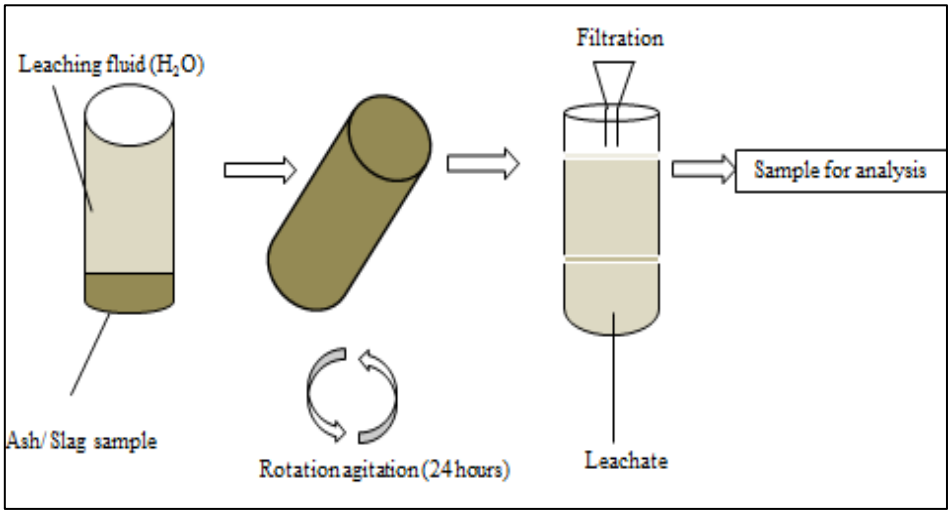

Figure 3.8: Diagram of the batch leaching procedure (Pendowski, 2003)

3.13.2 Column leaching method

Column leaching experiments are aimed to mimic the movement of groundwater through a porous bed of coarse solids (Van der Sloot *et al*., 1997). The leachate solution may flow in different directions, either down or up. The flow through the substrate may be continuous or interrupted. The flow rate may be controlled. During continuous leaching, the ash is exposed uniformly to the leachate solution. Factors that can affect the results of column experiments include precipitation or sorption within the column.

The leachate solutions normally used during column experiments are as follows: 0.009 M acetic acid ($C_2H_4O_2$) solution; 0.5 M sulfuric acid (H_2SO_4); 2.0 M nitric acid (HNO_3); 0.05 M sodium carbonate ($NaCO_3$); 1.0 M sodium hydroxide (NaOH), and deionised water (neutral) (Kim, 2003; Kim, 2002; Kim and Kazonich, 2004; Kim, 2006). Saturated and unsaturated conditions can be used to study a column leaching test. Unsaturated conditions are irregular additions of a specific volume of leachate

solution at the top of the column (Kim, 2002). This unsaturated condition provides even circulation of the fluid and ensures a continual lixiviant movement through the unsaturated column. Saturated columns are attained by a continuous lixiviant flux, letting the solution stay in the upper section of the column for a particular residence time (Kim, 2002). Some of the experimental variables that can be obtained during the column experiments include leachate flow rate, duration of the experiment and leachate collection time (Van der Sloot *et al*., 1997). **Figure 3.9** shows a simple schematic representation of a column leaching setup.

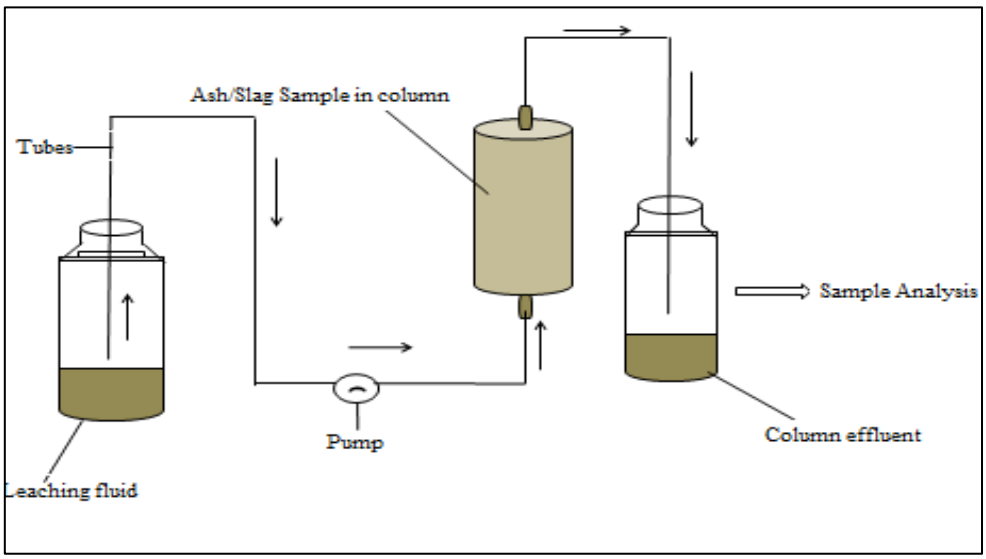

Figure 3.9: Diagram of the Column Leaching Procedure (Pendowski, 2003)

3.13.3 Approaches to leaching investigations

Pendowski, (2003) described three approaches to leaching methods . These include regulatory methods, standard methods and research methods.

Regulatory methods are those enacted and accepted by a regulator to develop specific knowledge for submission as legal content.

Standard methods are those adopted by standard organisations, such as the Standard Test Method for Shake Extraction of Solid Waste with Water (ASTM) or the International Organization for Standardization (ISO). These procedures include the

Leachate Extraction Procedure (LEP) and the Toxicity Characteristic Leaching Procedure (TCLP), etc., for specific sets of conditions and for specific materials.

Research methods are those developed by researchers for a particular purpose.

Chapter 4: Experimental methods

4.1 Introduction

The experimental procedures and conditions used in this study will be discussed in this chapter. The sample preparation and the instrumental specifications for the different analytical techniques used will be presented in detail. The analytical method for the surface area and porosity analysie will be given in detail. Finally, the leaching procedures that were used in this study will be discussed.

4.2 The Origin of the coal sample

The raw coal, floor and roof samples used in this study were supplied by Africary and originated from the Theunissen underground coal gasification site in Free State Province, South Africa. The samples were received in particle sizes ranging from fine -75 µm to 10 mm.

4.3 Sample preparation

Mechanical size reduction was used to decrease the particle size of the raw coal, floor and roof samples to the required sizes needed for ashing and analyses. Raw coal, floor and roof samples were pre-ground to less than 3 mm using a jaw crusher (Samuel Osborne (SA) LTD, Model: 66YROLL) and a grinder mill (Usborn Coal equipment). The laboratory ball mill with stainless steel balls was used to grind all samples to I mm particle size. The 1 mm particle size was used in order to prevent the breakdown of mineral-mineral interaction in the coal sample. Before using the steel balls, they were cleaned with compressed air in order to avoid contamination with the previously crushed sample. Further reduction of the <1 mm size particles was performed using a Fritsch P-14 rotary mill with a speed of 600 rpm for 30 minutes and a 280x230 ceramic macro crusher (Model number: 46-126) containing 10 mm ceramic balls.

After crushing of the samples, individual samples (raw coal, floor and roof) were mixed together by mass in the ratio: 80% raw coal, 15% roof and 5% floor. The mixed samples were further homogenised using the ball mill without the stainless steel balls. The milling process was repeated until 40 kg of the blended sample that

was used for ashing at different temperatures was collected. The blended coal sample was oven dried to prevent it from oxidising before the heat treatment.

4.4 Ash Preparation

40 kg of the less than 1 mm coal blend sample was submitted to Mintek for the ashing process. These samples were initially mixed to form a single composite sample. From the composite sample, seven sub-samples, weighing 5 kg each, were taken and subjected to ashing experiments. Coal ashing involved firstly placing the sample, using a sample feeding scoop, into the middle zone of the kiln, i.e. the hot zone of the kiln furnace. The photograph of the rotary kiln set-up including the hearth furnace is shown in **Figure 4.1**. The test was conducted under a flow of air to facilitate combustion of the organic component and removal of volatiles. The two ends of the kiln were left open to allow for easy removal of the generated volatiles and gases, which were extracted by an off-gas extraction unit.

Figure 4.1: Open furnace showing heating elements (left), two kilns used for the ashing test with open front and back end (right)

The rotary kiln furnace temperature was initially set to 1000°C, as all 7 batches of the sample were initially subjected to ashing at 1000°C. At a temperature of about 600°C, the sample combusted into a big flame, causing the temperature to increase drastically. Upon reaching 1000^{o}C, the furnace temperature was kept isothermal until all emissions had ceased, after a residence time of 3 hours, before being cooled

down to room temperature. Once the ash was at ambient temperature, it was taken out of the kiln and the mass recorded. The respective mass losses resulting from the ashing process at 1000°C for the 7 batches of the sample, including the mass of the ashes, are presented in **Table 4.1**. The same ashing conditions were applied to all 7 sample batches.

Table 4.1: Mass % loss after ashing at 1000°C

Batch	1	2	3	4	5	6	7
Mass loss (%)	62.03	59.92	58.43	65.17	63.18	53.21	59.99
Ash mass (g)	1898.5	2004.1	2078	1741.3	1841.2	2339.4	1975.4
Initial mass of coal sample (g)	5000	5000	5000	5000	5000	5000	5000

The ash products, excluding ash obtained from Batch 1, were blended to form a composite homogenous ash sample. The Batch 1 product was not blended because it had flakes that needed further characterisation. The flakes were a result of contamination from the furnace and the Batch 1 sample was thus excluded from further research. The newly combined bulk sample was split into five sub-samples. The first sub-sample was kept as a test sample from 1000°C ashing and the other four sub-samples were reserved for testing at respective temperatures of 1100°C, 1200°C, 1300°C and 1400°C in a muffle furnace, using fire clay trays as sample holders, as shown in **Figure 4.2**. Each sub-sample was weighed into a fire clay tray and heated at the predetermined temperature for 3 hours before being cooled down to ambient temperature.

The sample prepared at 1300°C sintered and caused the material to stick onto the fire clay tray. Consequently, the fire clay tray was broken to retrieve the sample. Consequently, the planned test at 1400°C was abandoned. The percentage mass changes for the respective ashes at the three different temperatures relative to the test sample at 1000°C are summarised in **Table 4.2**.

Figure 4.2: Fireclay trays used during ashing at 1100, 1200, and 1300°C.

Table 4.2: Percent mass changes after further heating of the ash up to 1300°C

Test	Temperature°C	Mass loss (%)
1	1100	0.74
2	1200	0.85
3	1300	1.31

The individual ash and sintered samples after the ashing process at the various temperatures used for this study are shown as a pictorial representation in **Figure 4.3**.

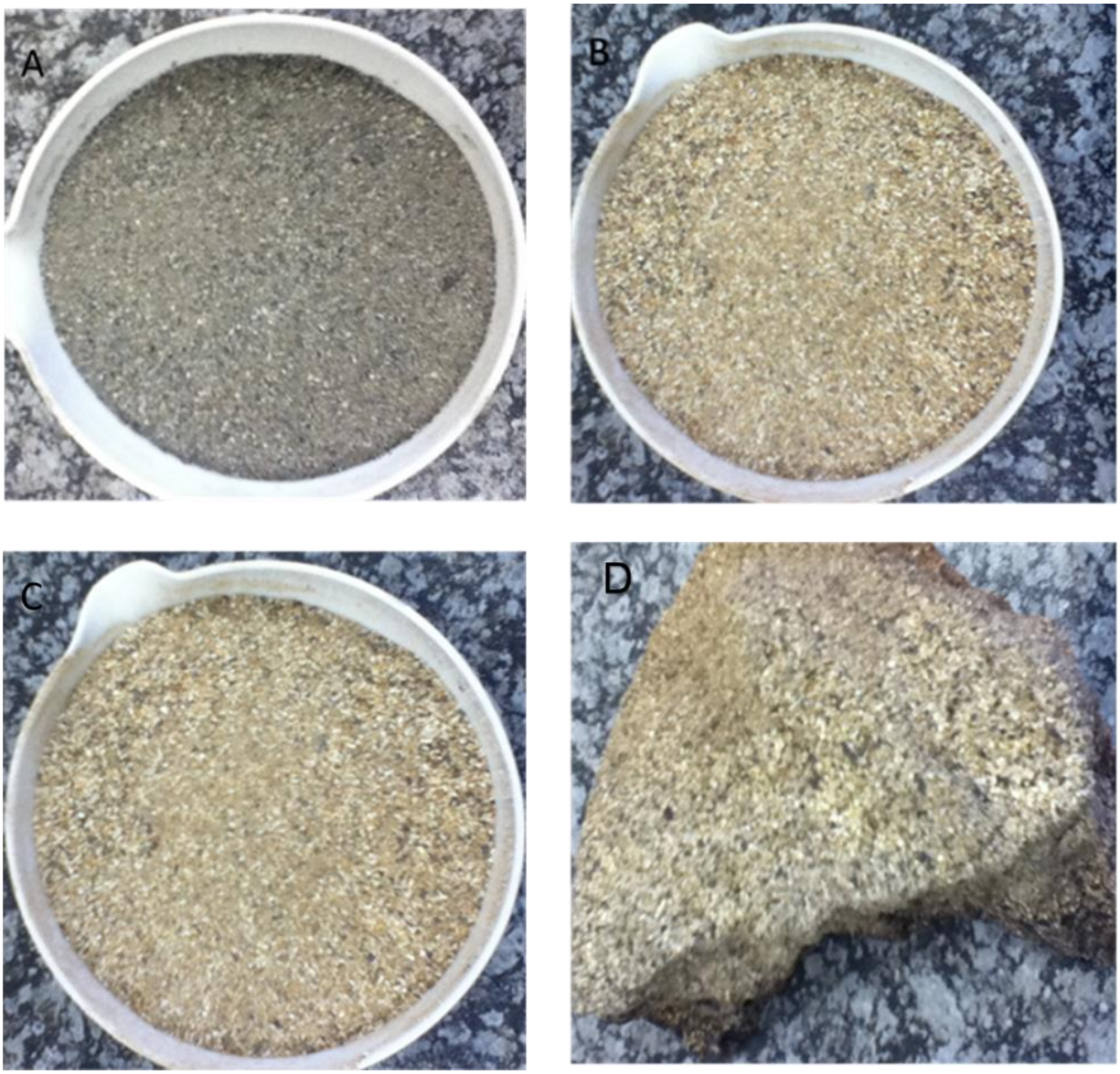

Figure 4.3: Pictures of the ash samples after the ashing process. A = Ash 1000°C, B = Ash 1100°C, C = Ash 1200°C and D = sintered Ash 1300°C

The 1 mm sieve was used to screen the 1000°C ash sample. Particles larger than 1 mm were collected and crushed further until 100% passed through the 1 mm sieve. The crushed ash particles were combined with the <1 mm ash particles obtained during the initial screening to produce a final representative 1000°C ash sample. This final material was used for the leaching steps. This procedure was repeated for the remaining 3 samples, except for the 1300°C sample, where sintering had been observed.The sintered ash particle was initially crushed in a jaw crusher to break down the particles to ± 2 mm, before using the ball mill to crush them to <1 mm particle sizes. After this, the final sample crushing and preparation procedure was applied to the 1300°C ash sample.

Thus, the following four ash samples were prepared for the leaching tests:

- ✓ <1 mm ash particles produced at 1000°C (named Ash 1000°C)
- ✓ <1 mm ash particles produced at 1100°C (Ash 1100°C)
- ✓ <1 mm ash particles produced at 1200°C (Ash 1200°C)
- ✓ <1 mm crushed sintered ash particles produced at 1300°C (Sintered 1300°C).

100 g of the representative samples from each of the different temperature ash samples was further pulverised to <75 µm with the rotary mill. A milling time of 30 minutes was used to ensure that a 100% passing through the <75 µm sieve was obtained. The same milling time was used to avoid variation in the particle size of the representative sample. The pulverised ash samples were used for various characterisation analyses including proximate, ultimate and total sulfur analyses; XRD and XRF analyses; SEM; surface area and porosity analyses; particle size distribution (PSD) analysis; Fourier transform infrared spectroscopy (ATR-FTIR), inductive coupled plasma (ICP) analysis; and ion chromatography (IC).

The contaminated ash sample that was produced during the ashing of the first batch of coal blend was screened to recover the flakes for XRD and XRF analyses. This contaminated ash sample was not subjected to the leaching experiments.

4.5 Proximate and ultimate analyses

The proximate and ultimate analyses of the raw coal, roof, floor, blended coal and the ash samples at various temperatures used for the study were conducted at the Coal laboratory of the North West University, Potchefstroom Campus. The analyses were essential for this study to evaluate the influence of water leaching on the reduction of the mineral matter contents in the coal sample. The proximate analysis was employed to quantify the percentages of fixed carbon (FC), volatile matter (VM), moisture and ash yield in the blended coal, ash and slag. The ultimate analysis was done to evaluate and quantify the elemental constituents, i.e. carbon, hydrogen, nitrogen, oxygen and sulfur (CHNOS) contents in the coal. The elemental oxygen content of the coal was determined by difference. **Table 4.3** present the analytical methods and standards that were used for the proximate and ultimate analyses.

Table 4.3: Analytical methods used for the chemical analyses

Items	Standard method
Sample preparation	SABS 0135: Part 1 &2. (1997)
Proximate analysis (wt.%, adb)[a]	
Inherent moisture content	SABS 925
Ash content	SABS ISO 1171 (1997)
Volatile matter content	SABS ISO 562 (1998)
Fixed carbon content	By Difference
Ultimate analysis (wt.%, dmmfb)[b]	
Carbon	ISO 12902
Hydrogen	ISO 12902
Nitrogen	ISO 12902
Oxygen	By Difference

[a]- weight percent, air-dried basis; [b]- weight percent, dry mineral matter free basis

4.6 X-ray fluorescence (XRF) analysis

For the XRF analysis, the samples were prepared by first drying at 105°C for ~3 hours to determine the loss of moisture (moisture content). High-temperature ashing (HTA) was initiated on the samples in an oven at 1000°C in air until completely ashed, in order to determine the loss on ignition (LOI). This was followed by a 15 min borate fusion (0.7 g sample + 6 g flux) using a Claisse® 66:33 LiT:LiM (Lithium Tetraborate:Lithium Metaborate) flux with a LiI (Lithium Iodide) releasing agent in a platinum crucible. The XRF analysis was performed using a PANalytical Epsilon 3 XL ED-XRF spectrometer, prepared with a 50 kV Ag-anode X-ray tube, six filters, a helium purge facility and a high-resolution silicon drift detector, calibrated using a number of internationally and nationally certified reference materials (CRMs). For the XRF data quantification, the strength of the distinctive lines of the elements was evaluated and the concentrations of the elements in the sample were calculated from the measured intensities (Loubser & Verryn, 2008; Sitko & Zawisza, 2012). Both the major and minor (trace) element analyses were done on the samples.

4.7 X-ray diffraction (XRD)

Samples were submitted for the XRD analysis to characterise and obtain qualitative and quantitative information on the mineral transformation between the blended coal and the ash and slag formed at the various temperatures. The mineralogy analysis was done in the Geology laboratory of North West University, Potchefstroom Campus.

The initially prepared samples of raw coal, roof, floor, blended coal, and the ash samples (<75 µm) were used for XRD analyses. A back-loading preparation method was used in the preparation of the samples. The powdered samples were moved to an appropriate sample container (made of aluminium) and the sample in the holder was packed moderately, but thoroughly, with the edge of a glass slide. After packing, the surplus sample was cut off with a glass slide (approximately 50x70 mm and 5 mm thick), while simultaneously compressing the sample in the container. The above procedure was repeated until a suitable surface (a smooth surface of uniform texture) was obtained.

The samples were subsequently tested in a PANalytical X'Pert Pro powder diffractometer with X'Celerator detector, adjustable divergence and fixed receiving slits with Fe-filtered Cu-Kα radiation. Identification of phases was done using X'Pert Highscore Plus software. The Rietveld method was used in estimating the relative phase amounts (weight %). As the experiment progressed, the X-ray intensities were measured and recorded by the X'Pert High Score Plus software. The intensities obtained were computed to enable the conversion of reduced intensities (Okolo, 2010). This can be achieved by the following procedures. Firstly, the raw diffractograms of the ash and blended coal were obtained and also the diffractogram of the sample spike of the reference material with a peak at a known value. Pure silicon was used for the spiking of the samples. The combination of the resultant diffractograms, that is the resulting spike and the raw diffractograms, is corrected in case of any shift observed for a peak. Finally, X'Pert Highscore plus application was used to correct for the polarisation and geometric factors (Frankline, 1951; Okolo, 2010; Lu *et al.,* 2001).

4.8 Elemental analysis by inductively coupled plasma optical emission spectroscopy (ICP-OES)

An Agilent 725 Radial ICP-OES instrument was used to measure concentrations of leachants present in the water from the UCG site, raw samples (coal blend and ash samples) and leachate samples from the leaching experiments. The samples were shaken or agitated thoroughly, before an aliquot of the samples was taken and put into a clean borosilicate glass beaker. The sample was firstly spot-treated with 30 vol. % H_2O_2. The beaker containing the sample was then placed in a sand bath at 100°C. The sample was not completely dried. It was removed from the sand bath, and 10 ml of 56% HNO_3 and 2 ml of 10% Br in $HC_2H_3O_2$ (acetic acid) were added to the heated samples. The mixture was subsequently placed on the sand bath at 100°C and taken to incipient dryness. To the dried sample, 5 ml of 56% HNO_3 was added before it was dried again. This step was repeated twice. Finally, 5 ml of 32% HCl was added to the resulting solution and warmed. The sides of the beaker were washed down after cooling, and the sample was diluted to the desired volume of 10 ml. Subsequently, the concentration of the leachants present in the liquid sample was determined using the ICP-OES instrument.

The Agilent 725 Radial ICP-OES spectrometer was allowed to warm up for 20 min, and a wavelength calibration was performed at the beginning of the session. A wavelength re-sloping procedure was performed at every 50^{th} sample of each analytical condition, as previously determined. Calibration was performed for every element to be determined, using the prepared standards. The calibration curves of all the elements of interest were performed and checked using the prepared standards. Finally, the samples were analysed, and the concentrations of the leachants present in these samples were reported in ppm, ppb and mg/l.

4.9 IC Method

About 20 µl samples was injected on a Metrosep A Supp 4-250/4 anion-exchange column (stationary phase) which was held at 25 °C, with a pressure of 5.83 MPa and a flow rate of 1.00 ml/min. Investigations of the samples were carried out under isocratic conditions using disodium carbonate (Na_2CO_3) (1.8 mmol/l) and sodium hydrogencarbonate ($NaHCO_3$) (1.7 mmol/l) as mobile phase with a pH 10.30. The

different standards used during the IC analysis includes Fluoride 2.0 mg/l, chloride 2.0 mg/l, nitrite 5.0 mg/l, bromide 10.0 mg/l and nitrate 10.0 mg/l.

4.10 CO_2 BET surface analysis

The CO_2 anf N_2 surface adsorption analyses were tested using a Micrometics ASAP 2010 instrument (**Figure 4.4**). The blended coal and ash samples were dried in a vacuum oven for about 6 hours in order to eliminate the moisture from the samples, which could prevent the accessibility of the absorbate. Samples of approximately 0.2 g were loaded in the sample tubes and tightly fitted onto the degassing port. To ensure a constant holding temperature, a thermal jacket was attached to the bottom of the sample tubes.

Figure 4.4: The Micrometrics ASAP 2020 surface area and porosity analyser used for CO_2 surface analyses

A	Degassing port	D	Analysis port
B	Sample tube being degassed	E	Sample tube being analysed
C	Thermal Jacket	F	Dewar holding cooling medium

Outgassing was done to remove air, moisture and other impurities before analysis was done on the samples. Outgassing of the samples was conducted at a temperature of 25°C and a pressure of 5 µm Hg for 48 hours. The ash samples were further degassed at 380°C. A ramp up of 2°C min^{-1} was used to reach the desired degassing temperature of 380°C and a holding time of 48 hours was used for the ash samples. On the completion of degassing, the glass tube was connected to the analysis port for adsorption analysis. Carbon dioxide gas was used as absorbate gas and an ice-water bath was used to keep the analysis temperature at 273.15 K. The BET surface area and the Dubinin-Radushkevich (D-R) micropore surface area were determined from the isotherm desorption data of CO_2 (Sobolik *et al.*, 1992).

The Horvart-Kawazoe (H-K) method was used to determine the micropore volume and average micropore diameter (Hovarth and Kawazoe, 1983, Joroniee *et al*., 1996; Kowalezyk *et al*., 2002; Micromeritics, 2006). The CO_2 adsorption data was used to calculate the porosity of the samples usually expressed in percentages and the cumulative volume of CO_2 was used to evaluate the volume of the pore openings. This was done using an integration method to obtain the cumulative pore volume over the measured pore diameter.

The N_2 adsorption test was done in a similar way to the CO_2 except that N_2 was used as the adsorbate gas and the analysis was performed at -196°C. The surface areas from the N_2 adsorption were assessed using different methods including BET, Langmuir and the Barrett–Joyner–Halenda (BJH) method. The pore volumes and average pore diameter from the N_2 adsorption results were measured using the Horvart-Kawazoe (H–K), BET and BJH models. The particle size distribution (PSD) of the samples from N_2 adsorption were obtained from the desorption isotherm using the BJH method (Clarkson *et al*., 1985)

4.11 Scanning electron microscopy (SEM) analysis

Surface analysis of the materials was performed with an FEI Quanta 200 scanning electron microscope (SEM) with an integrated Oxford Instruments INCA 200 energy dispersive X-ray spectroscopy (EDS) microanalysis system. This Microscope anaysising instrument (SEM) was used to show the change in morphological and qualitative characteristics, and for elemental characterisation of the coal, ash, and slag samples. The coal and ash samples were pre-coated with carbon tape to make

their surfaces conductive. Precaution was taken by covering the entire surface of the tape with the sample to avoid the interference of the carbon from the tape with the sample to be analysed. The SEM instrument was activated at the increased speed voltage of 20 keV for the mineral analysis of individual samples to deliver results on the physical and chemical properties.

4.12 Particle size distribution (PSD)

The particle size distribution values of the coal blend and ash samples used in this study were determined using a laser-based particle size analyser, Mastersizer 2000, manufactured by Malvern Instruments Ltd. The equipment uses Fraunhofer diffraction of light built for particles with diameters larger than the incident laser beam wavelength. A combination of an optical filter, lens and photodetector connected to a computer with Mastersizer software aids in measuring the particle size distribution (PSD) from the diffraction data. The results are displayed as volume percentage against the particle size.

4.13 Fourier transform infrared spectroscopy (ATR-FTIR) analysis

The ATR–FTIR spectra of the blended coal and ash samples were obtained from a Bruker Alpha-P FTIR spectrometer in transmittance mode, using the attenuated total reflection (ATR) platinum–diamond coupling. Analysis of the samples was done at ambient temperature. The wavenumber was taken from values ranging from 400-4000 cm^{-1} with total numbers of 32 scans and a spectral resolution of 4 cm^{-1}. Samples were dried in an oven for 2 hours at a temperature of 50°C to reduce the effect of moisture on the samples before analysis.

4.14 Batch leaching method

The batch leaching set-up used in this study is shown in **Figure 4.5**. The leaching cell is a round-bottomed container with a five-necked lid that contains the sample to be leached in the ratio of 1:10 with water: 10 g of coal blends, ash or slag and 100 ml of deionised water (DW) Deionized water (Millipore Milli-Q Plus® Q-pack CPMQ004R1) or water from the UCG site (GW) were used. The influence of liquid to solid ratio was also tested by increasing the amount of ash and the lixiviant kept the same i.e 20 g of coal blends, ash or slag and 100 ml (2:10), these was done for both

at room temperature and 50^{o}C leaching temperatures. The inflenuce of liquid to solid ratio was done only when GW was used as lixiviant. An overhead stirrer facilitated the suspension of the solid particles in the solution and also helped in the stirring of the mixture to to make the solution is homogeneous. The leaching test was conducted for 24 hours at a stirring speed of 200 revolutions per minute (rpm). At the end of this period, it was assumed that equilibrium was reached. The stirrer was inserted through the middle neck of the leaching cell lid. A Liebig cooler helped in the minimisation of evaporation.

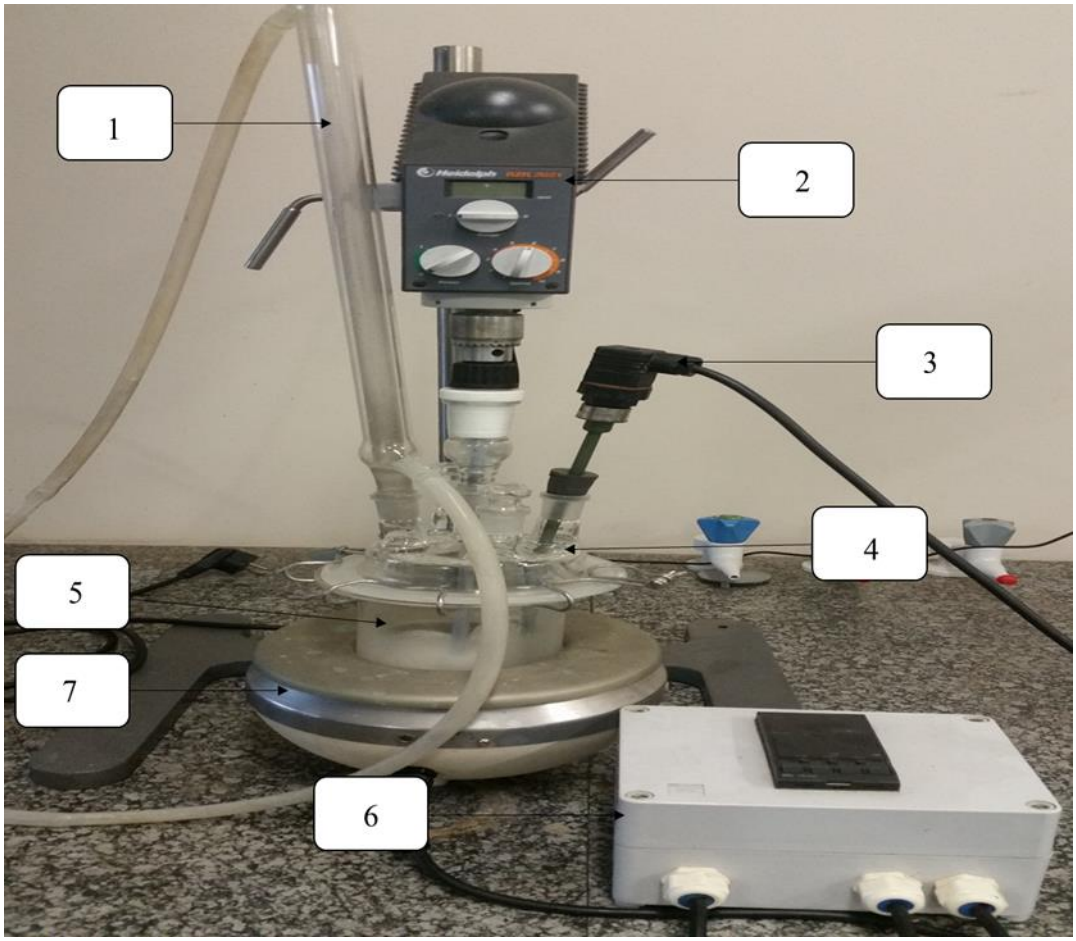

Figure 4.5: Leaching equipment used for the batch leaching

1	Liebig cooler	5	Leaching cell (round-bottomed container 500ml)
2	Overhead stirrer	6	Thermostat
3	Thermocouple	7	Heating mantle (temperature controller)
4	Five-necked lid		

The thermocouple, heating mantle and LCD display controller from the electronic temperature controller helped in the regulation of the leaching temperature. To ensure that the heat is distributed evenly an optimisation was done by inserting a piece of aluminium foil between the cell and the heating mantle. The samples were loaded into the leaching cell. The leaching cell was closed with a lid to limit the supply of air available during leaching, a provision necessary to simulate underground conditions.

Two sets of batch experiments were conducted:

Set 1: Experiments at ambient temperature and 50°C.

This set of leaching tests did not require sampling of the leachate during the experimental period. The leaching experiment was left for 24 hours and filtered after the time had elapsed. The filtrates were analysed for Ca, Si, Al, Fe, Mg, trace elements. The electron conductivity (EC), total dissolved solid (TDS), total alkalinity (TA) and pH of the filtered leachate were measured using Hana HI 991301 pH meter with potable EC/pH/TDS/temperature probe. A continuous batch leaching experiment was carried out on the ash samples (1000 °C, 1100°C and 1300°C) at 50°C leaching temperature. The continuous leaching test was done to ascertain the influence of recycling of the leachate after the initial leaching experiment. The continuous batch leaching test was achieved by initially leaching the samples for 24 hours and filtering the samples. Fresh ash was added to the already filtered leachate and the second leaching step was carried out with the initial leachate and fresh ash for another 24 hours.

Set 2: Experiments for temperature study.

This set of experiments was conducted to study the leaching time and temperature. This was carried out by varying certain operation conditions such as the leaching time and temperatures. The temperature was regulated using the thermostat. The leaching temperatures used for this part of the study were: 20°C, 30°C, 40°C and 50°C. These temperatures were chosen in order to be able to evaluate the influence of temperature and time during the leaching process. Leachate samples were collected during the experiment in the following time intervals: 0.5, 1, 2, 4, 8, 10, 12 and 24 hours. The samples were subsequently filtered with a 0.5 µm filter paper and the liquid residues were stored in the refrigerator prior to ICP-OES analysis to

identify the amounts of inorganic elements in the leachate. The leachates were analysed for Ca, Si, Al, Fe, and Mg. The resulting data was used to determine the rate of the reaction and the activation energy of the leaching process.

4.15 Column leaching method

A column leaching process was carried out to simulate the underground leaching process and also to compare the results with that obtained from the batch leaching process. The experiment was carried out inside a glass tube of 5 cm internal diameter and 60 cm length. The column has a gauge at the bottom end which was used to monitor the flow rate of the leachate during the test. The flow rate used for this study was 20 ml/hour. The bottom of the glass tube was coated with cotton wool to prevent the ash particles from entering the leachate. 20 g of the individual representative samples were loaded in the glass tube. The lixiviants used (water from the underground site and deionised water) were poured from the top of the column and a 10 cm level above the solid sample was maintained. The column leaching method was carried out at ambient temperature.

Two sets of column leaching tests were used in this study:
(1) In the first set, the leaching test ran for 24 hours. After 24 hours, filtration was done using a 0.5 µm filter paper and leachate was stored in the refrigerator, ready for further analysis. The leachate was analysed for Ca, Si, Al, Fe, Mg, trace elements. The electron conductivity (EC), total dissolved solid (TDS), total alkalinity (TA) and pH of the filtered leachate were measured using Hana HI 991301 pH meter with potable EC/pH/TDS/temperature probe.

(2) The second set of column leaching was carried out by taking aliquots of 10ml of the leachate and replacing it with the same volume of the lixiviant. The different time intervals for sampling were: 0.5, 1, 2, 3, 8, 10, 12, and 24 hours. After the leaching test, the leachate samples were collected and sealed in a reagent bottle. The packaged samples were stored in the refrigerator for ICP analysis. The leachates were analysed for Ca, Si, Al, Fe, Mg, trace elements. The electron conductivity (EC), total dissolved solid (TDS), total alkalinity (TA) and pH of the filtered leachate were

measured using Hana HI 991301 pH meter with potable EC/pH/TDS/temperature probe.

Chapter 5: Blended Coal and Ash Characterisation Results and Discussion

5.1 Introduction

In this chapter, the results obtained from the detailed physical and chemical characterisation of ash produced during the heating process, as well as the blended coal used in this study are discussed. This serves as a basis for better understanding of the mineralogical transformation from the feed material to the ash generated.

5.2 Physical appearance of the various ash samples at different temperatures

The appearance of the ash obtained by heating (described in section 4.2) the blended coal sample from the Theunissen site at different UCG temperatures varied as expected. The variation in the colour of the ash could be as a result of the removal of volatiles and fixed carbon, together with some mineral transformation as ashing temperature increases. After heating the feed coal to a temperature of 1000°C, there was a colour change from black to tan-grey. The change in colour could be as a result of the transformation of kaolinite to aluminium silicate (mullite and amorphous meta-kaolinite) and the combustion of some of the carbon. As expected, the ash produced at this temperature was more powdery than the original feed coal sample. As the temperature increased, the tan-grey colouration changed to a brown colour and a fine powder formed (1100^{o}C). The appearance of the brown colouration could be due to the transformation of pyrite to ferric oxides. Furthermore, at high temperatures the remaining material changed from dark-green to black, and it became a solid and hard material. The ash produced at 1300°C fused with the fire clay tray and it was assumed that a slag had thus formed. The slag that was produced at 1300^{o}C was highly aerated and was chipped from the tray to use for the leaching studies.

5.3 Proximate analysis

The proximate analysis results obtained for the raw coal, roof, floor, blended coal and the ash used in this study are summarised in **Table 5.1**. The background on the proximate analyses are described in Section 3.2. The experimental procedures and

the standard methods used for the various analyses are given in Section 4.6. The preparation of the samples is described in Section 4.4.

Table 5.1: Proximate analysis results (Air-dried basis (adb))

Sample	% Volatile Matter	% Moisture Content	% Ash Yield	% Fixed Carbon
Raw coal	20.7	6.5	35.3	37.4
Roof	1.8	0.8	93.5	3.9
Floor	2.0	0.5	93.6	4.4
Blended coal	16.6	7.2	40.1	36.1
Ash 1000°C	0.4	0.00	95.8	3.5
Ash 1100°C	0.3	0.00	97.5	2.3
Ash 1200°C	0.3	0.00	97.4	1.8
Sintered 1300°C*	0.2	0.00	98.0	1.5

The proximate analyses of the feed coal, roof material, floor material, blended coal and ash produced at various temperatures were performed to better understand the chemical composition of the samples before the leaching tests. The proximate analysis results are presented in weight percentages on an air-dried basis (adb). Data of the raw coal, roof and floor material are important in predicting how the mineral matter in the blended coal sample will perform during thermal treatment. The proximate analyses of the coal samples give an indication of the coal suitability for the coal utilisation processes. From **Table 5.1**, it was found that the moisture content of the floor and the roof material was found to be very low at 0.78 wt. % and 0.46 wt. %, respectively. Similarly, the volatile matter content of the roof and the floor material was also found to be low, approximately 1.8 wt. % and 2.0 wt. %, respectively. The fixed carbon content was found to be low for the roof and floor samples, but the ash yield for the roof and floor was, as expected, very high at 93.5 wt. % and 93.6 wt. %, respectively, suggesting that the roof and floor are composed of mineral matter. The similarity of the fixed carbon, volatile matter, moisture contents and ash yields of the roof and the floor samples indicated that the floor and the roof may be related with respect to their mineral matter contents.

It was observed from the proximate analysis results that the raw coal sample possessed a volatile matter content of 20.7 wt.%, fixed carbon content of 37.4 wt.%, inherent moisture content of 6.5 wt.% and ash yield of 35.3 wt. %. These shows that the feed coal has a high mineral matter content. These results are comparable to reported data obtained by previous researchers on bituminous coal of South Africa (; Matjie *et al.,* 2015; Okolo *et al*., 2015). The blended coal sample has a volatile matter content of 16.6 wt.%, moisture content of 7.2 wt.%, fixed carbon content of 36.1 wt.%, and ash yield of 40.1 wt.%. The ash yield of the blended coal sample increased, with a slight reduction in the fixed carbon content, which could be as a result of the relatively high percentages of the ash content in the roof and floor samples. It should be noted that the blended coal contains 80 wt. % of the feed coal, 15 wt. % of the roof and 5 wt. % of the floor samples.

The proximate analysis results for the ash yield of the four ash samples were similar, ranging between 95.8 wt. % - 98.0 wt. %. It seems that the ash samples contained mainly (>95%) transformed mineral matter. Small quantities of fixed carbon were observed in the ash samples (1.5 - 3.5 wt. %) which decreased with an increase in heating temperature. Proximate analyses were conducted on the ash samples for comparative reasons and to have an idea of the material that will be used for further leaching experiments.

5.4 Ultimate analysis

The ultimate analysis results obtained for the blended coal and the ash used in this study are summarised in **Table 5.2**. Backgrounds on the ultimate analyses are described in Sections 3.3. The experimental procedures and the standard methods used for the various analyses are given in Section 4.6. The preparation of the samples is described in Section 4.4.

Table 5.2: Ultimate Analysis (Dry mineral matter free basis (dmmfb))

Samples	% Carbon	% Hydrogen	% Nitrogen	%Sulfur	%Oxygen
Raw Coal	79.4	5.5	2.1	1.4	11.6
Blended coal	75.7	4.0	0.9	0.8	18.4
Ash 1000°C	1.1	0.03	0.11	0.3	-0.8
Ash 1100°C	0.7	0.04	0.12	0.3	-0.6
Ash 1200°C	0.5	0.01	0.15	0.3	-0.5
Sintered 1300°C	0.4	0.03	0.13	0.06	-0.5

The results from the ultimate analysis are presented in **Table 5.2** on dry mineral matter free basis. The elemental carbon, hydrogen, nitrogen oxygen and sulfur (by difference) contents (CHNOS) of the raw coal and blended coal samples were comparable to reported data on South African bituminous coals (Everson *et al.*, 2008; Everson *et al.*, 2013; Okolo, 2010; Matjie *et al*., 2015; Van Niekerk *et al.*, 2008,). The raw coal had a fixed carbon content of 79.4 wt. % (dmmfb) and that for the blended coal was 75.6 wt. % (dmmfb). This property makes the raw coal and blended coal samples useful as a feed material for the coal gasification process. The elemental oxygen content of the raw coal was 11.6 wt. % (dmmfb) and that of the blended coal 18.4 wt. % (dmmfb). The sulfur content of the raw coal was 1.4 wt. % (dmmfb) and for the blended coal 0.82 wt. % (dmmfb). The nitrogen content of the raw coal was found to be 2.1 wt. % (dmmfb) while that for the blended coal sample was found to be 0.8 wt. % (dmmfb), and hydrogen values ranged from 5.5 wt. % (dmmfb) for raw coal to 4.0 wt. % (dmmfb) for the blended coal. However, the elemental carbon, hydrogen, sulfur and nitrogen contents of the blended sample decreased slightly with an increase in oxygen (by difference) for the raw coal and blended coal samples. This could be as a result of the influence of the roof and floor sample additions.

The CHNOS contents of the ash decreased significantly after heat treatment and with increasing temperature, leaving a small amount of the organic elements in the ash sample as can be seen in **Table 5.2**, indicating that the volatile matter and organic contents of the blended sample have been consumed during the ashing (combustion) process. The values for the oxygen was found to be negative and also very small values (<1%) of the elemental carbon, hydrogen and sulfur were observed. This suggests that small organic fractions were found in the ash samples. Finally, from the results of the proximate and ultimate analyses, it can be concluded that the ash samples that were used for the leaching process consisted mainly of ash mineral matter (inorganic) with a relatively small fraction of organic elements (<1%).

5.5 Petrographic Analysis

The petrographic analysis results shown in **Table 5.3** reveal that the coal is moderately inertinite-rich with an inertinite maceral abundance of 63.3 vol. % (mmb). These results indicate that the organic matter of the coal was dominated by the inertinite maceral with small proportions of vitrinite and liptinite macerals.

Table 5.3: Petrographic analysis results

Reflectance properties		
Mean vitrinite random reflectance (Rr, %)	ISO 11760: 2005	0.99
Rank	ISO 11760: 2005	Bituminous medium rank C
Maceral composition (vol.%, mmb)		
Total vitrinite (TV)	ISO 7404-3:2009	10.3
Total liptinite (TL)	ISO 7404-3:2009	3.1
Reactive semifusinite (RSF)	ISO 7404-3:2009	23.0
Inert semifusinite (ISF)	ISO 7404-3:2009	39.4
Fusinite/secretinite	ISO 7404-3:2009	0.8
Micrinite	ISO 7404-3:2009	0.2
Total inertinite	Calculated	63.3
Visible minerals	ISO 7404-3:2009	34.7
Total reactives	Calculated	39.6
Total inerts	Calculated	40.4

The liptinite maceral content of the coal was 3.1 vol.% (mmb), which is similar to most reported liptinite contents of South African bituminous coals (Everson *et al.*, 2008; Everson *et al.*, 2013; Okolo, 2010; Van Niekerk *et al.*, 2008). The total volume of reactives (TV+TL+RSF), which refers to the maceral components that possess high tendency to react during heating, was 39.6 vol. % (mmb) for the coal sample. This is a good indication that the coal may be a good feedstock for combustion and gasification processes similar to the findings of other investigators (Everson *et al.*, 2008; Kaitano, 2007; Phiri, 2010; Okolo, 2010). The visible mineral content under the petrographic microscope was 34.7 vol. %, mmb for the coal sample, which is similar to the ash content from the proximate analysis results. The inertinites of the raw coal are mainly made up of semifusinite (39.4 vol. %, mmb) and a small proportion of

fusinite/secretine and micrinite. The reactive semifusinite content (RSF) was found to be relatively high with 23 vol. %, mmb. According to the ISO-11760:2005 standard, the coal is classified as bituminous medium rank C, with mean vitrinite random reflectance of 0.99 Rr%. The petrographic properties of this coal are comparable to the published petrographic data of South African bituminous coals (Everson *et al*., 2008b; Everson *et al*., 2013; Kruszewska, 2003; Okolo, 2010; Van Niekerk *et al*., 2008).

5.6 XRF analysis of blended coal and ash at different ashing temperatures

The background on the XRF analysis is described in Section 3.4, while the procedures used during the experiment are given in Section 4.6. The XRF results for the raw coal, blended coal and ash produced at 1000°C, 1100°C, 1200°C and sintered 1300°C are presented in **Tables 5.4, 5.5 and 5.6**.

The ash component or species were reported as oxides of the elements of loss on ignition free basis (lfb and sfb) (Loubser & Verryn, 2008; Sitko & Zawisza, 2012). Based on the classification of ash, the ash produced at various temperatures used in this work could be categorised as class F ash. This is because silica (SiO_2), alumina (Al_2O_3) and iron oxide (Fe_2O_3), make up about 90.5 - 91.5 wt. % of the ash as seen in **Table 5.5**. Similar results were also found for the raw coal sample and the roof and floor material. Also, the CaO content of the ash samples was < 2.2 wt. %. Ash can be classified as F if the quantity of the total major oxides: silica, SiO_2; alumina, Al_2O_3; and iron oxide, Fe_2O_3, in the ash is above 70 wt. % and the CaO content is < 5 wt. % (Singh and Kolay, 2002). Ash found in high-rank coals is usually classified as class C ash if the CaO content is above 5%. The concentration of the total major oxides: silica; alumina and iron oxide in the ash is also found to be < 70 wt. % (Singh and Kolay, 2002). The Si/Al ratio of the ash produced ranged from 2.0 to 2.3 wt. % and the total base to acid ratio ranged from 0.1 to 0.2. The high percentage composition of the acidic species (SiO_2 and Al_2O_3) indicated that the ash samples contained mainly (>95%) transformed mineral matter, suggesting a high alumina-silicate or clay composition. It is worthy to note that the amounts of CaO and SO_3 were low for all the ash samples at the different temperatures. The Si/Al and the base-acid ratio showed little variations, as their values were very close for all the ash samples, similar to the findings on the ash component (elemental) compositions of

the ash used in this study. However, significant differences were observed in the mineralogy of the ash samples and that will be discussed in detail in Section 5.9.

Table 5.4: XRF results of major elements in the blended coal and ash sample at different temperatures

Compound Name	Blended coal	Ash 1000°C (wt. %)	Ash 1100°C (wt. %)	Ash 1200°C (wt. %)	Sint 1300°C (wt. %)
Na_2O	0.6	0.8	0.8	0.7	0.7
MgO	0.9	0.8	0.8	0.6	0.7
Al_2O_3	25.9	28.4	28.4	25.3	25.9
SiO_2	55.3	57.3	57.5	58.3	57.3
P_2O_5	0.1	0.1	0.1	0.1	0.1
SO_3	0.8	0.6	0.6	0.2	0.4
K_2O	2.8	1.8	1.9	2.3	2.2
CaO	2.4	1.9	2.0	2.0	2.2
TiO_2	1.7	1.3	1.3	1.1	1.1
MnO	0.6	0.1	0.1	0.1	0.1
Fe_2O_3	9.0	6.9	6.6	9.4	9.3
Base to acid ratio	0.2	0.1	0.1	0.2	0.2
Silica to alumina ratio	2.2	2.0	2.0	2.3	2.2
Iron to calcium ratio	6.7	3.6	3.3	4.8	4.2
$SiO_2+Al_2O_3+ Fe_2O_3$	90.2	91.5	91.4	90.9	90.5

Table 5.5: XRF Analysis of the Feed coal, Roof and Floor material before Blending (wt. %)

Compound	Raw Coal	Roof	Floor
SiO_2	59.5	82.5	63.5
Al_2O_3	26.2	11.2	27.4
Fe_2O_3	4.5	1.4	3.1
TiO_2	1.6	0.3	1.3
P_2O_5	0.03	0.01	0.1
CaO	2.6	0.1	0.2
MgO	0.9	0.2	0.8
Na_2O	0.4	0.3	0.2
K_2O	1.3	3.7	3.0
MnO	0.02	<0.01	0.03
Base/acid Ratio	0.11	0.1	0.03
$SiO_2 + Al_2O_3 + Fe_2O_3$	90.2	95.1	94.0

From the XRF results for the major elements (**Table 5.4**), it was observed that SiO_2 and Al_2O_3 were the most abundant elements for all the samples at different ashing temperatures, with a minor composition of CaO, Fe_2O_3, TiO, K_2O, MgO and Na_2O. This also compares well with the XRD results for the ash samples obtained in this study (**Table 5.8**, Section 5.9). SiO_2 and Al_2O_3 are derived from clay minerals (quartz, kaolinite, and mullite) which form the majority of the minerals. The Al_2O_3 mineral present in the coal ash may be derived from clay such as kaolinite ($Al_2O_3.SiO_2.2H_2O$). The compound has been reported by other investigators as one of the major minerals found in bituminous coal ash (Matjie *et al*., 2008; Matjie *et al*., 2011; Matjie *et al*., 2012; Stach *et al*., 1982; Ward, 2002). In addition, the high quantity of acidic species in the ash suggests a high alumino-silicate or clay composition.

The presence of Fe_2O_3 in the blended coal and ash samples at different ashing temperatures can be attributed the transformation of pyrite to hematite, maghemite, and magnetite, as could be observed from the XRD results in Tables 5.8 and 5.9. MgO and CaO were seen in all the ash samples, which is a demonstration of the transformation of calcite and dolomite in the coal at different ashing temperatures (**Table 5.9**). The presence of TiO_2 in the sample can be a reflection of the anatase

and rutile in the blended coal and ash samples, respectively. K_2O in the ash samples could be attributed to the presence of muscovite and microcline in the blended coal before the ashing process.

Similarly, XRF of the initial material (raw coal, roof and floor material) before the blending are presented in **Table 5.5**. The results also show that the major elements in the initial material were SiO_2 and Al_2O_3 in the raw coal sample and roof and the floor material, with the roof and the floor material having the highest percentages of 82.5 and 63.5 wt. %, respectively. Other minor elements such as Fe_2O_3, CaO, MgO, NaO and K_2O were also found in the initial material. The acid to base ratio of the initial material was found to range from 0.03 - 0.11 and the $SiO_2 + Al_2O_3 + Fe_2O_3$ ranged from 90.2 - 94.0 wt. %.

The results of the minor and trace elements are summarised in **Table 5.6** in milligram per kilogram of the sample (mg/kg), which is equivalent to parts per million (ppm). From **Table 5.6**, it was found that the concentrations of the trace elements are very low, but the NiO concentration was relatively high in comparison with the other trace elements. The majority of the trace elements are typically related with coal minerals. Such trace elements include Hg, Bi, Sn, Mo,As, B, Ge, Ti, S, Se, Sb, and Pb (Querol *et al*., 1995). The leachability of these elements into the environment or underground water bodies depends on the solubility of the elements in the lixiviant used and the pH of the solution. XRF study of the trace elements enables an understanding of the trace element constituents of the initial ash before leaching tests.

Table 5.6: XRF data of trace elements in the ash samples at different temperatures (wt. %)

Compound Name	Ash 1000°C	Ash 1100°C	Ash 1200°C	Sint 1300°C
	mg/Kg	mg/Kg	mg/Kg	mg/Kg
NiO	1990	1730	3980	3660
CuO	119	122	192	264
ZnO	81	63	101	99
Ga_2O_3	23.2	32.3	4.16	37.1
GeO_2	-[a]	-	13.9	-
Rb_2O	85.8	97	131	138
SrO	304	345	450	503
ZrO_2	637	660	1110	1200
Nb_2O_5	20.5	0.638	30.3	33.4
MoO_3	-	-	3180	3330
BaO	850	1930	231	416
WO_3	116	236	-	132
PbO	92.1	76.9	114	29.5
ThO_2	43.1	59.8	58.9	71.3

[a]- Not determined

The significance of carrying out XRF analyses is to determine the concentrations of inorganic elements present in the blended coal and the ash samples produced. This will help in calculating the dissolution efficiencies of the elements that were leached out during the leaching tests.

5.7 Ash fusion temperature (AFT)

AFT tests were used within the context of this study to simulate the performance of the raw coal, roof and floor material and the blended coal when heated under oxidising or reducing conditions. All the AFT analyses were done at the laboratory of Bureau Veritas, Middelburg, South Africa, in both oxidising and reducing atmospheres. The background of the analyses are presented in Section 3.7. The summary of the results is presented in **Table 5.7**, showing the initial deformation temperatures, softening (spherical) temperatures and the fluid temperatures for both the reducing and oxidising conditions. From **Table 5.7** it can be observed that all the parameters investigated, ranging from initial deformation temperature (ID), softening temperature (SF), hemispherical temperature (HT), and fluid temperature (FT), for

the feed coal were lower compared with the roof and the floor samples' results. This could be attributed to the higher abundance of acidic components (SiO_2, Al_2O_3 and TiO_2) in the ash of the roof and floor material, as can be seen in the XRF ash component analysis results for the roof and the floor samples given in **Table 5.5**. Huggins *et al*. (1981), Prinsloo (2009) and Van Dyk and Waanders (2007) reported that the acidic components of coal ash, which are SiO_2, Al_2O_3 and TiO_2, have a significant impact on the AFT values, with aluminium exhibiting the strongest influence.

As indicated by the XRF results of the roof and the floor in **Table 5.5**, it can be seen that the roof and floor material has a high amount of K_2O. Vassilev *et al*. (1995) stated in their study that the presence of potassium species has an intermediate increasing influence on the AFT, suggesting it can increase the ATF and, more specifically, the hemispherical temperature (HT). The K_2O contents of the floor and the roof samples are higher when compared with the raw coal sample, as can be seen in **Table 5.5**. This may explain the higher AFT values of the roof and floor material when compared with the raw coal sample. The main reason for the higher AFT values of the roof and the floor material, however, is mainly due to the higher SiO_2 contents, but more specifically the high acidic contents of the roof and the floor material. The lower AFT values of the raw coal sample can be attributed to the high percentages of the fluxing elements and low acidic content of the raw coal in comparison to the other samples, as can be seen in **Table 5.5**. Similarly, the lower AFT of the blended coal sample in comparison to the roof and floor may be attributed to the lower percentage of the acidic species and the higher abundance of fluxing elements, CaO, Fe_2O_3, Na_2O, in the blended coal sample (**Table 5.4**).

Table 5.7: Ash fusion temperature under oxidising and reducing condition (^{o}C)

Properties/Sample ID	Raw coal	Roof	Floor	Blend Coal
Oxidizing condition				
Initial deformation (ID)	1358	1352	1486	1336
Softening temperature (ST)	1370	1408	1546	1386
Hemispherical temperature (HT)	1372	1480	1550	1440
Fluid temperature (FT)	1394	1546	1552	1460
Reducing condition				
Initial deformation (ID)	1356	1380	1486	1390
Softening temperature (ST)	1390	1400	1560	1360
Hemispherical temperature (HT)	1380	1450	1555	1380
Fluid temperature (FT)	1360	1560	1580	1375

Higman and Burgt (2008) stated that if both the calcium and iron contents are high in coal, the softening and the melting temperatures will be reduced. It thus seems valid to conclude that the initial deformation temperature of the raw coal sample, which makes up about 80% of the blended sample used for this study, is 1356°C. The reducing condition was used for this study because the values obtained were lower when compared with the values obtained under oxidising conditions. Ashing the samples above the AFT (1356^{o}C) of the raw coal sample will lead to the melting and possibly fusion of the ash sample with the sample holder, rendering further studies with the fused sample difficult.

Both Huffman *et al*. (1981) and Su *et al*. (2003) demonstrated in their work that for gasification uses, the AFT values of the coal to be used should be investigated under reducing conditions since the results obtained from the oxidising conditions are higher than those obtained during reducing conditions. The results obtained for the samples investigated in this study under the oxidising and reducing conditions do not differ significantly, as shown in **Table 5.7**. Matije *et al*. (2015) obtained similar results where the oxidising and reducing condition results did not differ significantly. This suggest that elements such as Fe, which have different valence states, do not have a significant influence on the AFT properties of the coal under reducing or oxidising conditions. Finally, the blended coal sample was found to exhibit slightly lower ash

fusion temperatures during reducing conditions, hence the choice of 1300^{o}C as the highest temperature used for this study.

The ash prepared from the blended coal sample at 1300°C already showed melting as described in the physical appearance section (Section 5.2).

5.8 Mineralogy of the Raw Coal Material

The XRD results of the raw coal, roof and floor material, which were blended in a proportion of 80, 10 and 5 wt. %, respectively, are presented in **Table 5.8**.

Table 5.8: XRD results for of the raw coal, floor and roof before blending (wt. %)

Mineral phase	Chemical formula	Raw coal	Floor	Roof
Kaolinite	$Al_2SiO(OH_4)$	37.7	35.1	8.9
Quartz	SiO_2	28.8	26.0	64.6
Microcline	$KAlSi_3O_8$,	10.0	10.0	14.4
Pyrite	FeS_2	4.1	0.3	0.4
Muscovite	$KAl_{l2}(AlSi_3O10(OH)_2)$	8.6	9.5	5.5
Anatase	TiO_2	5.3	3.1	0.5
Rutile	TiO_2	1.2	0.6	0.4
Plagioclase	$CaAl_2Si_2O_8$	4.4	0.9	3.2
Dolomite	$CaMg(CO_3)_2$	-	0.3	1.5
Siderite	$FeCO_3$	-	3.0	0.3
Amorphous	nd	nd	nd	nd

nd- not determined

From **Table 5.8**, it can be seen that the major minerals in the raw coal, floor and roof material are kaolinite, quartz, and microcline, with a small proportion of pyrite, muscovite, anatase plagioclase, dolomite, siderite and rutile. The coal sample had the following percentages of minerals: kaolinite (37.7 wt %), quartz (28.8 wt %), muscovite (8.6 wt %), and microcline (10.0 wt %) and the minor minerals were illites, calcite, rutile, plagioclase and pyrite. Similarly, the roof contained kaolinite (35.1 wt %), quartz (26.0 wt %), muscovite (9.5 wt %), and microcline (10.0 wt %) as major minerals, with minor percentages of illite, calcite, rutile, plagioclase pyrite, dolomite and siderite. The floor contained kaolinite (8.9 wt %), quartz (64.6 wt %), muscovite (14.4 wt %), and microcline (10.0 wt %) as the major minerals with minor percentages of illite, calcite, rutile, plagioclase pyrite, dolomite and siderite. The only

major difference in the minerals observed in the floor and the roof is that in the roof the amount of quartz (26.0 wt %) was found to be low when compared with the amount found in the floor (64.6 wt %). Also, the amount of kaolinite in the roof and the floor varied with the roof having 8.9 wt % and the floor having 35.1 wt %.

5.9 Mineral matter transformation during heat treatment of feed coal at a different temperatures.

The X-ray diffractograms of the blended coal and the ash samples generated at different temperatures are presented in **Figure 5.1**. These diffractograms were used for the identification and quantification of the mineral phases in the feed material and the ash.

From **Figure 5.1**, it was observed that diffractograms of ash looked almost similar but significantly different to the diffractogram of the blended coal sample. These variations can be attributed to the mineral transformations from the original blended coal sample to the different ash samples, following the high-temperature ashing process. The amount of the amorphous mineral phase of the ash sample prepared at 1300°C is less compared with the crystalline mineral phase (which is made of siliceous species). It can further be predicted that the concentration of species in the leachate at 1300°C will be low when compared with the concentration leachate species from the 1000°C and 1100°C ash. Full details of individual sample diffractogram are presented in Appendix (**Figure A1-5**).

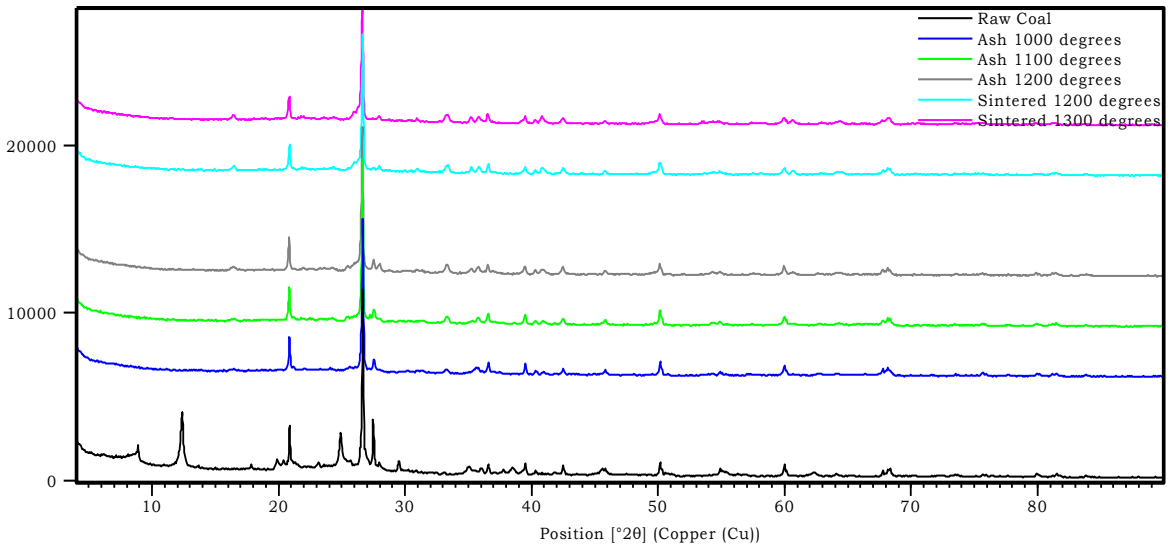

Figure 5.1: X-ray powder diffractograms of blended coal and ashes at 1000, 1100, 1200 and 1300°C showing peaks used to identify major mineral phases

The quantitative XRD results obtained during the coal mineral transformations to ash at different heating temperatures are summarised in **Table 5.9**. Some of the transformed mineral phases are mullite, cristobalite, anhydrite, hematite, magnetite, rutile, diopside and portlandite, which are in agreement with results from other studies on coal ash generated at high temperatures (Bayat, 1998; Grim, 1968; Matjie *et al.*, 2008; Matjie *et al.,* 2011; Matjie *et al*., 2012; Van Dyk *et al* ., 2009; Van Dyk and Waanders, 2007; Vassiev *et al.,* 1996; Ward *et al.,* 2006; Ward *et al*., 2014;)**.** These transformations are discussed in detail in Sections 5.9.1 - 5.9.9.

XRD quantitative analysis was obtained by the combination of XRD with the Rietveld method to determine the different compositions of the crystalline and amorphous (glassy) phases of the blended coal sample and ash at different temperatures used in this study (as described in Section 4.7). The quantification of the amorphous minerals was carried out by spiking of the samples with silica.

Table 5.9: XRD results of the blended coal and the ash samples at different temperatures (wt. %)

Mineral phases	Blended coal	Ash 1000°C	Ash 1100°C	Ash 1200°C	Sint 1300°C
Quartz	4.4	35.6	34.5	36.2	35.6
Kaolinite	14.1	-	-	-	-
Mullite	-	8.2	12.8	24.1	31.7
Rutile	-	2.3	1.7	2.4	0.6
Hematite	-	0.9	1	1	0.8
Pyrite	0.4	-	-	-	-
Anatase	0.2	-	-	-	-
Muscovite	0.3	-	-	-	-
Dolomite	7.4	-	-	-	-
Calcite	3.6	-	-	-	-
Graphite 3R	0.8	-	-	-	-
Maghemite	-	0.9	0.2	0.6	0.5
Magnetite	-	0.9	-	-	-
Diopside	-	0.4	0.3	0.4	0.2
Lime	-	0.2	0.1	-	-
Periclase	-	0.3	-	-	0.5
Anhydrate	-	1.1	1.0	1.1	0.1
Cristobalite	-	-	0.2	-	-
Portlandite	-	-	-	0.2	-
Goyazite	0.4	-	-	-	-
Amorphous phase	66.2	49.2	48.2	34	30

The samples were found to exhibit two main groups of phases, which are the crystalline phase and the amorphous phase. The amorphous phase is defined as material that is not in an orderly condition, or has a particular composition of elements or a phase that is not in a crystalline form. A summary of the XRD results is presented in **Table 5.9**. From the table, the blended coal sample was found to contain about 66.2 wt. % of the amorphous phase and the remaining 34 wt. % consisted of the crystalline mineral phases, with kaolinite, dolomite and quartz

having the highest abundances of 14.1 wt. %, 7.4 wt. % and 4.4 wt. %, respectively. Pyrite, anatase, muscovite, calcite, and goyazite occurred only in small proportions in the crystalline phase of the blended coal sample.

It was also observed that as the ashing temperature increased, the amorphous phases decreased with a commensurate increase in mullite content. The increasing mullite content can be attributed to the dissociation of the meta-kaolinite minerals in the amorphous phase. But, as expected, the quartz abundance in the four ash samples were almost the same, ranging from 34.5 - 36.2 wt. %. This shows that quartz is a very unreactive material even at high temperatures. Matije *et al*. , (2015) also reported similar findings for the unreactivity of quartz. The crystalline transformations that occurred from the blended coal and ash samples at various temperatures are presented in Appendix A.

5.9.1 Mullite

The mullite in the different coal ash samples generated in this study could be attributed to the transformation of kaolinite in the feed material (**Table 5.9**). The kaolinite loses water of crystallisation to form meta-kaolinite at around 450^{o}C (Moore and Reynolds, 1997). It has been reported that meta-kaolinite undergoes phase transformation at 900°C and further dissociates to give mullite and reactive quartz (French *et al*., 2001; Grim *et al*., 1968; Matjie *et al.*, 2015; Mitchell *et al*., 1976;). The transformation of kaolinite to mullite is in agreement with previously published results (Matjie *et al*, 2015; Matjie, 2008; Van Dyk *et al*., 2009; Van Dyk and Waanders, 2007; Yu *et al*., 2007). The mullite can remain in the solid phase to at least 1600^{o}C (Reifenstein *et al*., 1999), which makes it more stable at elevated temperatures. The proportion of mullite obtained for this study ranges from 8.0 - 31.7 wt. %. The mullite content was found to increase with increasing ashing temperature with the ash produced at 1300 °C exhibiting the highest abundance of mullite (**Table 5.9**).

5.9.2 Quartz

Quartz, which is one of the major minerals in the crystalline phase, ranges from 36.2-34.5 wt. % of the ash at different temperatures. As expected, the value for the quartz does not vary significantly due to the fact that quartz is very unreactive. Quartz is expected to persist and remain unchanged during heat treatment. This is predictable

as quartz is recognised as most stable form of crystalline phase under normaly circumstance (Matjie *et al.*, 2015). Thus quartz may pass from the feed coal to ash without any alterations due to it unreactive properties. Quartz is known to be very stable temperatures, although a change in quantity may transform into another crystalline form, cristobalite, through the alteration of amorphous phase when treated above 1470 °C for a certain period (Sakurovs *et al*., 2007, Van Dyk *et al*., 2008). Reactive quartz is transformed at elevated temperatures to cristobalite. For this study, mullite, dolomite and quartz were the predominant crystalline minerals in the ash samples.

5.9.3 Cristobalite

The cristobalite proportion in the coal ash was found to be very low at about 0.1% by weight. Cristobalite is a high-temperature polymorph of quartz which crystallises as the stable form above 1470°C. The low percentage of cristobalite could be attributed to the transformation of reactive silica from clay at the experimental conditions used for this study. The conversion temperature for quartz to cristobalite may fluctuate depending on the rate and direction of the temperature change (Hurlbut, 1971). Cristobalite is thus a metastable form, possibly present due to the rapid heating of the ash. Studies from different authors on Highveld coal during fixed bed combustion processes have shown that prolonged exposure of quartz to high temperatures may gradually transform quartz into cristobalite (Matjie *et al*., 2012a; Matjie *et al*., 2012b; Reifenstein *et al*., 1999).

5.9.4 Anorthite

The anorthite content was found to be very low at 0.1 wt. % for all the samples. The mineralogical changes observed for anorthite suggest that it could be formed either by solid state association of free Ca from the transformation of dolomite and high-temperature aluminosilicates (meta-kaolinite) (French, 2001), or by the crystallisation of molten aluminosilicates (glassy) (Matjie *et al*., 2008; Matjie *et al*., 2011). According to Bryers (1986), Ward (1984), and Raask (1985), CaO from the decomposition of calcite can react with kaolinite (reactive aluminosilicate) at high temperatures (1000-1200°C to form anorthite ($CaAl_2SiO_2O_8$). This shows that calcite that was found in the blended coal may have transformed at high ashing

temperatures used in this study to form CaO, which further reacts with kaolinite (reactive alumina silicate) to form anorthite.

5.9.5 Anhydrite

The anhydrite ($CaSO_4$) in the ash may have been derived from the reaction between SO_3 and CaO. Small proportions (0.8 - 2.2%) of anhydrite was found in the ash, which may be attributed to the small amount of CaO and SO_3 in the blended coal sample as can be seen from the XRF result in **Table 5.5**. The small quantity of CaO in the coal ash may have provided less opportunity for the capture of SO_3 during the heating process.

5.9.6 Hematite/magnetite

Pyrite in the blended coal undergoes a transformation to hematite and magnetite as could be seen in **Table 5.9**. Pyrite present in the coal undergoes intensive oxidation at elevated temperatures to form iron oxide (hematite), magnetite and sulfur dioxide during heat treatment (Hu *et al*., 2006; Matjie *et al*., 2011; Matjie *et al*., 2012; Van Alphen, 2005; Schobert, 2013; Srinivasacher, 1990; Yani, 2009). The percentage of hematite and magnetite in all the ash samples ranged from 0.8 to 1.0 wt. %, which is very low compared with the percentages of Fe_2O_3, ranging from 6.5 - 9.1 wt. % as seen in the XRF results in **Table 5.5**. This suggests that most of the Fe is fused in the amorphous phase (Matjie *et al*., 2011).

5.9.7 Rutile

The rutile, which is a Ti-bearing mineral, in the ash may have arisen from the anatase in the blended coal sample. The percentages of the rutile for all the ash samples in this study ranged from 0.6 - 2.4 wt. %.

5.9.8 Lime/periclase

Small percentages of lime (CaO) was found at 1000^{o}C and 1100^{o}C, while a small amount of periclase (MgO) was found at 1000 ^{o}C and later reappeared at 1300^{o}C. The occurrence of lime and periclase may be as a result of the dolomite in the blended coal undergoing a disassociation reaction which transformed the lime and the periclase. It may also may be in the ash sample, probably from the calcite and the dolomite in the blended coal sample. Reifenstein *et al*., (1999) reported that

calcite may decompose at 900^{o}C to form lime and the lime may interact with water from the atmosphere to form portlandite.

5.9.9 Diopside

The percentages of diopside ranged from 0.4 - 0.7% in the different ash samples. The occurrence of diopside in the ash samples may be as a result of the reaction between reactive silicon that was formed from the decomposition of meta-kaolinite (alumino-silicate) and CaO and MgO formed from the disassociation of dolomite.

From the transformation discussions in Section 5.9, it can be concluded that the initial minerals in the blended coal sample changes to different minerals during the heating (ashing) at the temperatures used in this study, which is similar to temperatures used during UCG. From the transformed minerals, it is possible to estimate the mineral species that will leach out during the leaching test, including anhydrite and some of the soluble minerals in the amorphous phase that are not in the crystalline phases.

From the XRF and XRD results in **Table 5.4** and **5.9**, respectively, the likely elements/compounds to be leached out will be potassium, sodium, sulfate, potassium sulfate, aluminium sulfate, and sodium silicate. These species/elements could be leached due to their high solubility in water. The blended coal sample was also found to be rich in aluminium and silicon, with lesser amounts of iron, magnesium, phosphorous, calcium and titanium; similar to previous studies on South African bituminous coals (Bunt *et al.*, 2012; ; Okolo, 2010; Everson *et al.*, 2008).

5.10 SEM analysis of blended coal and ashes at different temperatures

The use of SEM can help in understanding the micromorphology of solid surfaces and the internal physical structure of a material. Image enlargement was carried out on the samples with different morphologies, showing the heterogeneity of coal. The background and procedure of analysis are presented in Sections 3.7 and 4.10, respectively. The results of the SEM morphology are presented in **Figure 5.2**. The SEM results, including the SEM-EDX elemental analysis data, give an insight into the changes in the morphology of the samples after heat treatment.

The blended coal samples (**Figure 5.2**) were made up of irregular shapes, which showed the heterogeneity of the coal sample. The ash deposits at different temperatures (1000^{o}C - 1300^{o}C) were also composed of particles with different shapes and sizes. The SEM morphology of the samples showed that the shapes of the sample particles were of different forms, ranging from spherical to irregular shapes. Sintering and agglomeration of mineral matter during the thermal treatment can be recognised by the occurrence of spherically-shaped particles and rounding of edges (**Figure 5.2**). The smooth spherical shapes can be as a result of melting that occurs during heat treatment of the ash samples at the various temperatures, while the irregular shapes could be attributed to the particles that resist melting at these high temperatures.

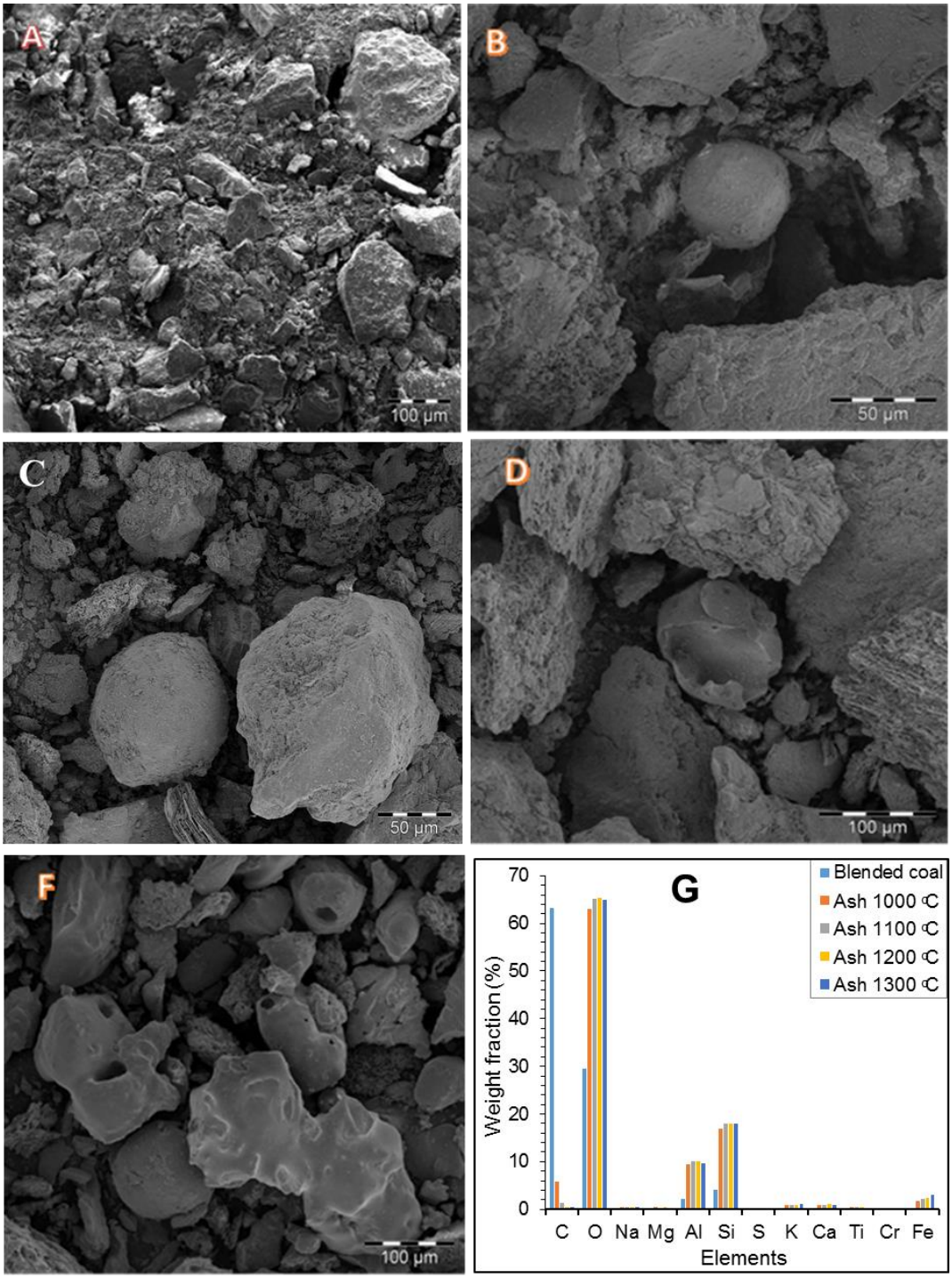

Figure 5.2: SEM micrographs for : A) Raw coal sample; B) Ash 1000^{o}C; C) Ash 1100^{o}C; D) Ash 1200^{o}C; F) Sint 1300^{o}C; and G) SEM-EDX elemental analysis data

As the ashing temperature increased, it was observed that the proportion of the spherically shaped particles increased, indicating melting of some of the ash particles at these elevated temperatures. The spherical shapes were more pronounced in the 1300^{o}C ash sample, suggesting that some of the mineral species

(e.g. aluminosilicates) have melted to form cenosphere particles, which can be formed by the agglomeration and sintering of the ash samples. Several authors have reported spherical shapes of ash at higher temperatures (Kutchko and Kim, 2006; Li *et al*., 2003; Saikia *et al*., 2006). The spherical shapes could be as a result of the melting of aluminium silicate due to fluxing elements: Fe^{2+} (ferrous), Ca, and Mg. These fluxing compounds were observed in the EDX results (**Figure 5.2(G**)). This is in agreement with the presence of aluminosilicate (mullite), hematite and lime from the XRD results presented in Table 5.9. The irregular shapes can be as a result of the unreactivity of SiO_2, which includes the quartz and feldspars (Li *et al*., 2016). These minerals are very unreactive at very high temperatures and often retain their shape during heating processes (Matjie *et al*., 2015).

Additionally, SEM images help in predicting the leachability of the ash materials that did not sinter, sintered and agglomerated particles when using water. The blended coal sample, as seen in the SEM images (**Figure 5.2**), is more porous than the ash sample, translating to a higher surface area, thereby having better water adsorption, which could lead to more leaching, but due to its high adsorption property (carbon content), the leachability of the inorganic compounds could be difficult. However, for the agglomerated samples with lower porosity and lower surface area, less water will get into contact with the leachable species. Nevertheless, the leachability of the sintered material (ash produced at 1300°C) may be very low as a result of the encapsulation or fusion of the inorganic species in the sintered ash.

From the SEM morphology of the blended coal sample and the ash at different temperatures, it may be concluded that there was significant transformation in the morphology of the samples as the temperature of heating (ashing) increased.

5.11 Surface area

The study of the surface area and porosity properties of the samples is premised on the expectations that, after the UCG progress, the burn cavity may collapse, leading to the cavity filled up over time with ground water and ash. Knowledge of the surface area and porosity properties of the ash at different temperatures will help in predicting the flow of the water to the surrounding underground water bodies. The background and procedures of analyses are presented in Section 3.9 and 4.9, respectively.

5.11.1 CO_2 adsorption data

The adsorption isotherms resulting from the low-pressure CO_2 adsorption on the raw coal and the ash produced at different temperatures are summerised in **Figure 5.3**, while a summary of the surface area and porosity properties of the samples is given in **Table 5.10**. The different analytical methods and models used to obtain the results are also given in **Table 5.10**.

As indicated in **Table 5.10**, the Dubinin-Radushkevich (D-R) micropore surface area and the Brunauer-Emmet-Teller (BET) surface area of the raw coal were found to be 73 m^2/g and 50 m^2/g, respectively. These values may be considered to be low in comparison with the published data of Okolo (2010) and Okolo *et al*. (2015), but compare well to the reported results of Mchabe (2012) on South African bituminous coals and elsewhere (Mahajan, 1991; Mahajan, 1984; Marsh, 1987; Nandi and Walker, 2003; Radovic *et al*., 1997; Şenel *et al.*, 2001; Walker, 1981). This may be attributed to the maturity (rank) of the raw coal, with a vitrinite reflectance of 0.99% R_0, used in this study. It is known that the surface areas of coals decrease with increasing maturity. A critical examination of the data of Okolo and co-workers reveals that the vitrinite reflectance of their coal samples was < 0.75 % R_0. , while the coals reported by Mchabe (2012) have a vitrinite reflectance > 0.75 Rr. %. The microporosity of the raw coal sample (<3%) calculated from the CO_2 adsorption data was also low compared with other reported results; with an average micropore volume of 2.96 cm^3/g. The microporosity of the ash samples was found to decrease drastically from that of the raw coal chars by a factor > 9.5 (**Table 5.10**).

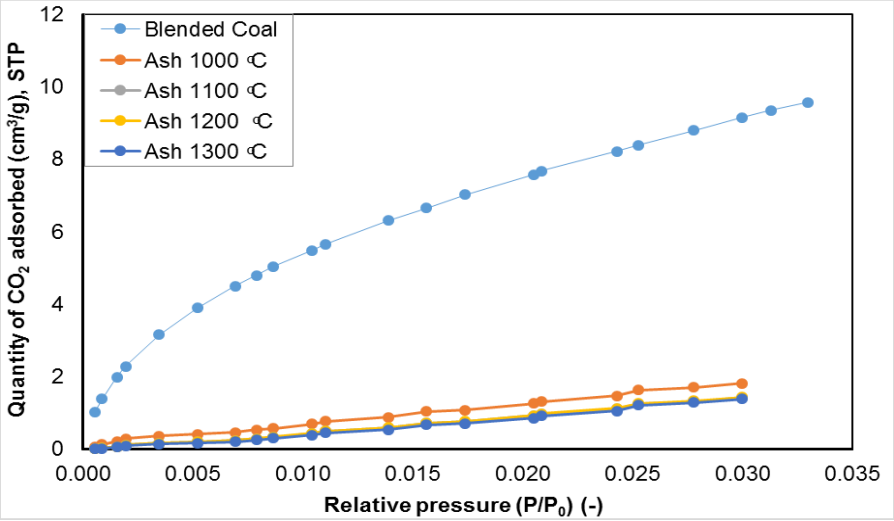

Figure 5.3: CO_2 adsorption isotherms of the raw coal and ash samples

For the ash samples, the D-R micropore surface area decreased with increasing ashing temperature, but increased slightly for the 1300°C, ash this could be as a result of the breaking of the pores during heat treatment. The BET surface area of the ash samples decreased significantly from the 1000°C (8.03 m^2/g) to a fairly constant value of between 3.87 to 3.97.m^2/g for the 1100 to 1300 °C ash. Similar trends were observed for the micropore volume and microporosity of the ash samples, while the average micropore diameters of the ash samples followed an opposite trend. This systematic behaviour of the ash samples may be due to slag formation, agglomeration and sintering of minerals in the ash, which were more significant for the 1300°C ash. Also, the decrease in surface area and porosity can be attributed to the consumption of the carbon part of the coal as ashing temperature increases.

Table 5.10: Physical–structural properties of samples from CO_2 gas adsorption

Properties / Sample ID	D-R micropore surface area (m^2/g)	BET surface area (m^2/g)	Average micropore diameter (Å)	Micropore volume ($x10^{-2}$ cm^3/g)	Microporosity (3 Å ≤ dp ≤ 5 Å) (%)
Methods used	D-R	BET	H-K	D-R	CO_2 Ads data
Blended Coal	73.74	50.38	3.96	2.96	2.76
Ash 1000°C	16.60	8.03	4.52	0.67	0.29
Ash 1100°C	14.14	3.97	4.57	0.57	0.12
Ash 1200°C	13.27	3.98	4.60	0.53	0.11
Ash 1300°C	14.62	3.87	4.60	0.59	0.11

Note: D-R - Dubinin-Radushkevich; BET - Brunauer-Emmet-Teller; H-K - Horvath-Kawazoe; CO_2 Ads data - CO_2 Adsorption data.

The micropore size distribution of all the samples obtained from CO_2 adsorption is given in **Figure 5.4**. The results show that the samples have a multimodal micropore size distribution in the range: 3Å ≤ d_p ≤ 5Å, where d_p, is the average pore diameter.

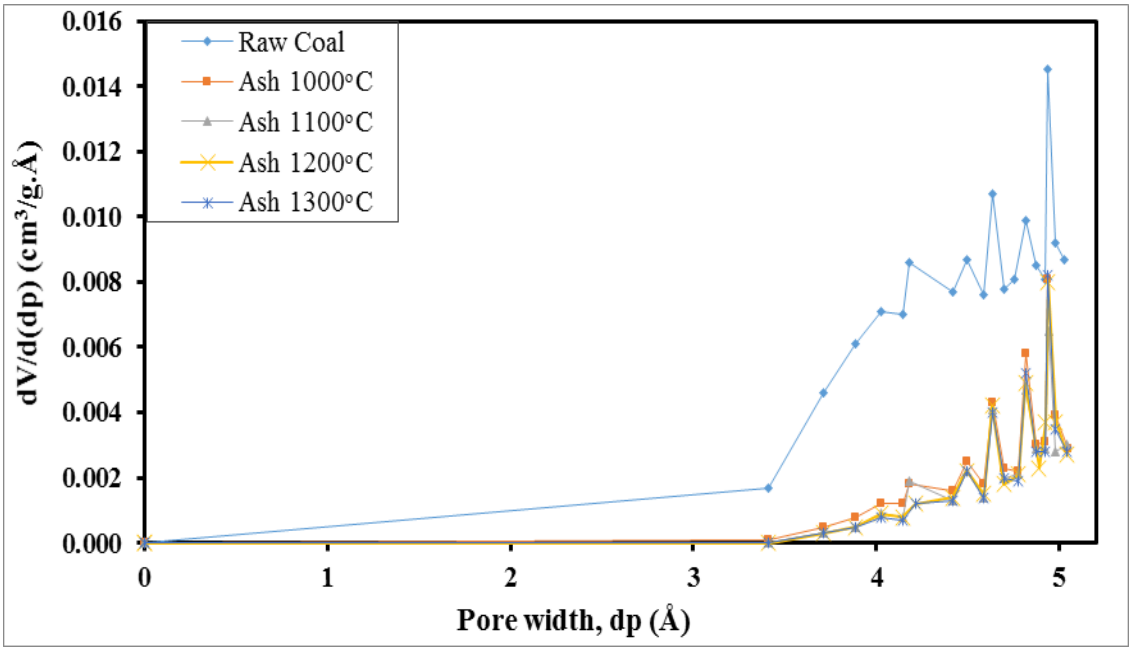

Figure 5.4: Micropore size distribution of the samples from CO_2 adsorption data

5.11.2 N_2 adsorption results

Figure 5.5 shows the N_2 adsorption-desorption isotherms of the raw coal and the ash produced at different temperatures, while a summary of the obtained results is given in **Table 5.11**. **Figure 5.5** illustrates that the N_2 adsorption-desorption isotherm of the coal sample exhibiteds a characteristic hysteresis loop arising from capillary condensation, peculiar to type IV isotherms (Sing *et al.,* 1985, Nandi and Walker, 1970). This means that the coal sample possesses both micropores and mesopores (Clarkson *et al*., 2012; Nie *et al.,* 2015; Okolo *et al.,*2015; Thommes, 2010), which is also evident from the relatively high CO_2 D-R micropore surface area (73.74 m^2/g) and N_2 BET surface area (7.62 m^2/g) (Table 5.11).

Contrary to the coal sample, the N_2 adsorption isotherms of all the ash samples followed a type III isotherm without the hysteresis loop, showing that the amount of N_2 gas adsorbed onto the ash pore surfaces increased without limit as its relative saturation approached unity. This shows that there was significant variation between the coal sample and ash produced at the various temperatures and it suggests that the ash samples may contain predominantly macropores and lesser proportions of mesopores (Thommes, 2010; Nie *et al.,* 2015; Okolo *et al.,*2015;). This can be corroborated by the relatively smaller N_2 BET surface areas (0.16 - 4.35 m^2/g), which decreased considerably with increasing ashing temperature. The total pore volume of the samples was found to decrease from the blended coal (2.18 $x10^{-2}$ cm^3/g) to the ash (0.019 - 1.31 $x10^{-2}$ cm^3/g); and further decreased with increasing ashing temperature. An opposite trend was observed for the N_2 adsorption determined BJH average pore diameter; with the Ash 1300°C having the highest value and the coal sample having the lowest value (**Table 5.11**). The results from the N_2 adsorption from this study compared well with the findings of other investigators (Schure *et al*., 1985). For all the surface area and porosity properties determined, CO_2 adsorption data returned higher values than results from N_2 adsorption, except for the average pore diameter.

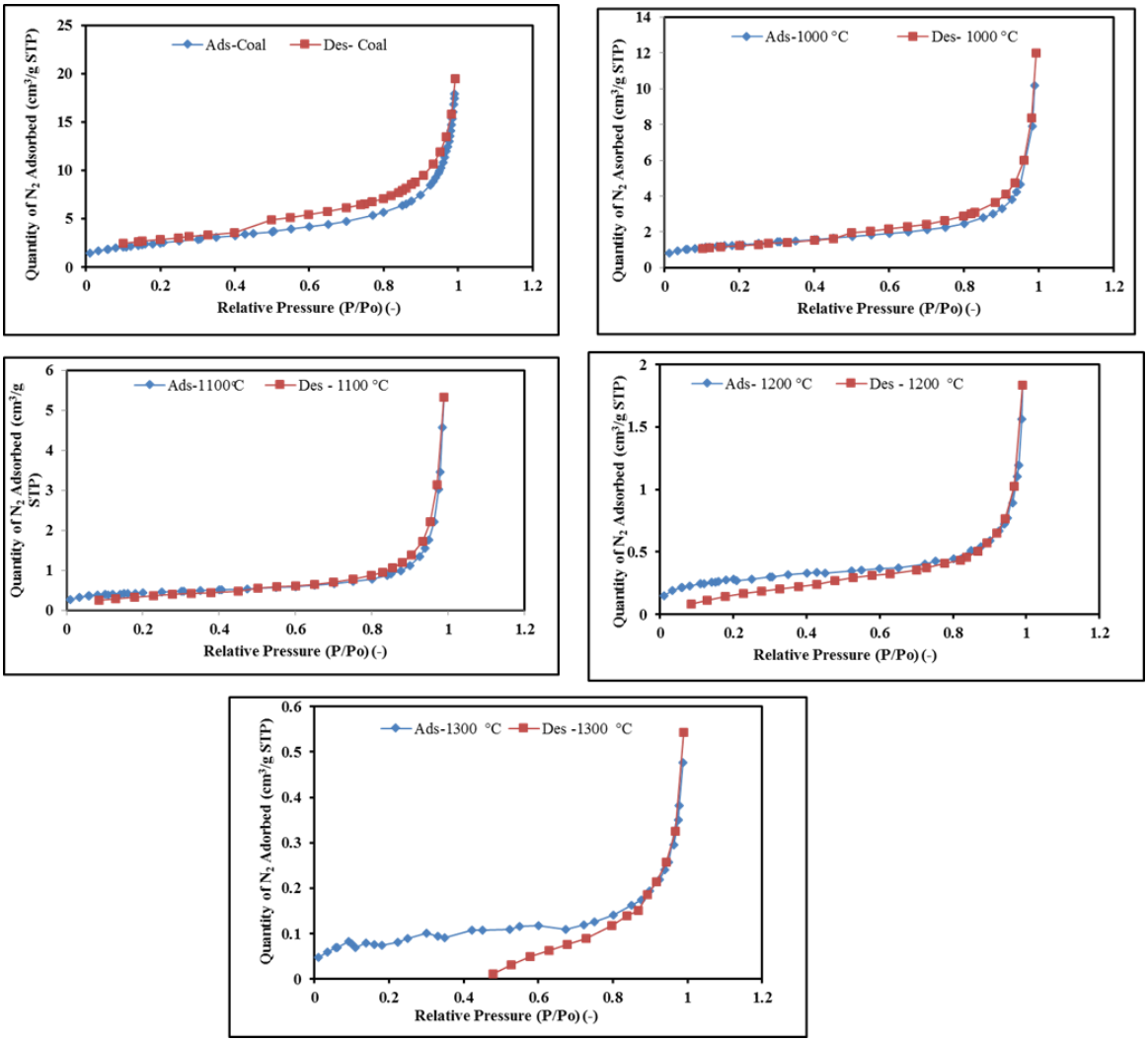

Figure 5.5: N_2 adsorption isotherms of the coal and ash samples

Table 5.11: Physical–structural properties of samples from N_2 gas adsorption

Properties / Sample ID	Surface area (m^2/g)	Total pore volume ($x10^{-2}$ (cm^3/g)	Average pore diameter (Å)
Methods used	BET	BJH	BJH
Blended Coal	7.62	2.18	85.29
Ash 1000°C	4.35	1.31	114.11
Ash 1100°C	1.43	0.47	138.72
Ash 1200°C	0.79	0.14	103.14
Ash 1300°C	0.16	0.019	358.71

Note: D-R - Dubinin-Radushkevich; BET - Brunauer-Emmet-Teller; BJH - Barrett-Joyner-Halenda.

5.12 Particle Size Distribution

Figure 5.6 shows the particle size distribution (PSD) profile of the blended coal samples and the ash produced at various temperatures used for this study. From **Figure 5.6**, a bimodal PSD was observed for all the samples, similar to the published findings of Jankowski *et al*. (2005). The major peaks were found between 1 µm - 100 µm and the minor peaks between 0.1 µm - 1 µm, except for the 1300°C sample with a minor peak around 25 µm. The particle size distribution is an important physical parameter that can aid during the characterisation of ash. Ash with smaller particles possesses higher surface areas compared with ash with larger particles, as can be seen from **Table 5.12** and **Figure 5.6**. Particle size distribution can also help in understanding the interaction between ash and the solution during the leaching process, as it affects the contact between the water and the material. It can thus affect the amount of ions that dissolve due to more or less contact between the water and the material. **Table 5.12** shows that the pulverised blended coal sample had the smallest particle sizes, and exhibited the highest surface area, which was greater than that of the ash produced at 1300°C by a factor of approximately 4 thus, particle size increased with increasing ashing temperature, resulting in a corresponding decrease in the surface area. Based on these results, it may be appropriate to infer that the blended coal sample has a better adsorption potential than the ash, with the ash produced at 1300°C having the lowest adsorption potential. These results corroborate the surface area and porosity results obtained from CO_2 and N_2 gas

adsorption, discussed in Section 5.11. Jankowski *et al*. (2005) noted that materials with high surface areas are prone to have particles that are irregular in shape compared with materials that have lower surface areas, which usually have particles that are spherical. SEM micro-morphology results of the ash (Section 5.10; **Figure 5.2**) support the findings. The finer texture of the ash produced at high temperatures used in this study shows some vital parameters such as water permeability and infiltration rate. Bayat (1998) stated in his study that low water permeability increases water runoff and the creation of hydraulic conditions in the ash structure, leading to retarding migration of trace elements and salt from the ash to the underground water.

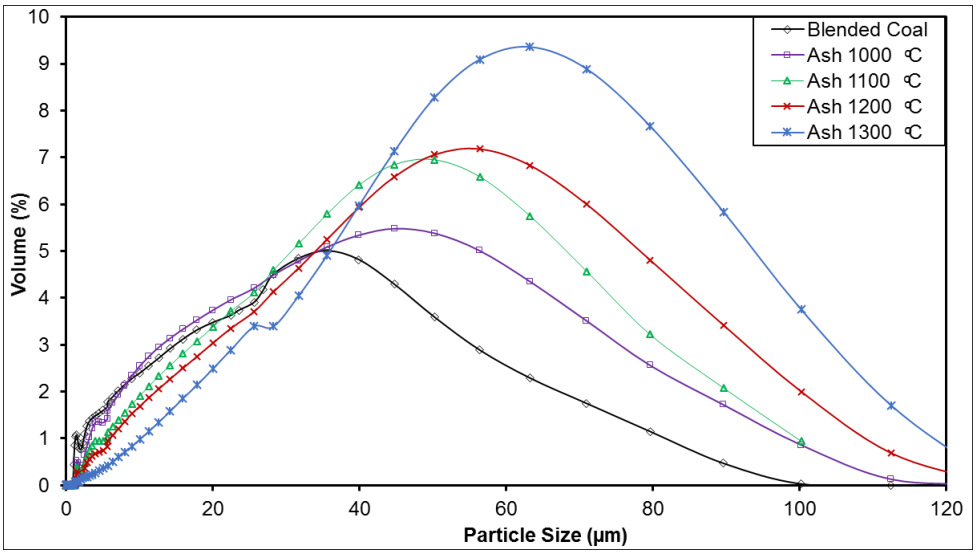

Figure 5.6: Percentage distribution of particle size in four fly ashes

Table 5.12: Selected physical parameters for particle size and surface area

Sample ID	Average particle size (µm)	Surface area (m^2/g)
Blended coal	67.617	0.721
Ash 1000 °C	68.571	0.479
Ash 1100 °C	72.273	0.384
Ash 1200 °C	81.282	0.327
Ash 1300 °C	91.606	0.193

5.13 Fourier Transform Infrared Spectroscopy (ATR-FTIR) analysis

FTIR analysis was done on the samples in order to show a change in the functional groups that occurred from the blended coal sample to the subsequent ash samples. The FTIR spectra of all the samples: blended coal and the four ash samples at different temperatures used for this study are shown in **Figure 5.7**. The procedure of analysis is presented in Section 4.10.

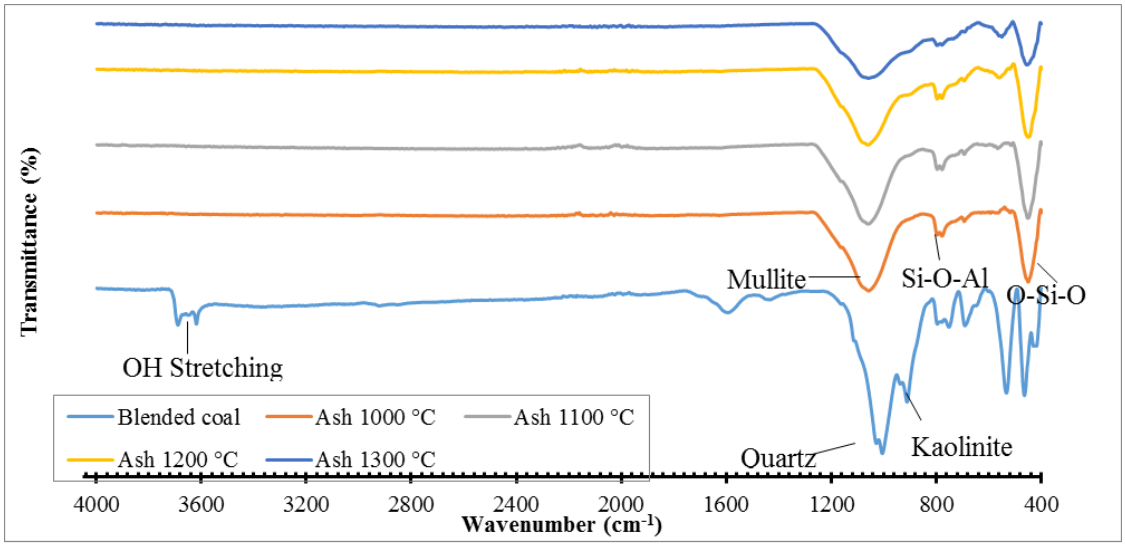

Figure 5.7: FTIR spectra of blended coal sample and ashes at 1000, 1100, 1200 and 1300°C

The FTIR spectra show the presence of some functional groups associated with silica: Si-OH, Si-O-Si, and O-Si-O groups. From **Figure 5.7**, small peaks were observed at 3618 cm^{-1} and 3689 cm^{-1} on the FTIR spectrum of the blended coal sample. This is attributed to the symmetric stretching vibration of the -OH group, thereby suggesting the presence of amorphous silica (glass), and clay minerals such as kaolinite and illite; $(Al(OH)_3$ and $Si(OH)_4$ or some other mineral containing water of crystallisation (Sembiring *et al*., 2014). The weak vibration at 1590 cm^{-1} signifies the presence of H_2O molecules in the blended coal sample (Adams, 2004), and the

peaks from 900-690 cm^{-1} are associated with the organic components of the blended coal sample (aliphatics, aromatics, trans and cis CH_2 saturated peaks, and C-H bending peaks).

Figure 5.7 also elucidates the effect of heat treatment on the functional groups in the samples. From **Figure 5.7**, it can be seen that all four ash samples have similar spectra. A distinctive peak at 1600 cm^{-1} for the blended coal sample was due to C=C stretching vibration with the aromatics rings of the blended coal. The peak observed at 1450 cm^{-1} could be observed to be the aliphatic C-H bending and 1490 cm^{-1} corresponds to the C=C aromatic stretching mode. The most significant transformation from that of the blended coal sample's spectrum is the absence of the peak from 1400-1600 cm^{-1}, which is associated with the organic (carbon) peaks, suggesting the liberation or release of some gases (CH_4, CO, CO_2) during the thermal treatment. Additionally, it was observed that the peak due to the stretching vibration of O-H at 3690 cm^{-1} disappeared in the spectra of the ash samples. This could be attributed to the evaporation of water molecules and the liberation of OH groups through the conversion of $Si(OH)_4$ and $Al(OH)_3$ into their various oxides (Alessio *et al*., 2000; Geng *et al*., 2009; Maity and Mukherjee, 2006; ; Mukherjee and Srivastava, 2006; Zhou *et al*., 2000).

The ash samples have bend vibrations at 444.78 cm^{-1}, a vibration possibly due to the bending vibration of the O-Si-O and Al-O functional groups. The doublet peak at around 1032 and 1008 cm^{-1}, together with a peak at around 912.01 cm^{-1}, is attributed to the presence of kaolinite (Mukherjee and Srivastava, 2006; Suraj *et al*., 1997). The band in the 1250-1000 cm^{-1} region of the blended coal became sharper and the small peaks at 1030 and 950 cm^{-1} combined to form only one peak at 1069.83 cm^{-1}, which suggests that, during heating, the disorderly phase of the kaolinite disappears, leading to the formation of orderly mullite.

The weak and wide peaks at 1069-1169 cm^{-1} are attributed to the Si-O-Si stretching vibration which is possibly due to the presence of mullite (Criado *et al*., 2005; Fernandez-Jimenez and Palomo, 2005a,b; ; Lee and van, 2002a,b; Swanepoel and Strydom, 2002; Sembiring *et al*., 2014). There was a shift in the wave number from 1069-1089 cm^{-1} with ash prepared at 1300°C to 1089 cm^{-1}, indicating the degree of mullitization. The intensity of this peak got broader as the temperature of heating

treatment increased. The peak at 692 cm^{-1} - 795 cm^{-1} implies the presence of quartz and amorphous silica/meta-kaolinite. These variations in the spectral features of the ash suggest the transformation of meta-kaolinite to mullite during the heat treatment process and further conversion of the meta-kaolinite in the amorphous phase to mullite.

Table 5.13: Peak assignment from FTIR spectra and characteristic transmittance intensity with respect to ashes.

Wavenumber (cm^{-1})	Band/peak assignment
3699-3588	OH stretch
3600-2200	H_2O Stretch
3217-3135	OH stretch
1700-1600	Bending vibration (HOH)
1200-950	Asymmetric stretching (Si-O-Si and Al-O-Si
1005-1068	Si–O stretch (SiO_4)
938-918	Al-Oh bending vibration
843-868	Al–O stretch (AlO_4)
673-721	T–O–T bend + Al-OH bend
547-576	Al–O stretch (AlO_6)
437-450	Bending (Si–O–Si and O–Si–O)
435 (s)	Kaolinite, bending (Si–O–Si and O–Si–O)

From the FTIR qualitative results, it is evident that significant transformation of mineral matter occurred during heat treatment of feed coal to ash. However, the influence of the ashing temperature on the spectra of the ash at different temperatures was only marginal. A summary of the band/peak assignment from the qualitative FTIR spectral analysis with respect to ash, compiled from the results from this study, as well as sthe reported findings of other investigators is given in **Table 5.13** (Beran *et al*., 2001; Denise *et al*., 2014; Suraj *et al*., 1997; Sembiring *et al*., 2014).

Chapter 6: Results and discussion of leaching of inorganic compounds into groundwater

6.1 Introduction

In this chapter, results obtained from the leaching experiments are presented and discussed. Leaching tests were conducted on the coal (which served as a control) and on the ash samples prepared at different temperatures. Three ashing temperatures: 1000°C, 1100°C, and 1300°C were used for the leaching experiments, since the ash samples prepared at 1200°C and 1300°C had similar chemical properties, as can be seen from the XRF and XRD results in Tables 5.4 and 5.9 (Sections 5.6 and 5.9, respectively). Particle sizes of < 1 mm were used for the leaching experiments in order to obtain maximum leaching effects. Two lixiviants were used, namely deionised water (DW) and water sampled from the UCG site (GW). The water from the underground site (i.e. GW) was sampled from the proposed UCG site in the Free State Province, South Africa.

Two sets of experiments were conducted during the batch and column leaching process: (1) the solution was left throughout the leaching process without sampling and (2) aliquot amounts of the leachate were taken over specified time intervals and at different leaching temperatures. The latter was conducted to study the effect of leaching temperature, ashing temperature and contact time on the dissolution of inorganic species. The results obtained from the two sets of experiments are discussed in detail in this chapter.

6.2 Groundwater analyses

Table 6.1 shows the composition of the groundwater that was used as a lixiviant during the leaching process. The analysis was done on the groundwater sample to evaluate the influence of groundwater during the leaching process. From **Table 6.1**, it can be seen that the groundwater sample was composed of relatively high amounts of Na species and Cl^- ions in the proportion of 5583.2 ppm and 5365.5 ppm, respectively. Other elemental species that were found in relatively high quantities were Ca: 79.45 ppm, K: 67.6 ppm, Mg: 13.0 ppm, NO_2^-: 14.9 ppm, NO_3^-: 5.4 ppm, Si: 5.0 ppm and Al: 1.2 ppm. Some of the species such as Fe and F^- were

found in minor quantities, while the trace elements were found in part per billion (ppb) amounts. The small amounts of the trace elements in the groundwater sample suggest that the water sample does not contain much of these pollutants.

The pH of the groundwater was found to be 7.65, therefore the water sample was slightly basic. The total dissolved solids (TDS), total alkalinity (TAL) and electron conductivity (EC) of the groundwater sample were found to be 8296.5 ppm, 143.8 ppm and 12.2 S/m, respectively.

Table 6.1: ICP-OES, ICP-MS and IC results of groundwater (GW) from the Theunissen (UCG) site.

Elements	Concentration (ppm)	Anions	Concentration (ppm)	Elements	Concentration (ppb)
Ca	79.5±3.0	SO_4^{2-}	5.3±1.3	Ba	2361.0±952.0
Mg	13.0±5.0	NO_2^-	14.9±3.9	Cu	58.2±3.6
Al	1.2±0.01	NO_3^-	5.4±2.14	Co	1.1±0.1
K	67.55±5.0	Cl^-	5365.5±180.0	Cr	90.0±10.0
Fe	0.87±0.13	F^-	1.0±0.01	Cd	3.0±0.3
Si	5.0±0.45			Pd	11.7±0.7
Na	5583.2±95.2			Au	0.23±0.004
TAL	143.8±27.0			Ag	29.82±3.2
pH	7.65±0.7			Ni	0.17±0.003
TDS	8296.5±161.7			Hg	0.06±0.003
EC	12.2±1.3 S/m			Se	119.5±30.28
				Zn	5.1±1.2

6.3 Batch leaching

The results obtained during the batch leaching tests at room temperature and at 50^{o}C leaching temperature will be discussed in detail in this section. The background and procedure were explained in Sections 3.13.1 and 4.14. The batch leaching tests were conducted in duplicate, the mean and the standard errors were calculated and reported in **Table 6.2**.

6.3.1 Batch leaching at room temperature

The following results obtained during the batch leaching at room temperature will be discussed in this section: leachate analyses and effect of pH, EC, total dissolved solids and alkalinity at room temperature.

6.3.1.1 Leachate analyses (ICP-OES)

Results obtained from the leaching experiments at room temperature are presented in **Table 6.2**. For the coal sample, it was observed from **Table 6.2** that the most leached were Ca species with a concentration of 96.0 ppm. Other leachants that were found during the leaching test at room temperature when DW was used as lixiviant included Mg: 5.2 ppm, Al: 1.6 ppm, K: 25.8 ppm, Fe: 0.9 ppm, Si: 1.7 ppm, Na: 55.43 ppm. The concentrations of these species in coal when groundwater (GW) was used as lixiviant were found to be Ca: 150 ppm, Mg: 17.5 ppm, Al: 2.4 ppm, K: 90.0 ppm, Fe: 1.81 ppm, Si: 6.5 ppm, Na: 5603.6 ppm. When comparing the leachants from coal when the two lixiviants were used, it was found that the concentrations of some of the species (Ca, K, Mg, K, and Na) were higher when GW was used as lixiviant, relative to when DW was used. The increase in concentrations could be attributed to the presence of these individual species and ions in the groundwater (**Table 6.1**).

The amounts of the leachants from the ash samples are also presented in **Table 6.2**. From the table, it was also observed that the most leached species is Ca, with values ranging from 125.5 - 265.0 ppm when DW was used as lixiviant at room temperature. The concentrations of other leachants were found to be smaller with values ranging from: Mg: 3.5 - 7.5 ppm, Al: 0.6 - 2.5 ppm, K: 25.4 - 40.0 ppm, Fe: 0.8 - 1.92 ppm, Si: 6.8 - 11.9 ppm, Na: 45.5 - 98.4 ppm, when DW was used as lixiviant. Consequently, when GW was used as lixiviant at room temperature, the concentration of the most leached species (Ca) ranged from 185.5 - 350 ppm, with a lower leaching of Mg: 19.2 - 21.9 ppm, Al: 2.1 - 4.0 ppm, K: 86.2 - 95.5 ppm, Fe: 1.8 - 3.8 ppm, Si: 12.0 - 18.5 ppm, Na: 5625.0 - 5657.0 ppm. When comparing the leachants from ash samples when the two lixiviants were used it was found that the concentrations of some of the elemental species (Ca, K, Mg, K, Na) were higher when GW was used as lixiviant to when DW was used. The increase in

concentrations could be attributed to the presence of these individual species and ions in the groundwater (**Table 6.1**).

It is worthy to note that the concentrations of the leachants were more for 1000^{o}C and 1100^{o}C ashing temperature samples but decreased for the 1300 ^{o}C ashing temperature sample. This decrease could be attributed to the mineralogy of the sintered ash and the fusion of the inorganics at 1300^{o}C, thereby inhibiting the dissolution of these individual species. Also, it was observed that the concentration of Na element species and Cl^- ions were relatively high when GW was used as a lixiviant compared with when DW was used. This increase may be as a result of the concentration of elemental Na and Cl^- ions in the groundwater (**Table 6.1**).

6.3.1.2 Leachate analyses (IC results)

IC results of the leaching experiments at room temperature are presented in **Table 6.3**. From **Table 6.3**, it can be observed that the most leached anion for the leachate from coal sample was SO_4^{2-} ions with a concentration of 69.5 ppm when DW was used as lixiviant. Other anions that were found when DW was used as lixiviant included NO_3^-: 6.7 ppm, NO_2^-: 1.0 ppm, Cl^-: 40.0 ppm, and F^-: 0.6 ppm. The concentrations of the anions when GW was used were found to be SO_4^{2-}: 89.1 ppm NO_3^-: 20.0 ppm, NO_2^-: 6.1, Cl^-: 5403.5 ppm, and F^-: 2.0 ppm. Nonetheless, when comparing concentrations of the anionic leachants from the coal sample at room temperature using the two lixiviants, it was found that the concentrations of the leachants from GW was relatively high compared with that observed for DW. This increase could be attributed to the concentration of these anions in the groundwater (**Table 6.1**).

The concentration of anions from the leachates obtained from the ash samples at room temperature was also investigated and results summarised in **Table 6.3**. From the results in **Table 6.3** it can be observed that the concentration of the most leached anions ranged from 75.2 - 696.7 ppm (SO_4^{2-}) when DW was used as lixiviant at room temperature. The concentrations of other anions were smaller when compared with the most leached anions, with values ranging from NO_3^-: 1.3 - 8.1 ppm, NO_2^-: 1.1 - 3.2 ppm, Cl^-: 30.0 - 78.5 ppm, and F^-: 0.6 - 2.8 ppm when DW was used as lixiviant at ambient leaching temperature. When GW was used as lixiviant at ambient

leaching temperature for the ash sample leachates, the concentration of the most leached anions (SO_4^{2-}) ranged from 87.9 - 738.7 ppm, with minor anionic concentrations ranging from NO_3^-: 14.3 - 21.0 ppm, NO_2^-: 5.1 - 9.2 ppm, Cl^-: 5385.5 - 5425.6 ppm, and F^-: 2.4 - 4.3 ppm. The concentrations of the anions were moderately higher when GW was used as lixiviant with respect to when DW was used as lixiviant for the ash sample leachates at ambient temperature. The concentration increase could be attributed to the concentrations of the anions in the groundwater sample (**Table 6.1**).

6.3.1.3 Influence of liquid to solid ratio on the leachants at room temperature

Liquid-to-solid ratios of the samples during leaching were evaluated to study the influence of an increase in the coal and ash samples to the release of the leachants. The ratios were set at 10:1 and 10:2. The results obtained using the different liquid-solid ratios are reported in Tables 6.2 and 6.4. When 10 g of ash was in contact with 100 ml of the lixiviants (10:1), the concentration of elemental Ca species dissolved in the deionised water ranged from 125.5 - 265.0 mg/l for DW and 185.5 - 350 mg/l for GW. Similarly, SO_4^{2-} anion values ranged from 75.2 - 696.7 ppm for DW and 87.9 - 738.7 ppm for GW. The concentrations of other species in the leachate were also slightly increased (**Table 6.2**). However, with a liquid-to-solid ratio of 10:2, the concentrations of the element were found to decrease as can be seen in **Table 6.4**

The concentrations of individual species decreased when the liquid to solid sample ratio decreased, showing that there was an inverse relationship between the amount of ash that came in contact with lixiviants and the amounts of species released into the groundwater. This decrease shows that, once saturation is reached during batch leaching, increasing the amount of ash in contact with water will have no effect on the amount of species and ions released to the groundwater.

Table 6.2: ICP-OES results of batch leaching of inorganic species from coal and ash samples used for this study at room temperature and 50°C leaching temperatures (10:1).

Samples	Ca	Mg	Al	K	Fe	Si	Na	TAl	pH	TDS	EC (S/m)
Coal DW	98.0±6.0	5.2±0.0	1.6±0.04	25.0±1.66	0.9±0.04	1.7±0.08	55.4±5.2	51.2±12.3	7.6±0.3	298.5±100.0	0.6±0.1
Coal GW	150.0±7.8	17.5.0±3.9	2.4±0.05	90.0±10.8	1.8±0.05	6.5±0.48	5603.8±120.2	175.0±29.0	8.1±0.39	7986.5±871.0	14.1±2.1
Ash 1000 °C DW	238.0±4.0	4.2±1.3	2.5±0.05	32.1±0.5	1.9±0.06	10.1±0.47	98.8±2.3	72.3±19.1	9.2±0.5	895.0±80.0	2.0 ±1.0
Ash 1000 °C GW	300.5±9.0	19.7±2.0	4 .0±0.2	92 .0±6.0	3.6±0.59	16.5±1.7	5657.0±85.2	168.8±7.3	10.3±0.6	8584.5±743.0	14.2±0.8
Ash 1100 °C DW	265.0±73.8	7.5±0.1	2.0±0.01	40.0±3.4	1.8±0.03	11.9±1.24	85.7±0.5	45.0±10.0	9.7±1.0	691.0±72.8	2.5±2.6
Ash 1100 °C GW	350.0±59.0	21.9±7.0	3.3±2.5	95.5±23.0	3.8±0.1	18.0±8.3	5636.2±104.2	178±5.0	10.9±0.2	8789.5±175.0	14.5±1.4
Ash 1300 °C DW	125.5±13.0	3.5±1.3	0.6±0.03	25.4±0.21	0.8±0.01	6.8±0.71	45.5±0.2	35.0±53	7.6±0.4	195.0±25.0	2.0±2.9
Ash 1300 °C GW	185.0±9.0	19.0±6.3	2.1±0.08	86.2±16.1	1.8±0.09	12.0±1.1	5625.0±64.2	170.0±10.0	8.2±0.4	8296.5±161.7	12.2±1.3
Groundwater	79.45±3.0	13.0±5.0	1.2±0.01	67.55±5.0	0.87±0.13	5.0±0.45	5583.2±95.2	143.8±27.0	7.65±0.7	8063.5±414.0	13.0±0.3
DWAF MR risk	-	-	0.43	-	9	-		-	-	-	-
Batch leaching 50°C (mg/l) (10:1) liquid/solid ratio											
Coal DW	120.0±12.0	6.8±0.7	2.7±0.01	30.9±0.7	1.2±0.04	3.2±1.5	108.0±12.2	84.0±10	8.0±0.2	375.8±86.0	0.9±0.2
Coal GW	204.0±10.0	20.0±2.3	3.3±0.6	105.3±9.3	2.8±1.1	8.7±1.0	5684.7±210.2	182.5±5.0	8.2±0.4	9635.5±147.0	15.6±1.2
Ash 1000 °C DW	317.0±29.4	9.3±0.2	2.5±0.08	40.0±5.0	1.8±0.1	13.3±2.0	104.4±1.2	61.5±8.0	10.9±0.0	923.0±101.0	2.0±1.3
Ash 1000 °C GW	410.5±9.0	21.9±1.4	4.6±0.3	116.7±6.4	3.8±0.6	19.6±3.0	5683.0±324.2	178.0±15.0	11.2±0.3	9968.5±247.0	16.0±0.9
Ash 1100 °C DW	373.0±20.0	11.2±0.4	2.8±0.4	60.2±4.7	2.5±0.06	15.0±1.0	99.0±1.2	45.0±19.0	10.4±0.2	893.0±119.0	2.3±0.2
Ash 1100 °C GW	463.0±15.0	24.0±6.0	4.2±0.8	136.5±21.6	4.8±0.04	24.5±2.0	5665.4±345.7	161.4±8.0	10.6±0.4	10111.5±375.0	16.2±0.6
Ash 1300 °C DW	155.3±8.2	7.2±0.05	1.7±0.02	32.7±0.5	1.2±0.03	7.0±3.0	76.5±1.3	38.3±12.3	7.3±1.0	293.8±257.0	1.4±2.2
Ash 1300 °C GW	225.0±20.0	21.6±2.3	3.2±0.3	95.9±13.4	2.5±1.2	14.0±1.0	5651.9±107.2	102.0±16.0	7.8±0.5	9262.3±612.0	14.1±1.2
Groundwater	79.45±3.0	13.0±5.0	1.2±0.01	67.55±5.0	0.87±0.13	5.0±0.45	5583.2±95.2	143.8±27.0	7.7±0.7	8063.5±414.0	13.0±0.3
DWAF MR risk	-	-	0.43	-	9	-		-	-	-	-

DW: deionised water; GW: groundwater; DWAF MR: Department of Water Affairs and Forestry Minimum Requirements; TDS: total dissolved solids; EC: electrical conductivity; TAl: Total alkalinity

Table 6.3: IC results of batch leaching of Ions from coal and ash samples at room temperature and 50°C.

Batch leaching room temperature (ppm) (10:1) liquid/solid ratio					
	SO_4^{2-}	NO_3^-	NO_2^-	Cl^-	F^-
Samples			*mg/l*		
Coal DW	69.5±8.7	6.7±4.9	1.0±0.01	40.0±2.2	0.6±0.2
Coal GW	89.1±6.0	20.0±2.7	6.1±0.2	5403.5±155.0	2.0±0.5
Ash 1000 °C DW	262.5±30.5	8.1±1.3	2.4±0.7	56.5±6.9	2.3±0.02
Ash 1000 °C GW	295.9±27.6	20.5±1.9	8.3±0.4	5415.0±37.2	4.3±4.25
Ash 1100 °C DW	696.7±22.8	3.2±4.0	3.2±0.1	78.5±32.3	2.8±0.02
Ash 1100 °C GW	738.7±7.1	21.0±5.8	9.2±0.4	5425.5±79.4	4.1±1.2
Ash 1300 °C DW	75.2±20.0	1.3±0.2	1.1±0.0	30.0±3.9	0.6±0.1
Ash 1300 °C GW	87.9±20.0	14.3±1.7	5.1±0.4	5385.5±2.9	2.4±0.2
Groundwater	5.3±1.3	14.9±3.9	5.4±2.14	5365.5±180.0	1.0±0.01
Batch leaching 50°C (ppm) (10:1) liquid/solid ratio					
Coal DW	126.4±7.1	9.1±1.9	2.2±0.4	60.2±4.9	1.5±0.35
Coal GW	143.9±19.7	24.0±1.0	7.9±2.0	5458.1±456.8	1.8±0.1
Ash 1000 °C DW	386.4±24.2	1.2±0.8	3.5±0.1	87.9±2.4	2.5±0.2
Ash 1000 °C GW	443.4±12.9	18.6±1.2	8.8±1.3	5490.0±247.0	3.7±0.01
Ash 1100 °C DW	872. 5±14.4	1.8±1.1	4.1±0.2	95.4±5.3	2.0±0.2
Ash 1100 °C GW	905.8±30.8	19.1±0.6	9.0±2.1	5502.3±200.5	4.7±1.23
Ash 1300 °C DW	88.5±6.8	1.2±2.1	2.1±0.1	50.75±3.6	0.9±0.02
Ash 1300 °C GW	105.4±9.1	17.6±1.3	6.55±0.12	5420.85±29.7	2.9±0.5
Groundwater	5.3±1.3	14.9±3.9	5.44±2.14	5365.5±180.0	1.0±0.01

DW: deionisedwater; GW: groundwater

Table 6.4: ICP-OES results for batch leaching at room temperature and 50 °C. Using GW with a liquid-solid ratio of 10:2.

Batch leaching at room temperature (mg/l**) (10:2)**							
Samples	**Ca**	**Mg**	**Al**	**K**	**Fe**	SO_4^{2-}	**Si**
Coal GW	110.0	13.1	1.2	42.3	0.3	45.0	3.7
Ash 1000°C GW	186.0	10.5	1.6	56.4	1.6	182.0	12.5
Ash 1100°C GW	254.0	12.0	1.8	68.0	3.0	543.0	9.2
Ash 1300°C GW	105.0	11.2	1.1	50.4	0.7	54.0	4.8
Batch leaching 50 °C (ppm) (10:2)							
Samples	**Ca**	**Mg**	**Al**	**K**	**Fe**	SO_4^{2-}	**Si**
Coal GW	124.2	15.0	1.6	65.2	1.3	122.3	4.3
Ash 1000°C GW	245.2	14.5	1.9	96.5	2.4	352.4	15.3
Ash 1100°C GW	380.6	15.4	2.5	79.5	4.0	780.9	16.6
Ash 1300°C GW	150.2	11.2	1.5	70.3	1.5	85.4	5.9

6.3.1.4 Change of pH, EC, total dissolved solids and alkalinity at room temperature

The change in pH, EC, total dissolved solids and alkalinity of the leachates was tested at room temperature and the results are presented in **Table 6.2**. The pH of the leachates from the coal sample for DW and GW was 7.80 and 8.26, respectively. The solutions were thus all slightly basic. For the leachates from 1000°C and 1100°C ash samples, there was an increase in the pH from 9.2 for the 1000 ^{o}C ash sample to 10.3 for the 1100^{o}C ash sample. The leachate pH values for the 1100^{o}C ash sample ranged from 9.7 - 10.9 for both lixiviants at room temperature. The pH of the leachate for 1300^{o}C ash decreased to a value ranging from 7.6 - 8.2 for both lixiviants at room temperature. Results from XRD in **Table 5.9** could be used to explain the drop in pH for the leachate from the 1300°C ash sample. From XRD, it was found that the ash produced at 1300°C contained the majority of the crystalline phase, which was fused together (**Table 5.9**). Since the ash produced at 1300°C agglomerated, it is expected that the dissolution of the inorganic species will be low, thereby having less influence on the pH.

Table 6.2 also shows the electrical conductivity (EC), which indicates the level of salinity of the water. It can be seen from **Table 6.2** that the groundwater EC was similar to that of the coal sample when GW and DW were used as lixiviants. However, EC of the leachates from the 1000°C and 1100°C ash were found to be high when compared with that of 1300°C ash. This increase may be due to the relatively high dissolution of the elemental species of the 1000°C and 1100°C ash samples. For the leachate from the 1300°C ash sample, the EC decreased as expected, which could be as a result of the decrease in the dissolution of the species and ions.

When comparing the EC of the leachate from the DW and GW experiments at room temperature, it was observed that the leachate from the GW experiment had a higher EC compared with the leachate from the DW experiment. This increase in EC could be as a result of the contribution of the dissolution of species and ions already in the groundwater when GW was used as lixiviant.

The total dissolved solids (TDS), which are not necessarily pollutants, but indicative of the amount of solids that dissolve in the lixiviants, increased for the leachates for the coal to the leachates from the 1000°C and 1100°C ash samples, but was reduced for the 1300°C ash samples. The TDS of the leachate obtained from the coal and the ash samples ranged from 8378.5 - 8963.5 mg/l when GW was used, which can be considered as moderately saline. On the other hand, when DW was used, the TDS ranged from 149.0 - 936.0 mg/l. The low values of TDS obtained for DW shows that the leachate produced by DW has less impurities when compared with leachants obtained when GW was used as lixiviant.

The National ground water association define total dissolve solid in water as follows; TDS lower than 1000 - 3800 mg/l is slightly saline, 3000 - 10000 mg/l is moderately saline and 10000 - 35000 mg/l is brine. These values suggest that the leachate obtained when groundwater was used as a lixiviant in this study at room temperature is moderately saline. The reason for the high salinity was attributed to the concentration of TDS in the groundwater (8272.5 mg/l).

The alkalinity was found to range from 168.8 - 175.0 mg/l when GW was used for the leaching test, indicating that the leachate is moderately or relatively hard water. Using DW, the alkalinity was low, ranging from 35.0 - 72.3 mg/l. The relatively high alkalinity for GW could be attributed to the alkalinity of the groundwater. Mato (2002) further demonstrated that water with an alkalinity of 0 - 60 mg/l is soft, 61 - 120 mg/l is moderately hard and 121 - 180 mg/l is described as hard water.

6.3.2 Leaching results for 50°C

The following results obtained during the batch leaching tests at 50°C will be discussed in this section: leachate analyses, change of pH, EC, total dissolved solids and alkalinity, results of the continuous leaching test at 50^{o}C and relative solubility of leachants from the coal and ash samples at 50°C.

6.3.2.1 Leachate analyses (ICP-OES)

The results of the leaching experiments at 50°C are given in **Table 6.2**. It was observed that the concentration of the most leached species (Ca) for the coal sample at 50^{o}C was 120.0 ppm. When deionised water (DW) was used as lixiviant, it

showed concentrations of Mg: 6.8 ppm, Al: 2.7 ppm, K: 30.9 ppm, Fe: 1.2 ppm, Si: 3.2 ppm, Na: 108.0 ppm. Similarly, the concentrations of the leachants from the coal sample when groundwater was used (GW) were: Ca: 204.0 ppm, Mg: 20.0 ppm, Al: 3.3 ppm, K: 105.2 ppm, Fe: 2.8 ppm, Si: 8.7 ppm, Na: 5684.7 ppm. The concentrations of these leachants when GW was used were relatively high compared with the leachants obtained when DW was used as a lixiviant. It was also observed that there was a relative increase in the concentrations of the leachants from the coal sample for both lixiviants at 50^{o}C when compared with leaching at room temperature.

The results of the concentrations of the leachants from the ash samples at 50^{o}C leaching temperature are presented in **Table 6.2**. Again it was observed that the most leached species was elemental Ca. The concentration of Ca ranged from 153.3 - 373.0 ppm using DW. Other leachants that were obtained from the ash samples at 50 ^{o}C leaching temperature include: Mg: 7.2 - 11.2 ppm, Al: 1.7 - 2.8 ppm, K: 32.7 - 60.2 ppm, Fe: 1.2 - 2.5 ppm, Si: 7.0 - 15.0 ppm, Na: 76.5 - 104.4 ppm, when DW was used as lixiviant. The concentrations of these individual leachants increased when GW was used as lixiviant for the different ash samples at 50^{o}C leaching temperature; Ca: 225.0 - 463 ppm, Mg: 21.6 - 24.0 ppm, Al: 3.2 - 4.6 ppm, K: 95.9 - 136.5 ppm, Fe: 2.5 - 4.8 ppm, Si: 14.0 - 24.5 ppm, Na: 5651.0 - 5685.0 ppm. Comparing the concentrations of the leachants when the two lixiviants were used, it was found that concentrations were relatively high when GW was used as lixiviant and this increase could be attributed again to the presence of these leachants in the groundwater (**Table 6.1**). The concentrations of leachants increased at 50°C, meaning that an increase in the leaching temperature influenced the concentrations of species and ions in the leachate.

6.3.2.2 Leachate analyses (IC)

IC results of the leaching experiments at 50^{o}C leaching temperature are presented in **Table 6.3**. The concentration of the most leached anion, SO_4^{2-}, was observed to be 116.5 ppm when DW was used as lixiviant for the coal sample leachate at 50^{o}C leaching temperature. Minor concentrations of the following anions were present; NO_3^-: 1.1 ppm, NO_2^-: 0.02 ppm, Cl^-: 60.2 ppm, and F^-: 1.53 ppm. Similarly, the anionic concentrations of the leachants when GW was used as lixiviant were SO_4^{2-}:

143.9 ppm, NO_3^-: 20.0 ppm, NO_2^-: 7.9 ppm, Cl^-: 5458.0 ppm, and F^-: 1.73 ppm. The concentrations of these anions when GW was used as lixiviant were relatively high when compared with results obtained when DW was used as lixiviant for the coal sample leachate at 50^{o}C leaching temperature. This increase could be attributed to the concentrations of the anions in the groundwater (**Table 6.1**). It was also observed that there was a slight increase in the concentration of the anions from the coal sample leachate for both lixiviants at 50^{o}C when compared with the leaching at room temperature.

The results of the anionic concentrations from the ash sample leachates at 50^{o}C are presented in **Table 6.3**. Again it was observed that SO_4^{2-} was the most leached anion with concentration ranges of 366.4 - 852.5 ppm when DW was used as lixiviant. Other anionic leachants from the ash sample leachates at 50^{o}C leaching temperature included NO_3^-: 1.2 - 1.8 ppm, NO_2^-: 0.01 - 0.05 ppm, Cl^-: 50 - 87.9 ppm, and F^-: 0.23 - 1.04 ppm when DW was used as lixiviant. The concentrations of the individual anions increased when GW was used as lixiviant for the different ash sample leachates at 50 ^{o}C leaching temperature with values ranging from SO_4^{2-} : 105.4 - 905.8 ppm, NO_3^-: 17.6 - 19.1 ppm, NO_2^-: 4.5 - 9.0 ppm, Cl^-: 5420.3 - 5502.3 ppm, and F^-: 0.23 - 4.7 ppm.

When comparing the concentrations of the anionic leachants when the two lixiviants were used for the ash sample leachates, it was found that concentrations were relatively high when GW was used as lixiviant and this could be attributed again to the presence of these leachants in the groundwater (**Table 6.1**). The concentrations of leachants increased at 50°C leaching temperature, meaning that an increase in the leaching temperature influenced and specifically increased the concentration of anions in the leachate.

6.3.2.3 Influence of liquid to solid ratio on the leachants from 50^{o}C

The amounts of species released per gram of ash in contact with water were calculated to evaluate the influence of the liquid-to-solid ratio on the leachate. **Table 6.4** presents the results, which followed the same trend as that observed at room temperature, but the concentrations at 50°C increased when compared with that obtained at room temperature. For example, for the 1000°C ash, the amount of Ca

released for 20 g of ash per 100 ml of water and 10 g of ash per 100 ml of lixiviant were 245.2 mg/l and 366.5 mg/l, respectively. For SO_4^{2-}, the values were 352.4 mg/l and 852.5 mg/l for 20 g of ash per 100 ml of lixiviant and 10 g of ash per 100 ml of water, respectively. This decrease in the concentration when the ash was increased and the liquid kept the same shows that the increase of ash in the solution did not increase the concentration of elements or ions leached into groundwater. A similar trend, but lower concentrations of the leachants, was observed for leaching at room temperature. At 50°C leaching temperature, it was also observed that the concentration of leachants from the 1300°C sintered ash (when the inorganic compounds were fused, sintered and encapsulated into the ash matrix) was lower compared with the 1000°C and 1100°C ash samples.

6.3.2.4 Change in pH, EC, total dissolved solids and alkalinity at 50°C

The change of pH, EC, total dissolved solids and alkalinity were also tested at 50°C leaching temperature and the results are presented in **Table 6.2**. It was found that the EC and TDS increased as the leaching temperature increased, indicating that the leaching temperature influences the concentrations of dissolved inorganic species in the leachate. A drop in pH was also observed from 11.0 for the 1000 °C ash sample to 10.0 for 1100°C ash sample, and 8.0 for 1300°C ash sample. The drop in pH could be attributed to the lower dissolution of species in the water following high-temperature ashing. Similar findings in the reduction of the concentration of species and pH in the leachate at higher temperatures of ashing were reported by Dalton and Campbell (1978). The pH values at 50°C followed similar trends than that obtained at room temperature.

6.3.2.5 Results of continuous leaching test at 50ºC

A continuous batch leaching experiment was carried out on the ash samples (1000 °C, 1100°C and 1300°C) at 50°C leaching temperature. The continuous leaching test was done to ascertain the influence of recycling of the leachate after the initial leaching experiment. The continuous batch leaching test was achieved by initially leaching the samples for 24 hours and filtering the samples. Fresh ash was added to the already filtered leachate and the second leaching step was carried out with the initial leachate and fresh ash for another 24 hours. The results after the second leaching step are summarised in **Table 6.5**. It was evident that the concentrations of

some of the species obtained in the leachate increased two-fold when compared with the concentrations of species in the 50°C leachate (**Table 6.5**). The increase in the leachant concentrations could be attributed to the dissolution of species from the fresh ash samples added. Furthermore, introducing fresh ash will invariably increase the concentration of the dissolved species or elemental species in the initial lixiviants, but at some stage saturation of the leachant will occur.

Table 6.5: ICP-OES results of batch leaching of inorganic elements from coal and ash samples used for this study at room temperature and 50°C continuous leaching process.

	Batch at 50°C Continuous leaching process (ppm)										
	Ca	Mg	Al	K	Fe	SO_4^{2-}	Cl^-	NO_3^-	AL	pH	TDS
Ash 1000 °C DW	619.4	15.76	3.33	57.23	1.48	1009.93	8.71	24.65	60.00	8.67	185.
Ash 1000 °C GW	680.6	30.77	6.30	176.60	2.63	1432.55	8493.72	30.95	172.50	9.85	13000
Ash 1100 °C DW	475.1	19.56	4.48	89.93	1.11	1484.09	5.96	19.68	40.00	9.89	1215
Ash 1100 °C GW	743.3	40.05	7.51	158.60	3.77	1858.36	7304.44	21.23	180.00	9.54	11459
Ash 1300 °C DW	350.97	12.13	2.56	62.75	1.12	277.98	2.93	16.18	35.00	8.02	312.
Ash 1300 °C GW	450	25.66	4.31	120.49	2.50	207.33	7379.78	24.87	120.00	8.01	10647
Ground water	79.45±3.0	13.0±5.0	1.2±0.01	67.55±5.0	0.87±0.13	5.3±1.3	5365.5±180.0	14.9±3.9	143.8±27.0	7.65±0.7	8063.5±

6.3.2.6 Relative solubility of leachants in the coal and ash samples during leaching at 50 °C

The relative solubility of each of the species leached out from the coal and ash samples used for this study were evaluated using Equation 6.2 as proposed by (Kim *et al.*, 2003). The relative solubility was calculated for the leachate at 50°C because at this temperature the concentrations of the species in the leachate were high compared with that at ambient temperature. This was achieved by first calculating the aggregate quantity of leachants per unit sample mass and dividing it by the concentration of that species in the ash sample. The agregate quantity of an leachant extracted per unit sample (M_L) corresponds to the totality of the concentrations evaluated in each leachate sample multiplied by the volume of lixiviant used and divided by the total mass of the sample used during the experiment (Equation 6.1).

$$M_L = \frac{\sum C*V}{S} \tag{6.1}$$

where:

M_L = Agregate quantity extracted in mg/kg;

C = concentration of the individual leachants species (mg/l);

V = volume of lixiviant in ml;

S = sample mass in g.

The relative solubility of each element of the ash ($M_{L/T}$) was defined as the agregate quantity extracted per unit sample (M_L) divided by the concentration of that leachants in the in the initial ash sample (M_T) (Equation 6.2).

$$M_{L/T} = \frac{M_L}{M_T} \tag{6.2}$$

where:

$M_{L/T}$ = mass extracted relative to the total concentration in the ash;

M_L = agregate quantity extracted from the ash sample in mg/kg;

M_T = total concentration of the leachants in the initial ash composite in mg/kg.

Table 6.6 summarises the relative values from the M_L and M_T of the samples, and the relative solubility is reported in **Table 6.6** and **Figure 6.1**. From the M_T values in **Table 6.6**, it was observed that the M_T for Si and Al were much higher than the other element in the coal and ash samples, which implies that the major species in the coal and the ash samples were Si and Al. The M_T results was obtained using ICP-OES method and the results determind is in agreement with the XRF analyses of the coal and ash samples as shown in **Table 5.4**. The concentrations of the trace elements were found to be low. The M_L data shows the cumulative amount of the leachant extracted from the samples.

Table 6.6: Elemental concentration (MT) obtained by ICP-MS of coal and ash samples and cumulative amount leached (ML in mg/kg) at 50°C.

Elements	A M_T	A M_L	B M_T	B M_L	C M_T	C M_L	D M_T	D M_L
Ca	5500	1245	12200	3305	12500	3855	13300	1455
Mg	2200	70	4200	82	3600	110	4100	86
Al	54900	20	92900	34	92600	30	92100	20
K	12300	378	61800	492	61600	679	63800	284
Fe	10200	19	18100	28	16900	39	17400	16
Si	175100	37	311400	146	312300	195	308100	90
As	8.1	0.06	11.5	0.29	12.4	0.14	11.9	0.09
Ba	152.2	7.56	462.8	8.14	416.6	7.96	357.4	5.64
Co	6.1	0.02	21.3	0.01	16.1	0.01	17.1	0.008
Cu	151.7	0.19	694.2	0.19	340.3	0.18	630.6	0.12
Cr	14.9	0.55	80.8	0.35	82.9	1.02	84.8	0.54
Hg	0.3	0.0003	0.01	0.0003	0.02	0.0001	0.01	0.0001
Ni	58.9	0.17	3600	0.13	1885.7	0.13	1757	0.11
Se	0.3	0.19	0.27	0.28	0.2	0.31	0.1	0.01
Zn	17.7	0.011	52.5	0.03	53.14	0.06	44.9	0.03

A M_T= Total concentration of species in coal, AM_L= Agregate quantity extracted from coal mg/kg, B M_T= Total concentration of species in Ash 1000 ^oC, BM_L = Agregate quantity extracted from Ash 1000^oC mg/kg, C M_T= Total concentration of species in Ash 1100 ^oC, CM_L= Agregate quantity extracted from Ash 1100^oC mg/kg, D M_T= Total concentration of species in Ash 1300^oC, DM_L= Agregate quantity extracted from Ash 1300^oC mg/kg

Table 6.7: Relative solubility at 50^oC leaching temperature of the leachants and trace elements from the coal and ash samples

	Coal	Ash 1000^oC	Ash 1100^oC	Ash 1300^oC
Ca	0.2265	0.2709	0.3084	0.1094
Mg	0.0318	0.0195	0.0306	0.0210
Al	0.0004	0.0004	0.0003	0.0002
K	0.0307	0.0080	0.0110	0.0045
Fe	0.0019	0.0015	0.0023	0.0009
Si	0.0002	0.0005	0.0006	0.0003

The aggregate weight of Fe leached per unit mass of the sample (M_L) for all the samples ranged from 16.0 - 39.0 ppm, meaning that less than 0.04 g/kg (40 ppm) of Fe was leached from coal and ash samples used for this study. The portion of Fe extracted comparative to the Fe concentration in the coal and ash sample ($M_{L/T}$) ranged from 0.0009 - 0.0023. The M_L for Al ranged from 20.0 - 34.0 ppm, i.e. Al was extracted from the coal and ash samples. The $M_{L/T}$ value of Al ranged from 0.0002 - 0.0004, which was slightly lower than that of Fe. Ca was the most soluble major element leached out with M_L values ranging from 1.3 - 3.85 g/kg (1300 - 3850 ppm) for all the samples. The $M_{L/T}$ for Ca was more than 0.1, ranging from 0.1 - 0.3 g/kg. For Si, the M_L ranged from 0.037 - 0.195 g/kg, with a relative solubility of 0.0002 - 0.0006, showing a very low solubility under the conditions used for this study.

K and Mg had low $M_{L/T}$ values (0.284 - 0.678 g/kg and 0.07 - 0.11 g/kg, respectively), with relative solubility ranging from 0.005 - 0.01 mg/l for K, and 0.02 - 0.032 mg/l for Mg. It was observed that Mg and K solubilities was higher compared with that of Si, Al, and Fe. Kim *et al*. (2003) reported that the relative solubility of fly ash could be measured based on the following conditions: species leached out during leaching of ash with relative solubility of ≤ 0.002 are insoluble, 0.002 - 0.02 is moderately insoluble, 0.20–0.65 is slightly soluble and > 0.65 is soluble. Based on these values, it can be concluded that of all the inorganic leachants from the coal ash, Ca had a relative solubility of 0.1 - 0.3 (slightly soluble) and the relative solubility of K, Si, Al, and Fe were < 0.02. These species can, therefore, be regarded as insoluble under these study conditions.

The relative solubility of Se, which forms oxy-anions, tended to be higher with $M_{L/T}$ values of ≥0.65. Kim *et al*., (2003) also reported a relatively higher solubility of Se in their study. Reports from Furr *et al*. (1977), Gutenmann *et al*. (1976) and Hower *et al*. (1996) shows that Se in coal ash is one of the most mobile trace elements under alkaline and acidic conditions. However, the relative solubility of other trace elements was below or equal to 0.1 for all the samples (**Figure 6.1**), indicating that the solubility of these trace elements in the lixiviants (deionised water and ground water) used in this study was low. The relative solubility of the trace elements implies that the leachability of trace elements will not pose any threat to the groundwater or the environment.

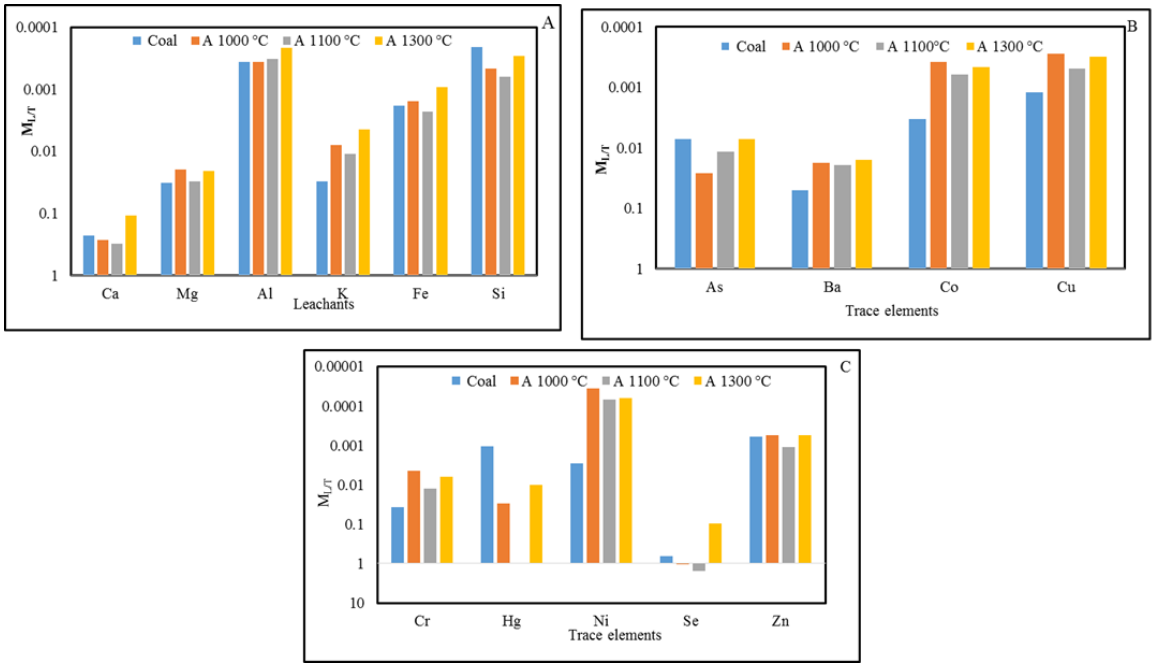

Figure 6.1: A graph of relative solubility (ML/T) values for leachants for coal and ash samples: (A) leachants from coal and ash samples at 50°C leaching temperature, (B and C) trace elements from coal ash at 50°C leaching temperature

6.4 Effect of contact time and temperature

Time is one of the significant factors which influences the concentration of species in the leachate from coal and ash samples. One of the objectives of this study was to estimate the influence of leaching time on the concentrations of leachants from the ash samples generated at different temperatures. Results obtained helped in accessing the time for the dissolution of leachants in the ash. Many leachants would be dissolved or undergo physical and chemical reactions and then be transferred from coal and ash after a long period of leaching. The concentrations of the species leached for different time intervals were investigated. The time intervals chosen for this study were 30 min, and 1, 2, 3, 4, 8, 10, 12 and 24 hours, and the experiements to determine the effect of time and temperature was caried using GW as lixiviants. The change in leaching concentration of species over time and the effect of leaching temperatures (trend curves) are shown in **Figures 6.2 - 6.4**. **Figures 6.2 - 6.4** show the graphical representation of concentration versus time observed during the experiments. The values used in obtaining the change in time and leaching temperature are shown in Appendix (**Table B-D**).

Three different leaching patterns were obtained during the leaching of the species under investigation:

(1) A slow but steady concentration decrease at the initial stage of the experiments. The slow concentration decrease may be attributed to a slow dissolution of the individual leachants over time;

(2) A rapid concentration increase followed by a slower release of the leachant. This rapid increase in concentration could be due to the leaching of species from the amorphous phase of the ash;

(3) A slow initial concentration increase and a rapid release of the leachant towards the end of the experiment.

Estimations by Gong *et al*. (2009) and other investigators have shown that some trace elements are concentrated on the surface of the ash after gasification (Hasen and Fisher, 1980; Kaakinen *et al.,* 1980; Querol *et al*., 1995; Ugurlu, 2004). These elements have a tendency to leach out very readily since they are located on the surface of the ash material. The concentrations of all the species increased

throughout the experiment with respect to time in the batch leaching experiments Other investigators have reported similar findings, where leaching of inorganic species increased with time of the experiment (Ibrahim, 2015; Tan and Xiano, 2010). Some of the curves exhibited a combination of one or two of the leaching patterns. It was evident that temperature of leaching played a role in the leaching steps (**Figures 6.2 - 6.4**). An increase in leaching temperature led to a slight increase in the amount of substances dissolved in the lixiviants.

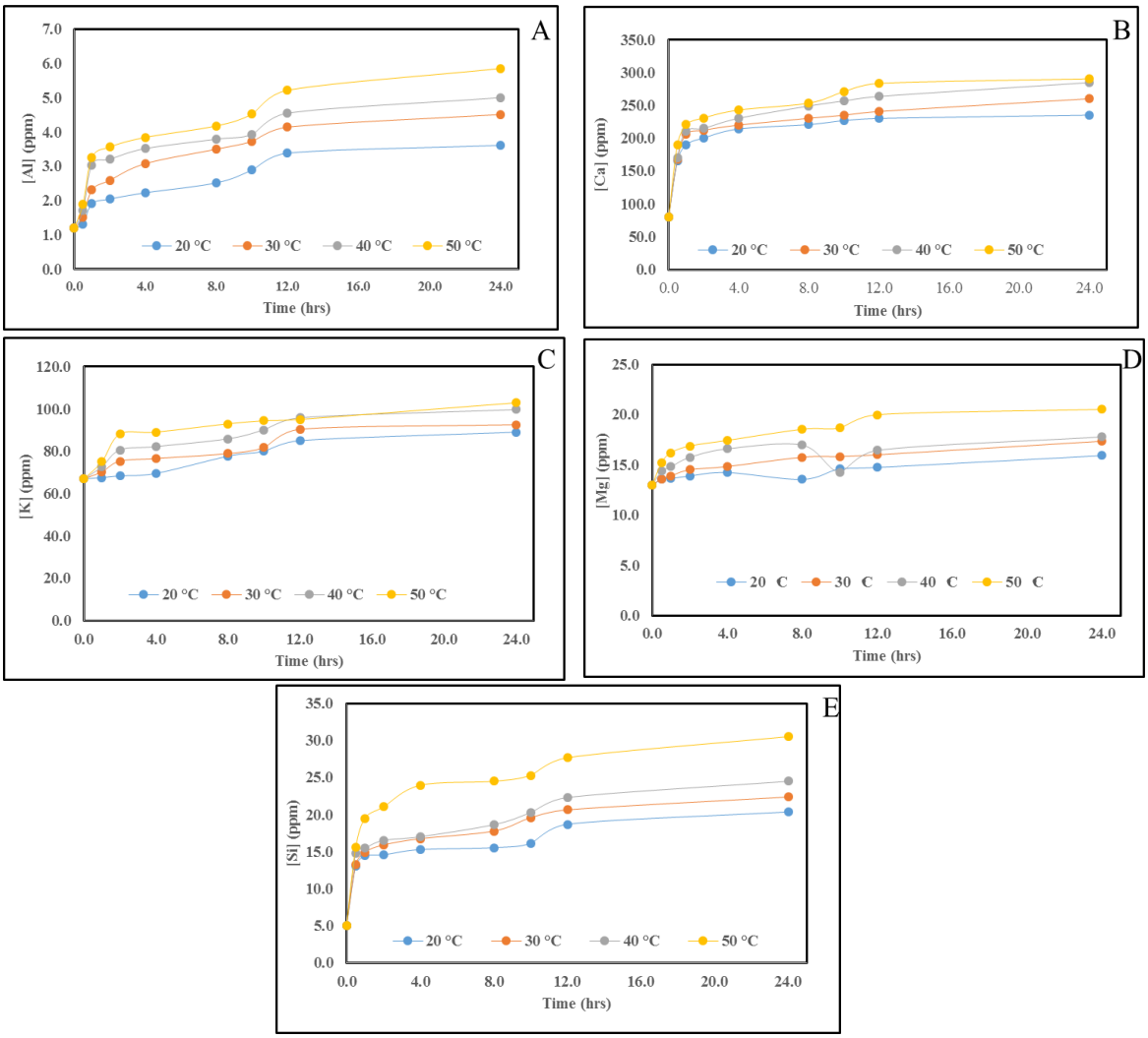

Figure 6.2: Concentration of leachants against time at different leaching temperatures of the1000°C ash when GW was used as lixiviant . (A) Al, (B) Ca, (C) K, (D) Mg, (E) Si.

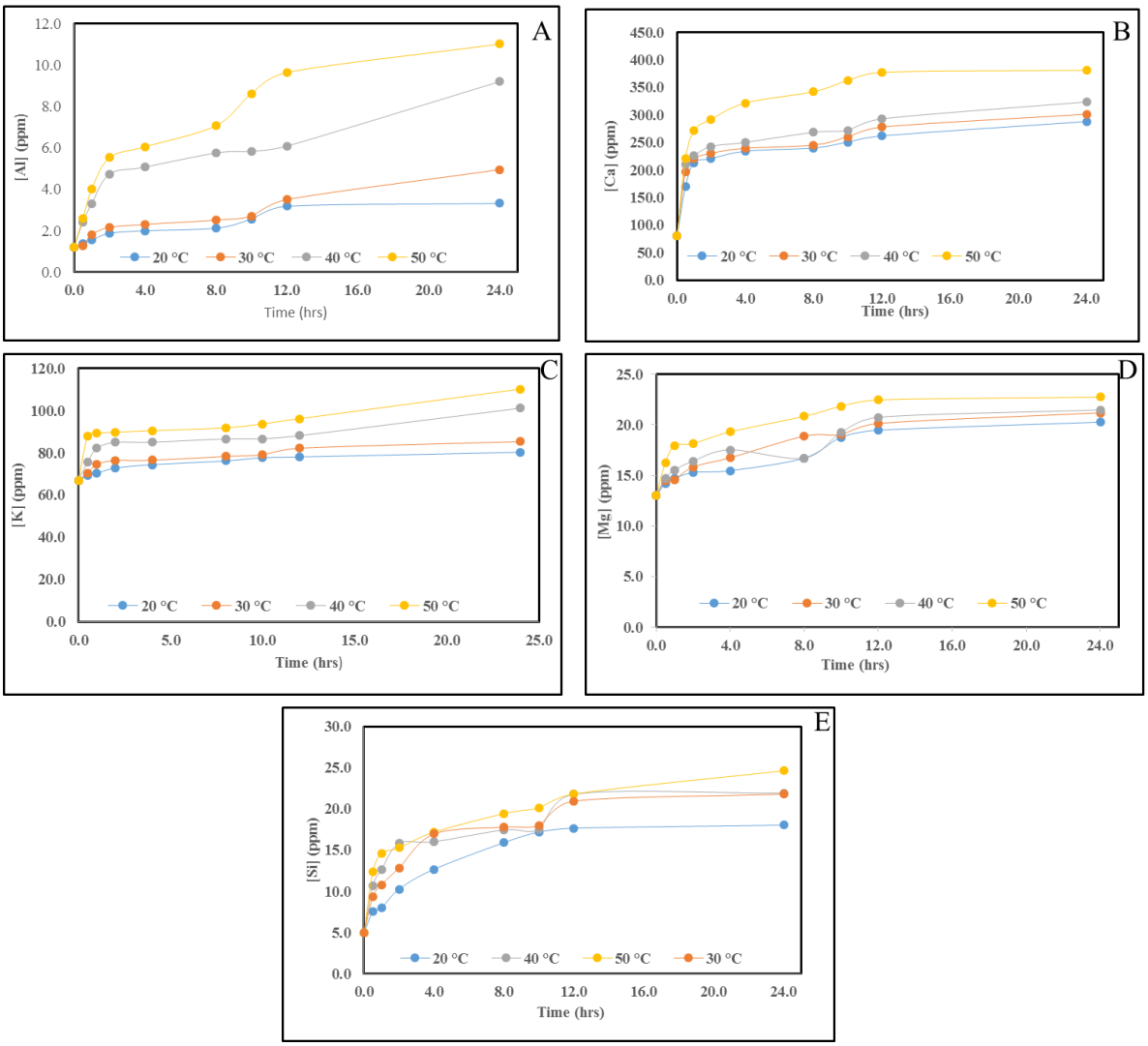

Figure 6.3: Concentration of leachants against time at different leaching temperatures of the 1100°C ash when GW was used as lixiviant. (A) Al, (B) Ca, (C) K, (D) Mg, (E) Si.

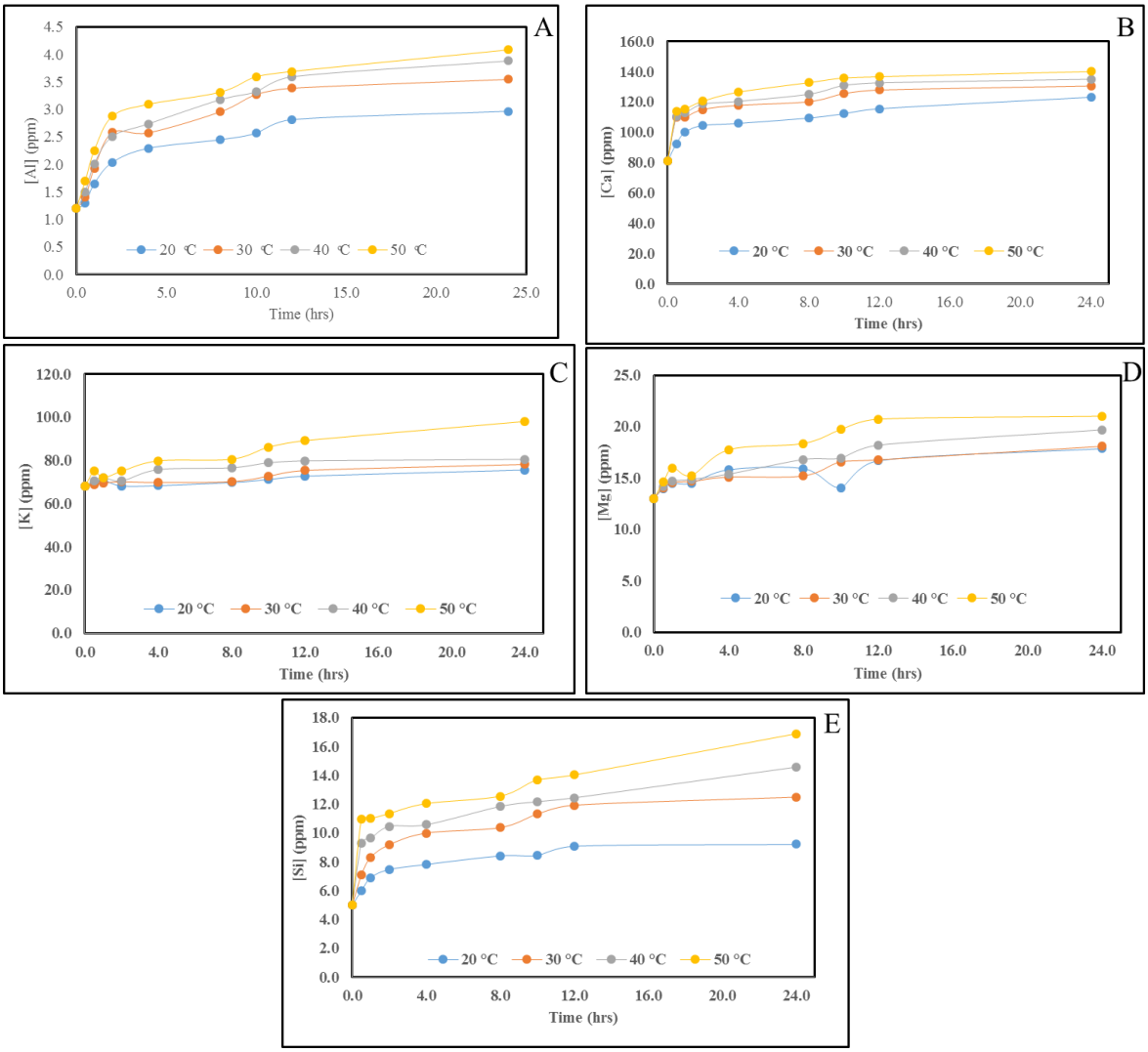

Figure 6.4: Concentration of leachants against time at different leaching temperatures of the1300°C ash when GW was used as lixiviant. (A) Al, (B) Ca, (C) K, (D) Mg, (E) Si.

6.5 Column leaching method

The column leaching method was carried out on the samples to stimulate and predict the inorganic compounds that could be leached out after an underground gasification process. Unsaturated column leaching was used in this study and involved the addition of lixiviants to maintain a given volume of lixiviant solution at the top of the column, following the method of Kim (2002). This method of leaching provides an even supply of the fluid and ensures continual lixiviant movement through the column.

The results obtained during the column leaching test at room temperature will be discussed in detail. The background and procedures are explained in Sections 3.13.2 and 4.15. The column leaching tests were conducted in duplicate, the mean and the standard errors were calculated and reported in **Table 6.8** and **6.9.**

6.5.1 Leachate analyses (ICP-OES)

The results of species and ions leached out using the column method are presented in **Table 6.8**. Similar trends observed during the batch leaching method were also found for the column leaching method. The concentration of the most leached leachant for coal when DW was used during the column method was found to be Ca: 162.0 ppm. The minor leachants were found to have the following concentrations: Mg: 7.2 ppm, Al: 1.9 ppm, K: 32.2 ppm, Fe: 1.1 ppm, Si: 2.8 ppm, Na: 114.0 ppm. The concentrations obtained when GW was used as lixiviant during the column method for the coal sample were: Ca: 231.25.0 ppm, Mg: 21.3 ppm, Al: 2.6 ppm, K: 102.9 ppm, Fe: 2.2 ppm, Si: 8.1 ppm, Na: 5697.5 ppm. When comparing the results from the two lixiviants during the column method for the coal sample, it was observed that some of the leachants had relatively high concentrations when GW was used as lixiviant when compared with leachants obtained when DW was used during the leaching test. A similar trend was observed during the batch leaching method.

Table 6.8: ICP-OES results of column leaching from coal and different ash samples at ambient leaching temperature

	Column leaching at ambient temperature (ppm)									
	Ca	Mg	Al	K	Fe	Si	Na	AL	pH	TDS
Coal DW	162.0±13.8	7.2±1.0	1.9±0.6	32.2±1.3	1.1±0.2	2.8±1.1	114±25.2	67.5±4.9	8.00±0.4	423.5±51.9
Coal GW	231.3±7.4	21.3±2.0	2.6±0.3	102.9±2.9	2.2±0.3	8.1±1.0	5697.5±120.2	170±19.6	8.16±0.14	8665.5±418
Ash 1000 °C DW	351.3±17.2	11.6±3.1	2.8±0.4	65.7±1.4	2.7±0.5	7.5±1.7	98.0±15.4	70±2.9	9.9±0.6	730.5±85.2
Ash 1000 °C GW	519.2±57.2	22.3±6.3	3.6±0.7	129.8±2.6	3.7±1.3	16.7±1.6	5702.2±170.2	149.3±13.2	10.03±0.3	9782.5±445
Ash 1100 °C DW	729.5±8.7	9.5±1.1	2.7±0.7	68.2±1.16	2.3±1.8	14.9±0.7	110.7±170.24	73.25±21.1	9.75±0.2	1275±499
Ash 1100 °C GW	928.3±56.2	23.5±9.3	3.7±1.0	122.3±9.6	3.4±1.0	20.3±1.7	5698.1±130	170±9.8	10.3±0.3	10048±397
Ash 1300 °C DW	188.4±3.1	6.7±1.3	1.8±0.5	37.8±1.5	0.8±0.7	5.1±2.9	52.7±17.2	65.75±4.4	7.69±0.5	357±62.7
Ash 1300 °C GW	267.1±13.8	15.9±3.2	2.6±1.4	100.7±2.6	2.0±1.0	10.2±3.7	5625.0±10.6	165±9.8	8.09±0.17	8981.5±53.9
Groundwater	79.5±2.8	13.3±4.8	1.2±0.01	67.6±5.0	0.87±0.13	5.0±0.45	5583.2±95.2	143.8±27.0	7.65±0.7	8063.5±414
DWAF MR risk	-	-	0.43	-	9	-		-	-	-

DW: deionised water; GW: groundwater; DWAF MR: Department of Water Affairs and Forestry Minimum Requirements; TCLP: toxicity characteristic leaching procedure.

Table 6.8 presents the results of the concentration of the leachants as determined with the column technique for the ash samples at ambient temperature. It was observed, as seen in **Table 6.8**, that the leachants obtained when DW was used as lixiviant were: Ca: 188.4 - 729.5 ppm, Mg: 14.7 - 19.5 ppm, Al: 1.8 - 2.8 ppm, K: 45.8 - 68.2 ppm, Fe: 0.8 - 2.7 ppm, Si: 3.9 - 18.0 ppm, Na: 52.72 - 110.7 ppm. The concentrations of these individual leachants increased when GW was used as lixiviant during column leaching for the different ash compositions with the following ranges of concentrations: Ca: 267.1 - 928.3 ppm, Mg: 15.9 - 23.5 ppm, Al: 2.6 - 3.7 ppm, K: 100.7 - 129.8 ppm, Fe: 2.0 - 3.7 ppm, Si: 10.2 - 20.3 ppm, Na: 5625.0 - 5702.2 ppm.

From the results in **Table 6.8**, it is evident that Ca elemental species were the most leached species and ions during the column leaching method, with lower concentrations of Fe, Al, Si, and K. The concentrations of these individual species and ions were higher when GW was used as lixiviant compared with when DW was used. The increase in the concentration when GW was used could be attributed to the presence of these individual species in the groundwater (**Table 6.2**).

6.5.2 Leachate analyses (IC)

IC results of the leaching experiments using the column method at ambient leaching temperature are presented in **Table 6.9**. The concentration of the most leached anion ,SO_4^{2-}, was found to be 119.4 ppm when DW was used as lixiviant for the coal sample at ambient leaching temperature, with low concentrations of the following anions: NO_3^-: 10.7 ppm, NO_2^-: 3.2 ppm, Cl^-: 65.6 ppm, and F^-: 1.5 ppm. The anionic concentrations of the leachants when GW was used as lixiviants were SO_4^{2-}: 130.2 ppm, NO_3^-: 24.0 ppm, NO_2^-: 8.3 ppm, Cl^-: 5422.5 ppm, and F^-: 2.3 ppm. The concentrations of these anions when GW was used as lixiviant were moderately higher when related to results obtained when DW was used as lixiviant for the coal sample at ambient leaching temperature for the column method. The increase in anion concentrations when GW was used as lixiviant could be attributed to the presence of the anions in the groundwater (**Table 6.1**).

The results of the anionic concentrations from the ash sample leachates at ambient leaching temperature for the column method are presented in **Table 6.9**. Again it

was observed that SO_4^{2-} was the most leached anion with a concentration range of 250.3 - 1360.0 ppm when DW was used as lixiviant. Other anionic leachants from the ash samples at ambient leaching temperature during the column method include NO_3^-: 1.3 - 8.1 ppm, NO_2^-: 1.2 - 3.1 ppm, Cl^-: 56.0 - 114.3 ppm, and F^-: 1.3 - 2.7 ppm when DW was used as lixiviant. The concentrations of the individual anions increased when GW was used as lixiviant for the different ash samples at ambient leaching temperature during the column method, with values ranging from SO_4^{2-} : 265.4 - 1400.4 ppm, NO_3^-: 14.2 - 24.0 ppm, NO_2^-: 5.0 - 7.0 ppm, Cl^-: 5414.0 - 5480.5 ppm, and F^-: 2.6 - 3.0 ppm.

From the results in **Table 6.9**, it was obvious that the SO_4^{2-} ion from the coal ash samples was the most leached anion during the column leaching method, with lower concentrations of NO_3^-, NO_2^-, Cl^-, and F^-. The concentrations of these individual ions were higher when GW was used as lixiviant compared with when DW was used.

Finally, the column leaching method results (Section 6.4) showed that the concentrations of the Ca species and SO_4^{2-} ions increased for the 1000°C and 1100°C ash samples, but decreased for the 1300°C ash sample. A similar trend was observed during the batch leaching tests. Several researchers have reported the higher concentration of SO_4^{2-} ions and Ca species relative to the other ions during column leaching and batch leaching tests (Campbell and Washington, 1976; Dalton and Campbell, 1978; Edgar *et al*., 1979; Humenick and Mattox, 1977; Humenick *et al*., 1983).

Table 6.9: IC results of column leaching of ions from coal and different ash samples at ambient leaching temperature.

Column leaching at ambient temperature (ppm)					
	SO_4^{2-}	NO_3^-	NO_2^-	Cl^-	F^-
Samples			*mg/l*		
Coal DW	119.4±10.6	10.7±0.9	3.2±0.001	65.6±5.5	1.5±0.7
Coal GW	130.2±42.7	24.0±2.7	8.3±2.1	5422.5±342.0	2.3±0.2
Ash 1000 °C DW	582.9±70.3	8.1±1.3	2.2±0.02	96.75±7.4	1.3±0.1
Ash 1000 °C GW	827.5±57.7	20.0±1.9	6.4±1.7	5460.0±488.0	2.6±0.01
Ash 1100 °C DW	1360.9±205.0	7.2±4.0	3.1±0.01	114.3±12.25	1.5±0.03
Ash 1100 °C GW	1400.4±404.0	21.0±5.8	7.0±2.75	5480.5±149	3.3±1.20
Ash 1300 °C DW	250.3±118.0	1.3±2.2	1.2±0.001	56.0±10.7	2.7±0.8
Ash 1300 °C GW	265.4±105.0	14.3±1.7	5.9.0±1.2	5414.0±341.0	3.0±2.1
Groundwater	5.3±1.3	14.9±3.9	5.44±2.14	5365.5±180.0	1.0±0.01

DW: deionised water; GW: groundwater; DWAF MR: Department of Water Affairs and Forestry Minimum Requirements; TCLP: Toxicity characteristic leaching procedure.

6.5.3 Change of pH and total alkalinity during the column leaching tests

During the column method, the change in pH and total alkalinity of the leachate samples collected over a specific time were investigated. The time intervals chosen determine the change in pH and total alkalinity were 30 min, and 1, 2, 3, 4, 8, 10, 12 and 24 hours, the change in pH and total alkalinity was carried using GW as lixiviant. It was found that there was a fluctuation in pH and alkalinity as the leaching time increased (**Figure 6.5**). The pH increased during the initial stage of the experiment and gradually decreased as leaching time increased, but the total alkalinity decreased with an increase in time. The drop in the total alkalinity and pH could have been as a result of the leaching of some soluble hydroxyl compounds as the leaching experiment progressed (Humenick *et al*.,1985) (see Equations 6.3 and 6.4).

$$OH^- + HCO_2^{3-} \longrightarrow CO_3^{2-} + H_2O \quad (6.3)$$

$$Ca^{2+} + CO_3^{2-} \longrightarrow CaCO_3\downarrow \quad (6.4)$$

The reaction pathway in Equations 6.3 and 6.4 could be explained by the following:

(1) The formation of a hydroxyl (Ca, Mg, K, Al) compound when the ash came into contact with water, thereby increasing the pH of the solution. The formed hydrolysed compound could further react with the bicarbonate to form carbonates and water.

(2) The carbonate ions may react with the free calcium ions in the solution to form an insoluble calcium carbonate, which could be removed from the leaching solution, thereby decreasing the pH and the alkalinity of the solution as leaching time increased. A similar decrease in the pH and total alkalinity was also observed by Humenick *et al*. (1985) when they investigated water leaching of lignite coal ash.

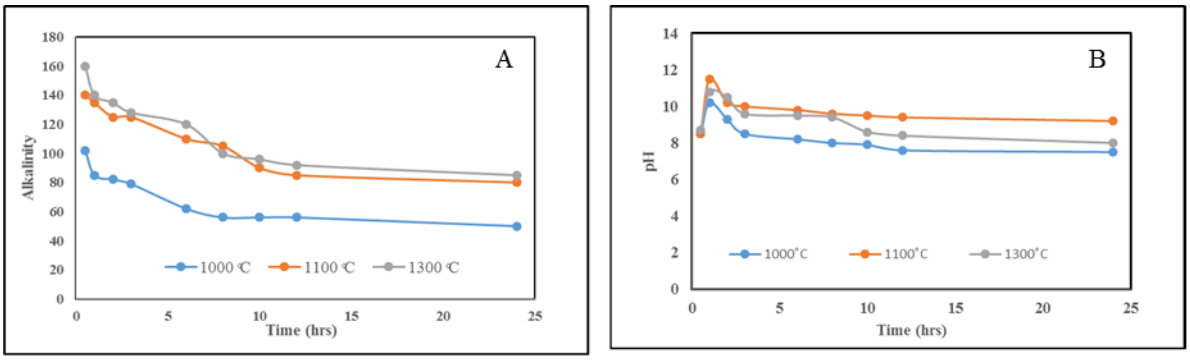

Figure 6.5: (A) Alkalinity vs. time and (B) pH vs. time observed during the column leaching method when GW was used as lixiviant.

6.6 Comparison of the batch and column methods at room temperature

The batch and column leaching methods were compared (**Figure 6.6**, **Table 6.4** and **6.8**) for leaching at room temperature. The concentrations of the Ca species increased approximately two-fold when a column leaching method was used; similarly SO_4^{2-} ions also increased about two-fold (**Table 6.10**) during the column method. The reason for this difference could be attributed to the flow of the lixiviant over the ash samples. The high liquid-to-solid ratio could have been one of the factors that led to higher concentrations of individual species during the column leaching tests in comparison to lower concentrations during the batch leaching tests at ambient temperature. Similar results were also obtained in other studies (Ogunro and Inyang, 2003).

The batch leaching method required vigorous agitation of samples, which may have improved the surface contact of the lixiviant and the solid particulates. Concentrations of species and ions such as Mg, Al, Si, K, NO_2^-, NO_3^- and F^- obtained for the batch leaching process were similar or varied slightly when compared with the column leaching method (**Figure 6.6**), whereas the Fe concentration was found to be slightly higher in the batch leaching method when compared with the column

leaching method. Also observed in **Figure 6.7**, there was not much difference in the trace element concentrations when comparing the two leaching methods. Some of the trace elements (Zn and Se) exhibited higher leachability during the batch leaching method as compared with the column method at room temperature. Other parameters such as TDS and EC increased slightly for the column leaching method as compared with the batch leaching method at ambient temperature, as expected (**Table 6.2** and **6.7**).

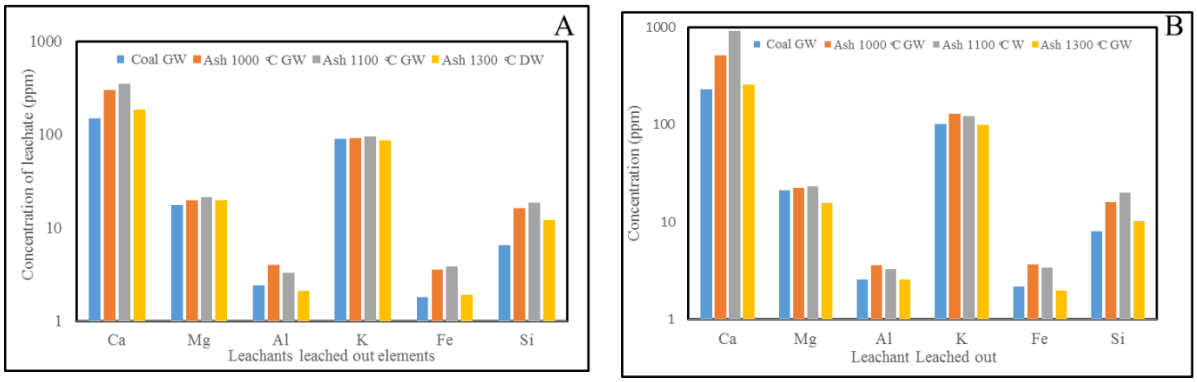

Figure 6.6: Graphs showing the concentrations of leachants and trace elements using the batch and column leaching methods (room temperature), (GW) as lixiviant, A) Batch leaching method at room temperature and B) Column leaching method at room temperature (leachants)

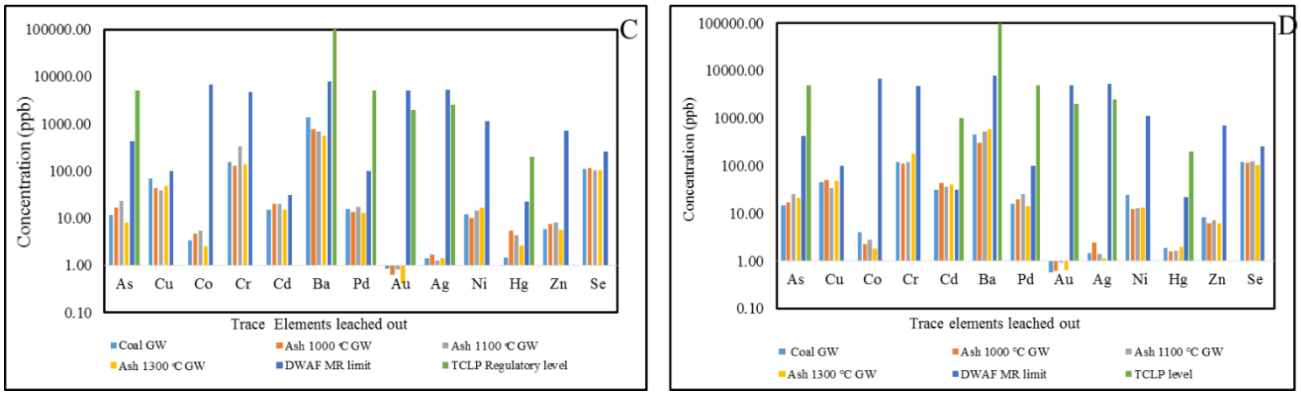

Figure 6.7: Graphs showing the concentration of leachants and trace elements using the batch and column leaching methods (room temperature), (GW) as lixiviant, C) Batch method at room temperature (trace elements), (D) Column method at room temperature(trace elements) DWAF MR: Department of Water Affairs and Forestry Minimum Requirements; TCLP: toxicity characteristic leaching procedure.

6.7 Contribution of coal and ash samples to groundwater leaching

The contributions of the individual leachants from the coal and ash samples were estimated to correlate the amounts of species that were leached out from the coal and ash samples into the groundwater with the concentrations of the species in the

groundwater prior to leaching. The estimation of the leachants released from coal and ash samples was achieved by subtracting the amount obtained during the leaching processes when groundwater was used as lixiviant from the concentration of the individual leachants in groundwater (**Table 6.1**). The results are presented in **Table 6.10** for the batch leaching method at room temperature, 50^{o}C and the column leaching method at room temperature.

The amounts of the leachants released were compared with the results obtained when DW (**Table 6.2**) was used as lixiviant and similar concentrations were observed with some slight difference. The difference in concentrations could be attributed to the following reasons, which include method of handling the samples prior to analysis, low concentrations and precision of the analytical instrument used.

Table 6.10: Concentrations of leachants released from coal and ash samples during groundwater leaching.

Room temperature (ppm) (Batch method)							
	Ca	Mg	Al	Fe	K	Si	Na
Coal	70.2	4.5	1.2	0.9	22.5	1.5	20.6
Ash 1000 °C	220.6	6.7	2.8	2.7	23.0	11.2	73.8
Ash 1100 °C	270	8.9	2.1	2.9	27.9	13.5	53.0
Ash 1300 °C	105.8	6.0	0.9	1.0	18.7	7.0	41.8
50 ^{o}C (ppm) (Batch method)							
	Ca	Mg	Al	Fe	K	Si	Na
Coal	124.6	7.0	2.0	1.9	37.8	3.7	101.5
Ash 1000 °C	330.6	8.2	3.4	2.8	49.2	14.6	99.8
Ash 1100 °C	385.6	11.0	3.0	3.9	67.9	19.5	82.2
Ash 1300 °C	145.6	8.6	2.0	1.6	28.4	9	68.7
Room temperature (ppm) (column method)							
	Ca	Mg	Al	Fe	K	Si	Na
Coal	151.8	8.0	1.4	1.3	35.3	3.1	114.3
Ash 1000 °C	439.7	9.0	2.4	2.8	62.2	11.2	119.0
Ash 1100 °C	848.8	10.2	2.5	2.5	54.7	15	114.9
Ash 1300 °C	187.6	2.6	1.4	1.1	33.1	5.2	41.8

6.8 Effect of ashing temperature on leachants

The effect of the ashing temperature on the leaching process was also investigated in this study. The results of the influence of the ashing temperature are presented in **Figure 6.8**. The leachants from ash produced at 1100°C and 1000°C have higher concentrations than those from the ash produced at 1300°C (**Figure 6.8**). This leaching behaviour could be attributed to the following:

(1) XRD results (**Table 5.9**) showed that the amorphous phase of the ash material decreases as temperature increased, with the 1300°C ash sample having the lowest amount of amorphous material. The sintered ash material at 1300°C has inorganic compounds encapsulated in the ash matrix, which will hinder the leaching of these inorganic species during the leaching process. Xu and Sarkar, (1994) estimated in their study that some of the glassy or amorphous phases of ash samples may be thermodynamically unstable during the leaching process. **Figure 6.8** shows a significant decrease in the concentrations of all inorganic species that leached out of the ash formed at 1300^{o}C. The decrease in concentration observed from leachate of ash samples produced at 1300^{o}C could be as a result of the low amount of the amorphous phase of the 1300°C ash and high percentages of crystalline phases, as observed from the XRD data (**Table 5.9**). Also, since the ash produced at 1300^{o}C are fused and sintered, there is a high probability of inorganic species encapsulation inside the ash matrix leading to the low leachability of these species.

(2) The proximate analyses results in Section 5.3 can also be used to explain the lower leachability of species for the ash sample produced at 1000^{o}C ash, when compared with the ash formed at 1100^{o}C. Since there is a remnant amount of carbon at 1000^{o}C (as observed in **Table 5.1**), the carbon parts may absorb some of the inorganic species, thereby leading to the lower leachability of some species when compared with ash at 1100 ^{o}C with lower carbon content.

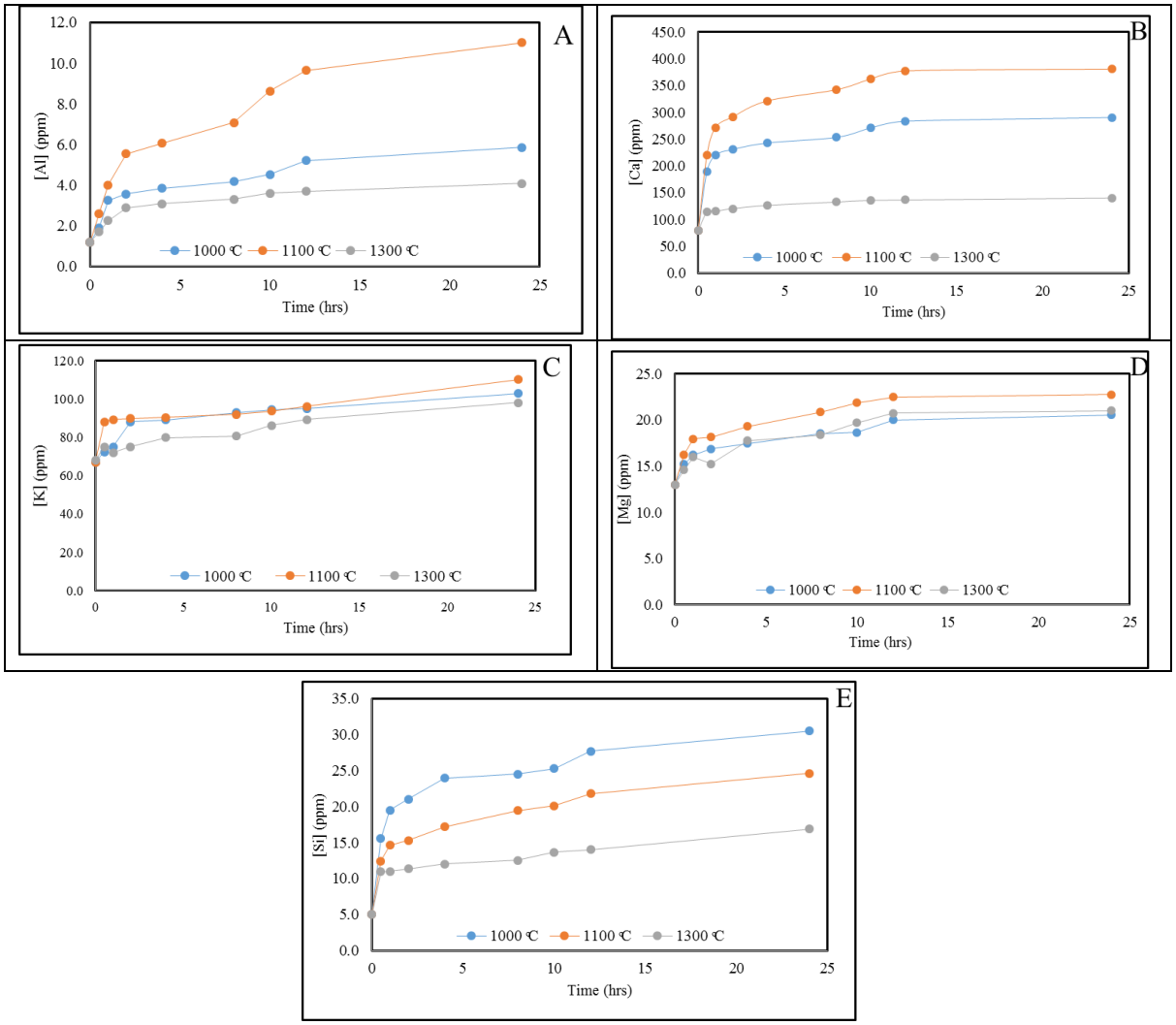

Figure 6.8: Concentration of leachants against time at 50 ºC leaching temperature (comparison of different ashing temperatures) Batch leaching (A) Al, (B) Ca, (C) K, (D) Mg, (E) Si.

6.9 Environmental impact of leached species

The ICP analysis showed that there were some amounts of trace and leached species that could be released to the environment or groundwater (**Table 6.2** and **6.11**). The majority of these species do not pose a threat to groundwater quality because of their low concentrations in the ash samples. Toxicity characteristic leaching procedures (TCLPs) are mostly used to estimate the levels of hazard of waste materials. TCLPs help in identifying the mobility of certain hazardous leachates (Matjie *et al*., 2005). The waste handling and disposal of the South African Department of Water Affairs and Forestry Minimum Requirements (DWAF MR) document indicates that water from industrial waste, such as coal ash, should not be excluded from rules binding hazardous waste. For this reason, the concentrations of species in the leachate obtained during the leaching tests were compared with the limits based on the DWAF MR and the USA Environmental Protection Agency (US EPA) TCLP values. The limits for US EPA TCLP and DWAF MR allowable risks are presented in **Table 6.11** for the following trace elements, which have been termed hazardous: Ag, As, Ba, Be, Cd, Cr, Hg and Pb. Other elements that will possibly need environmental monitoring include Al, Co, Cu, Fe, Mn, Ni, V and Zn.

Individual amounts of leachants and trace elements obtained at 50°C were compared with the standard for DWAF and TCLP. The concentration of the specific leachants at 50°C leaching temperature was used for the comparison because the highest concentration of the leachant was attained at 50°C leaching temperature. Similarly, the comparison for trace elements obtained at batch leaching at ambient temperature and column leaching at ambient temperature are presented in Appendices E1 and E2. The results are discussed in detail in the following paragraphs.

Aluminum (Al): The amounts of Al for all the samples obtained at 50^{o}C leaching temperature ranges from 3.2 - 4.6 ppm (**Table 6.2**). The percentages of Al leached out for all the samples were very low when compared with the relative abundance of Al in the ash samples at the various temperatures (**Table 6.6**). The low values of Al obtained could be attributed to the slow dissolution of Al from the glassy and crystalline phases (Dudas, 1981). Al appeared in the form of mullite (**Table 5.9**). Mullite is normally considered a non-reactive mineral in alkaline ash solutions.

Therefore, Al that leached out could have been as a result of the dissolution of Al species in the glassy phase (Dubokora *et al*., 2006; Querol *et al*., 2001). Based on the low percentages of Al in the leachates, it can be suggested that the ash produced in this study had a low content of soluble Al in the glassy phase that is leachable into groundwater

Al is not regarded as one of the US EPA-regulated inorganic species. The leachant results, however, showed that the Al concentration exceeded the risk levels of the DWAF MR, which gives the limit as 0.43 ppm

Calcium (Ca) in the ash was in the form of lime, anhydrite and calcite and some in the amorphous phase as seen from the XRD results (**Table 5.9**). Although Ca was the most dominant element leached, the amount of Ca for all the samples at 50^{o}C leaching temperature ranged from 225.0 - 463.0 ppm (**Table 6.2**). The amounts were low relative to the amount of Ca in ash samples (**Table 6.6**). An investigation by Kim *et al*. (2003) revealed that, irrespective of the lixiviant used during the leaching experiment, the most leached element was Ca. In most cases, the amount of Ca dissolved in lixiviants depended on the forms of Ca (mineralogy of Ca) in the ash.

XRD results (**Table 5.9**) showed that Iron (Fe) in the ash samples were in the form of magnetite and hematite. The amounts of Fe for all the samples at 50^{o}C leaching temperatures ranged from 2.5 - 4.8 ppm (**Table 6.2**). These values showed a very low leachability of Fe from the coal and ash samples used for this study. Results of the species for all samples showed that a small amount of Fe was leached out from the ash and this should not have an effect on the environment. Kukier *et al*. (2003) indicated that some portion of Fe is found in the amorphous phase. Seidel and Zimmel (1998) found that Fe leachability depends on the pH of the lixiviant and concluded that Fe could only be leached out when the pH of the lixiviant is ≤ 1.5. The low leachability of Fe in this study could, therefore, be attributed to the slightly basic conditions of the leaching process and was largely dependent on the mineralogy of Fe. Kim *et al*. (2003) showed that the concentration of Fe leached in neutral or alkaline solutions is < 10 mg/kg and, in some instances, the Fe concentration was below the detection limit.

Table 6.11: ICP-OES results of batch leaching of heavy elements from coal and ash samples at 50°C leaching temperature.

	Heavy element extraction at 50°C (ppb) (batch method)										
	A	B	C	D	E	F	G	H	GW	DWAF limit	TCLP limit
As	7.0±1.4	6.10±3.2	10.0±0.1	31.0±8.2	31.7±4.2	15.4±37.1	7.7±12.2	9.7±8.6	1.12±0.2	430	5000
Cu	10.2±1.9	49.1±7.6	13.8±1.3	50.1±4.1	15.3±0.6	47.2±9.5	22.9±1.5	50.4±10.2	30.5±3.6	100	-
Co	0.1±0.0	3.1±1.2	1.1±0.03	1.9±1.3	1.4±0.9	2.1±1.5	0.3±0.01	1.9±0.12	1.1±0.1	6900	-
Cr	39.4±1.5	144.7±14.3	39.2±21.2	125.3±29.8	26.5±26.6	191.8±13.2	55.0±14.3	143.7±17	90.0±10.0	4700	-
Cd	38.4±3.6	42.6±4.8	45.7±2.5	51.5±6.3	41.8±7.0	52.7±9.2	33.3±3.3	52.0±7.6	3.0±0.3	31	1000
Ba	463.5±8.9	992.0±74.4	572.2±103.5	1049.5±77.4	604.2±97.7	1033.5±104.9	640.8±25.8	799.9±0.1	236.0±95.2	7800	-
Pd	2.1±0.9	14.2±1.8	8.0±0.7	17.1±2.2	6.6±1.2	19.3±1.5	0.8±0.2	12.9±1.0	1.7±0.7	100	5000
Au	0.07±0.1	0.12±0.2	0.64±1.2	1.22±1.8	0.12±0.01	0.23±0.07	0.29±0.05	0.14±0.02	0.23±0.04	5000	2000
Ag	0.07±0.01	0.14±0.02	0.18±0.03	0.23±0.04	0.27±0.045	0.60±0.12	0.09±0.00	0.14±0.02	0.8±3.2	5300	2500
Ni	17.2±3.9	17.4±6.1	9.0±1.0	13.0±0.4	7.0±1.0	13.0±1.5	6.0±1.1	11.5±1.0	0.17±0.31	1140	-
Hg	0.073±0.03	0.087±0.06	0.12±0.13	0.09±0.1	0.02±0.02	0.05±0.00	0.06±0.02	0.07±0.016	0.06±0.03	22	200
Zn	2.8±1.18	6.15±0.69	1.2±2.35	8.0±1.1	2.5±2.24	10.85±1.08	1.2±2.16	7.6±1.96	5.1±1.18	700	-
Se	21.7±5.49	138.5±10.78	25.8±2.35	147.2±19.2	10.7±6.86	150.95±47.14	18.9±0.78	120.5±6.86	119.55±30.28	260	-

DW: deionised water; GW: groundwater; DWAF MR: Department of Water Affairs and Forestry Minimum Requirements; TCLP: toxicity characteristic leaching procedure. A= Coal DW, B= Coal GW, C= Ash 1000 °C DW, D= Ash 1000°C GW, E= Ash 1100°C DW, F= Ash 1100°C GW, G= Ash 1300°C DW, H= Ash 1300°C GW.

Magnesium (Mg) in the ash samples occurred in the form of periclase. The amounts of Mg for all the samples at 50^{o}C leaching temperatures ranged from 21.6 - 24.0 ppm (**Table 6.2**). The low concentrations of Mg will likely not have any effect on the groundwater or the environment. Dadas (1981) attributed this to slow dissolution and hydrolytic reactions of carbonate compounds. Ward *et al*. (2003) indicated that the reason for the poor leaching of Mg may be due to the enrichment of Mg in the glassy fraction of the ash, which leads to low solubility.

Sulfur is one of the most leached ions in the form of SO_4^{2-}, along with elemental Ca. The amounts of SO_4^{2-} for all the samples at 50 ^{o}C leaching temperatures ranged from 105.0 - 905.8 ppm (**Table 6.2**). Irrespective of the concentration that was released to the groundwater, sulfur does not have any negative effects in these amounts on the groundwater as it is a major nutrient needed for the growth of plants. Iwashita *et al*. (2005) and Izquierdo *et al.* (2008) showed that the concentration of sulfur leached out during their leaching experiments correlated with the amount of sulfur in the ash. Querol *et al*. (2001) and Ward *et al*. (2003) noted that approximately 40 - 80% of sulfur could be leached out from coal ash when water is used as a lixiviant. The amounts of sulfur do not pose a threat to groundwater quality because the sulfur content of the feed coal and ash samples at different ashing temperatures were very small, as can be seen from the XRF results in **Table 5.4** and the ICP results in **Table 6.6**.

Silicon (Si) in the ash is in the form of quartz or aluminosilicate (mullite) with smaller amounts in the amorphous phase (**Table 5.9**). The amounts of Si for all the samples at 50 ^{o}C leaching temperatures ranged from 14.0 - 24.5 ppm (**Table 6.2**). The percentages of Si leached for all the samples were very low when compared with the relative abundance of Si in the ash samples at various temperatures (**Table 6.6**). Querol *et al*. (2001) found that the Si-bearing phase is the main element in the amorphous phase. These authors go on to illustrate that the dissolution of glass is influenced by the presence of OH^- in the solution. Irrespective of the leaching procedure, Si is poorly leached in an alkaline solution. Ward *et al*., (2003) and Moreno *et al*. (2005) estimated that < 0.5 mg/l of Si was leached out during alkaline leaching from coal ash.

The quantity of Silver (Ag) in coal ash is very low and is not leached into groundwater. The percentages of Ag leached out for all the samples were very low when compared with the abundance of Ag in the ash samples at various temperatures (**Table 6.6**). The amounts of Ag for all the samples at 50^{o}C leaching temperatures ranged from 0.14 - 0.64 ppb (**Table 6.11**). When comparing the value with the standard from EPA TCLP and DWAF MR allowable risks, it was found that the values were far below the acceptable limits (**Figure 6.9**).

Arsenic (As) in coal ash is mainly related to As-bearing pyrite (Finkelman, 1995). Low concentrations of As (mostly occurring as As(V)) are found in South African coal (Matjie *et al*., 2005). This form of As is less toxic than the As(III) species. The amounts of As for all the samples at 50^{o}C leaching temperature ranged from 6.9 - 31.9 ppb (**Table 6.11**). When comparing the value with the standard from EPA TCLP and DWAF MR allowable risks, it was found that the values were far below the acceptable limits (**Figure 6.9**).

Barium (Ba) in coal ash forms a sparingly soluble compound with sulfate and carbonate ions (Fruchter *et al*., 1990) and its leachability is relatively low with regards to its regulatory limit. The amounts of Ba for all the samples at 50 ^{o}C leaching temperature ranged from 604.0 - 1033.5 ppb (**Table 6.11**). When comparing the values with the standard from DWAF MR allowable risks, it was found that the values were far below the acceptable limit (**Figure 6.9**).

Cadmium (Cd): The concentration of Cd was very low in the coal ash and will likely not to be an environmental hazard to waterbodies when leached. Results from a leaching experiment conducted by Matjie *et al*. (2005) showed that the concentration of Cd in the leachate was below detection limit. The amounts of Cd for all the samples at 50 ^{o}C leaching temperature ranged from 33.55 - 52.73 ppb (**Table 6.11**). When comparing the values with the standard from EPA TCLP it was found to be below the acceptable limit but it was above the standard for DWAF MR (**Figure 6.9**).

Chromium (Cr) occurs mainly in two oxidation states in water bodies, namely Cr(VI) and Cr(III). The hexavalent oxidation states, which can be in the form of chromate or dichromate, are known to be soluble in aqueous solutions and are carcinogenic (Huggins and Hoffman, 2004). Cr(III) is less soluble and is of concern to human health. Coal ash from bituminous coal is made up of insoluble Cr(III), which is mostly

related to illite (Huggins and Huffman, 2004; Huggins *et al*., 2000). The amounts of Cr for all the samples at 50 ^{o}C leaching temperature ranged from 125.3 - 291.75 ppb (**Table 6.11**). When comparing the values with the standard from DWAF MR allowable risks, it was found that the values were far below the acceptable limit (**Figure 6.9**).

The amounts of Mercury (Hg) in the coal ash samples were very low and a small quantity of this element was leached out during the leaching experiments for all the leaching experiments using ash samples prepared at different temperatures. The amounts of Hg for all the samples at 50^{o}C leaching temperature ranged from 0.05 - 0.09 ppb (**Table 6.11**). When comparing the values with the standard from DWAF MR allowable risks, it was found that the values were far below the acceptable limit (**Figure 6.9**). Nathan *et al*. (1999) and Sanchez *et al*. (2006) showed that the concentration of Hg leached out during their study was relatively low (0.2 (µg/l)) at a pH of 4.5 - 13.0, suggesting that the solubility of Hg does not depend on pH. However, because of the toxicity of Hg, a small concentration will be harmful to the environment or waterbodies. Nonetheless, the concentration of Hg in the ash samples was low enough to not have an environmental effect and is not deemed detrimental to the environment. Other trace elements such as Zn, Ni, Cu, Co, Pd and Se were also found to be below the standards stipulated by DWAF and EPA as seen in **Table 6.11** and **Figure 6.9**.

The species mentioned above were the possible leachants found in the coal and ash samples used in this study, which may likely cause damage to the environment. From **Tables 6.9**, and **Figure 6.9**, the concentration of elements in the leachant obtained was compared with the detection limits for US EPA and DWAF MR limits. As shown in **Table 6.11**, the concentrations of all the trace elements did not exceed the concentration of the two regulatory bodies, except for Cd, which exceeded the DWAF MR limit but not the TCLP limit. Therefore, the trace and heavy element leachants released from the coal ash at different leaching temperatures and via different leaching methods used for this study did not pose a health or environmental risks, with the exception of Cd.

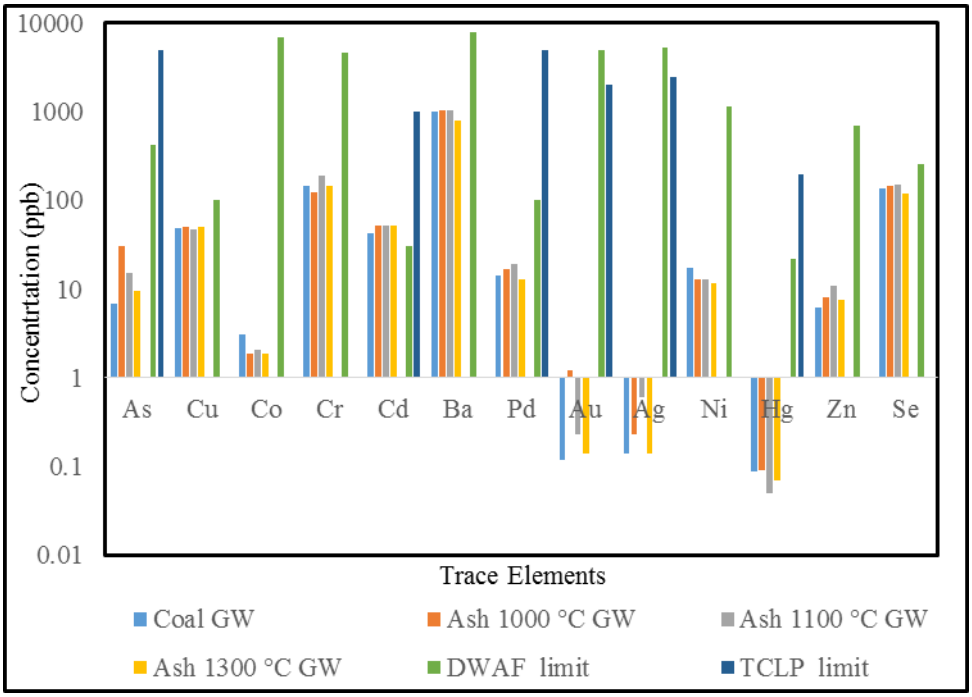

Figure 6.9: Amounts of trace elements leached from coal and ash samples at 50°C leaching temperature in comparison with the standard limits (DWAF and TCLP regulatory level)

Chapter 7: Conclusion and Recommendation

7.1 Introduction

The mineralogical transformations of minerals in the blended coal sample (feed coal, floor and roof) from the Theunissen UCG site in Free State, South Africa, to ash and slag, and the possible subsequent influence of the inorganics on groundwater bodies have been elucidated in this dissertation. This chapter deals with the summary of the main findings and the conclusions derived during the investigation. Recommendation for future work will be provided in this chapter.

7.2 General Conclusion from the study

- The ultimate and proximate analysis results from the feed coal sample were found to be similar in chemical properties with that of some South African bituminous coal samples. When the samples were blended with 15% of the floor sample and 5% of the roof sample, the composition of the blended coal changed with a reduction in the carbon content and an increase in the ash yield, as expected.

- The petrographic results of the feed coal sample revealed that the sample was inertinite-rich, with an inertinite maceral abundance of 63.3 vol. %, mmb, and a small proportion of vitrinite and liptinite. The feed coal sample was found to be a bituminous medium rank C coal.

- It was found from the ash fusion temperature results that there was no significant influence of the floor and the roof samples on the AFT values for the coal ash of the blended coal sample in comparison to the coal sample. Since the blended coal had an ash fusion temperature which varied from 1356 - 1530 ^{o}C under reducing and oxidising conditions, 1300^{o}C was chosen as the maximum temperature for the heat treatment experiments.

- XRF analyses was carried out on the feed coal material, roof, floor and the blended coal samples. The XRF results for all coal ash samples analysed indicated that these samples contained SiO_2 and Al_2O_3 as major elements with a small proportion of Fe_2O_3, TiO_2, CaO, MgO, Na_2O and MnO. The ash sample

was classified as F due to the fact that the samples contained about 92.1 - 93.4% of SiO_2 + Al_2O_3 + Fe_2O_3, with CaO ranging from 1.2 - 1.3wt %. The acid to base ratio was found to be 0.1- 0.2 wt. %

- XRD analyses of the coal, floor and roof samples showed that minerals such as kaolinite and quartz, were the major crystalline minerals found in the samples prior to blending, while minerals such as microcline, muscovite, anatase, rutile, dolomite and siderite were found in minor percentages in the coal, roof and the floor samples.

- The blended coal sample showed two phases (amorphous and crystalline phase), with the amorphous phase having the highest percentages of 66.2 wt. %. Also, the crystalline phase of the blended coal sample showed that kaolinite and quartz were the major crystalline minerals with minor percentages of pyrite, anatase, microcline, illite and dolomite.

- It was found that the ash samples contained an amorphous phase ranging from 49.2 - 30 wt. %, with ash produced at 1300^oC having the lowest percentage of the amorphous phase (30 wt. %). The crystalline phase of the ash samples was found to contain major minerals such as mullite and quartz with minor percentages of rutile, hematite, magnetite, maghemite, diposide, lime, periclase, anhydrite, cristobalite, and portlandite. As expected, the percentages of mullite increased with a decrease in the amorphous phase, suggesting the transformation of kaolinite to meta-kaolinite which subsequently formed mullite. Based on the results from XRD, it is clear that some minerals found in the coal, roof, floor, and blended coal samples transformed to ash minerals during heat treatment.

- BET surface area measurements, using N_2 and CO_2, of the blended coal sample and the ash samples formed at the different heating temperatures revealed that the surface area of the blended coal sample was relatively higher when compared with the ash samples produced at the different temperatures. This was

attributed to the formation of minerals which melted and agglomerated at high temperatures. The surface area and the porosity also showed that the blended coal sample had a higher surface area and porosity when compared with the ash samples and this could be as a result of the collapsed pores during heat treatment. Also, as the temperature of ashing increased, the surface area and the microporosity decreased simultaneously with the ash generated at 1300^{o}C having the lowest surface area of 3.87 m^2/g and microporosity of 0.11 Å.

- It was found that the particle size distribution of the blended coal was lower with a higher surface area when compare with the ash samples. This is in agreement with the BET surface area results.

- Batch leaching experiments at room temperature when DW and GW was used as livivrants at 10:1 liquid to solid ratio indicated that the Ca species and SO_4^{2-} ions were released to groundwater from the ash with minor releases of Al, Si, Mg, and Fe species. Minor anions that were leached out from the ash samples included NO_3^-, NO_2^-, Cl^- and F^- during the batch leaching method.

- A slight increase in the releases of elemental species and ions was observed as leaching temperatures increased from ambient to 50^{o}C, showing that temperature has a slight influence on the leachability of the mentioned ions and elemental species. The total dissolved solids (TDS) and electron conductivity (EC) were also found to increase as leaching temperature increases. This was attributed to the dissolution of individual species during the leaching process.

- It was observed that the liquid to solid ratio of 10:1 had higher concentrations of the leachants of interest compared with when a ratio of 10:2 was used. It could be concluded from the results of liquid to solid ratio that increasing the quantity of the ash during the leaching process will not have any influence on the

concentration of the leachants to be released to the environment, but more leachants will be observed should the amount of groundwater increase.

- Column leaching experiments at ambient temperature showed that the Ca species and SO_4^{2-} ions were dominated elemental species and ions released to groundwater from the ash, with minor releases of Al, Si, Mg, and Fe species. Similarly to the batch leaching process, the minor anions that were leached included NO_3^-, NO_2^-, Cl^- and F^-.

- It was found that the column method had about 2-fold concentrations of the most leached species and ions (Ca and SO_4^{2-}) when compared with the batch leaching method at room temperature. Other species of interest in this study did not show much difference between the two leaching methods. It is advised that in studying the leachability of species during the UCG process, the column method should be used. This is because the column method is a more practicable approach, similar to what is obtainable in the field study.

- The temperature of gasification will have a large effect on the amounts of ions and species released to groundwater. Ash produced at 1300^{o}C (fused), yielded lower concentrations of ions and elemental species when compared with leachants obtained from ash produced at 1000^{o}C and 1100^{o}C. This was attributed to the mineralogy of the ash produced at 1300^{o}C and the slow dissolution of the fused ash material at 1300^{o}C. It was concluded that ash generated at high temperatures (1300^{o}C) produced less inorganic contaminants when compared with ash produced at 1000 ^{o}C and 1100^{o}C. In terms of inorganic contaminants in groundwater, it is concluded that 1300^{o}C and higher temperatures will be better temperatures for the UCG process since at these temperatures lower concentrations of the leachants and trace elements were obtained in the groundwater.

- The amounts of trace and heavy elements in the leachates were compared with the limits or standards from the Department of Water and Forestry in South Africa (DWAF) and the Environmental Protection Agency of USA (EPA). It was found that the trace and heavy elements in all the leachates were lower than the recommended limits (DWAF and EPA), except for Cd and Al. Cd and Al concentrations were slightly higher than the accepted DWAF limits.

7.3 Recommendation and future studies

Based on the findings from this study, the following recommendations are made for possible further investigations:

- A continuous leaching process should be carried out at least 2 or 3 more times in order to determine the saturation point of the various inorganic compounds that were leached.

- A study should be carried out on a continuous leaching process where fresh lixiviants are added to the already leached coal or ash samples in order to evaluate the inorganic species and ions to be leached out after the initial leaching of the coal ash.

- A scrubber solution method should be used during the combustion and pyrolysis tests in other to capture the inorganic volatiles. By using the principle of mass balance, the amount of inorganic volatiles during the UCG process could be estimated.

- An investigation of a combustion process with a mixture of two or more combustion agents (air, steam and oxygen) is recommended, in order to study the efficiency of the amount of syngas generated at a different case study. This will give a more pragmatic application to combustion studies and will yield results that can best describe the typical underground gasification process.

- An investigation of the influence of tar addition on coal during pyrolysis and combustion and the effect of leaching of char formed from coal with added tar at typical underground coal combustion process temperatures is recommended. This will aid to understand the influence of organic contaminants during UCG.

- It is recommended to investigate the influence of char and ash produced during UCG using coal of different ranks; this will help to understand the influence of different ranks of coal during underground gasification processes.

- The influence of different lixiviants on the char and ash samples should be investigated during the batch leaching method: neutral (deionised water), acidic medium (acetic acid), and basic medium (sodium hydroxide) to understand the influence of pH of the individual lixiviants during underground gasification processes.

- A more detailed analytical techniques characterisation method of the coal and ash samples using Qemscan and Electron microprobe (EMP) is recommended to give better insight into the mechanism of mineral transformation from blended coal to ash used during UCG.

References

Adam, F., & Chua, J. H., 2004. The adsorption of palmytic acid on rice husk ash chemically modified with Al (III) ion using the sol–gel technique. Journal of colloid and interface science, 280(1), 55-61.

Ahern, J. J., & Frazier, J. A., 1982. Water quality changes at underground coal gasification sites—a literature review. Laramie Energy Technology Center, US Department of Energy, under contract.

Alessio AD, Vergamini P, Benedetti E., 2000. Investigation of the structural changes of Sulcis and South Africa coals under progressive heating in vacuum. Fuel; 79:1215-20.

Attalla, M.I., Morgan, S., Riley, K., Bryant, G. and Nelson, P.F., 2004. Trace element deportment incombustion processes, Research report 50, Cooperative Research Centre for Coal inSustainable Development (CCSD), CSIRO, University of Newcastle, MacquarieUniversity, Australia.

Bayat, O.,1998. Characterisation of Turkish fly ashes. Fuel, 77(9), 1059-1066.

Bell, D.A., Towler B.F. & Fan, M., 2011. Coal gasification and its applications. Elsevier, Burlington, MA. 399 pp.

Benfell, K. E., Liu, G. S., Roberts, D. G., Harris, D. J., Lucas, J. A., Bailey, J. G., & Wall, T. F., 2000. Modelling char combustion: The influence of parent coal petrography and pyrolysis pressure on the structure and intrinsic reactivity of its char. Proceedings of the Combustion Institute, 28(2), 2233-2241.

Benson, S.A., 1987. Laboratory studies of ash deposit formation during the combustion of Western U.S. coals, PhD Thesis, the Pennsylvania State University. Pennsylvania, US.

Benson, S.A. & Holm, P.L., 1985. Composition of inorganic constituents in three low-rank coals. Industrial & Engineering Chemistry Product Research & Development, **24**(1):145-149.

Blinderman, M. S., & Friedman, S. J., 2006. Underground Coal Gasification with Carbon Capture and Storage: A Pathway to a Low-Cost, Low-Carbon Gas for

Power Generation and Chemical Syntheses, NETL 5th Annual Conference on Carbon Sequestration, Alexandria, VA. Exchange Monitor Publication.

Bohor, B.F., & Triplehorn, D.M., 1993. Tonsteins: Altered Volcanic-Ash Layers in Coal-bearing Sequences. Special Paper of the Geological Society of America, Volume 285. 42 pp.

Bolat. E; Saglam, S. & Piskin, S., 1998. Chemical demineralization of Turkish high ash bituminous coal. Fuel Processing Technology, **57**:93-99.

Bool, L.E., Helble, J.J., 1995. A laboratory study of the partitioning of trace elements during pulverized coal combustion. Energy Fuels **9**: 880-887.

Borrego, A. G., Marbán, G., Alonso, M. J. G., Alvarez, D., & Menéndez, R., 2000. Maceral effects in the determination of proximate volatiles in coals. Energy & fuels, **14**(1): 117-126.

Buhre, B., Elliott, L., Sheng, C., Gupta, R. and Wall, T., 2005. Oxy-Fuel Combustion Technology for Coal-Fired Power Generation. Progress in energy and combustion science, **31**(4): 283-307.

Burwell, E. L., 1984. Potential of underground coal gasification. Chem. Eng. Prog. (United States), 80(2).

Burton, E., Friedmann, J. & Upadhye, A. 2008. Best practices in underground coal gasification. Lawrence Livermore National Laboratory, U.S. Department of Energy Contract W-7405-7448.0.

Bunt, J. R., Waanders, F. B., & Schobert, H., 2012. Behaviour of selected major elements during fixed-bed gasification of South African bituminous coal. Journal of Analytical and Applied Pyrolysis, 93, 85-94.

Britten, J.A. & Thorsness, C.B., 1988. A Mechanistic Model for Axis Symmetric cavity growth During Underground Coal Gasification. https://web.anl.gov/PCS/acsfuel/preprint%20archive/Files/33_2_TORONTO_06-88_0126.pdf. Date of access 02-04-2015

Bryers, R.W., 1986. Influence of segregated mineral matter in coal, In: Mineral matter and ash. In Vorres, K., (Ed.). Coal, Symposium of American Chemical Society, pp. 351-374.

Cairncross, B., 2001. An overview of the Permian (Karoo) coal deposit of Southern Africa. Journal of African Earth Sciences, **33**(3-4):529-562.

Campbell, J.H. Pellizzari, E. & Santor, S., 1978. Results of groundwater quality study near an underground coal gasification experiment (Hoe Creek I), Lawrence Livermore Laboratory, Report No.: UCRL-52405.

Campbell J.H. & Washington, H., 1976. Preliminary Laboratory and Modeling Studies on the Environmental Impact of "In-Situ" Coal Gasification. Lawrence Livermore Laboratory, Report No.: UCRL-178303.

Chen, C., & Rubin, E. S., 2009. CO_2 control technology effects on IGCC plant performance and cost. Energy Policy, 37(3), 915-924.

Choudhury, N., Chaudhuri, S.G., Chakraborty, C.C., Boral, P., 2004. Studies on char morphology in relation to petrographic characteristics of some Permian coals of India. Journal of Scientific and Industrial Research, **63**(4):383-385.

Clarke, L. B., 1993. The fate of trace elements during coal combustion and gasification: an overview. Fuel, 72(6), 731-736.

Clarkson, C. R., Freeman, M., He, L., Agamalian, M., Melnichenko, Y. B., Mastalerz, M., & Blach, T. P., 2012. Characterization of tight gas reservoir pore structure using USANS/SANS and gas adsorption analysis. Fuel, 95, 371-385.

Cloke, M., Wu, T., Barranco, R. & Lester, E., 2003. Char characterisation and its application in a coal burnout model. Fuel, **82**(15-17):1989-2000.

Creelman, R.A. and Ward C.R., A., 1996. Scanning electron microscope method for automated, quantitative analysis of mineral matter in coal, International Journal of Coal Geology, 30, pp. 249-269.

Criado, M.; Palomo, A.; Fernandez-Jimenez, A., 2005. Alkali activation of fly ashes. Part 1. Effect of curing conditions on the carbonation of the reaction products. Fuel, **84**: 2048–2054.

Dalton, V.A. & Campbell, J.H., 1978. Laboratory Measurement of Groundwater Leaching and Transport of Pollutants Produced During Underground Coal Gasification. Lawrence Livermore Laboratory, Report No.: UCRL-80834.

DeGraeve, G.M., Overcast, R.L., Bergman, H.L., 1980.Toxicity of underground coal gasification condenser water and selected constituents to aquatic biota. Archives of Environmental Contamination and Toxicology, **9**(5):543–555.

Department of Water Affairs and Forestry., 1998. Minimum Requirements for Handling, Classification and Disposals of Hazardous Waste. Second Edition.

Dubikova, M., 2006. Modelling Element Mobility in Water-flyash Interactions. QCAT Technology Transfer Centre.

Dudas, M. J., 1981. Long-term leachability of selected elements from fly ash. Environmental Science & Technology, 15(7), 840-843.

Edgar, T.F., Humenick, M.J., Kaiser, W.R., Charbeneau, R.J., 1981. Environmental Effects of In-Situ Gasification of Texas lignite. Project Summary. USEPA, EPA-600/S7- 81-035.

England, T., Hand P.E. & Michael, D.C., Falcon, L.M. & Yell, A.D., 2002. Coal Preparation in South Africa. The South African Coal Processing Society. Pietermaritzburg: Natal Witness Commercial Printers (Pty) Ltd. 298 pp.

Environmental Protection Agency (EPA)., 1986. Federal Register, page 1750 – 1759

Everson RC, Neomagus HWJP, Kaitano R, Falcon R, Van Alphen C & Du Cann VM., 2008. Properties of high ash char particles derived from inertinite-rich coal: 1. Chemical, structural and petrographic characteristics. Fuel, 87 (13-14):3082-3090.

Everson RC, Okolo GN, Neomagus HW & Dos Santos J-M., 2013. X-ray diffraction parameters and reaction rate modeling for gasification and combustion of chars derived from inertinite-rich coals. Fuel, 109:148-156.

Eskom. 2008. Eskom Annual Report. http://www.eskom.co.za/annreport08/ar_2008/downloads.htm. Accessed: 26-10-2015.

Eskom. 2010. Eskom Annual Report. http://www.eskom.co.za/Whatweredoing/ElectricityGeneration/PowerStations/Pages/Majuba_Power_Station.aspx. Accessed: 26-10-2015.

Falcon, L.M. & Falcon, R.M.S., 1987. The petrographic composition of Southern African coals in relation to friability, hardness, and abrasive indices. Journal of the South African Institute of Mining and Metallurgy, **87**(10): 323-336.

Falcon, R.M.S. & Snyman C.P., 1986. An Introduction to Coal Petrography: Atlas of Petrographic Constituents in the Bituminous Coals of Southern Africa. Johannesburg: The Geological Society of South Africa. pp.27.

Falcone, S.K. Schobert, H.H. Rmdt, D.K. & Braun, S., 1984. Mineral transformations during ashing and slagging of selected low-rank coals. American Chemical Society, Division of Fuel Chemistry Preprints, **29**(4):76-83.

Falcone, S.K. & Schobert, H.H., 1986. Mineral transformations during ashing of selected low- rank coals. In Vorres, K.S. (Ed.). Mineral matter and ash in coal. ACS Symposium Series No. 301. pp 114-127.

Fernandez-Jimenez, A.; Palomo, A., 2005. Composition and microstructure of alkali activated fly Ash binder: Effect of the activator. Cem. Concr. Res, **35**: 1984–1992.

Furr, A. K., Parkinson, T. F., Hinrichs, R. A., Van Campen, D. R., Bache, C. A., Gutenmann, W. H., & Lisk, D. J., 1977. National survey of elements and radioactivity in fly ashes. Absorption of elements by cabbage grown in fly ash-soil mixtures. Environmental Science & Technology, 11(13), 1194-1201.

Franklin, R. E.. 1951. The structure of graphitic carbons. Acta crystallographica, 4(3), 253-261.

Finkelman, R. B., 1995. Modes of occurrence of environmentally-sensitive trace elements in coal. In Environmental aspects of trace elements in coal (pp. 24-50). Springer Netherlands.

French, D., Dale, L., Matulis, C., Saxby, J., Chatfield, P., & Hurst, H. J., 2001. Characterization of mineral transformations in pulverized fuel combustion by dynamic high-temperature X-ray diffraction analyzer. InProceedings of 18th Pittsburgh International Coal Conference, Newcastle, Australia (Vol. 20018).

Fruchter, J. S., Rai, D., & Zachara, J. M., 1990. Identification of solubility-controlling solid phases in a large fly ash field lysimeter. Environmental Science & Technology, 24(8), 1173-1179.

Galbreath, K.C., Zygarlicke, C., 2004. Formation and chemical speciation of arsenic-, chromium-, and nickel-bearing coal combustion PM2.5. Fuel Process. Techno **85**,701-726.

Gavals, George R. A., 1980. Random capillary model with application to char gasification at chemically controlled rates. AIChE Journal 26.4: 577-585.

Geng W, Nakajima T, Takanashi H, Ohki A., 2009. Analysis of carboxyl group and coal aromaticity by Fourier transform infrared (FTIR) spectrometry. Fuel 2009; 88:139-44.

Gibbs, B. M., Thompson, D., & Argent, B. B., 2004. A thermodynamic equilibrium comparison of the mobilities of trace elements when washed and unwashed coals are burnt under pf firing conditions. Fuel, 83(17), 2271-2284.

Given, P.H. and Yarzab, R.F., 1978. Analysis of the organic substance in coals: problems posed by the presence of mineral matter, In: Karr, C. (Ed.), Analytical Methods for Coal and Coal Products, Volume II, Academic, Press, New York, pp. 3-41.

Given, P.H., 1984 An essay on the organic geochemistry of coal, In Gorbaty, M.L., Larsen, J.W. & Wender, I. (Eds.), Coal Science, vol. 3, pp. 137.

Gluskoter, H., 1975. Mineral matter and trace elements in coal. In trace elements in coal; Babu, S. Advances in Chemistry. American Chemical Society. Trace elements in Coal.

Gluskoter, H.J., Ruch, R.R., Miller, W.G., Cahill, R.A., Dreher, G.B., & Kuhn, J.K., 1977. Trace elements in coal: occurrence and distribution. Illinois State Geological Survey Circular, **499**. 154 pp.

Goblirsch, G.M., Benson, S.A., Karner, F.R., Rindt, D.K. & Hajicek, D.R., 1984. AFBC bed material performance with low-rank coals. In kube, W.R., Sondreal, E.A. & Rao, C.D. (Eds.), Proceedings of the Twelfth Biennial Lignite Symposium: Technology and Utilization of Low-Rank Coal. DOE/METC/84-13-2. Pp. 557.

Gomez, M. R., Cerutti, S., Sombra, L. L., Silva, M. F., & Martínez, L. D., 2007. Determination of heavy metals for the quality control in argentinian herbal medicines by ETAAS and ICP-OES. Food and Chemical Toxicology, 45(6), 1060-1064.

Gong, X., Wu, T., Qiao, Y., & Xu, M., 2009. In Situ Leaching of Trace Elements in a Coal Ash Dump and Time Dependence Laboratory Evaluation. Energy & Fuels, 24(1), 84-90.

Gupta, R.P., Yan, L., Kennedy, E.M., Wall, T.F., Masson, M. and Kerison, K., 1999 System accuracy for CCSEM analysis of minerals in coal, In: Gupta, R.P., Wall, T.F., Baxter, L. (Eds.), Impact of Mineral Impurities in Solid Fuel Combustion, Kluwer Academic Publishing/Plenum, New York, pp. 225-235.

Gupta, R., 2007. Advanced coal characterization: A review. Energy Fuels, **21**:451-460.

Gupta, S.K, Wall, T.F., Creelman, R.A., Gupta, R.P., 1998. Ash fusion temperatures and the transformation of coal ash particles to slag. Fuel Process. Techno: 56, 33-43.

Gutenmann, W. H., Bache, C. A., Youngs, W. D., & Lisk, D. J., 1976. Selenium in fly ash. Science, 191(4230), 966-967.

Gregg, S.J., Sing, K.S.W., 1967. Adsorption, Surface Area and Porosity. Acad. Press, London. 371 pp

Gregg, D.W. & Edgard, T.F., 1978. Underground Coal Gasification. AIChE Journal, **24**:753-781.

Gregg, S.J., Sing, K.S.W., 1982. Adsorption area and porosity (second ed.)Academic Press Inc., New York, USA p. 303.

Grim, R.E., 1962. Applied clay mineralogy, University Of Illinois, Urbana, Illinois, Mcgraw-Hill book company Inc., New York. Pp. 97-113.

Harvey, R.D. & Ruch, R.R., 1986. Mineral matter in Illinois and other US coals. In: Vorres, K.S. (Ed.), Mineral Matter in Coal Ash and Coal. American Chemical Society Symposium Series, **301**:10-40.

Hansen, L. D., & Fisher, G. L., 1980. Elemental distribution in coal fly ash particles. Environmental Science & Technology, 14(9), 1111-1117.

Higman, C., & Van der Burgt, M., 2011. Gasification. Gulf professional publishing.

Horvath, G., & Kawazoe, K., 1983. Method for the calculation of effective pore size distribution in molecular sieve carbon. Journal of Chemical Engineering of Japan, 16(6), 470-475.

Hower, J. C., Robertson, J. D., Thomas, G. A., Wong, A. S., Schram, W. H., Graham, U. M., ... & Robl, T. L., 1996. Characterization of fly ash from Kentucky power plants. *Fuel*, *75*(4), 403-411.

Hu, G., Dam-Johansen, K., Wedel, S., & Hansen, J. P., 2006. Decomposition and oxidation of pyrite. Progress in Energy and Combustion Science, 32(3), 295-314.

Huffman, G.P. & Huggins, F.E., 1983. Investigation of partial ash melting by phase analysis of quenched samples, proceedings of the 1981, Engineering Foundation Conference at Henniker, N.H., fouling and slagging resulting from impurities in combustion gases, Bryers, R.W., Ed., Engineering Foundation, N.Y.

Huggins, F. E., 2002. Overview of analytical methods for inorganic constituents in coal. International Journal of Coal Geology, 50(1), 169-214.

Huggins, F. E., Kosmack, D. A., & Huffman, G. P., 1981. Correlation between ash-fusion temperatures and ternary equilibrium phase diagrams. Fuel, 60(7), 577-584.

Huggins, F. E., Najih, M., & Huffman, G. P., 1999. Direct speciation of chromium in coal combustion by-products by X-ray absorption fine-structure spectroscopy. Fuel, 78(2), 233-242.

Huggins, F. E., & Huffman, G. P., 2004. How do lithophile elements occur in organic association in bituminous coals?. International Journal of Coal Geology, 58(3), 193-204.

Humenick, M.J., Melissa, L. & Kenneth, F.J., 1983. Leaching Characteristics of Lignite Ash. Journal (Water Pollution Control Federation), **55**(3):310-316.

Humenick, M. J., & Mattox, C. F., 1978. Groundwater pollutants from underground coal gasification. Water Research, 12(7), 463-469.

Hurlbut Jr, C. S.,1971. Dana's Manual of Mineralogy, John Wiley and Sons Inc. New York.

Hurt, R. H., Sarofim, A. F., & Longwell, J. P., 1991. The role of microporous surface area in the gasification of chars from a sub-bituminous coal. Fuel, 70(9), 1079-1082.

Huang CYL, Schulte EE., 1985. Digestion of plant tissue for analysis by ICP emission spectroscopy. Communications in Soil Science and Plant Analysis 16, 943–958.

Ibrahim lAA., 2015. Chemical characterization and mobility of metal species in fly ash–water system. Water Science, 29 (2):109-122.

Illingworth, S. R., 1922. The Action of Solvents on Coal. Fuel in Science and Practice, 1, 213-219.

Iwashita, A., Sakaguchi, Y., Nakajima, T., Takanashi, H., Ohki, A., & Kambara, S., 2005. Leaching characteristics of boron and selenium for various coal fly ashes. Fuel, 84(5), 479-485.

Izquierdo, M., Moreno, N., Font, O., Querol, X., Alvarez, E., Antenucci, D.,& Fernández-Pereira, C., 2008. Influence of the co-firing on the leaching of trace pollutants from coal fly ash. Fuel, 87(10), 1958-1966.

Jankowski, J., Ward, C. R., French, D., & Groves, S., 2006. Mobility of trace elements from selected Australian fly ashes and its potential impact on aquatic ecosystems. Fuel, 85(2), 243-256.

Jaroniec, M., Gadkaree, K. P., & Choma, J.,1996. Relation between adsorption potential distribution and pore volume distribution for microporous carbons. Colloids and Surfaces A: Physicochemical and Engineering Aspects, 118(3), 203-210.

Johnson, R., Sellers, G., & Fleming, S.,1989. USGS Bulletin 1823, Methods for sampling and inorganic anlaysis of coal. Retrieved July 22, 2015, from USGS Publications Warehouse: http://www.pubs.usgs.gov/bul/b1823/05.htm.

Kaakinen, J. W., Jorden, R. M., Lawasani, M. H., & West, R. E. 1975., Trace element behavior in coal-fired power plant. Environmental Science & Technology, 9(9), 862-869.

Kahraman, H., Bos, F., Reifenstein, A., Coin, C.D.A., 1998. Application of a new ash fusion test to Theodore coals. Fuel 77 (9110), 1055-1011.

Kaitano, R., 2007. Characterisation and reaction kinetics of high ash chars derived from inertinite-rich coal discards (Doctoral dissertation, North-West University).

Kapusta, K., & Stańczyk, K., 2011. Pollution of water during underground coal gasification of hard coal and lignite. Fuel, 90(5), 1927-1934.

Karayigit, A. I., Gayer, R. A., Ortac, F. E., & Goldsmith, S., 2001. Trace elements in the Lower Pliocene fossiliferous kangal lignites, Sivas, Turkey. International Journal of Coal Geology, 47(2), 73-89.

Keaton Energy., 2009. About SA Coalfields. (Web) http:/www.keatonenergy.co.za/cm/sa_coal.asp. Accessed: 20-03-2015.

Kershaw, J., & Taylor, G., 1992. Properties of Gondwana coals with emphasis on the Permian coals of Australia and South Africa. Fuel Processing Technology, 127-168.

Kim, A.G. & Kazonich, G., 2004. The Silicate/non-silicate distribution of metals in fly ash and its effect on solubility. Fuel, **83**(17-18):2285-2292.

Kim, A.G., 2006. The effect of alkalinity of class F PC fly ash on metal release. Fuel, **85**:1403-1410.

Kim, A.G., Kazonich, G., and Dahlberg, M., 2003. Relative Solubility of Cations in Class F Fly Ash. Environmental Science & Technology, **37**(19):4507-4511.

Kim, A.G., 2002. Physical and Chemical Characteristics of CUB. In Vories, K.C. & Throgmorton, D. (Eds.). Proc. Coal Combustion By-Products and Western Coal Mines, US Department of Interior, Office of Surface Mining Coal Research Center, Southern Illinois University at Carbondale, 18 pp.

Kim, A.G., 2003. Leaching Methods Applied To CUB: Standard, Regulatory And Other. 15th International Symposium on Management and Use of Coal combustion Products, Jan. 27-30, 2003; St. Petersburg, Russia. Pp. 29-1-29-12

Khadse, A., Qayyumi, M., Mahajani, S. & Aghalayam, P., 2007. Underground coal gasification: A new clean coal utilization technique for India. Energy, **32**(11):2061-2071.

Kleiner, K., 2008. Nuclear energy: assessing the emissions. Nature Reports Climate Change, 130-131.

Kowalczyk, P., Terzyk, A. P., Gauden, P. A., & Solarz, L., 2002. Numerical analysis of Horvath–Kawazoe equation. Computers & chemistry, 26(2), 125-130.

Kühn, L., & Plogmann, H., 1983. Reaction of catalysts with mineral matter during coal gasification. Fuel, 62(2), 205-208.

Kukier, U., Ishak, C. F., Sumner, M. E., & Miller, W. P., 2003. Composition and element solubility of magnetic and non-magnetic fly ash fractions. Environmental Pollution, 123(2), 255-266.

Kutchko, B.G. & Kim, A.G., 2006. Fly ash characterization by SEM-EDS. Fuel, **85**(17-18):2537-2544.

Kruszewska, K. J., 2003. Fluorescing macerals in South African coals. International journal of coal geology, 54(1), 79-94.

Larsen, J. W., Hall, P., & Wernett, P. C., 1995. Pore structure of the Argonne premium coals. Energy & Fuels, 9(2), 324-330.

Lee, W.K.W.; Van Deventer, J.S.J., 2002a. The effects of inorganic salt contamination on the strength and durability of geopolymers. Colloids Surf. A, **211**, 115–126.

Lee, W.K.W.; Van Deventer, J.S.J., 2002b. Structural reorganization of class F Fly Ash in alkaline silicate solutions. Colloids Surf. A, **211**, 49–66.

Lee, S.-R., Wu, C.-Y., 2002. Study of vanadium emission control in combustion systems by thermodynamic equilibrium analyses. Adv. Environ. Res. **7**:1-10

Lee, S., 2007. Gasification of coal. In Lee, S., Speight, J.G and Loyalka, S.K (Eds.), Handbook of alternative fuel technologies. CRC Press, New York. Pp: 25-79.

Li, J., Zhu, M., Zhang, Z., Zhang, K., Shen, G., & Zhang, D., 2016. Characterisation of ash deposits on a probe at different temperatures during combustion of a Zhundong lignite in a drop tube furnace. Fuel Processing Technology, 144, 155-163.

Linc Energy Ltd., 2008. Underground coal gasification: Industry review and an assessment of the potential of UCG and UCG value added products. http://www.lincenergy.com/data/media_news_articles/relatedreport-02.pdf. Accessed: 12-05-2015).

Liu, S., Wang Y., Yu, L. & Oakey, J., 2006a. Thermodynamic equilibrium study of trace element transformation during underground coal gasification. Fuel Processing Technology, **87**(3):209-215.

Liu, S., Wang, Y., Yu L. & Oakey J. 2006b. Volatilization of mercury, arsenic and selenium during underground coal gasification. Fuel, **85**(10-11):1550-1558.

Liu, S-Q., Li J-G., Mei, M. & Dong D-L., 2007. Groundwater Pollution from Underground Coal Gasification. Journal of China University of Mining & Technology, 4:467-472.

Loubser, M. & Verryn, S., 2008. Combining XRF and XRD analysis and sample preparation to solve mineralogical problems. South African Journal of Geology, **11**:229-238.

Lu, L., Sahajwalla, V., Kong, C., & Harris, D., 2001. Quantitative X-ray diffraction analysis and its application to various coals. Carbon, 39(12), 1821-1833.

Mackowsky, M.T. & Stach, E., 1982. Coal Petrology 3rd revised edition, Gebruder Borntraeger, Berlin: Pp. 153-171.

Mahajan, O. P., 1991. CO_2 surface area of coals: the 25-year paradox. Carbon, 29(6), 735-742.

Mahajan, O. P.,1984. Physical characterization of coal. Powder technology, 40(1), 1-15.

Magee E.H., Hall H.J., & Varga, G.H. Jr., 1973. Potential Pollutants in Fossil Fuels. Esso Research and Engineering Co., Linden, N. J., Public #PB-225-039. EPA. EPA# R2-73-249. 151 p.

Maity S, Mukherjee P., 2006. X-ray structural parameters of some Indian coals. Curr Sci; **91**(3):337- 40.

Malumbazo, N., 2011. Chemical and physical structural studies on two inertinite-rich lump coals (Doctoral dissertation, University of the Witwatersrand. Johannesburg).

Marsh H., 1987. Adsorption methods to study microporosity in coals and carbons – a critique. Carbon; 25(1):49–58.

Massaquoi JGM., 1981. Combustion in underground coal conversion. Dissertation, West Virginia University.

Martelli, E., Kreutz, T., & Consonni, S., 2009. Comparison of coal IGCC with and without CO 2 capture and storage: shell gasification with standard vs. partial water quench. Energy Procedia, 1(1), 607-614.

Matjie, R.H., 2008. Sintering and slagging of mineral matter in South African coals during the coal gasification process. PhD Thesis, University of Pretoria. http://www.upetd.up.ac.za/thesis/available/etd-11112008-1259131/. Accessed: 30-04-2015.

Matjie, R.H., van Alphen, C. & Pistorius, P.C., 2006. Mineralogical characterisation of Secunda gasifier feedstock and coarse ash. Minerals Engineering, **19**:256-261.

Matjie, R.H., Li, Z., Ward, C.R. & French D., 2008. Chemical composition of glass and crystalline phases in coarse coal gasification ash. Fuel, **87**:857-869.

Matjie, R. H., French, D., Ward, C. R., Pistorius, P. C., & Li, Z., 2011. Behaviour of coal mineral matter in sintering and slagging of ash during the gasification process. Fuel Processing Technology, 92(8), 1426-1433.

Matjie, R.H., Ward, C.R., Li, Z., 2012a. Mineralogical transformations in coal feedstocks during carbon conversion, based on packed-bed combustor tests: Part 1. Bulk coal and ash studies. Coal Combustion and Gasification Products 4, 45–54

Matjie, R. H., Ward, C. R., & Li, Z., 2012b. Mineralogical transformations in coal feedstocks during carbon conversion, based on packed bed combustor tests, Part 2: Behaviour of individual particles. Coal Combustion and Gasification Products, 4, 55-67.

Matjie, R. H., Ginster, M., Van Alphen, C., & Sobiecki, A., 2005. Detailed characterisation of Sasol ashes. In World of coal ash conference.

Matjie, R. H., Li, Z., Ward, C. R., Kosasi, J., Bunt, J. R., & Strydom, C. A., 2015. Mineralogy of Furnace Deposits Produced by South African Coals during Pulverized-Fuel Combustion Tests. Energy & Fuels, 29(12), 8226-8238.

Mato, R. R. A. M., 2002. Groundwater pollution in urban Dar es Salaam, Tanzania: assessing vulnerability and protection priorities.

Maroto-Valer, M. M., Love, G. D., & Snape, C. E., 1994. Relationship between carbon aromaticities and HC ratios for bituminous coals. Fuel, 73(12), 1926-1928.

Marrero, J., Polla, G., Rebagliati, R. J., Plá, R., Gómez, D., & Smichowski, P., 2007. Characterization and determination of 28 elements in fly ashes collected in a thermal power plant in Argentina using different instrumental techniques. Spectrochimica Acta Part B: Atomic Spectroscopy, 62(2), 101-108.

Mead, S.W., Wang, F.T., Stuermer, D.H., Raber, E., Ganow, H.C. & Stone, R., 1980. Implications of Groundwater Measurements of the Hoe Creek UCG Site in Northeastern Wyoming. Lawrence Livermore Laboratory Report No. UCRL-84083.

Meany, R.A. & Maynard, A., 2009. A Review of the Potential for Underground Coal Gasification and Gas to Liquids Applications in. Pedirka Basin, Onshore Northern Territory and Pela 77 Pedirka Basin, Onshore South Australia Australia., Mulready Consulting Services Pty Ltd.

Meng, X., Xiao, X., Le, D. D., & Takarada, T., 2011. Two-stage steam gasification of waste biomass in fluidized bed at low temperature: Parametric investigations and performance optimization. Bioresource technology, 102(2), 1975-1981.

Meyers, R., 1982. Coal structure. California: Academic Press, INC.

Mitchell, R. S., & Gluskoter, H. J.,1976. Mineralogy of ash of some American coals: variations with temperature and source. Fuel, 55(2), 90-96.

Micromeritics instrument corporation., 2006. Accelerated surface area and porosimetry system (ASAP2020), Operator's manual V3.01, Pg: C1-44.

Miller, B.G., 2004. Coal energy systems. Elsevier Academic Press Publications.

Molina, A., & Mondragon, F.,1998. Reactivity of coal gasification with steam and CO 2. Fuel, 77(15), 1831-1839.

Moitsheki, L.J., Matjie, R.H., Baran, A., Mooketsi, O.I. & Schobert, H.H., 2010. Chemical and mineralogical characterization of a South African bituminous coal and its ash, and effect of pH of ash transport water. Minerals Engineering, **23**(3):258-261.

Moreno, N., Querol, X., Andrés, J. M., Stanton, K., Towler, M., Nugteren, H., & Jones, R., 2005. Physico-chemical characteristics of European pulverized coal combustion fly ashes. Fuel, 84(11), 1351-1363.

Moore, D., & Reynolds Jnr, R., 1997. X-ray diffraction and the identification and analysis of clay minerals. New York: Oxford University Press.

Moreno, I. M., González-Weller, D., Gutierrez, V., Marino, M., Cameán, A. M., González, A. G., & Hardisson, A., 2008. Determination of Al, Ba, Ca, Cu, Fe, K, Mg, Mn, Na, Sr and Zn in red wine samples by inductively coupled plasma optical emission spectroscopy: evaluation of preliminary sample treatments. Microchemical Journal, 88(1), 56-61.

Mukherjee S, Srivastava SK., 2006. Minerals transformation in north eastern regions coals of Indian on heat treatment. Energy Fuels; 20(3):1089-96.

National Ground Water Association., 2010. *Brackish Groundwater* (National Ground Water Association, Westerville, OH), Information Brief. Assessed 10-02-2016 .

Nandi S, Walker Jr P., 1970. Activated diffusion of methane in coal. Fuel; 49(3):309–23.

Nathan, Y., Dvorachek, M., Pelly, I., & Mimran, U., 1999. Characterization of coal fly ash from Israel. Fuel, 78(2), 205-213.

Narukawa, T., Riley, K. W., French, D.H., Chiba, K., 2007. Speciation of chromium in Australian fly ash. Talanta 73, 178-184.

Nel, S., 2011. Catalytic steam gasification of large coal particles (Doctoral dissertation, North-West University).

Nie, B., Liu, X., Yang, L., Meng, J., & Li, X., 2015. Pore structure characterization of different rank coals using gas adsorption and scanning electron microscopy. Fuel, 158, 908-917.

Nishiyama, Y.,1991. Catalytic gasification of coals—features and possibilities. Fuel processing technology, 29(1), 31-42.

Nobbs, D.M., Barford, I.P., Carroll, B.I., Peters, G.M., 1997. An integrated investigation of anthropogenic selenium contamination in Lake Macquarie. Pure Appl. Chem. 69(11): 2387- 2401.

OECD., 2012. Working Paper: The Global Value of Coal IEA Coal Industry Advisory Board OECD, Paris. http://www.desmogblog.com/sites/beta.desmogblog.com/files/global_value_of_coal.pdf assessed 12/07/2015

O'Gorman, J.V. & Walker, P.L., 1973. Thermal behaviour of mineral fraction separated from selected America coal. Fuel, **52**(1):71-79.

Okolo, G.N., 2010. The effects of chemical and physical properties of chars derived from inertinite-rich, high ash coals on gasification kinetics. M.Eng. Dissertation, North West University, Potchefstroom, South Africa. Pp. 276.

Okolo, G.N., Everson, R.C., Neomagus, H.W.J.P., Roberts, M.J. & Sakurovs, R., 2015. Comparing the porosity and surface areas of coal as measured by gas adsorption, mercury intrusion and SAXS techniques. Fuel, **141**:293-304.

Ogunro, V. O., & Inyang, H. I., 2003. Relating batch and column diffusion coefficients for leachable contaminants in particulate waste materials. Journal of environmental engineering, 129(10), 930-942.

Osborne, D.G., 1988. Coal Preparation Technology. Graham & Trotman. London. pp.1175.

Özbayoğlu, V. & Özbayoğlu, M.E., 2006. A new approach for the prediction of ash fusion temperatures: A case study using Turkish lignite. Fuel, **85**(4):545-552.

Pendowski, J. J. (2003). An Assessment of Laboratory Leaching Tests for Predicting the Impacts of Fill Material on Ground Water and Surface Water Quality.

Pinetown, Kaydy Lavern, Colin R. Ward, and W. A. Van der Westhuizen., 2007. "Quantitative evaluation of minerals in coal deposits in the Witbank and Highveld Coalfields, and the potential impact on acid mine drainage." *International Journal of Coal Geology* 70.1 166-183.

Pinheiro, H. J., Pretorius, C. C., Boshoff, H. P., & Barker, O. B., 1999. A techno-economic and historical review of the South African coal industry in the 19th and 20th centuries AND analyses of coal product samples of South African collieries 1998–1999. Bulletin, 113, 97.

Phiri, Z., 2010. Nitric Oxide Reduction by Chars Derived from High Ash Inertinite-rich Discard Coals (Doctoral dissertation, North-West University, Potchefstroom Campus).

Prevost XM., 2003. SA coal resources and reserves, a present-day outlook. Paper presented at: Application of Computers and Operations Research in the Minerals Industries (APCOM). Proceedings of the South African Institute of Mining and Metallurgy; 2003 May 14-16; Cape Town, South Africa. Johannesburg: SAIMM; 2003. p. 99-102.

Pricewaterhouse Coopers (PwC)., 2008. Linc Energy Limited underground coal gasification: industry review and an assessment of the potential of UCG and UCG value added products. Assessed 05-03-2015.

Prabu, V. & Jayanti, S., 2011. Clean Coal Utilization Based on Underground Coal Gasification Integrated Solid Oxide Fuel Cells and Carbon dioxide Sequestration. In the Proceedings of the World Renewable Congress, Sweden. Pp. 697-704.

Prinsloo, C. B., 2008. A study into the fundamental understanding of iron-transformations and the effect of iron as fluxing agent on Highveld fine coal sources during gasification/by Christoffel Bernardus Prinsloo (Doctoral dissertation, North-West University).

Profomo, A., Spini, G., Cucca, L., Pesavento, M., 2003. Determination of inorganic nickel compounds in the particulate matter of emissions and workplace air by selective sequential dissolutions. Talanta 61, 465-472.

Quanta 250 FEG., 2012: Discover the “any sample, all data” solution for ultimate versatility and high resolution SEM. https://www.fei.com/WorkArea/DownloadAsset.aspx?id=214748386688. Accessed: 12-07-2015.

Querol, X., Fernández-Turiel, J., & López-Soler, A., 1995. Trace elements in coal and their behaviour during combustion in a large power station. Fuel, 74(3), 331-343.

Querol, X., Umana, J. C., Alastuey, A., Ayora, C., Lopez-Soler, A., & Plana, F., 2001. Extraction of soluble major and trace elements from fly ash in open and closed leaching systems. Fuel, 80(6), 801-813.

Querol, X., Juan, R., Lopez-Soler, A., Fernandez-Turiel, J., & Ruiz, C. R.,1996. Mobility of trace elements from coal and combustion wastes. Fuel, 75(7), 821-838.

Ray, A., Adria, D., Sara, H., Doug, P. & Robert B.S., 2003. An Assessment of Laboratory Leaching Tests for Predicting the Impacts of Fill Material on Ground

Water and Surface Water Quality. A Report to the Legislature. http://www.ecy.wa.gov/programs/tcp/cleanup.html. Assessed 20/03/2015.

Rao, C. P., & Gluskoter, H. J., 1973. Occurrence and distribution of minerals in Illinois coals. Urbana: Illinois State Geological Survey.

Raask, E., 1985. Mineral impurities in coal combustion: Behaviour Problems and Remedial Measures. Hemisphere Publishing Company, New York, pp 484.

Radovic, L. R., Menon, V. C., Leon, C. L. Y., Kyotani, T., Danner, R. P., Anderson, S., & Hatcher, P. G., 1997. On the porous structure of coals: evidence for an interconnected but constricted micropore system and implications for coalbed methane recovery. Adsorption, 3(3), 221-232.

Reed, G.P., Dugwell, D.R., Kandiyoti, R., 2001. Control of trace elements in gasification: distribution to the output streams of a pilot scale gasifier. Energy Fuels 15, 794-800.

Reid, W.T., 1981. Coal ash – its effect on combustion systems, in chemistry of coal utilisation, M.A. Elliot, Ed., John Wiley, N.Y., Chapter 21, pp. 1389-1446.

Reifenstein, A. P., Kahraman, H., Coin, C. D. A., Calos, N. J., Miller, G., & Uwins, P., 1999. Behaviour of selected minerals in an improved ash fusion test: quartz, potassium feldspar, sodium feldspar, kaolinite, illite, calcite, dolomite, siderite, pyrite and apatite. Fuel, 78(12), 1449-1461.

Renton, J.J., 1986 Semiquantitative determination of coal minerals by X-ray diffractometry, In: Vorres, K.S. (Ed.), Mineral Matter and Ash in Coal, American Chemical Society Symposium Series 301, pp. 60.

Russell, S.J. and Rimmer, S.M., 1979. Analysis of mineral matter in coal, coal gasification ash, and coal liquefaction residues by scanning electron microscopy and X-ray diffraction, In: Karr, C. (Ed.), Analytical Methods for Coal Products, vol. 3. Academic Press, NewYork, pp. 133-162.

Saikia, N., Kato, S., & Kojima, T., 2006. Compositions and leaching behaviours of combustion residues. Fuel, 85(2), 264-271.

Sakurovs, R., French, D., & Grigore, M., 2007. Quantification of mineral matter in commercial cokes and their parent coals. International Journal of Coal Geology, 72(2), 81-88.

Sanchez, F., Keeney, R., Kosson, D. S., Delapp, R., & Thorneloe, S., 2006. Characterization of mercury-enriched coal combustion residues from electric utilities using enhanced sorbents for mercury control. Contract No. EP-C-04-023, Work Assignment, 1-31.

Sarwar, A., Khan, M. N. and Azhar, K. F., 2014. The Physicochemical Characterization of a Newly Explored Thar Coal Resource. Energy Sources, Part A: Recovery, Utilization, and Environmental Effects, **36**(5): 525-536.

Schumann, R., 1952. Metallurgical Engineering Volume l Engineering Principles. Addison-Wesley.

Schobert, H. H., 2013. Chemistry of Fossil Fuels and Biofuels. New York: Cambridge University Press.

Senel, I. G., Gürüz, A. G., Yücel, H., Kandas, A. W., & Sarofim, A. F.,2001. Characterization of pore structure of Turkish coals. Energy & fuels, 15(2), 331-338.

Seggiani, M., 1999. Empirical correlations of the ash fusion temperatures and temperatures of critical viscosity for coal and biomass ashes. Fuel 78, 1121-1125.

Seidel, A., & Zimmels, Y., 1998. Mechanism and kinetics of aluminum and iron leaching from coal fly ash by sulfuric acid. Chemical Engineering Science, 53(22), 3835-3852.

Sembiring, S., Simanjuntak, W., Manurung, P., Asmi, D., & Low, I. M., 2014. Synthesis and characterisation of gel-derived mullite precursors from rice husk silica. Ceramics International, 40(5), 7067-7072.

Singh, D. N., & Kolay, P. K., 2002. Simulation of ash–water interaction and its influence on ash characteristics. Progress in Energy and Combustion Science, 28(3), 267-299.

Sitko, R., Zawisza, B., & Malicka, E., 2012. Modification of carbon nanotubes for preconcentration, separation and determination of trace-metal ions. TrAC Trends in Analytical Chemistry, 37, 22-31.

Skoog, D., Holler, F., & Nieman, T., 1998. Principles of instrumental analysis. USA: Harcourt Brace & Company.

Skoog, D., Holler, F., & Crouch, S., 2007. Principles of Instrumental Analysis 6th Edition. Belmont, USA: BROOKS/COLE CENGAGE Learning.

Shafirovich, E. & Varma, A., 2009. Underground Coal Gasification: A Brief Review of Current Status. Industrial & Engineering Chemistry Research, **48**(17):7865-7875.

Sharma, D.K. & Gihar, S., 1988. Chemical cleaning of low grade coals through alkali-acid leaching employing mild conditions under ambient pressure. Fuel, **70**:663-665.

Speight, J. G., 1994. The Chemistry and Technology of Coal. New York: CRC Press.

Speight, J., 2005. Handbook of Coal Analysis. John Wiley & Sons. Inc.

Smoot, L.D., & Smith, P.J., 1985. Coal combustion and gasification. The Plenum Chemical Engineering Series. New York: Plenum Press.

Snyman, C.P. & Botha, J.W., 1993. Coal in South Africa. Journal of African Earth Science, **16**:171-180.

Snyman CP ., 1998. Coal in the mineral resources of South Africa. In: Wilson MGC and Anhaeusser CR (eds) Handbook, council for geoscience 16, p 136–205.

Sobolik, J. L., & Ludlow, D. K., 1992. Parametric sensitivity comparison of the BET and Dubinin-Radushkevich models for determining char surface area by CO 2 adsorption. Fuel, 71(10), 1195-1202.

Solcova, O., Karel, S., Jan, R., Krzysztof, S. & Petr, S., 2009. Gas transport through porous strata from underground reaction source: The influence of the gas kind,

temperature and transport-pore size. Fuel Processing Technology, **90**(12):1495-1501.

Speight, J., 2005. Handbook of Coal Analysis. John Wiley & Sons. Inc.

Su, S., Pohl, J.H., & Holcombe, D., 2003. Fouling propensities of blended coals in pulverized coal-fired power station boilers. Fuel, **82**:1653-1667.

Suárez-Ruiz, I., & Crelling, J. C. (Eds.)., 2008. Applied coal petrology: the role of petrology in coal utilization. Academic Press.

Subramoney, S., 2010. Africa has the advantage–it now needs to win the game. Retrived from http://www. nepad. org/nepad/news/1502/africa-has-advantage-it-now-needs-win-game. Assessed 20/05/2015.

Subramoney J, Van Wyk J, Dithupe M, Molapo A, Mahlangu N & Morumudi R. 2009. *Digest of South African energy statistics*. Pretoria: Department of Energy, Republic of South Africa.

Suraj, G.; Iyer, C. S. P.; Rugmini, S.; Lalithumbika, M., 1997. The effect of micronization on kaolinites and their sorption behaviour. Applied Clay Science 12, 111-130.

Suzuki, T., Mishima, M., Takahashi, T., & Watanabe, Y., 1985. Catalytic steam gasification of Yallourn coal using sodium hydridotetracarbonyl ferrate. Fuel, 64(5), 661-665.

Srinivasachar, S., Helble, J. J., & Boni, A. A., 1990. Mineral behavior during coal combustion 1. Pyrite transformations. Progress in Energy and Combustion Science, 16(4), 281-292.

Stanczyk, K., Howaniec, N., Smoliński, A., Świądrowski, J., Kapusta, K., Wiatowski, M., Grabowski, J. & Rogut, J., 2011. Gasification of lignite and hard coal with air and oxygen enriched air in a pilot scale ex-situ reactor for underground gasification. Fuel, **90**(5):1953-1962.

Stach, E., Mackowsky, M-Th., Teichmuller, M., Taylor, G.H., Chandra, D. and Teichmuller, R., 1982. Textbook of coal petrology, 2nd. Rev. Ed. Berlin. Gebruder Borntraeger, pp.314-328; 535.

Stuermer, D.H., Ng, D.J., & Morris, C.J., 1982. Organic contaminants in ground water near an underground coal gasification site in North Eastern Wyoming. Environmental Science & Technology, **16**(9):582-587.

Swaine, Dalway J., 1994. Trace elements in coal and their dispersal during combustion. Fuel Processing Technology 39.1-3 121-137.

Swaine, Dalway J., 2000. Why trace elements are important. Fuel Processing Technology 65: 21-33.

Swanepoel, J.C.; Strydom, C.A., 2002 Utilisation of fly Ash in a geopolymeric material. Appl. Geochem, **17**:1143–1148.

Thomas Jr J, Damberger HH., 1976. Internal surface area, moisture content, and porosity of illinois coals: variations with coal rank. Circular 493, Illinois State Geo. Survey, Urbana; p. 44.

Thommes, M., 2010. Physical adsorption characterization of nanoporous materials. *Chemie Ingenieur Technik*, *82*(7), 1059-1073.

Thorsness, C.B., & Rozsa, R.B., 1976. In-situ coal gasification: model calculations and laboratory experiments. SPE Paper 6182. 51st Annual Fall Technical Conference and Exhibition, New Orleans, Louisiana, October 3–6.

Tomita, A., 2001. Catalysis of carbon-gas reactions. Catalysis Surveys from Japan, **5**:17-24.

Van Alphen, C., 2005. Factors influencing fly ash formation and slag deposit formation (slagging) on combusting a South African pulverised fuel in a 200 MWe boiler (Doctoral dissertation, Faculty of Engineering and the Built Environment, University of the Witwatersrand, Johannesburg).

Van Alphen, C., 2007. Automated mineralogical analysis of coal and ash products–challenges and requirements. Minerals Engineering, 20(5), 496-505.

Van Dyk. J.C., 2006. Understanding the influence of acidic components (Si, Al, and Ti) on ash flow temperature of South African coal sources. Mineral Engineering, **19**:280-286.

Van Dyk, J.C., Baxter, L.L., Van Heerden, J.H.P. & Coetzer, R.L.J., 2005. Chemical fractionation tests on South African coal sources to obtain species-specific information on ash fusion temperatures (AFT). Fuel, **84**(14-15):1768-1777.

Van Dyk, J.C. & Waanders, F.B., 2007. Manipulation of gasification coal feed in order to increase the ash fusion temperature of the coal enabling the gasifiers to operate at higher temperatures. Fuel, **86**:2728-2735.

Van Dyk, J.C., Waanders, F.B., Benson, S.A., Laumb, M.L. & Hack, K., 2009. Viscosity predictions of the slag composition of gasified coal, utilizing FactSage equilibrium modelling. Fuel, **88**:67-74.

Van Dyk, J., Brand, J. F., Strydom, C., & Waanders, F., 2015 Update on the 50-MWe Theunissen Underground Coal Gasification Project.

Van der Sloot, H.A., L. Heasman, & Quevauviller Ph., 1997. Harmonization of Leaching/Extraction Tests. Studies in Environmental Science, **70**:1-281.

Van Niekerk, D., 2008. Structural elucidation, molecular representation and solvent interaction of vitrinite-rich and inertinite-rich South Africa coals. Doctoral dissertation. Penn state university, U.S.A.

Van Krevelen, D.W., 1981. Coal: Typology- Physical, Chemistry, Construction. Coal Science and Technology Series, Volume 3. Anderson, L.L. (Ed.), Elsevier, Amsterdam. Pp: 58-88, 111-126, 160-174, 309-341.

Van Nierop, P., Erasmus, H. B., & van Zyl, J. W., 2000. Sasol's achievements in the 20th century as a building block for the 21st.Gasification Technologies Council, San Francisco, California, USA, 8-11.

Van der Riet, M., 2008. Underground coal gasification. In Proceedings of the SAIEE Generation Conference. Eskom College, Midrand (19 Feb 2008).

Van Dyk, J. C., Benson, S. A., Laumb, M. L., & Waanders, B., 2009. Coal and coal ash characteristics to understand mineral transformations and slag formation. *Fuel*, *88*(6), 1057-1063.

Van Dyk, JC and Waanders, F.B., (2007). Manipulation of gasification coal feed in order to increase the ash flow temperature of the coal enabling the gasifiers to operate at higher temperatures. FUEL, **86**: 2728-27365.

Van Dyk, J. C., Waanders, F. B., & Van Heerden, J. H. P. ,2008. Quantification of oxygen capture in mineral matter during gasification. *Fuel*, *87*(12), 2735-2744.

Vassilev, S.V. & Vassileva, C.G., 2005. Methods for characterization of composition of fly ashes from coal-fired power station: A critical overview. Energy & Fuels, **19**(3):1084-1098.

Vassilev, Stanislav V., and Christina G. Vassileva., 2007. "A new approach for the classification of coal fly ashes based on their origin, composition, properties, and behaviour." Fuel 86.10: 1490-1512.

Vassilev, S. V., & Tascón, J. M., 2003. Methods for characterization of inorganic and mineral matter in coal: a critical overview. Energy & Fuels, 17(2), 271-281.

Verma, R.P., Mandal, R., Chaulya, S.K., Singh, P.K., Singh, A.K. & Prasad, G.M., 2014. Contimatination of underground water due to underground gasification. International Journal of Water Resources & Environmental Engineering, **6**(12): 303-311.

Vorres, K.S. (Ed.)., 1986. Mineral matter and ash in coal. http://pubs.acs.org/doi/pdf/10.1021/bk-1986-0301.ch001. Assessed 05-06-2015.

Walker, P. L., Verma, S. K., Rivera-Utrilla, J., & Davis. A., 1988. Densities, porosities and surface areas of coal macerals as measured by their interaction with gases, vapours and liquids. Fuel, 67(12), 1615-1623.

Walker, L.K., Blinderman, M.S., Brun K., 2001. An IGCC Project at Chinchilla, Australia, based on UCG, in Gasification Technologies Conference, San Francisco, USA.2001. p. 8–10.

Walker, P. L., 1981. Microporosity in coal: its characterization and its implications for coal utilization. Philosophical Transactions of the Royal Society of London A: Mathematical, Physical and Engineering Sciences, 300(1453), 65-81.

Wall, T.F., Creelman, RA., Gupta, R.P., Gupta, S.K., Coin, C., Lowe, A., 1998. Coal ash fusion temperatures - new characterization technique, and implications for slagging and fouling. Prog. Energy. Combust. Sci. 24, 345-353.

Wall, T.F., Gupta, S.K., Gupta, R.P., Sanders, RR, Creelman, RA., Bryant, G.W., 1999. False deformation temperatures for ash fusibility associated with the conditions for ash preparation. Fuel 78, 1057-1063.

Wang, B., Li, W., Li, B., Wang, G., 2007. Study on the fate of As, Hg and Pb in Yima coal via subcritical water extraction. Fuel 86, 1822-1830.

Ward, C.R., 2002. Analysis and significance of mineral matter in coal seams. International Journal of Coal Geology, **50**:135-168.

Ward, C.R., 1991. Mineral matter in low-rank coals and associated strata of the Mae Moh basin, Northern Thailand. International Journal of Coal Geology, **17**:69-93.

Ward C.R. & French, D., 2004. Analysis and significance of mineral matter in coal, The Society for organic petrology, Short Course Notes, The University of New South Wales, Sydney, NSW, Australia, pp. 7-68.

Ward, C.R., French, D., 2006. Determination of glass content and estimation of glass composition in fly ash using quantitative X-ray diffractometry. Fuel 85, 2268–2277.

Ward, C.R., 1974. Isolation of mineral matter from Australian bituminous coals using hydrogen peroxide, Fuel, **53**:220-221.

Ward, C.R., 1977. Mineral matter in the Harrisburg-Springfield (No.5) Coal Member of the Carbondale Formation, Illinois Basin, Illinois State Geological Survey, Circular 498, pp. 35.

Ward, C.R., 1978 Mineral matter in Australia bituminous coals, Proceedings, Australasian Institute of Mining and Metallurgy 267, pp. 7-25.

Ward, C.R., 1989. Minerals in bituminous coals of the Sydney Basin (Australia) and Illinois Basin(U.S.A.), International Journal of Coal Geology 13, pp. 455-479.

Ward, C. R., French, D., & Jankowski, J., 2003. Comparative evaluation of leachability test methods and element mobility for selected Australian fly ash samples. Co-operative Research Centre for Coal in Sustainable Development, 22.

Ward, C.R., 1984. (Editor), Coal Geology and Coal Technology, School of applied geology, University of New South Wales, Australia, Blackwell Scientific publications, Melbourne, Oxford, London, 40-113.

WCI., 2003. Ecoal. The quarterly Newsletter of the World Coal Institute. http://www.org/resources/ecoal/ecoal---back-issues/. Accessed: 25-10-2015.

WCI., 2007. Coal Statistics. http://www.worldcoal.org/resources/coal-statistics/index.php. Accessed: 25-10-2015.

Wild, S., 2014. The battle of Majuba goes underground. http://mg.co.za/article/2014-01-17-the-battle-of-majuba-goes-underground. Accessed: 12-04-2015.

Wolf, R.E., 2005. What is ICP-MS? ... and more importantly, what can it do? USGS/Central Region/Crustal Imaging and Characterization Team.

Wood, B. J., & Sancier, K. M., 1984. The mechanism of the catalytic gasification of coal char: a critical review. Catalysis Reviews Science and Engineering, 26(2), 233-279.

Xu, A., & Sarkar, S. L., 1994. Microstructural development in high-volume fly-ash cement system. Journal of materials in Civil Engineering, 6(1), 117-136.

Xu, M., Yan, R., Zheng, C., Qiao, Y., Han, J., & Sheng, C., 2004. Status of trace element emission in a coal combustion process: a review. Fuel Processing Technology, 85(2), 215-237.

Yang L, Liang J, & Yu L., 2003. Clean coal technology – study on the pilot project experiment of underground coal gasification. Energy, **28**:1445-60.

Yang, L.H., Zhang, X., Liu, S.Q., Yu, L., & Zhang, W.L., 2008. Field test of large-scale hydrogen manufacturing from underground coal gasification (UCG). International Journal of Hydrogen Energy, **33**:1275-1285.

Yani, S., 2009. Sulphur Transformation during Pyrolysis of an Australian Lignite. University of Western Australia.

Ye, R., Xiang, C., Lin, J., Peng, Z., Huang, K., Yan, Z., & Ceriotti, G., 2013. Coal as an abundant source of graphene quantum dots. Nature communications, 4.

Yi, H., Hoo, J., Duan., L., Tang, x., Ning, P., Li, x., 2008. Fine particle and trace element emissions from an anthracite coal-fired power plant equipped with a bag-house in China. Fuel 87, 2050- 2057.

Yu, J., Lucas, J., & Wall, T., 2007. Formation of the structure of chars during devolatilization of pulverized coal and its thermoproperties: a review. Progress in Energy and Combustion Science, **33**:135-170.

Zahir, F., Rizwi, S.J., Haq, S.K., Khan. R.H., 2005. Low dose mercury toxicity and human health. Environ. Toxicol Pharmacol. 20: 351-360.

Zhou Y, Lemaignen L, Chatzakis IN, Reed GP, Dugwell DR, Kandiyoti R., 2000. An attempt to correlate conversions in pyrolysis and gasification with FT-IR spectra of coals. Energy Fuels; **14**:1049-58.

Appendix

Appendix A

Table A: Crystalline phase of the ash sample without spiking

Mineral Identification (%)	Formula	Ash 1000 ^{o}C	Ash 1000 ^{o}C	Ash 1100 ^{o}C	Ash 1200^{o}C	Sintered 1300^{o}C
Quartz	SiO_2	68.8	62.7	52.4	52.1	49.7
Mullite	$3Al_2O_32SiO_2$	19.1	27.9	39.8	42.9	46.5
Cristobalite	SiO_2	0.7	0.6	-	0.1	-
Anorthite	$CaAl_2SiO_8$	0.1	0.1	0.1	-	0.1
Rutile	TiO_2	2.9	3	2.7	1.4	1
Hematite	FeO_3	1.7	1.8	1.3	1.4	1.2
Maghemite	Fe_2O_3	1.7	0.8	0.8	0.7	0.6
Magnetite	Fe_3O_4	1.7	-	-	-	-
Diopside	$MgCaSi_2O_6$	0.7	0.6	0.5	0.3	0.4
Lime	CaO	0.6	0.2	0.1	-	-
Periclase	MgO	-	-	0.3	-	-
Anhydrate	$CaSO_4$	2	2.1	1.7	0.8	0.3
Portlandite	$Ca(OH)_2$	-	0.1	0.3	0.3	0.1

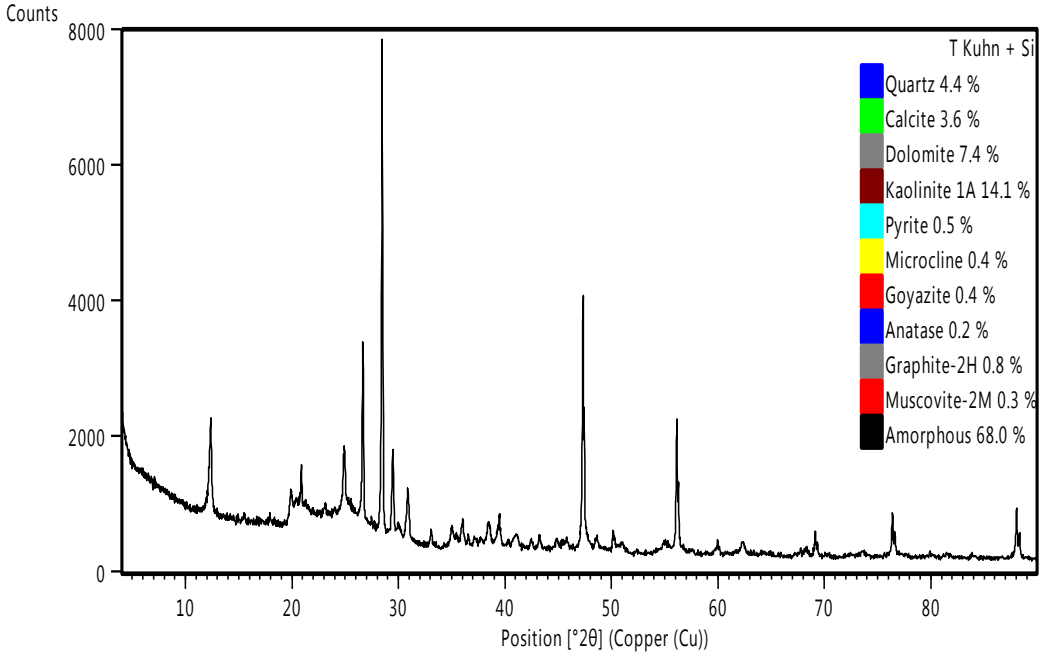

Figure A1: Diffractograph of Blended coal sample

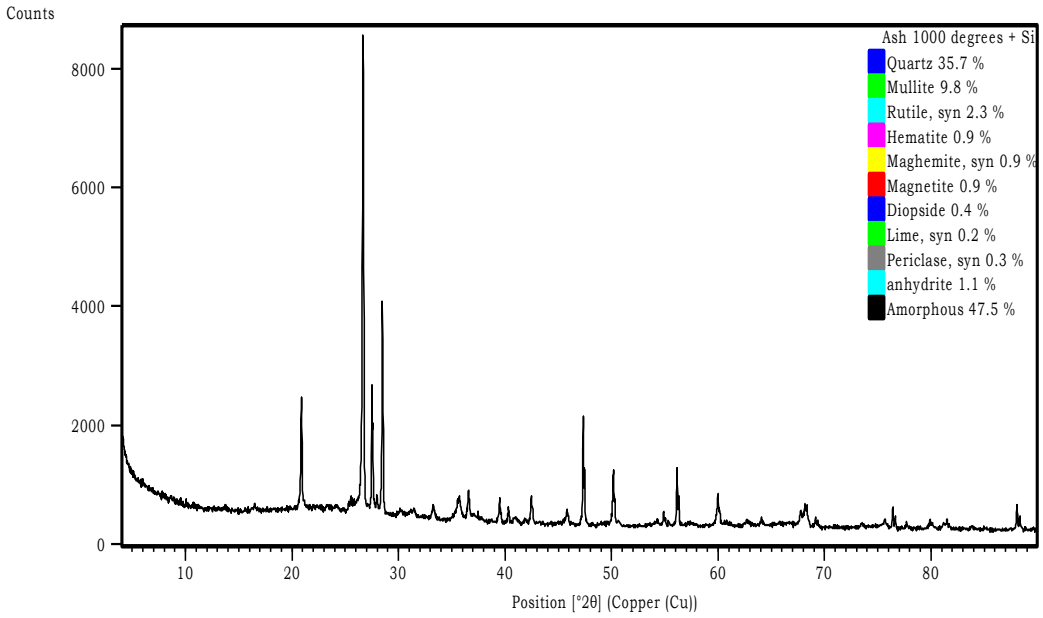

Figure A2: Diffractograph of ash at 1000 ºC

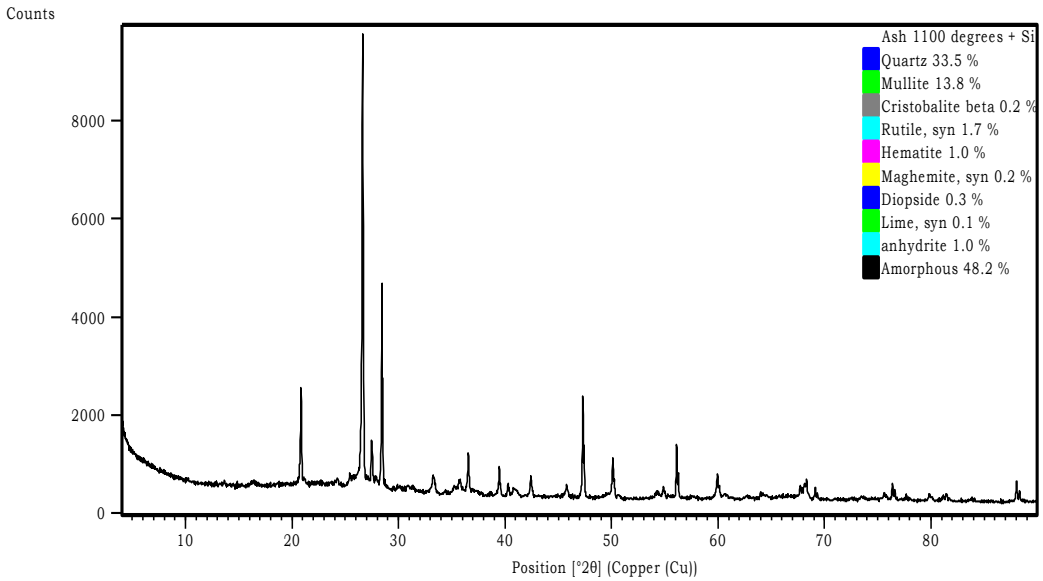

Figure A3: Diffractograph of ash at 1100 ºC

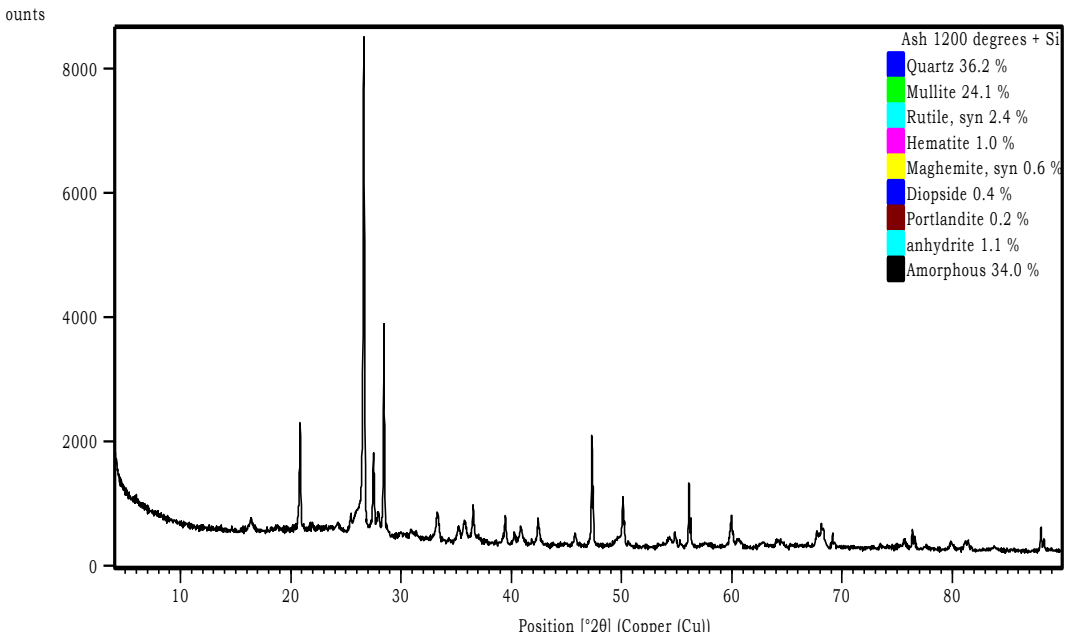

Figure A4: Diffractograph of ash at 1200 ºC

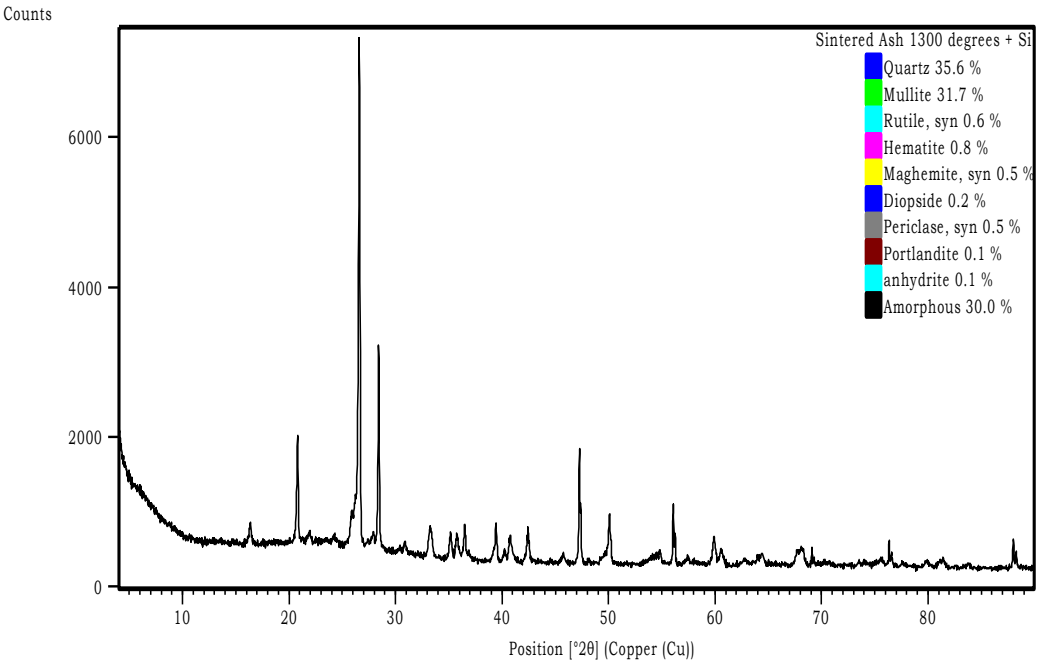

Figure A5: Diffractograph of ash at 1300 ºC

Appendix B

Table B1: Concentration of Al with respect to time at different leaching temperatures (1000°C ash) Al

Time(hrs)	20°C(ppm)	30°C(ppm)	40°C(ppm)	50 °C(ppm)
0	1.20	1.20	1.20	1.20
0.5	1.32	1.52	1.71	1.91
1	1.91	2.31	3.04	3.25
2	2.05	2.59	3.21	3.56
4	2.23	3.08	3.52	3.84
8	2.52	3.50	3.79	4.18
10	2.89	3.73	3.93	4.52
12	3.38	4.14	4.55	5.22
24	3.61	4.51	5.00	5.85

Table B2: Concentration of Si with respect to time at different leaching temperatures (1000°C ash) Si

Time(hrs)	20°C(ppm)	30°C(ppm)	40°C(ppm)	50°C(ppm)
0	5.03	5.03	5.03	5.03
0.5	13.05	13.25	14.78	15.58
1	14.44	14.94	15.48	19.51
2	14.58	15.90	16.52	21.04
4	15.28	16.75	17.02	23.96
8	15.54	17.78	18.65	24.50
10	16.12	19.58	20.27	25.30
12	18.70	20.65	22.30	27.68
24	20.37	22.38	24.50	30.53

Table B3: Concentration of Mg with respect to time at different leaching temperatures (1000°C ash) Mg

Time(hrs)	20°C(ppm)	30°C(ppm)	40°C(ppm)	50°C(ppm)
0.0	13.00	13.00	13.00	13.00
0.5	13.56	13.60	14.37	15.21
1.0	13.64	13.91	14.81	16.21
2.0	13.89	14.51	15.74	16.88
4.0	14.24	14.84	16.59	17.44
8.0	13.55	15.76	16.97	18.54
10.0	14.60	15.83	14.28	18.67
12.0	14.74	16.00	16.44	20.00
24.0	15.92	17.36	17.79	20.53

Table B4: Concentration of Ca with respect to time at different leaching temperatures (1000°C ash) Ca

Time(hrs)	20°C(ppm)	30 °C(ppm)	40°C(ppm)	50°C(ppm)
0.00	80.00	80.00	80.00	80.00
0.50	165.56	168.27	170.36	190.04
1.00	190.15	205.74	210.88	220.68
2.00	200.47	212.26	215.15	230.98
4.00	214.09	220.04	230.40	243.00
8.00	220.89	230.38	249.12	253.51
10.00	226.88	235.10	256.80	270.99
12.00	230.19	240.75	263.72	283.57
24.00	235.28	260.24	284.74	290.61

Table B5: Concentration of K with respect to time at different leaching temperatures (1000°C ash) K

Time(hrs)	20°C(ppm)	30°C(ppm)	40°C(ppm)	50°C(ppm)
0.0	67.0	67.0	67.0	67.0
0.5	67.5	69.2	70.1	72.4
1.0	67.6	70.3	72.7	75.1
2.0	68.4	75.4	80.6	88.2
4.0	69.6	76.6	82.2	89.1
8.0	77.7	78.9	85.9	93.0
10.0	80.0	81.8	90.2	94.4
12.0	85.0	90.4	95.8	95.1
24.0	89.1	92.6	99.7	102.9

Appendix C

Table C1: Concentration of K with respect to time at different leaching temperatures (1100°C ash)

Time(hrs)	20°C(ppm)	30°C(ppm)	40°C(ppm)	50°C(ppm)
0.0	67.0	67.0	67.0	67.0
0.5	69.3	70.4	75.6	88.0
1.0	70.3	74.6	82.2	89.3
2.0	72.8	76.3	85.0	89.8
4.0	74.4	76.5	85.1	90.5
8.0	76.2	78.3	86.6	91.9
10.0	77.7	79.1	86.7	93.7
12.0	78.1	82.2	88.1	96.2
24.0	80.3	85.4	101.1	110.2

Table C2: Concentration of Al with respect to time at different leaching temperatures (1100°C ash)

Time(hrs)	20°C(ppm)	30°C(ppm)	40°C(ppm)	50°C(ppm)
0.0	1.2	1.2	1.2	1.2
0.5	1.4	1.3	2.4	2.6
1.0	1.5	1.8	3.3	4.0
2.0	1.9	2.2	4.7	5.5
4.0	2.0	2.3	5.1	6.1
8.0	2.1	2.5	5.8	7.1
10.0	2.6	2.7	5.8	8.6
12.0	3.2	3.5	6.1	9.6
24.0	3.3	5.0	9.2	11.0

Table C3: Concentration of Ca with respect to time at different leaching temperatures (1100°C ash)

Time(hrs)	20°C(ppm)	30°C(ppm)	40°C(ppm)	50°C(ppm)
0.0	80.0	80.0	80.0	80.0
0.5	170.0	196.9	210.6	220.9
1.0	213.2	220.6	225.9	272.1
2.0	220.5	230.5	242.8	292.0
4.0	234.2	239.5	250.3	321.7
8.0	240.2	245.5	268.6	342.4
10.0	251.0	260.3	272.4	362.6
12.0	262.1	278.1	293.0	377.6
24.0	288.1	301.6	323.8	381.3

Table C4: Concentration of Mg with respect to time at different leaching temperatures (1100°C ash)

Time(hrs)	20°C(ppm)	30°C(ppm)	40°C(ppm)	50°C(ppm)
0.0	13.0	13.0	13.0	13.0
0.5	14.2	14.5	14.8	16.3
1.0	14.7	14.6	15.5	18.0
2.0	15.3	15.9	16.4	18.2
4.0	15.5	16.8	17.5	19.3
8.0	16.7	18.9	16.7	20.9
10.0	18.8	19.1	19.3	21.8
12.0	19.5	20.1	20.8	22.5
24.0	20.3	21.2	21.5	22.8

Table C5: Concentration of Si with respect to time at different leaching temperatures (1100°C ash)

Time(hrs)	20°C(ppm)	30°C(ppm)	40°C(ppm)	50°C(ppm)
0.0	5.0	5.0	5.0	5.0
0.5	7.5	9.4	10.7	12.4
1.0	8.0	10.8	12.7	14.6
2.0	10.3	12.9	15.8	15.3
4.0	12.7	17.0	16.0	17.2
8.0	15.9	17.8	17.5	19.4
10.0	17.2	18.0	17.5	20.1
12.0	17.7	20.9	21.8	21.8
24.0	18.0	21.8	21.9	24.6

Appendix D

Table D1: Concentration of Ca with respect to time at different leaching temperatures (1300°C ash)

Time(hrs)	20°C(ppm)	30°C(ppm)	40°C(ppm)	50°C(ppm)
0.0	80.9	80.9	80.9	80.9
0.5	92.5	110.0	110.4	114.0
1.0	100.1	110.1	112.8	115.5
2.0	104.5	115.1	118.6	120.5
4.0	105.9	117.8	120.4	126.5
8.0	109.4	120.2	125.2	132.8
10.0	112.3	125.6	131.0	135.9
12.0	115.6	127.9	132.6	136.7
24.0	123.2	130.6	135.1	140.1

Table D2: Concentration of Si with respect to time at different leaching temperatures (1300°C ash)

Time(hrs)	20°C(ppm)	30°C(ppm)	40°C(ppm)	50°C(ppm)
0.0	5.0	5.0	5.0	5.0
0.5	6.0	7.1	9.3	10.9
1.0	6.9	8.3	9.6	11.0
2.0	7.5	9.2	10.5	11.3
4.0	7.8	10.0	10.6	12.0
8.0	8.4	10.4	11.8	12.6
10.0	8.4	11.3	12.2	13.7
12.0	9.1	11.9	12.4	14.0
24.0	9.2	12.5	14.6	16.9

Table D3: Concentration of Al with respect to time at different leaching temperatures (1300°C ash)

Time(hrs)	20°C(ppm)	30°C(ppm)	40°C(ppm)	50°C(ppm)
0.0	1.2	1.2	1.2	1.2
0.5	1.3	1.4	1.5	1.7
1.0	1.7	1.9	2.0	2.3
2.0	2.0	2.6	2.5	2.9
4.0	2.3	2.6	2.7	3.1
8.0	2.5	3.0	3.2	3.3
10.0	2.6	3.3	3.3	3.6
12.0	2.8	3.4	3.6	3.7
24.0	3.0	3.5	3.9	4.1

Table D4: Concentration of K with respect to time at different leaching temperatures (1300°C ash)

Time(hrs)	20 °C(ppm)	30 °C(ppm)	40 °C(ppm)	50 °C(ppm)
0.0	68.0	68.0	68.0	68.0
0.5	69.5	68.7	70.7	75.0
1.0	70.7	69.5	72.1	72.0
2.0	68.2	70.2	70.5	75.0
4.0	68.3	69.8	75.8	79.8
8.0	69.8	70.2	76.7	80.6
10.0	71.2	72.7	78.9	86.1
12.0	72.7	75.4	79.8	89.2
24.0	75.6	78.2	80.5	98.1

Table D5: Concentration of Mg with respect to time at different leaching temperatures (1300°C ash)

Time(hrs)	20°C(ppm)	30°C(ppm)	40°C(ppm)	50°C(ppm)
0.0	13.0	13.0	13.0	13.0
0.5	14.0	14.0	14.2	14.6
1.0	14.5	14.6	14.7	16.0
2.0	14.5	14.7	14.9	15.2
4.0	15.8	15.1	15.4	17.8
8.0	15.9	15.2	16.8	18.4
10.0	14.1	16.6	16.9	19.7
12.0	16.7	16.8	18.2	20.7
24.0	17.9	18.1	19.7	21.0

Appendix E

Table E1: ICP-OES results of batch leaching heavy elements from coal and different ash samples used for this study at ambient leaching temperature.

	Heavy element extraction at room temperature (µg/L) Batch method									
	A	B	C	D	E	F	G	H	GW	DL
As	9.8	11.5	12.3	16.9	19.4	23.3	6.8	8.0	1.12±0.2	430
Cu	19.0	70.0	5.0	43.5	4.3	38.6	7.7	47.4	30.5±3.6	100
Co	1.2	3.3	1.7	4.7	0.8	5.4	1.2	2.5	1.1±0.1	6900
Cr	78.8	153.9	71.1	126.5	225.0	327.6	66.1	137.2	90.0±10.0	4700
Cd	10.4	14.9	15.8	20.4	14.7	19.8	10.5	15.2	3.0±0.3	31
Ba	480.7	1377.0	343.7	760.7	413.0	682.7	400.8	554.9	236.0±95.2	7800
Pd	10.1	15.7	8.1	13.6	12.6	17.3	10.7	13.1	1.7±0.7	100
Au	0.2	0.8	0.1	0.6	0.3	0.8	0.3	0.4	0.23±0.04	5000
Ag	0.6	1.4	0.4	1.7	0.5	1.3	0.4	1.4	0.8±3.2	5300
Ni	11.2	12.1	7.7	10.1	10.9	14.3	8.3	16.8	0.17±0.31	1140
Hg	0.5	1.5	3.3	5.5	2.5	4.3	1.5	2.6	0.06±0.03	22
Zn	1.3	5.9	2.3	7.4	3.3	8.1	2.7	5.6	5.1±1.18	700
Se	11.7	110.5	10.6	116.3	5.5	102.0	0.4	101.7	119.55±30.28	260

DW: deionised water; GW: groundwater; DL: Department of Water Affairs and Forestry Minimum Requirements; TL: toxicity characteristic leaching procedure limit. A= Coal DW, B= Coal GW, C= Ash 1000°C DW, D= Ash 1000°C GW, E= Ash 1100 °C DW, F= Ash 1100°C GW, G= Ash 1300°C DW, H= Ash 1300°C GW

Table E2: ICP-OES results of column leaching heavy elements from coal and different ash samples used for this study at ambient leaching temperature.

Heavy element extraction room temperature (µg/L) column method											
	A	B	C	D	E	F	G	H	GW	DL	TL
As	12.9	14.6	10.4	17.0	18.7	25.3	12.4	20.9	1.12±0.2	430	5000
Cu	7.4	44.7	9.3	51.1	2.7	34.4	7.6	48.7	30.5±3.6	100	-
Co	1.1	4.0	0.5	2.3	1.8	2.8	0.6	1.8	1.1±0.1	6900	-
Cr	22.7	119.5	9.8	110.1	43.5	120.2	93.7	175.2	90.0±10.0	4700	-
Cd	26.3	31.6	33.2	43.8	28.2	35.8	32.8	40.9	3.0±0.3	31	1000
Ba	182.8	459.0	145.8	307.3	232.7	521.7	160.1	587.0	236.0±95.2	7800	100000
Pd	9.4	16.0	10.1	20.0	11.2	25.0	9.4	14.1	1.7±0.7	100	5000
Au	0.3	0.6	0.3	0.6	0.3	0.9	0.3	0.6	0.23±0.04	5000	2000
Ag	0.4	1.4	0.4	2.4	0.4	1.4	0.4	1.1	0.8±3.2	5300	2500
Ni	3.4	24.9	11.1	12.2	8.7	12.9	8.7	13.0	0.17±0.31	1140	-
Hg	0.6	1.9	0.5	1.6	0.7	1.6	0.9	2.0	0.06±0.03	22	200
Zn	2.8	8.3	4.5	6.2	2.3	7.2	3.2	6.3	5.1±1.18	700	-
Se	16.1	119.9	6.2	115.0	11.6	123.7	1.0	105.0	119.55±30.3	260	-

DW: deionisedwater; GW: groundwater; DL: Department of Water Affairs and Forestry Minimum Requirements; TL: toxicity characteristic leaching procedure. A= Coal DW, B= Coal GW, C= Ash 1000°C DW, D= Ash 1000°C GW, E= Ash 1100°C DW, F= Ash 1100°C GW, G= Ash 1300 °C DW, H= Ash 1300^{o}C G